LabSTAF and RunSTAF

Handbook

Doc No. 2408-014-HB | Issue F

Approved	Kevin Oxborough	13/12/2022
Checked	Nina Schuback	05/12/2022
Originated	Kevin Oxborough	--
Issue	ECN	Date
F	NA	16/12/2022

Contents

Authorship

Main author:	Kevin Oxborough[1,2]
Additional scientific:	Nina Schuback[1,3], Mary Burkitt-Gray[1], C. Mark Moore[2]
Additional technical:	Sam Saragi[1], Salman Mian[1], Jack O'Byrne[1], John Attridge[1], Tony Foord[1], Cameron Hughes[1], Drew Phillpot[1]

[1]Chelsea Technologies Ltd., West Molesey, KT8 2QZ, UK

[2]University of Southampton, Southampton, SO14 3ZH, UK

[3]Swiss Polar Institute, Rue de l'Industrie 17, 1950 Sion, Switzerland

Acknowledgements

OCEANIDS programme (NE/P020844/1)

Technologies for Ocean Sensing | TechOceanS Project | H2020 | CORDIS | European Commission (europa.eu)

Changes since 2408-014-HB Issue E

This section provides a brief overview of the changes made since Issue E. At the time of release, this version of the handbook is matched with RunSTAF v8.9.1.

The **Pre E** ST curves are on the same **SU** scale as the main ST curves.

The updating of data files, including curve fit updates, is now incorporated within a single option:
File → Run a folder-based version update

A fluorescence amplitude-based method for deriving 'transient' values of E_k (E_{kt}') and tau (τ_t') has been implemented. These parameters can be accessed as **Step parameter values** on the home screen and as **Plot selections** on the data plot screen.
See: **Data processing within RunSTAF**

New spectral processing functions have been added. These allow external actinic light spectra to be imported and applied to existing FLC data. The External Spectral Data ESD function can incorporate data acquired directly or indirectly from CTL's Spectral PAR (SPAR) sensor or indirectly from a calibrated third-party spectrometer. The ESD may, for example, be logged from a photosynthetron light source or ambient light.
See: **working with External Spectral Data (ESD)**

Plot selections on the data screen now includes F_b and F_o' under **Primary fluorescence values** plus **[oc]** and **[cc]** under the **Dimer fit parameters** list.

A COM port data stream has been added to RunSTAF. This provides real time data streaming of SPAR data, Saq group data and FLC step data in CSV format.
See: **Data access: COM port output**

The Package Effect Correction and PEP-based spectral correction applied are now quantified through the values of **cPEC** and **cPEP**, respectively. The file-specific values of cPEC and cPEP are shown under the **Data processing** section of the home screen and are also included in the standard Clipboard header. The cPEC and cPEP values are both applied at the level of a_{LHII}, rather than JV_{PII}.

The Clipboard menu now includes an option to turn off the Footer.
See: **The Clipboard footer**

The automated **High $\mathbf{E}$** setting for running FLCs used to be fixed at four times the E_k from the preceding FLC. There is now a field under **FLC setup** (**x $\mathbf{E_k}$**) that allows the end user to set the multiple of E_k used to define the value of **High $\mathbf{E}$**.
See: **Auto FLC mode setup**

A dual incubation method for simultaneous assessment of ^{14}C-fixation and JV_{PII} from samples within scintillation vials has been developed:
See: **Non-standard experimental procedures**

Updates

New releases of this document will be uploaded to **oceanbestpractices.org**.

The DOI for the previous release is…

http://dx.doi.org/10.25607/OBP-1029.3

The most recent release of this document is also included within the RunSTAF download link…

https://1drv.ms/u/s!AkUtV8PHZSmVvJ9wn1f32TiIViBbZw?e=n2TFwe

1 Introduction

This introductory section provides a brief overview of the development of LabSTAF and RunSTAF and future aims for the development of Single Turnover Active Fluorometry (STAF). It also includes a description of the major differences between LabSTAF and the previous generation of active fluorometers. A comprehensive overview of the acronyms and terms used within this document is provided within **Glossary of terms**.

1.1 The STAFES-APP and TechOceanS projects

LabSTAF is the first of a new generation of research-grade active fluorometers developed by Chelsea Technologies Ltd (CTL) in collaboration with The University of Southampton (UoS) and the National Oceanographic Centre, Southampton (NOCS) as part of the STAFES-APP project within the NERC-funded OCEANIDS programme (NE/P020844/1). Additional, ongoing funding for STAF development is being provided through the EU-funded Technologies for Ocean Sensing (TechOceanS) programme (Technologies for Ocean Sensing | TechOceanS Project | H2020 | CORDIS | European Commission (europa.eu)).

The STAFES-APP acronym expands to Single Turnover Active Fluorometry of Enclosed Samples – for Autonomous Phytoplankton Productivity. The overall aim of the project was to develop highly sensitive benchtop and deployable systems that can be used to improve our understanding of the global carbon cycle and aquatic ecosystem function.

Primary productivity by phytoplankton (PhytoPP) accounts for approximately half of the carbon fixed by photosynthesis on a planetary scale. It follows that measurement of PhytoPP on wide spatial and temporal scales has enormous potential for developing our understanding of ocean productivity and improving climate change models. Arguably the most important way in which this target can be achieved is through the validation and development of satellite remote sensing, which operates on the widest possible spatial scales, but which currently includes large errors for the estimation of PhytoPP. Historically, validation of remote sensing algorithms for the estimation of PhytoPP has relied on data from ^{14}C tracer-based methods, including photosynthetron-based measurement of ^{14}C-fixation as a function of incident light (Geider and Osborne, 1992; Sakshaug et al. 1997). Because this method cannot be applied on meaningful spatial or temporal scales, there is currently extreme undersampling of the oceanic environment for PhytoPP at acceptable levels of accuracy (e.g., Lee et al. 2015). A key target for the STAFES-APP project was to develop new, STAF-based methods for the assessment of PhytoPP that can be used on much wider spatial and temporal scales than ^{14}C-fixation, at comparable levels of accuracy and precision.

1.1.1 Fluorescence Light Curves (FLCs) and P-E curves

The combination of LabSTAF and RunSTAF allows for the highly automated acquisition of fluorescence light curves (FLCs). A FLC comprises a set of STAF measurements made at several photon irradiance levels between darkness and saturating light. It follows that a FLC allows for an assessment of the light-dependence of photosynthesis in a way that is comparable to the ^{14}C tracer-based photosynthesis – photon irradiance (P-E) curve. The LabSTAF system can typically run between two and four FLCs per hour, incorporating eight to twelve photon irradiance levels. For comparison, ^{14}C tracer-based P-E curves normally require the incubation of a range of samples exposed to different levels of incident photon irradiance within sealed containers for several hours (Marra, 2002; Milligan et al., 2015).

Within this document, the primary FLC-generated dataset is defined as a relative P-E (rP-E) curve. The rP values are generated as the product of a STAF-derived fluorescence parameter, F_q'/F_{mc}', and incident photon irradiance, E. The F_q'/F_{mc}' parameter provides a proxy for PSII photochemical efficiency (ϕ_{PII}) and the incident photon irradiance is provided by the calibrated and spectrally characterised actinic light source incorporated within the LabSTAF unit. There are three parameters

that are routinely derived from P-E curve fits: α, E_k, and P_m. The value of α provides the initial slope of the relationship between incident photon irradiance and the rate of photosynthesis. E_k is an inflection point along the P-E curve which has been described as the light saturation parameter (Platt and Gallegos, 1980). P_m is the maximum rate of photosynthesis.

The chemical energy required to drive PhytoPP is derived from the light reactions of oxygenic photosynthesis. The combination of LabSTAF hardware and RunSTAF software allows the evaluation of oxygenic photosynthesis through measurement of photosystem II (PSII) photochemical flux per PSII (J_{PII}) and PSII photochemical flux per unit volume of ocean (JV_{PII}) using the so-called Sigma and Absorption methods, respectively. Comparison of rP values from different cultures or communities and the scaling of rP values to J_{PII} and JV_{PII} invariably require spectral correction. In the case of JV_{PII}, accuracy can also be improved by correction for the so-called package effect (Boatman, Geider and Oxborough, 2019). The combination of LabSTAF and RunSTAF allows for highly automated spectral correction and correction for the package effect.

Figure 1.1 shows an example of output from a RunSTAF-generated FLC. In this example, the rP data have been scaled to JV_{PII}, providing units of µmol photons m^{-3} s^{-1}. Calculated values of J_{PII} are also shown, with units of photons $PSII^{-1}$ s^{-1}.

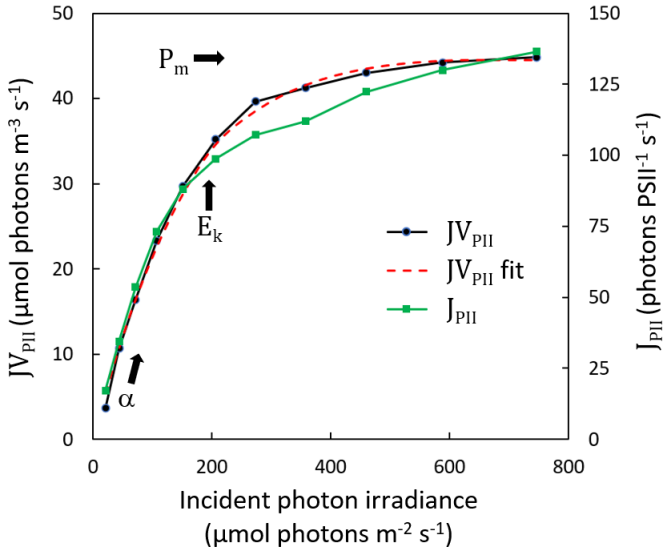

Figure 1.1: Example P-E curves from a RunSTAF-generated FLC. The sample was cultured cells of the diatom *Conticribra weissflogii*.

Converting rP data to JV_{PII} P-E data involves a straightforward rescaling of values, using the Absorption method. This retains the original shape of the rP-E curve. In the case of J_{PII}, there are two widely used methods for deriving values. The first method incorporates a STAF-derived estimate of the absorption cross section of PSII photochemistry from the dark measurement (σ_{PII}) at every point along the curve. As with JV_{PII}, this approach generates values that track the rP-E curve. The alternative method, which is the one used within RunSTAF, incorporates a separate light-adapted value for the absorption cross section of PSII photochemistry (σ_{PII}') at each point along the curve. This can result in a significant and potentially informative divergence in shape between the JV_{PII} P-E and J_{PII} P-E curves, as seen in Figure 1.1.

Importantly, it is much easier to scale PhytoPP (units of moles of carbon per unit volume per unit time) with JV_{PII} (units of moles of photons per unit volume per unit time) than with J_{PII} (units of photons per PSII per unit time).
See: **Generating values of J_{PII} and JV_{PII}**

1.2 Essential Ocean Variables (EOVs)

Global assessment of PhytoPP falls within the remit of the Global Ocean Observing System (GOOS) which defines and prioritises a range of Essential Ocean Variables (EOVs). The fundamental criteria

employed for defining EOVs are impact and feasibility: to make it on to the GOOS list, an EOV must have high impact and be measurable on meaningful scales using cost effective technology. Although PhytoPP clearly satisfies the impact criterion, the feasibility requirement means that measurements must be made on the same spatial and temporal scale as the environmental drivers of PhytoPP, which includes light, temperature and nutrient fluxes.

Because ^{14}C tracer-based methods for the assessment of PhytoPP fall cannot be applied on meaningful spatial and temporal scales, they score very low on the feasibility scale. In sharp contrast, STAF systems are relatively easy to deploy and have the potential to generate data on spatial scales from a few metres up to oceanic basin scales and temporal scales of seconds to tens of minutes, depending on the level of detail required. It follows that STAF has potential for the provision of meaningful EOVs for use in the assessment of PhytoPP, particularly when combined with nutrient and other EOV data.

Direct comparison between ^{14}C tracer-based and STAF-based assessment of PhytoPP is far from straightforward. One widely acknowledged issue is that while STAF provides a method for direct assessment of PSII photochemical flux, it does not provide a direct quantitative assessment of the proportion of the reducing equivalents derived from PSII photochemistry that are ultimately used to drive carbon assimilation. In contrast, the link between PSII photochemistry and the oxidation of water by the PSII Oxygen Evolving Complex (OEC) means that PSII photochemical flux is generally well correlated with gross oxygen release by PSII (GO_{PII}). It follows that development of a STAF-based EOV for the assessment of GO_{PII} with acceptable levels of accuracy and precision looks perfectly feasible but that a STAF-based EOV for PhytoPP is likely to require additional input. The degree to which these additional input requirements will constrain STAF-based assessment of PhytoPP will depend on the spatial and temporal scales at which these additional inputs can be monitored and their scales of variability within the environment. For example, the spatial and temporal scales at which nutrient availability can be assessed are well below the scales for STAF measurements but usually within environmental scales of variability. In addition, confidence in STAF-based EOVs for PhytoPP is highly dependent on a thorough assessment of variability in and the predictability of the coupling of JV_{PII} and carbon assimilation.
See: **The dual incubation method (^{14}C-fixation + STAF)**

1.2.1 STAF-derived EOVs for the assessment of PhytoPP

Because JV_{PII} and PhytoPP all respond rapidly to changes in incident light, there is value in making STAF measurements over a range of incident photon irradiances. Within RunSTAF, this process is centred around the automation of FLCs and rP-E curve analysis. A target for future development is to increase the frequency at which FLCs are run, from samples with contrasting light histories. The current default FLC protocol runs through a set of increasing incident photon irradiances, from dark to saturating light. For a sample that was previously light-adapted, there is often a requirement to run the sample through a combination of several minutes of low light plus dark-adaptation before the FLC is started. While this is generally not an issue when working with cultures, it seems likely that modification of the standard protocol could significantly shorten the assessment time and generate more meaningful information from samples loaded directly from the natural environment.

Although only a small number of STAF-derived parameters can be applied directly to the assessment of PhytoPP, a much broader range of parameters have the potential to improve the accuracy of this assessment. When considering appropriate parameters to use as EOVs, it is important to define exactly how such parameters are derived and to allow for future recalculation, where this is justified by the availability of new information. This criterion is currently met by archiving all primary data and calibration data within RunSTAF data files. While this strategy is ideal for systems that can be recovered for data download, a central aim of the TechOceanS project is to develop STAF systems for use on platforms that may never be recovered, such as Argo Floats. For such deployments, the available bandwidth is too low to allow for the transmission of all primary data. This bandwidth

limitation generates a significant challenge for the transmission of EOV-standard data from unrecovered platforms: acquisition needs to be at high enough frequency to meet the spatial and temporal scales requirements for assessment of PhytoPP, while data need to be processed in such a way that the recalculation criterion can be met.

1.3 Changes from FastOcean and Act2

LabSTAF represents a significant update to the well-established combination of FastOcean Fast Repetition Rate fluorometer (FRRf) and Act2 laboratory system. The list of advantages that LabSTAF has over FastOcean plus Act2 includes:

- More than ten times the sensitivity
- Much lower optical filter breakthrough
- Two fluorescence detection wavebands instead of one
- Seven fluorescence excitation LED wavebands instead of three
- DC actinic light source providing 10 to > 1600 µmol photons m^{-2} s^{-1}
- A circulating water jacket that avoids intersection with all optical paths
- Increased FLC automation
- Extended data analysis
- Improved access to primary data

The increased sensitivity is the result of a switch from 1 µs FRRf 'flashlets' on a 2 µs pitch to a solid excitation pulse from the excitation LEDs, plus a more efficient optical arrangement. An added advantage of the switch from FRRf to a solid pulse is that the same number of data points can be collected in half the time. Consequently, the default Single Turnover (ST) pulse has been shortened from 200 µs (FastOcean) to 100 µs (LabSTAF).

The much lower filter breakthrough is the result of the change in optical configuration and the use of better optical filters. The most obvious benefit is lower and more consistent blank values when sampling within extreme oligotrophic regions.

The incorporation of two fluorescence detection wavebands within LabSTAF, centred at 685 nm and 730 nm, allows for correction of the package effect (Boatman, Geider and Oxborough, 2019).
See: **Applying the Package Effect Correction (PEC)**

The seven Measurement LED (MLED) wavebands incorporated within LabSTAF allow for routine spectral analysis based on variable fluorescence (F_v) and the absorption cross section of PSII photochemistry (σ_{PII}). This analysis includes automated spectral correction of primary data using the F_v values.
See: **Spectral correction**

The blue-enhanced DC Actinic LED (ALED) light source incorporated within LabSTAF improves signal to noise and avoids the potential for measurement artefacts associated with Pulse Width Modulation (PWM).
See: **The actinic light source (ALED)**

Avoiding intersection between the water jacket and all optical paths allows underway water (for example) to be used to maintain the temperature of the sample. The LabSTAF optics and electronics are sealed to prevent condensation in situations where there is a need to maintain the sample temperature at well below ambient. The relative humidity within the LabSTAF unit is reported by RunSTAF each time it is attached.
See: **Sample temperature control**

The improved FLC automation allows for the inclusion of a pre-illumination and a dark step after sample exchange between successive FLCs. The ST data collected during these steps are archived within the standard data file.
See: **Auto FLC mode setup**

The extended data analysis includes a new ST curve fitting function that assumes connectivity among PSII complexes is entirely attributable to dimerization.
See: **Data processing within RunSTAF**

RunSTAF incorporates a range of functions for real time data analysis. In addition, straightforward transfer of primary data and derived parameters is possible, through the Windows Clipboard and/or bulk generation of CSV files. Access to primary data is provided to allow for analysis with user-formulated algorithms and database integration.
See: **Data access: Clipboard functions** and **Data access: CSV functions**

2 Key features and terminology

This section describes key features of the LabSTAF system and provides an overview of the acronyms and terminology used within this document.
See: **Glossary of terms**.

2.1 The Surface Go computer

The LabSTAF system includes a Surface Go computer and keyboard to provide a consistent, reference platform for the RunSTAF software. Most screenshots within this document were captured from a Surface Go 3 computer screen. RunSTAF can also be installed and used on most computers running the Windows 10 or Windows 11 operating system.

2.2 New terms

Introduction of a Dual ST Pulse (DSP) method, the dimer fitting procedure and other new features have necessitated the introduction of new terminology. Although this has led to the use of alternatives to some established terms, most terms used are identical or very close to ones that have been in widespread use for several decades.
See: **Glossary of terms**.

2.3 Irradiance and photon irradiance

Irradiance is the radiant flux (power) received at a surface, with SI units of W m^{-2}. Photon irradiance is the photon flux received at a surface, with SI units of mol photons m^{-2}. As is generally the case for biological processes, photon flux is more useful than radiant flux when quantifying photosynthesis. Throughout this document, photon irradiance is reported in preference to irradiance, with units of µmol photons m^{-2} s^{-1}.

2.4 Conformance with the SI system

The units used throughout this document conform with the SI system (International System of Units). When discussing the derivation of quantities, base SI units are used. Reported units include commonly used standard SI prefixes, where appropriate. For example, photon irradiance within an equation will have units of photons m^{-2} s^{-1} or mol photons m^{-2} s^{-1} (depending on context) while actinic photon irradiance is usually reported with units of µmol photons m^{-2} s^{-1}.

2.5 Photosystem II Reaction Centre (RCII)

Each RCII includes all subunits required for stable charge separation between P_{680} (the PSII primary electron donor) and Q_A (the first stable electron acceptor). An RCII can be in the open state (capable of photochemistry) or the closed state (where charge separation is inhibited by reduction of Q_A).

2.6 Photosystem II Light Harvesting System (LHCII)

The term LHCII is applied to any structure that can absorb and transfer photons to the RCII.

2.7 Photosystem II (PSII) complex

A PSII complex comprises a RCII plus a LHCII. When a PSII complex is described as open or closed, it is referencing the status of the RCII within the complex. A PSII complex can be photochemically active (open or closed state) or photoinactivated (requiring repair before absorbed photons can be used to drive photochemistry).

2.8 PSII photochemical flux per photosystem (J_{PII})

This term is used to quantify the photon flux through the absorption cross section for PSII photochemistry provided by a single PSII complex (units of photons $PSII^{-1}$ s^{-1}). The Sigma method is

used to generate values of J_{PII}.
See: **Generating values of J_{PII} and JV_{PII}**

2.9 PSII photochemical flux per unit volume (JV_{PII})

This term is used to quantify the photon flux through the absorption cross section for PSII photochemistry provided by all PSII complexes within a unit volume of ocean or other medium (SI units of photons m^{-3} s^{-1} or mol photons m^{-3} s^{-1}, reported units of µmol photons m^{-3} s^{-1}). The Absorption method is used to generate values of JV_{PII}.
See: **Generating values of J_{PII} and JV_{PII}**

2.10 Photosynthetic Gross Oxygen release by PSII photochemistry (GO_{PII})

This is the moles of oxygen molecules released by PSII photochemistry per unit volume per unit time (SI units of mol O_2 m^{-3} s^{-1}, reported units of mmol O_2 m^{-3} h^{-1}). Values reported by RunSTAF assume that each O_2 released requires four stabilised charge separation events at PSII and is calculated as JV_{PII} divided by four.

2.11 Electron Transport Rate (ETR)

While it is generally accepted that the ultimate source of the electrons being transferred through the photosynthetic electron transfer chain is the oxidation of water by the Oxygen Evolving Complex (OEC), the value of ETR can be defined as electrons transferred to, as examples, the plastoquinone pool or NADP. While no parameter termed ETR is reported by RunSTAF, the assumption that each photon used to drive PSII photochemistry results in the transfer of an electron out of PSII makes it perfectly reasonable to substitute 'electrons' for 'photons' in the units of J_{PII} and JV_{PII}. This allows J_{PII} and JV_{PII} to be repurposed as clearly defined ETR parameters, where required.

2.12 Phytoplankton Primary Productivity (PhytoPP)

This term is used as a catch-all for carbon assimilation by phytoplankton that is dependent on oxygenic photosynthesis. No distinction is made between gross and net primary productivity and values for PhytoPP are not reported by RunSTAF.

2.13 Downregulation

This term is used to define the process underlying non-photochemical quenching of PSII fluorescence, which is widely assumed to compete directly with PSII photochemistry. The term does not include changes in the amplitude of PSII fluorescence due to state transitions.
See: **The Stern-Volmer relationship, NPQ and NSV**

2.14 STAF Units of fluorescence (SU)

Although the reported fluorescence values are unitless, the LabSTAF calibration procedure places the fluorescence output on a defined STAF Unit (**SU**) scale. Importantly, this allows for derivation of the absorption coefficient for PSII light harvesting (a_{LHII}) which is used in the calculation of JV_{PII}.
See: **LabSTAF calibration**

2.15 Single Turnover (ST)

With this method, it is essential that the intensity of the ST pulse is high enough to drive a high (>> 90%) of PSII complexes into the closed state. Figure 2.1 shows a representative LabSTAF 100 µs ST pulse where this criterion is satisfied. Although 'Single Turnover' implies that each PSII reaction centre undergoes one charge separation event during each ST pulse, simple modelling suggests that approximately 12% of centres are likely to undergo a second charge separation event when a default 100 µs ST pulse is applied. This value more than doubles with a 200 µs ST pulse, to approximately 27%.

In the dark-adapted state, the fluorescence value at t = 0 is termed F_o. The asymptote is termed F_m and the difference between F_m and F_o is termed F_v. The σ_{PII} term shown in Figure 2.1 is the absorption cross section of PSII photochemistry, with reported units of nm^2 PSII^{-1}.
See: **Glossary of terms**

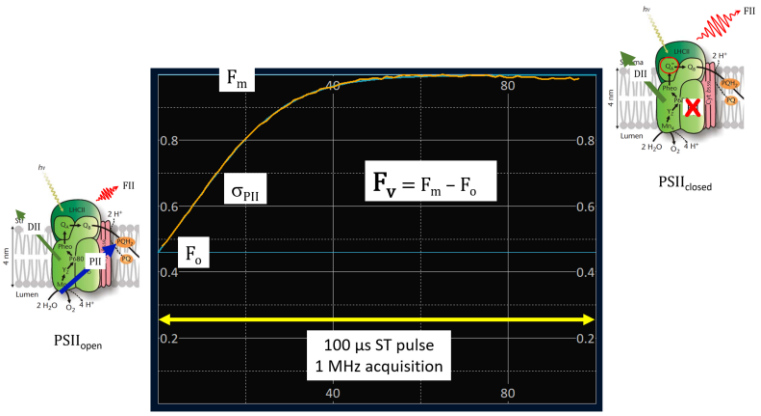

Figure 2.1: Screenshot crop from the RunSTAF home screen showing a 100 µs ST pulse.

The PSII$_{open}$ and PSII$_{closed}$ graphics are from Govindjee et al. (2010)

2.16 The interrogated volume

The LabSTAF sample chamber can hold up to 20 mL of sample. The entire sample is evenly illuminated by the actinic light source. ST data are acquired from a sub-volume of approximately 0.5 mL (the interrogated volume). The measurement LEDs (MLEDs) are focussed on a slightly larger volume to ensure that the interrogated volume is evenly illuminated by the MLEDs. A minimum of 10 mL is required to adequately incorporate the interrogated volume. Scintillation vials can be used to decrease the required volume or to facilitate rapid measurement from a set of samples.
See: **Using scintillation vials**

2.17 Data averaging terminology

At low biomass, averaging of ST data may be required to generate reliable curve fits. The base level of ST data is termed the **Seq** (sequence). Several Seqs can be averaged to generate the next level of ST data, the **Acq** (acquisition) and several Acqs averaged to generate the next level of ST data, the **Saq** (super acquisition). These relationships are illustrated by the example in Figure 2.2.

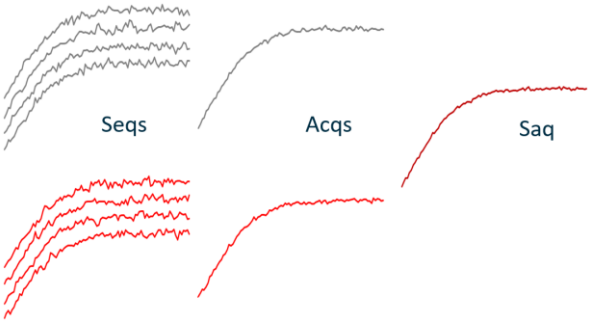

Figure 2.2: Sample ST data acquired at 4 Seqs per Acq and 2 Acqs per Saq.

Seqs are not archived within RunSTAF data files. Saqs are archived within RunSTAF data files, processed, and displayed in real time. If the number of Acqs per Saq is greater than one, the Acqs are archived by RunSTAF but can only be accessed through Clipboard functions.
See: **Data access: Clipboard functions**

The data averaging structure provides a high degree of control over data acquisition and archiving. For example, one Seq per Acq and eight Acqs per Saq could be set for a low biomass sample to provide the highest level of temporal resolution while generating a high enough S:N to allow real time fitting of the Saq level data. At the other end of the scale, setting eight Seqs per Acq and one Acq per Saq minimises the size of the data file for a defined temporal resolution.

2.18 Dual ST Pulse (DSP)-based relaxation phase (tau) measurement

The established FRRf method (Kolber, Prášil and Falkowski, 1998) uses a series of very short, very intense 'flashlets' to form a ST pulse. Typically, each flashlet is 1 µs and the interval between successive flashlets is also 1 µs. As an example, the default FastOcean ST pulse comprises 100 flashlets over 200 µs.

With the FRRf method, the reopening of closed RCIIs can be tracked by applying a relaxation phase measurement that typically comprises tens of widely spaced 1 µs flashlets. Analysis of the relaxation phase is complicated because a correction must be applied to account for the proportion of the reopened RCIIs that are reclosed by each relaxation phase flashlet. Multiple turnovers (mostly double turnovers) of PSII complexes add an additional complication.

The relaxation phase measurement incorporated within LabSTAF uses a Dual ST Pulse (DSP) method to track the reopening of closed PSII complexes. A sample pair of ST pulses is shown in Figure 2.3.

The paired ST pulses are normally of the same duration, with a variable gap between them. The default set incorporates eleven gaps of between 400 and 12800 µs between the end of the first ST pulse and the start of the second ST pulse.

DSP data are acquired by looping through the programmed sequence of gaps until the required level of data averaging has been met (**Seqs / Acq** x **Acqs / Saq** x **Saqs**). Although the DSP method generates fewer relaxation phase points than a typical FRRf relaxation phase measurement, these points have much higher precision and require fewer assumptions to be made when deriving relaxation phase parameters.

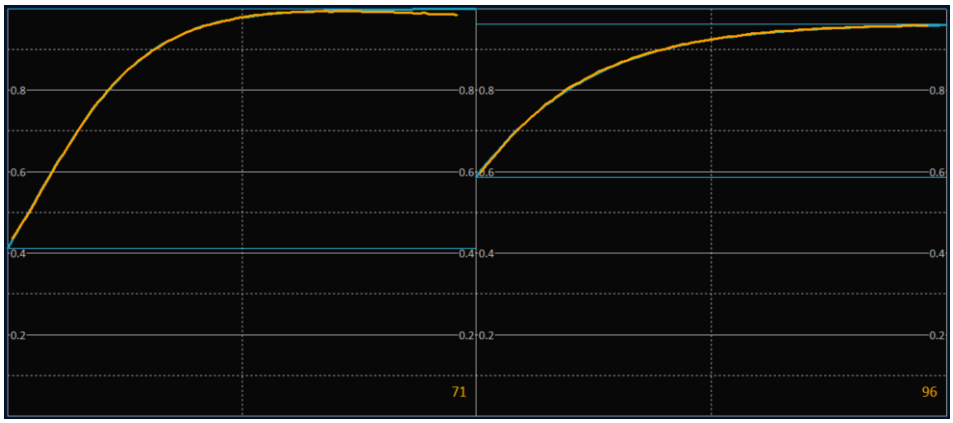

Figure 2.3: This DSP example has been cropped from the RunSTAF data plot screen. The gap between the end of the first pulse and the start of the second pulse is 800 µs.

The default sequence interval (**Seq interval**) for DSP measurements is 120 ms. Although RCIIs closed by a single ST pulse normally reopen on a much shorter timescale than this, the continuous application of pairs of ST pulses to a static dark sample can result in the accumulation of closed RCIIs, over several seconds to tens of seconds, due to the reduction of electron carriers downstream of PSII. This feeds back to PSII and increases the time required for RCIIs to reopen. With LabSTAF, the passive exchange of cells between the interrogated volume and the rest of the sample decreases the accumulation of closed PSII complexes. Using the supplied stirrer unit increases the rate of exchange and further decreases the accumulation of closed PSII complexes.
See: **The relaxation phase (tau) fit** and **LabSTAF hardware setup**

When the DSP method is used, the programmed level of data averaging is applied to each gap length within the range of **Gap steps**. The entire sequence of **Gap steps** is defined as a **Group**. When running in the Auto FLC mode, all first ST pulses from the Saqs within a Group are averaged to generate a Group acquisition (**Gaq**), such that:

Seq / Gaq = **(Seqs / Acq)** x (**Acqs / Saq)** x **Gap steps**

The example in Figure 2.4 shows eight **Seq / Acq**, a single **Acq / Saq** and eleven **Gap steps**, which makes each Gaq an average of 88 Seqs.

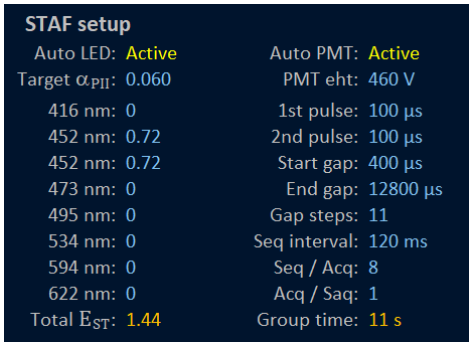

Figure 2.4: Crop from the home screen showing the default settings under **STAF setup**. The dual ST pulse function is set to run with 100 µs ST pulses and 11 **Gap steps** between 400 µs and 12800 µs.
The **Seq interval** between the end of the second ST pulse in one pair and the start of the first ST pulse in the next pair is constant, with a default value of 120 ms.

During acquisition, the most recent Gaq ST curve generated is shown within the ST plot window on the home screen. Once acquisition has completed in the Auto FLC mode, the last Gaq at the Up step selected within the rP-E plot is shown within the ST plot window. All Gaq traces are accessible through data export functions.
See: **The rP-E data fit**

2.19 Photochemical Excitation Profiles (PEPs)

The Measurement LEDs (MLEDs) within LabSTAF emit within narrow spectral bands while the Actinic LED (ALED) within LabSTAF provides a broad spectral output. It follows that derivation of a_{LHII}, J_{PII} and JV_{PII} values must include a spectral step to correct for the difference between the overall output from the combination of MLEDs used to generate the primary ST data and the output of the ALED.

The spectral correction protocol incorporated within RunSTAF generates values of F_v and σ_{PII} for each of the MLED wavebands through the Photochemical Excitation Profile (PEP) function. The PEP data are then used to generate values of F_v and σ_{PII} that are normalized to the ALED.
See: **Spectral correction**

Figure 2.5 shows the $\mathbf{F_v}$ PEP and $\boldsymbol{\sigma_{PII}}$ PEP values. The numbers next to each key lines are for the selected MLED waveband. In this example, the 594 nm waveband is selected (Figure 2.3) but the actual central wavelength of 593.9 nm (from calibration) is reported. The numbers in brackets are the ratios of the selected MLED waveband to ALED values for each parameter. In this case, the photon yield of F_v for the 594 nm waveband is **0.491** x the ALED value and the σ_{PII} value for the 494 nm waveband is **0.493** x the ALED value.

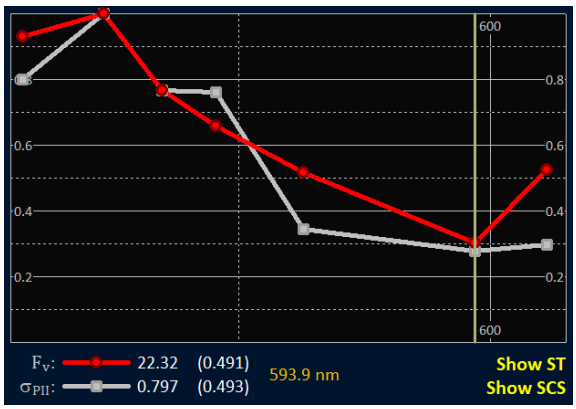

Figure 2.5: This PEP crop shows the F_v and σ_{PII} values for each MLED waveband. The sample was cultured cells of the diatom, *Conticribra weissflogii* (CCAP 1085/18). The differences observed between F_v and σ_{PII} values were consistent over a series of reps.

2.20 Spectral Correction Spectra (SCS) and flat white coefficients

Figure 2.6 shows an extended version of the F_v PEP data in Figure 2.5. Only F_v PEP values are used to apply a spectral correction. The MLEDs and ALED spectra are recorded at 1 nm resolution as part of the LabSTAF calibration procedure. Collectively, these constitute the Spectral Correction Spectra (SCS).
See: **Spectral correction**

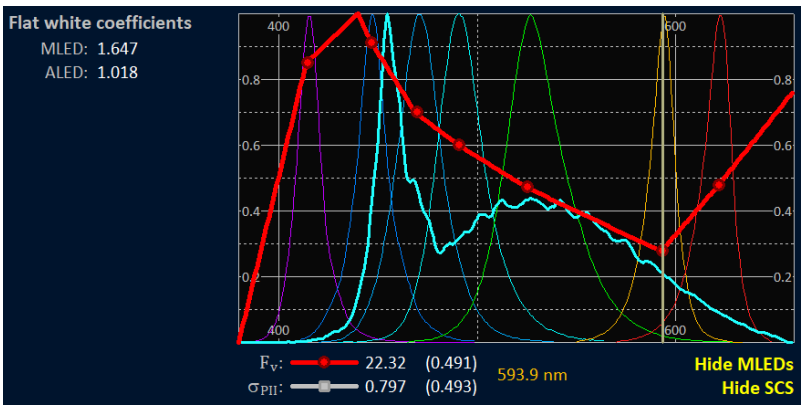

Figure 2.6: The SCS are used by RunSTAF within the spectral correction protocol. The SCS range is between 380 nm and 660 nm.

Figure 2.6 includes **Flat white coefficients** for the MLEDs and ALED. The MLED value indicates that the MLEDs used for the ST pulses have a photon yield of F_v that is **1.647** x that of a theoretical white light source with a completely flat emission spectrum over the SCS range of 380 to 660 nm. The equivalent value for the ALED is **1.018**.

2.21 External Spectral Data (ESD)

In addition to the SCS, RunSTAF allows for the import and application of spectral data from an external device. The example in Figure 2.7 shows the spectral data from a SPAR sensor reading under ambient light as a dashed or solid yellow line. Pressing the **Applied** option switches between application of the **ALED** and **ESD** flat white coefficient to dependent parameters, including the **cPEP** and a_{LHII} values shown within the insets to each panel. In this instance, the values are within 3% of each other. The impact on the dependent parameters is within the same margin.
See: **Working with External Spectral Data (ESD)**

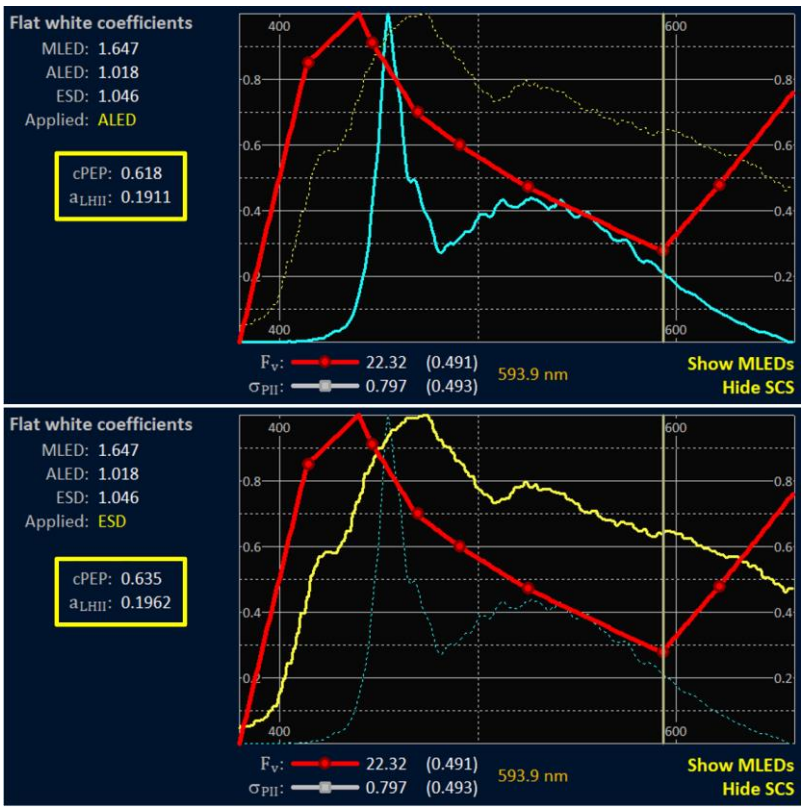

Figure 2.7: illustration of the switch between **ALED** and **ESD**. The inset **cPEP** and a_{LHII} values were cropped from the **Data processing** section of the home screen with each option.

2.22 Correcting for the package effect

The Absorption method, which is used to generate values of a_{LHII} and JV_{PII} is sensitive to the so-called package effect (Boatman, Geider and Oxborough, 2019). Within RunSTAF, a Package Effect Correction (PEC) can be applied. A value for the PEC parameter can be set manually by the user or generated by the Automated Dual Waveband Measurement (Auto DWM) function.
See: **Applying the Package Effect Correction (PEC)**

2.23 Baseline correction

In addition to spectral correction and correction for the package effect, scaling of rP values to JV_{PII} requires an assessment of, and possible correction for, baseline fluorescence. In this context, baseline fluorescence is defined as fluorescence from a dark-adapted sample generated by all sources other than photochemically active PSII complexes.

The curve in Figure 2.8 was generated by applying a ST pulse to a dark-adapted sample. This has generated an F_v/F_m of 0.382, which is significantly lower than the 0.5 to 0.65 range that is widely seen from cultured cells under nutrient replete conditions. This lower value may be the result of locked-in downregulation of PSII photochemistry or may indicate a high level of fluorescence from sources other than photochemically active PSII complexes (including photoinactivated PSII complexes) coupled with an intrinsic PSII photochemical efficiency within the healthy range.

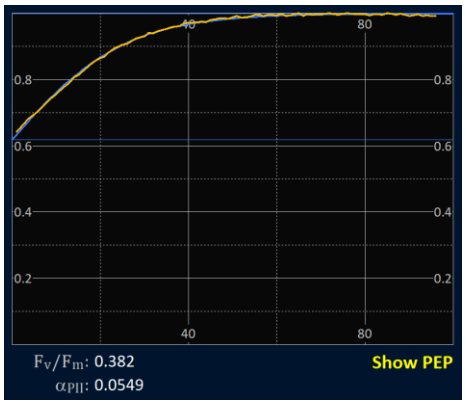

Figure 2.8: Screenshot crop from the home page of RunSTAF showing a ST curve recorded from a dark-adapted sample of cultured cells of the diatom, *Conticribra weissflogii*.

Fluorescence from sources other than photochemically active PSII complexes is termed F_b.
See: **Derivation of F_b and F_{oc}'**

3 The RunSTAF menu bar

This section provides a brief overview of the functions available through the RunSTAF menu bar.

3.1 File

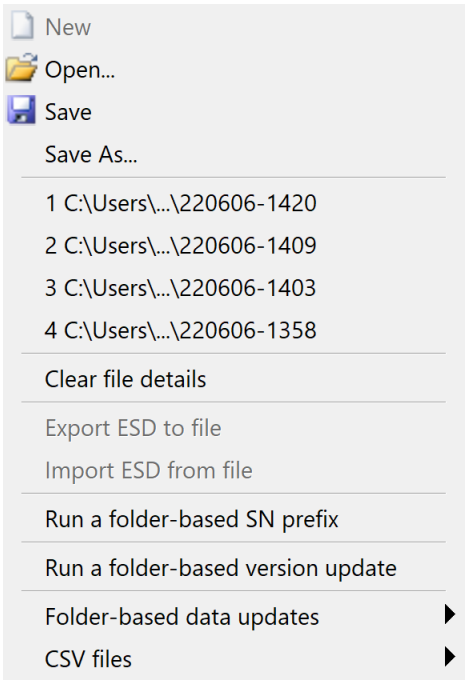

Figure 3.1: The **New** command is only active when relevant.

The **Clear file details** function empties all fields within the File details section of the home screen.

The **Export ESD to file** and **Import ESD from file** options are only active when relevant.
See: **Working with External Spectral Data (ESD)**

The **Run a folder-based SN prefix** function adds the RunSTAF serial number from within the file to the start of every filename within a folder.

The **Run a folder-based version** update also includes updated curve fits, as required.
See: **Update the file version (and refit data)**

The **Folder-based data updates** functions provide a number of functions for reprocessing RunSTAF data.
See: **Folder-based file version and data updates**

The **CSV files** functions provide a number of options for extracting data from RunSTAF files in CSV format.
See: **Data access: CSV functions**

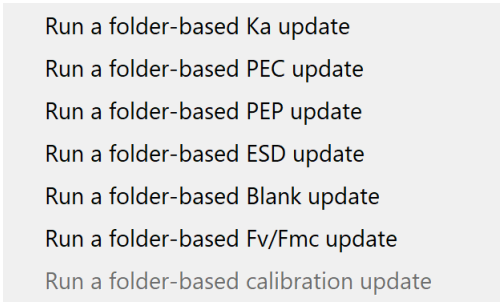

Figure 3.2A: Options for folder-based updates when the active file contains relevant data. All active options overwrite all files within the selected folder with the relevant parameter(s) from the current RunSTAF file.

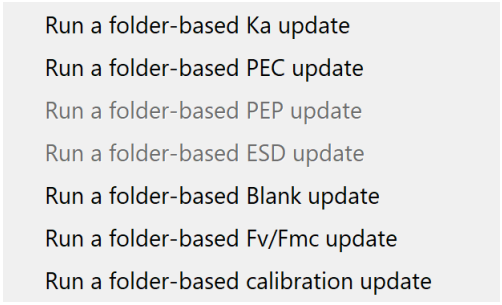

Figure 3.2B: Options for folder-based updates when the active file is empty. All active options overwrite all files within the selected folder with the relevant parameter(s) that are currently set within the empty file.
See: **Folder-based refitting and reprocessing**

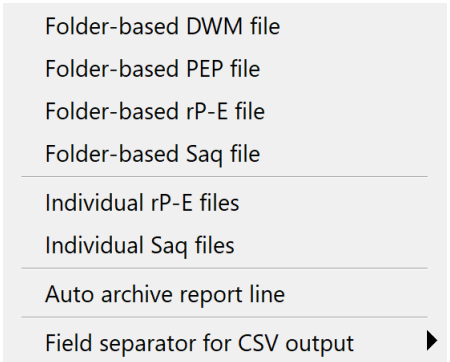

Figure 3.3: The **CSV files** option opens a sub-menu of functions for generating CSV files. The **Folder-based file** and **Individual files** options are only available when RunSTAF is first started.

If the **Auto archive report line** option is checked, a CSV summary file is created to match with each data file generated by RunSTAF.
See: **Data access: CSV functions**

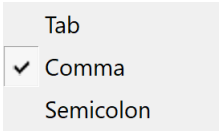

Figure 3.4: The **Field separator for CSV output** option opens a sub-menu that allows the default **Comma** field separator to be replaced with a **Tab** or a **Semicolon**. The selection is applied across all CSV files generated by RunSTAF.

3.2 Settings

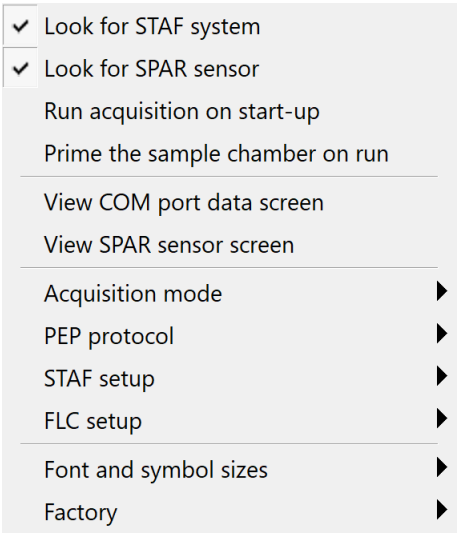

Figure 3.5: The **Look for STAF system** option must be active for data acquisition.

The **Look for SPAR** sensor option must be active for RunSTAF to access a SPAR sensor connected through a COM port.

When **Run acquisition on start-up** is active, acquisition starts as soon as the connected LabSTAF is attached to RunSTAF.

If **Prime the sample chamber on run** is active, RunSTAF will implement the **Exchange** settings from **FLC Setup** before starting acquisition.

The **View COM port data screen** and **View SPAR sensor screen** options switch from the currently active screen to the selection.

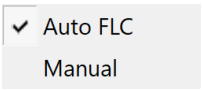

Figure 3.6: The **Acquisition mode** sub-menu allows for selection between the **Auto FLC** and **Manual** modes.

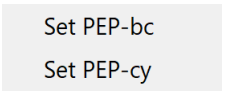

Figure 3.7: The PEP mode sub-menu can be used to set the MLED output for **PEP-bc** or **PEP-cy**. The selected option is saved as the default for new files.

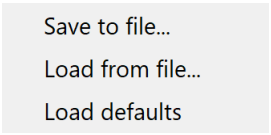

Figure 3.8: The **STAF setup** and **FLC setup** menus both provide options to save and load settings to a named file and to reset to the default values.

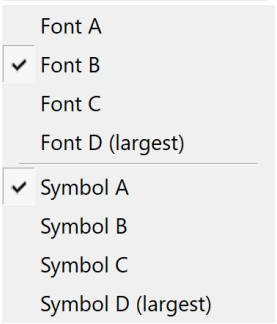

Figure 3.9: The **Font** and **Symbol** sizes sub-menu provides options that can be used to improve the screen layout on computers other than the supplied Surface Go.

RunSTAF must be restarted to implement a change in font size. Symbol size changes are implemented immediately.

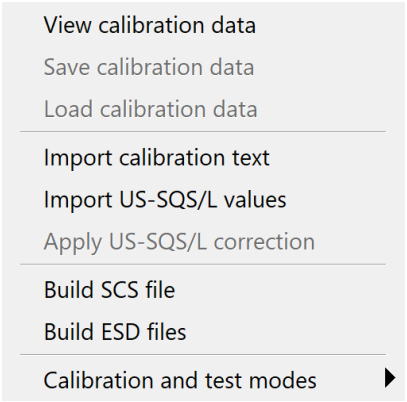

Figure 3.10: The **Factory** sub-menu provides access to a range of functions required for instrument calibration and setup.

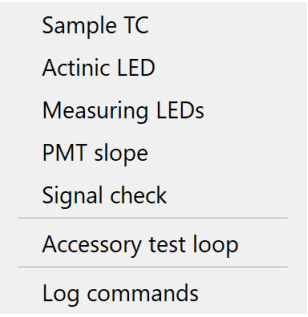

Figure 3.11: The Calibration and test modes sub-menu provides access to functions for factory use.

3.3 Clipboard

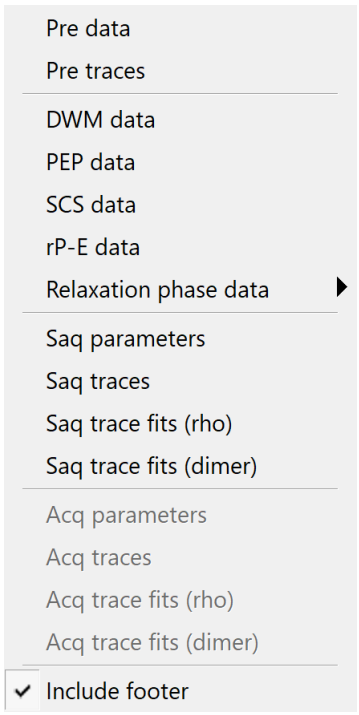

Figure 3.12: The **Clipboard** menu incorporates options for copying data from an open RunSTAF file to the Windows Clipboard.

The Include footer option is active by default. The footer provides a record of the calibration values used to generate the parameter values within the Clipboutput.

See: **Data access: Clipboard functions**

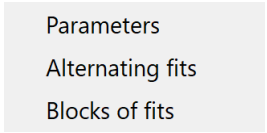

Figure 3.13: The **Relaxation phase data** sub-menu includes the options shown here.

See: **Clipboard → Relaxation phase data**

4 An introduction to the LabSTAF system running in Auto FLC mode

For many users, the most important application of LabSTAF is the fully automated acquisition of consistent FLC data. This section starts with a detailed overview of how to run a LabSTAF system in the standard **Auto FLC** mode.
See: **Auto FLC mode setup**

4.1 Overview of the standard Auto FLC mode

The standard **Auto FLC** mode within RunSTAF incorporates a wide range of features for protocol design. The LabSTAF system includes a range of accessories which can be combined with these features to provide different levels of automation. A high proportion of the accessories provided are included within the setup shown in Figure 4.1.
See: **LabSTAF hardware setup**

Figure 4.1: A compact arrangement of the LabSTAF system. The Power Pack, which provides 24 V DC to the LabSTAF unit and peristaltic pump unit and 15 V to the Surface Go, is located behind and to the left of the LabSTAF. The peristaltic pump and solenoid unit on top of the LabSTAF are plumbed in and connected. The flow-through stir unit is also plumbed in and connected. This plumbing arrangement allows for sample exchange between successive FLCs and programmed cleaning cycles. The LabSTAF unit is plumbed directly to a circulating water bath through the two connectors at the back right of the unit. This circulating system is very effective in maintaining sample temperature without intercepting any of the optical paths.

The first part of this section provides basic descriptions of many of the settings and data parameters that are accessible through the home screen or data plot screen. More detailed descriptions are provided within later parts of this section.

The main objective for this section is to introduce the **STAF setup**, **Data processing** and **FLC setup** sections of RunSTAF by running sequential FLCs using the **Auto FLC** mode. The setup for this introductory run was much simpler than shown in Figure 4.1. 20 mL of MilliQ was placed in the sample chamber and combined with a few drops from a mixture of cultured cells of *Chlorella*

vulgaris and *Anabaena* sp. (both freshwater species). The flow-through stir unit was used to stir the sample but was not plumbed in for sample exchange or system cleaning.

4.2 Booting up into the Auto FLC mode

The screenshot below shows the RunSTAF home screen when the **Auto FLC** acquisition mode is active and before a LabSTAF unit has been attached. Values in teal blue are editable. The values in orange are set by RunSTAF. Yellow text fields are buttons.

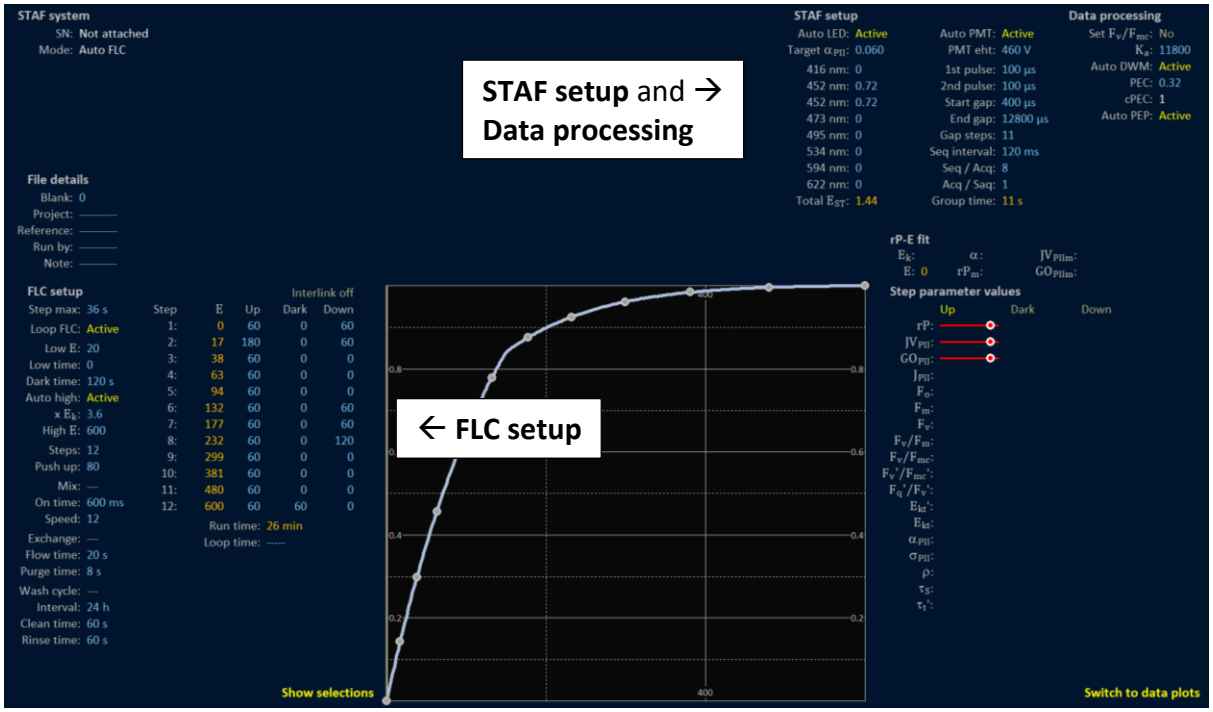

Figure 4.2: Screenshot of RunSTAF in Auto FLC mode before a LabSTAF unit has been attached. The lower left of the screen incorporates the **FLC setup**. The Top right of the screen incorporates the **STAF setup** and parameters for **Data processing**. All default values are shown.

The LabSTAF unit takes around 30 s to boot up and attach to RunSTAF. This is a fully automated process which includes the uploading of stored calibration data from the LabSTAF unit. Figure 4.3 shows the default values for the FLC setup. These values were used for this introductory run.

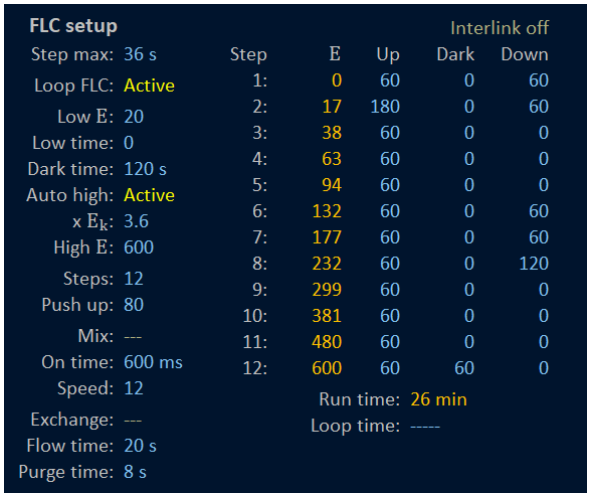

Figure 4.3: This crop from the home screen shows the default options for the **FLC setup**. These settings are suitable for running a sequence of FLCs on a single sample, as is the case here.

4.3 Start and the pre-FLC steps

This section works through the changes that take place at the **STAF system** level between the Acquisition **start** button being pressed and the FLC starting.

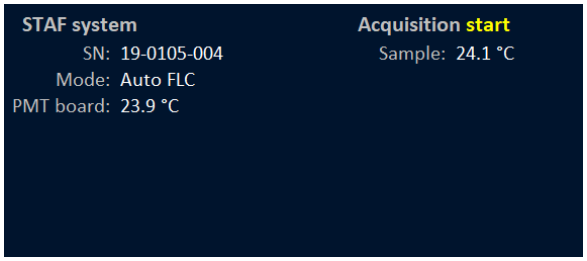

Figure 4.4: The Acquisition **start** button appears once the boot up sequence has completed. The **PMT board** and **Sample** temperatures are updated approximately once a second.

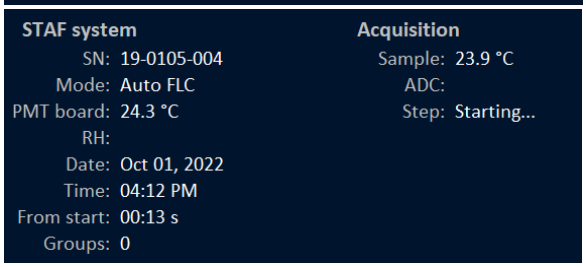

Figure 4.5: Pressing the **start** button triggers the programmed pre-FLC steps and FLC sequence.

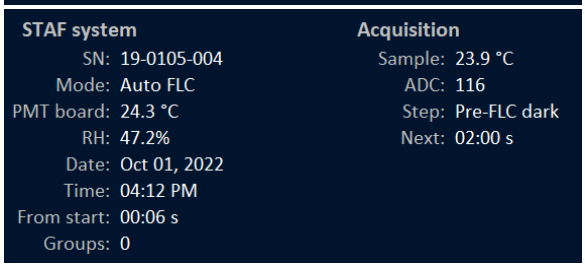

Figure 4.6: The pre-FLC steps within this example excludes a pre-FLC low (light) step but includes a 120 s pre-FLC dark step. Initially, the **ADC** value is over 100, indicating that the PMT eht is set too high. The **Auto PMT** function brings the ADC within range before acquisition starts.

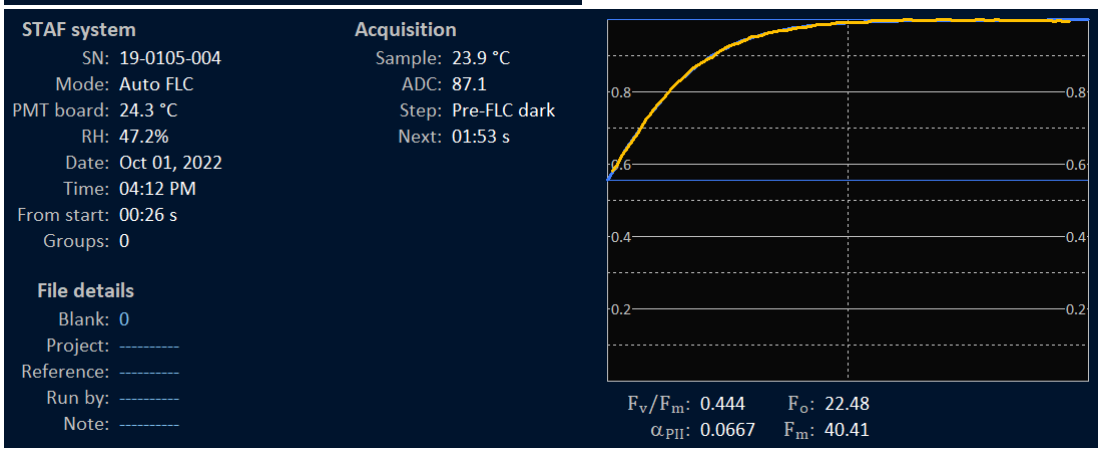

Figure 4.7: The ST curve within this crop from the home screen was recorded during the pre-FLC dark step. The four parameters below the ST curve are derived from the automated RunSTAF curve fit.

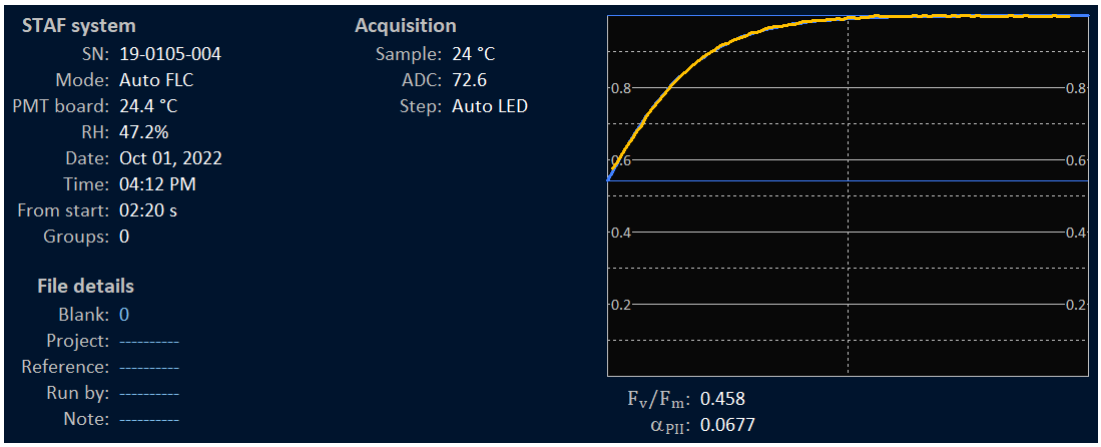

Figure 4.8: Once the pre-FLC dark step has completed, RunSTAF implements the **Auto LED** function.

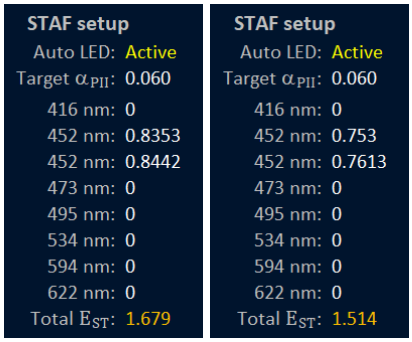

Figure 4.9: The pre-**Auto LED** values are shown left, the post-**Auto LED** values are shown right. Because the **Auto LED** step is run after the pre-FLC **Low** and **Dark** steps, the α_{PII} value during these earlier steps may deviate significantly from the **Target** α_{PII}**.** For example, the α_{PII} in Figure 4.8 (before the Auto LED correction has been applied) is more than 10% above the target value, at 0.0667. After the Auto LED correction, the α_{PII} dropped to 0.0599.

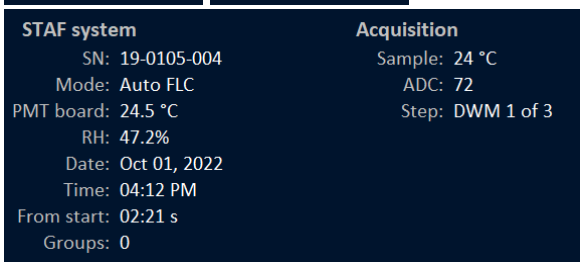

Figure 4.10: Once the Auto LED step has completed, the **Auto DWC** step runs to generate a correction for the package effect. The DWM step always runs through three reps.
See: **Applying the Package Effect Correction (PEC)**

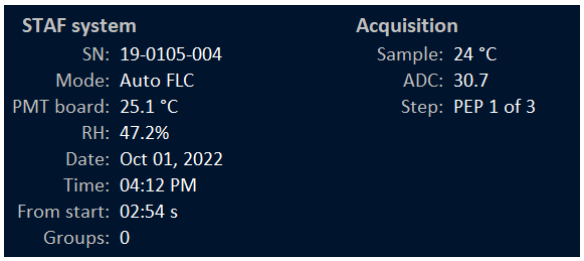

Figure 4.11: The **Auto PEP** step runs immediately after the **Auto DWC** step. This step also incorporates a sequence of three reps.

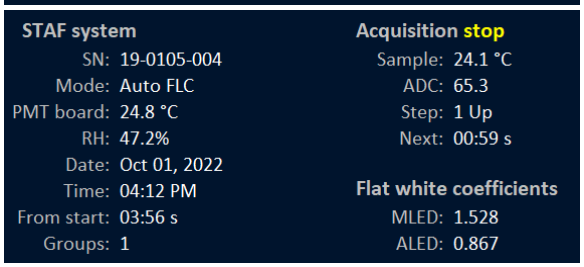

Figure 4.12: Once the **Auto PEP** step has completed, the FLC starts. At this point, the **stop** button and **Flat white coefficients** appear on the home screen.

4.3.1 Pre-FLC changes in STAF setup

This section works through the changes that take place at the **STAF setup** level between the Acquisition **start** button being pressed and the FLC starting.

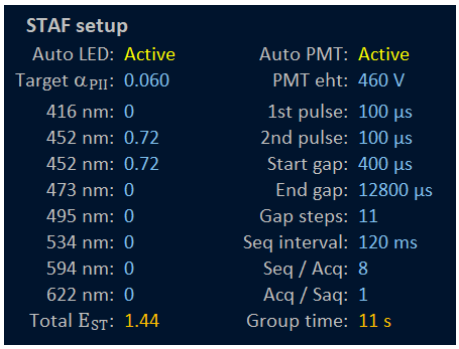

Figure 4.13: Before the LabSTAF unit is attached, the default MLED values are as shown here. The default settings include the dual ST pulse function with **100 µs** pulses and **11 Gap steps** between **400 µs** and **12800 µs**.

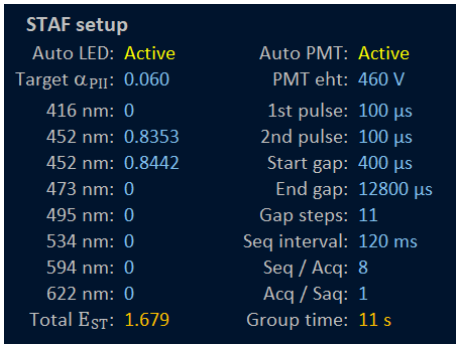

Figure 4.14: Once the LabSTAF unit has attached, the default MLED drive current for both of the **452 nm** channels is set at 360 mA. The E_{ST} values at this drive current are calculated from the calibration data stored within the LabSTAF unit. All values in blue can be edited by the user at this point. Changed values are saved and applied the next time a LabSTAF unit is attached.

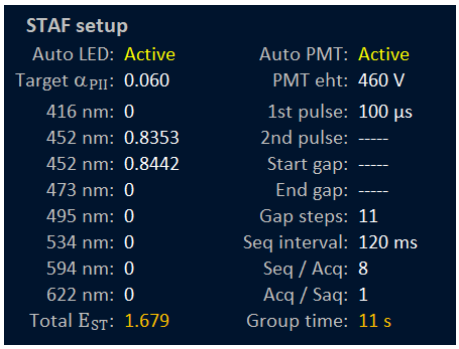

Figure 4.15: For all pre-FLC steps, the **2nd pulse** is turned off. All blue fields are changed to white to show that they can't be edited by the user from this point on.

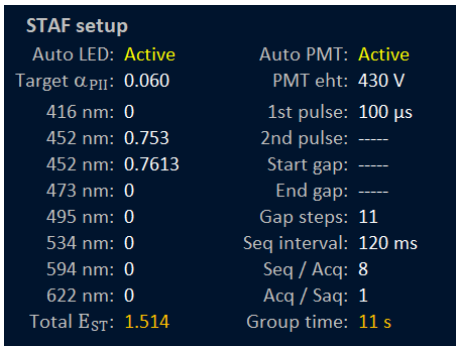

Figure 4.16: The **Auto LED** function adjusts the intensity of the MLED channels to try and achieve the **Target** α_{PII} value. The optimised E_{ST} values are used for the **Auto DWC** step.
See: **Applying the Package Effect Correction (PEC)**

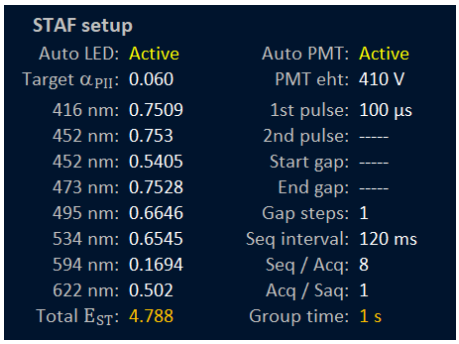

Figure 4.17: During the **Auto PEP** step, the E_{ST} values for all eight channels are based on the MLED values set by the **Auto LED** function.
See: **Spectral correction**

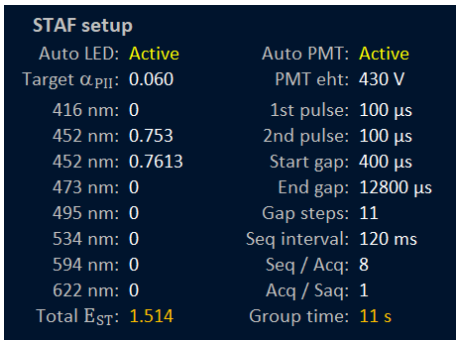

Figure 4.18: Once the **Auto PEP** step has completed, the second ST pulse is set back to its original value and the E_{ST} values are reset to the MLED values generated by the **Auto LED** function. These values are maintained while the FLC is run.

4.4 Viewing the PEP and SCS

The Photochemical Excitation Profile (PEP) is central to the application of spectral correction of STAF data. If the PEP is absent from a RunSTAF data file, values for spectrally dependent parameters are not calculated. Construction of the Spectral Correction Spectra (SCS) is dependent on RunSTAF having access to the LabSTAF unit-specific SCS file generated as part of the calibration process. RunSTAF includes functions to allow for the import of PEP data from a separate file.
See: **PEP update**

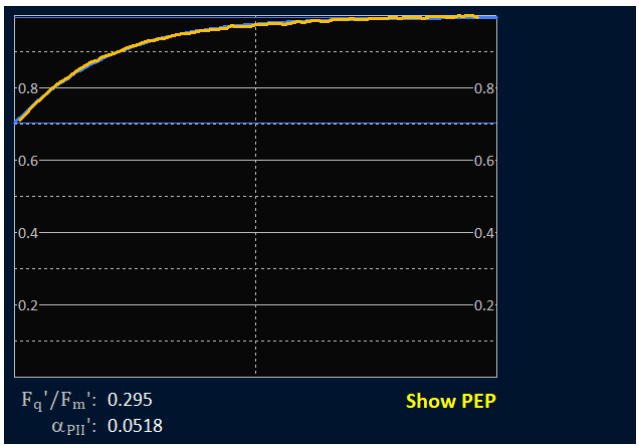

Figure 4.19: Once the **Auto PEP** step has completed and normal acquisition has started, it is possible to view the PEP on the home screen by pressing the **Show PEP** button below the ST pulse.

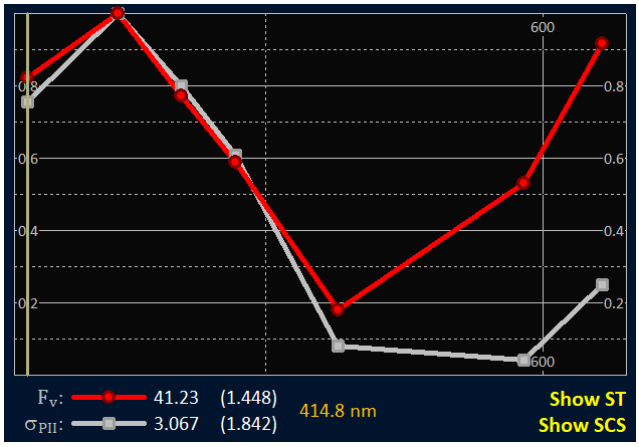

Figure 4.20: The PEP view shows normalized plots of the F_v PEP and σ_{PII} PEP data. The actual values for the selected point are shown next to the key bars below the plots. Note the sizeable gap between the F_v and σ_{PII} values at the red end of the PEP spectrum (the 496 nm and 622 nm points).
See: **Working with Photochemical Excitation Profiles (PEPs)**

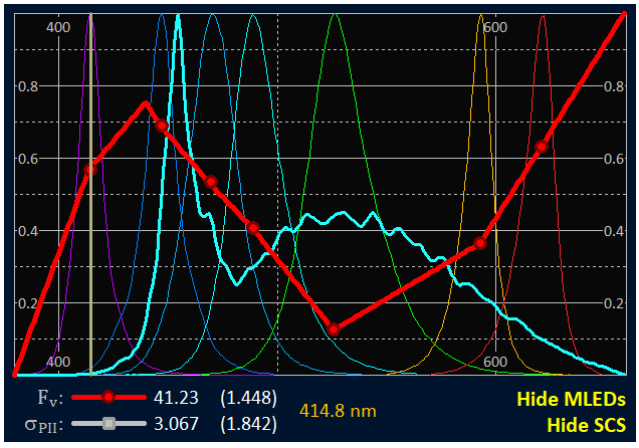

Figure 4.21: The Spectral Correction Spectra (**SCS**) view shows an extended F_v PEP (the bright red line) plus the emission spectrum of the ALED incorporated within LabSTAF (the bright blue line). This view includes an option to also show the emission spectra of the seven MLED wavebands within LabSTAF.
See: **Spectral correction**

4.5 The FLC steps

Once the Pre-FLC functions have completed, RunSTAF runs through the FLC steps. Figure 4.22 shows the actinic photon irradiance (**E**) values at each step for this example.

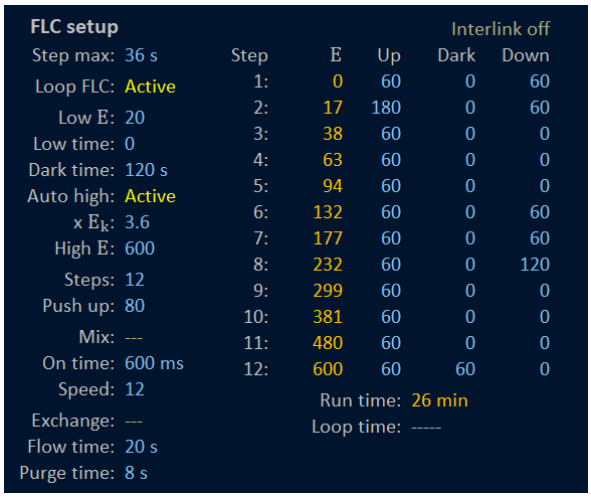

Figure 4.22: The FLC steps used for the example described below. The **High E** value (at step 12) is set to the default of **600** µmol photons m^{-2} s^{-1}. All step times are the default values.

The FLC runs through the **Up** column from **1** to **12**. If a non-zero time is set within the **Dark** column at any step, it is run after the **Up** at the same step before moving to the next **E**. With the default setup, the only non-zero **Dark** time is at step **12**. This is run immediately after **Up 12**. The **Down** column then runs from **12** to **1**. The default setup includes five non-zero values within the **Down** column.

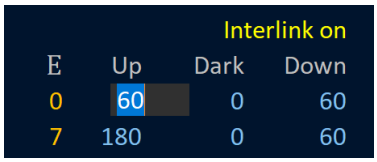

Figure 4.23: When the Interlink button is active, changing one step value will change all identical values in the same column to the new value. For example, changing the **Up 1** value from **60** to **90** would also change **Up 3** through **Up 12** to 90 but leave **Up 2** unchanged at **180**.

Figure 4.24 shows the ST pulse from the most recent (live) Gaq. In this example, the Gaq was acquired during **Up 2**. As with the ST curves generated during the pre-FLC steps, RunSTAF has applied a curve fit to the raw data values. This fit generates the values of F_v/F_m and α_{PII} shown below the curve. The **Next** field shows the minimum remaining time for this step. Once this time has counted down to zero, the current Gaq will complete before the next Step is started. While data are being acquired, this window on the home screen always shows the most recent Gaq-level ST curve.

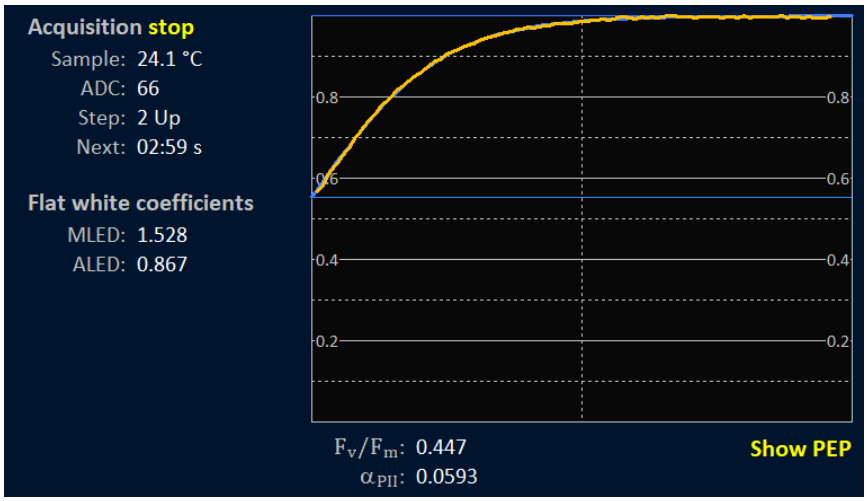

Figure 4.24: Crop from the home screen showing the most recent Gaq-level ST curve, acquired during **Up 2** of the FLC.

4.6 The Step parameters plot window

The options for plotting data within the rP-E plot become visible on the home screen when the **Show selections** button is pressed (Figure 4.25).

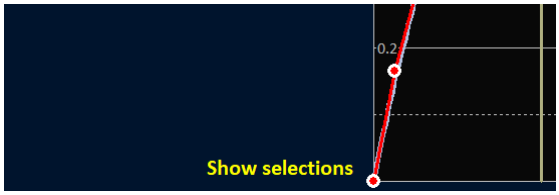

Figure 4.25: Crop of the home screen showing the **Show selections** button, to the lower-left of the plot window.

Figure 4.26 shows the default **Step data selections** and the selections made for this test run.

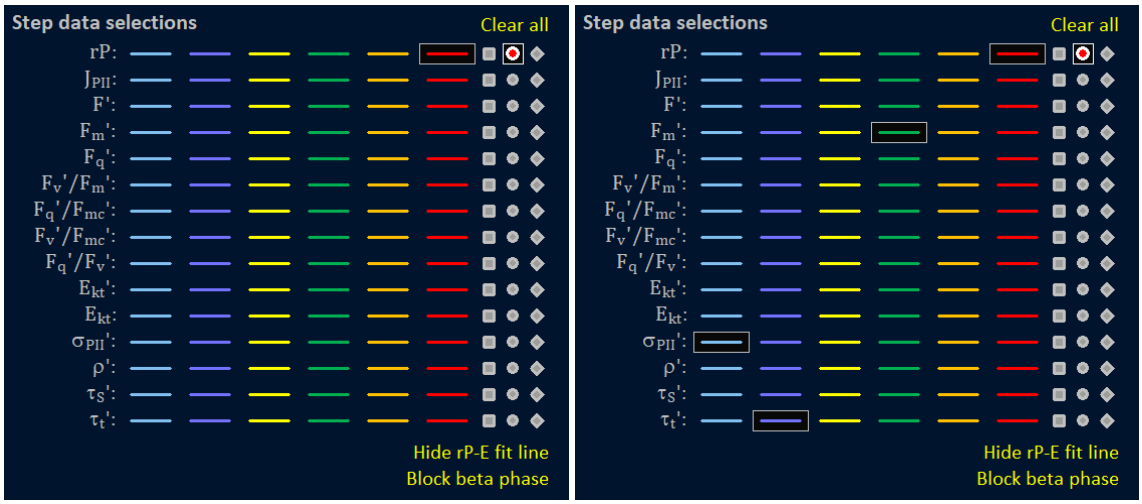

Figure 4.26: Crops from the home screen with the **Show selections** option active. The left panel shows the default selections, the right panel shows the selections used during this test run. The light-adapted version of each parameter is shown.

Figure 4.27 shows the Step parameters plot with the FLC at **Up 6** (E = 132 µmol photons m^{-2} s^{-1}).

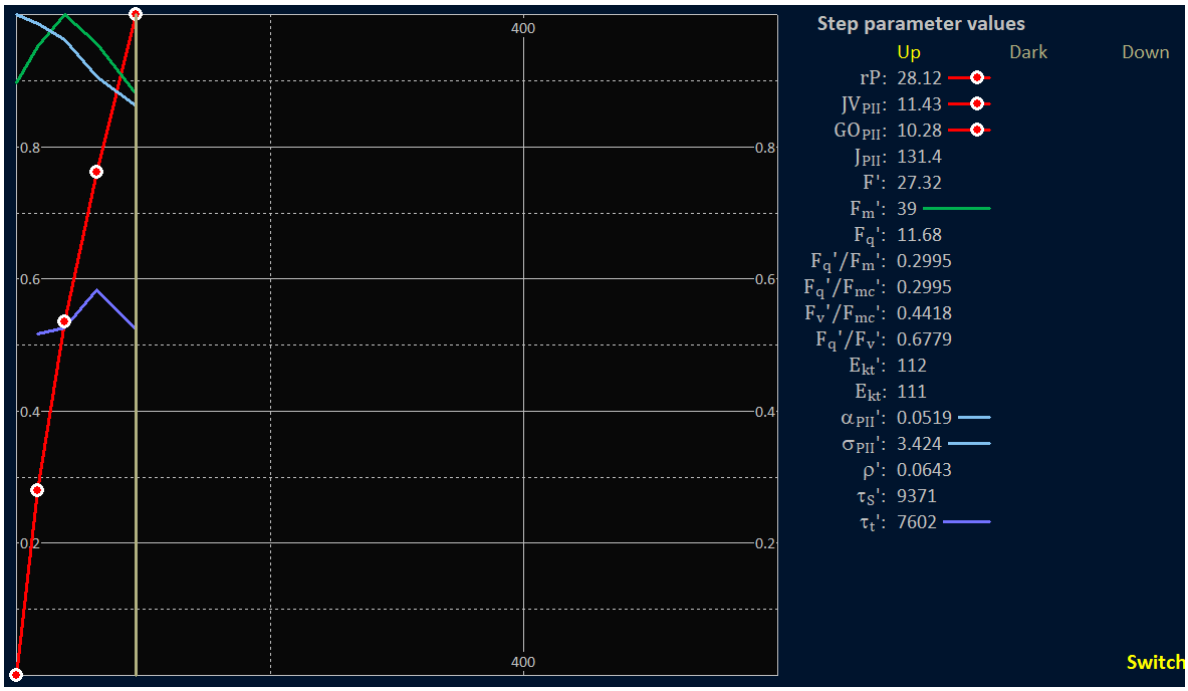

Figure 4.27: Crop from the home screen showing the Step parameter plot with **Up 6** selected.

Because **Up 6** is still running, the values shown are from **Up 5** (the last completed step, at 94 µmol photons m^{-2} s^{-1}). The **rP**, JV_{PII} and GO_{PII} values are all plotted with the same line. This is because the JV_{PII} and GO_{PI} values are scaled directly from the **rP** values, such that the **rP**, JV_{PII} and GO_{PII} P-E curves are the same shape.

See: [Generating values of J_{PII} and JV_{PII}]

4.7 The rP-E curve fit

The curve fitting algorithm within RunSTAF normally generates the first fit to the rP data to generate an rP-E curve after **Up 6** has completed (i.e. at the start of **Up 7**). Figure 4.28 shows the plot at this stage. The curve fit value of E_k at this point is 104 µmol photons m^{-2} s^{-1}.

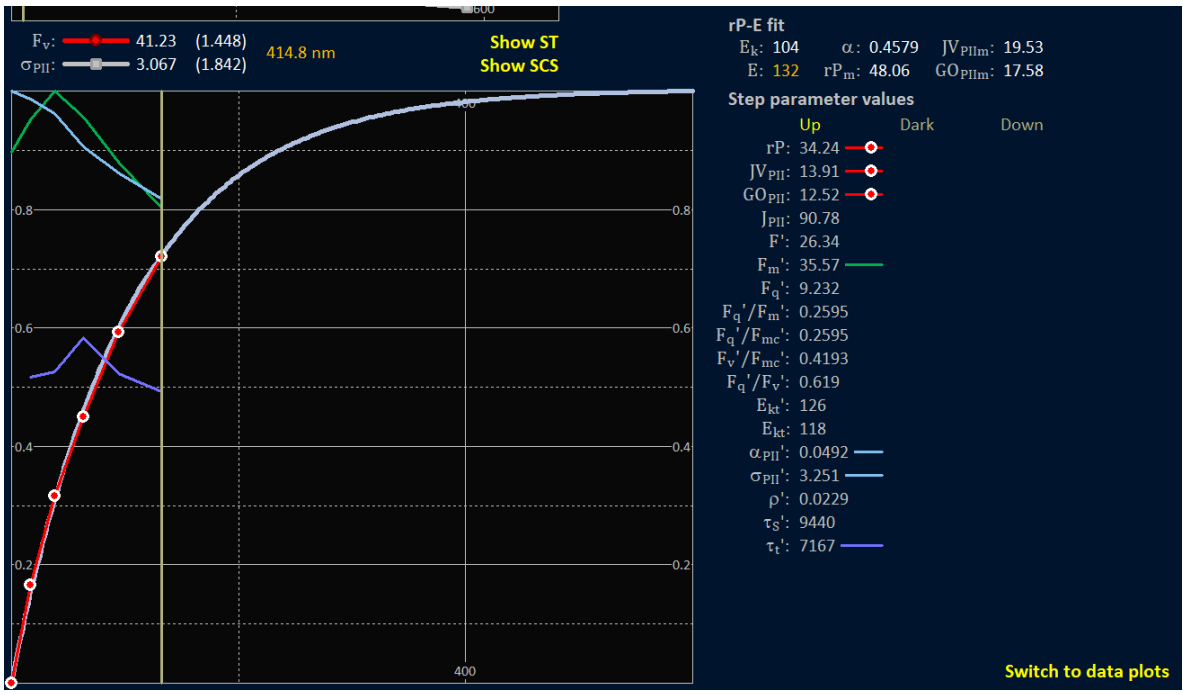

Figure 4.28: The Step parameter window at **Up 7**.

RunSTAF refits the rP-E curve after each Gaq is completed and added and the Step parameter values are updated. Figure 4.29 shows the fit during **Up 10** (after **Up 9** has completed). The E_k is now 110 µmol photons m^{-2} s^{-1}.

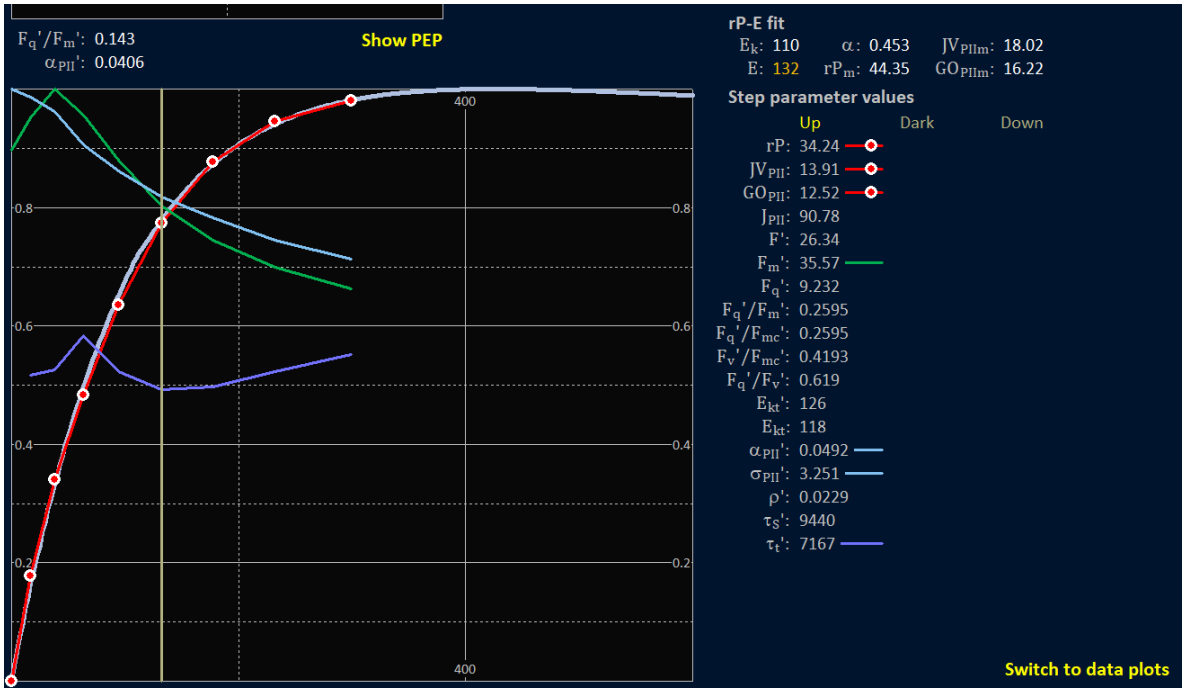

Figure 4.29: The Step parameter window at **Up 10**.

The FLC protocol used for this example includes five Down steps at locations **8**, **7**, **6**, **2** and **1**. The aim of the Down steps is to track the reversal of downregulation that may have formed during the Up

phase. The Down steps are positioned around E_k as this is where downregulation usually starts. Figure 4.30 shows the Step parameter window with **Down 2** selected. Overall, these data are consistent with downregulation having not completely reversed during the Down phase of the FLC.

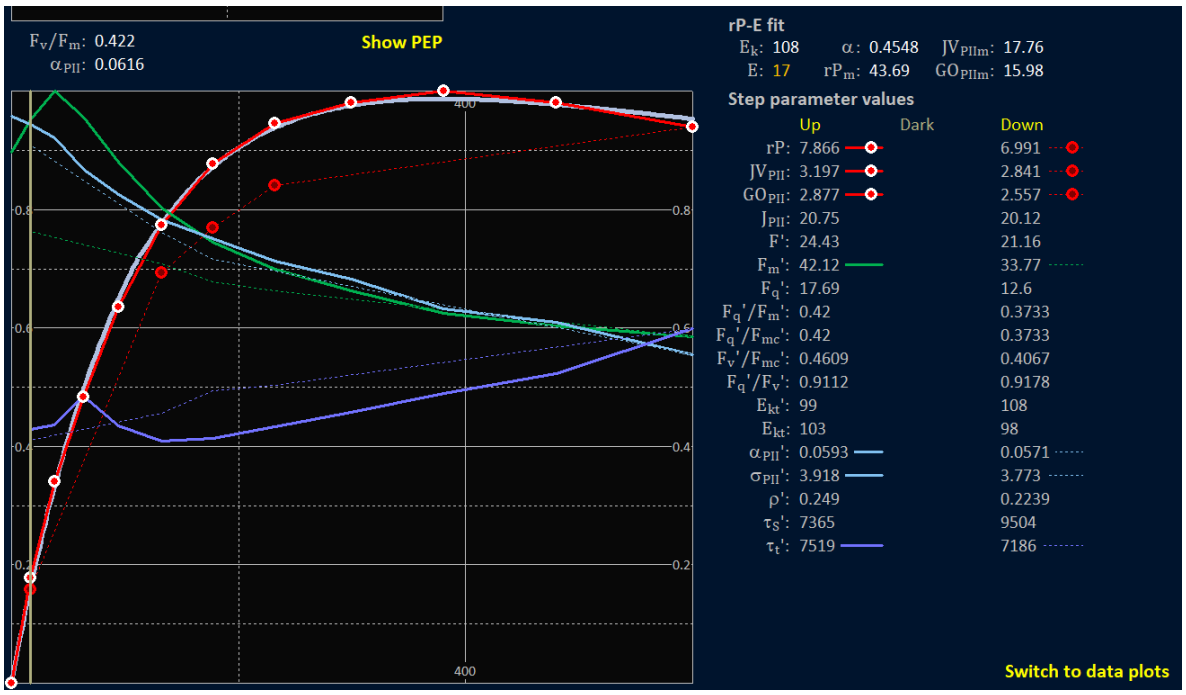

Figure 4.30: The Step parameter window at **Down 1**.

4.8 The data plots view

Pressing the **Switch to data plots** button at bottom right on the home screen switches to the data plot screen. Figure 4.31 shows the initial data plot screen for this example.

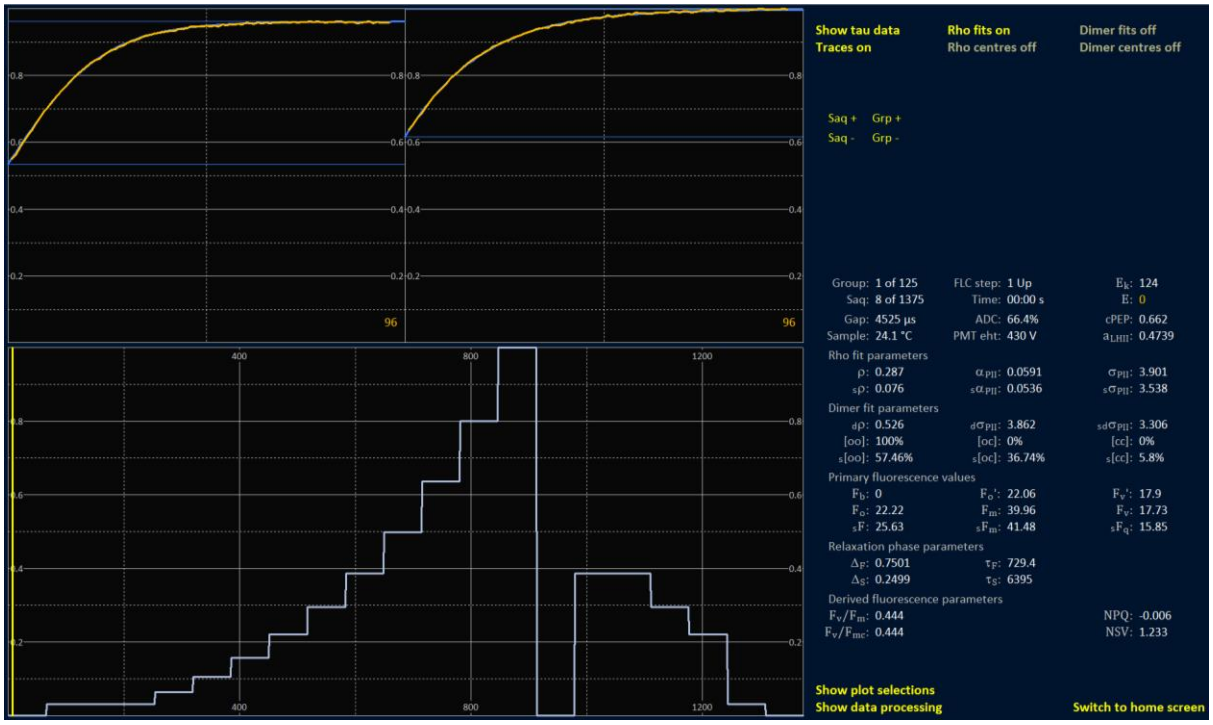

Figure 4.31: The initial view of the data screen for this example.

In Figure 4.31, the first Saq in the file is selected by default and the Dual ST Pulse (DSP) sequence for this Saq is showing in the top part of the screen. By default, there are no STAF data plotted within

the lower panel. The one line always showing in the lower panel is photon irradiance (E). In Figure 4.31, the FLC has completed and the photon irradiance line tracks the entire Up and Down phases, separated by the Dark step between the end of the Up phase and the start of the Down phase. The x-axis for the lower plot is Saq index, rather than time.

Pressing the **Show plot selections** button (to the right of the lower panel) replaces the DSP sequence with the options for plotting STAF parameters, organised within groups (Figure 4.32). A high proportion of these parameters have different terms for the dark-adapted and light-adapted versions. In these cases, the dark-adapted term is shown.
See: **Glossary of terms**

Figure 4.32: The data plot screen with the plot selections showing.

Each of the plot selection parameters has six pen options, plus a dashed line. Selecting and deselecting a pen is achieved using the left mouse button. If the dashed line is also selected, the pen switches from a solid line to a dashed line of the same colour. A single pen colour can be used for more than one parameter and there is no specified limit to the number of lines that can be plotted simultaneously.

Figure 4.33 shows red pen selections for plotting σ_{PII} and $s\sigma_{PII}$ (the absorption cross section of PSII photochemistry from the first and second ST pulses in a DSP sequence, respectively) under **Rho fit parameters**. The $s\sigma_{PII}$ line has been switched from solid to dashed. Under **Primary fluorescence values**, the green pen has been selected to plot values of F_m. Under **Relaxation phase parameters**, the purple pen has been selected to plot values of τ_t'. Finally, the yellow pen has been selected to plot values of JV_{PII} under **Derived fluorescence parameters**. The selected lines are plotted against each of the selected parameters in the list of values for the selected Saq, to the right of the data plot.

Figure 4.33: The data plot screen with a number of parameters selected.

Pressing the **Hide plot selections** button replaces the plot selections with the dual ST pulse sequence for the currently selected Saq. In Figure 4.34, the **Dimer fits** and **Dimer centres** options (top right of the screen) have both been selected for the dual ST pulse plot. The cursor in the data plot has been moved to select Saq **444 of 1175** and the cursor in the upper panel has selected the **50 µs** point within the second ST pulse. Because Saq 444 is a light-adapted acquisition, all of the terms shown to the right of the data plot have changed from the dark-adapted form (shown in Figure 4.33) to the light-adapted form. In addition, the light-adapted parameters with no dark-adapted equivalent (such as $\mathbf{JV_{PII}}$) are now showing.

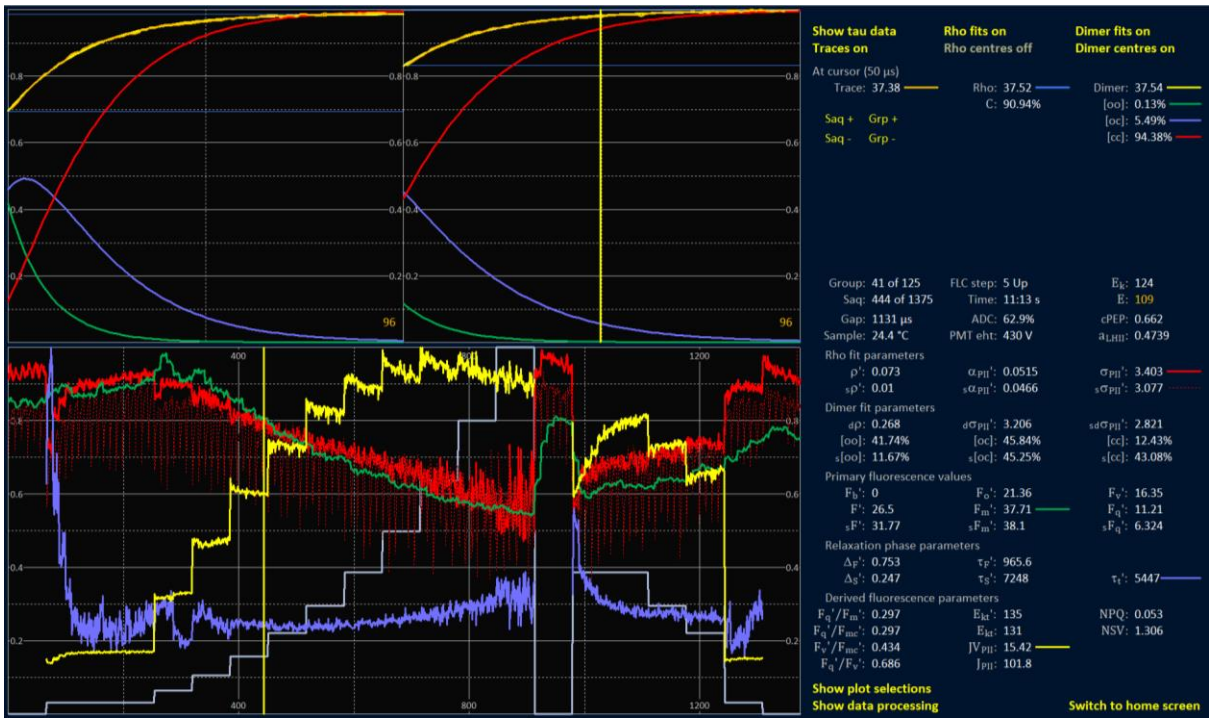

Figure 4.34: The data plot screen with a light-adapted Saq selected and the Dimer fits showing.

4.8.1 The relaxation phase traces (tau data)

Figures 4.35 and 4.36 show two selections from the data plot with the **Show tau data** option active. The selection within Figure 4.35 is the very first (dark-adapted) Saq within the file. The selection within Figure 4.35 is light-adapted at 109 µmol photons m^{-2} s^{-1}. It is perfectly normal for the three relaxation phase fits (**Fv**, **Rho** and **Dimer**) to be highly separated in the dark-adapted state and to be much closer to each other in the light-adapted state, as seen here.

See: **The relaxation phase (tau) fit**

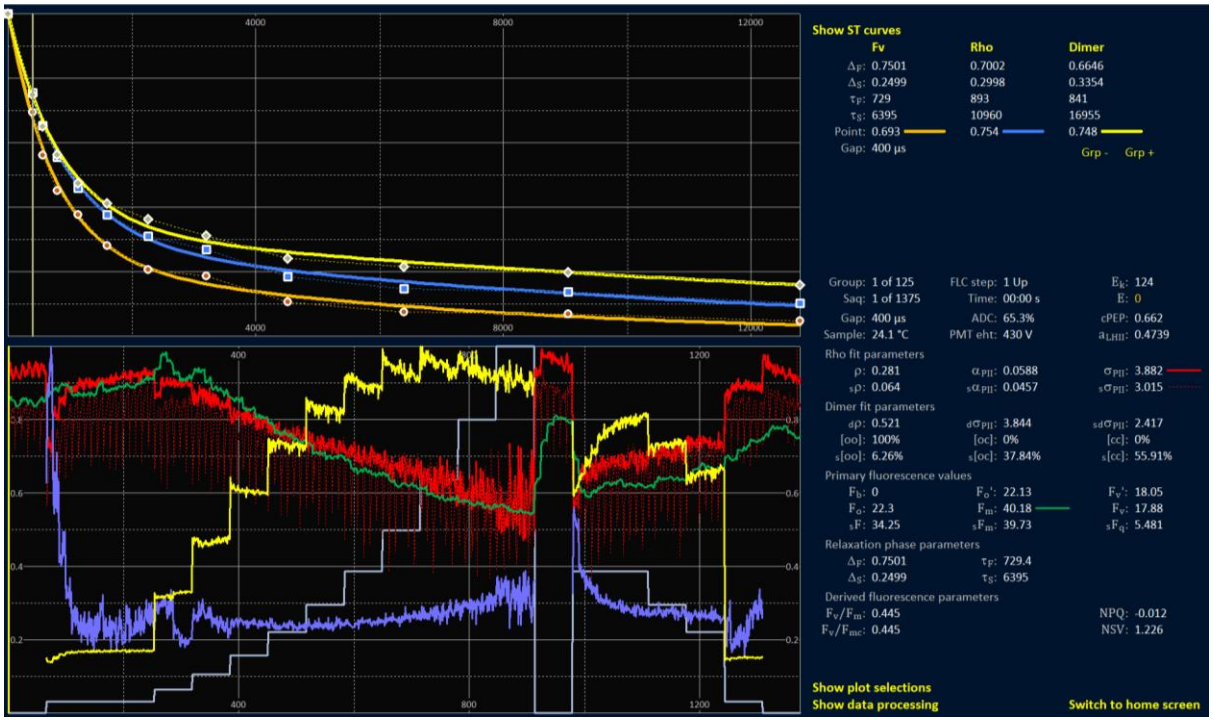

Figure 4.35: Saq 1 selected with the **Show tau data** option active.

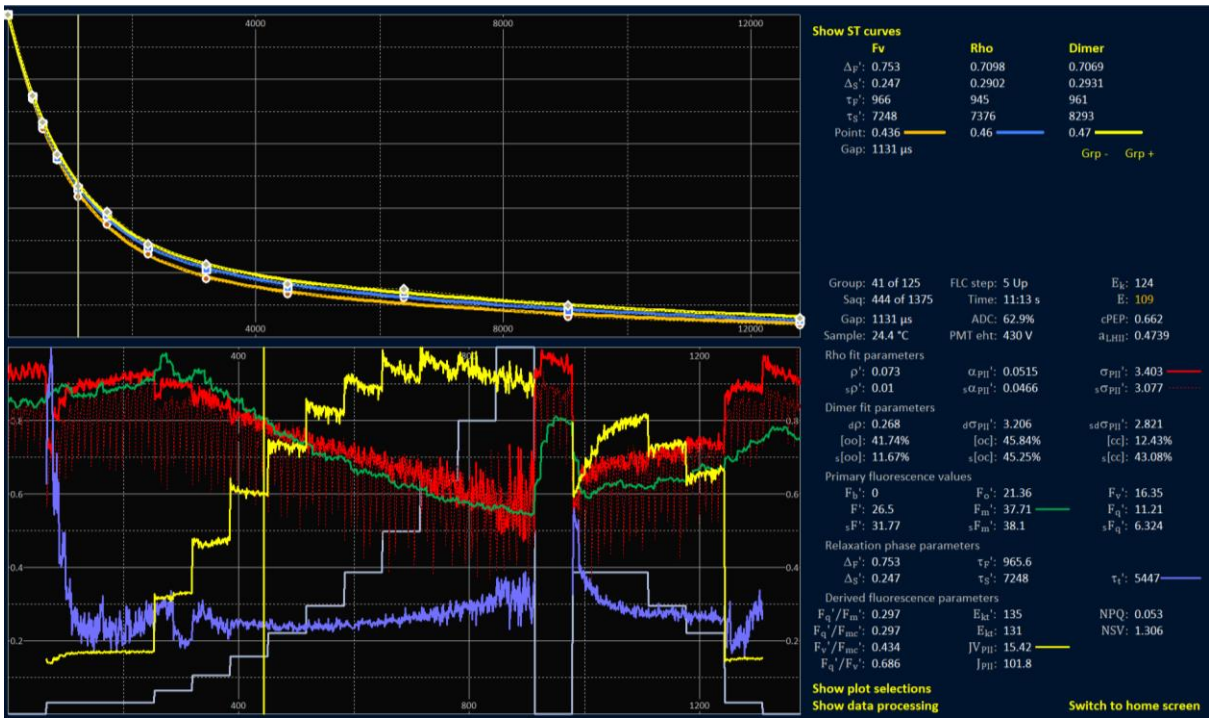

Figure 4.36: Saq 444 selected with the **Show tau data** option active.

5 STAF setup and Data processing

All functions within **STAF setup** and **Data processing** are available for both the Auto FLC and Manual modes. This section provides an overview of the individual functions.

5.1 The STAF setup section

Figures 5.1 to 5.7 are crops from the home screen at different stages of the automated STAF setup process. All settings in the left column of **STAF setup** are for the MLEDs. The editable E_{ST} value for each of the eight MLED channels is the photon flux delivered to the interrogated volume by each LED channel with units of photons nm^{-2} (100 µs) $^{-1}$. The **Total E_{ST}** field provides the sum of values from all active channels. To provide a guide, 1.0 photons nm^{-2} (100 µs)$^{-1}$ is the equivalent of 16 603 µmol photons m^{-2} s^{-1}.

If **Auto LED** is **Active**, the **Set α_{PII}** value provides the target initial slope of RCII closure during the first ST pulse. The value of **0.06** in Figure 5.1 is equivalent to 6% of the RCII population in the open state at $t = 0$ being closed at $t = 1$ µs. The **Auto LED** function adjusts the photon flux from MLEDs that are set to a non-zero E_{ST} value to try and achieve the **Target α_{PII}** value. LED channels set to zero by the user are left unchanged. The **Auto LED** function will always run if the **Auto DWM** or **Auto PEP** is **Active**, even if it is not set as **Active**.

The top two settings in the right column of **STAF setup** set the **Auto PMT** function and the starting **PMT eht**. The **Auto PMT** function is set to **Active** every time RunSTAF is started.

Below the PMT settings are the **1st Pulse**, **2nd Pulse**, **Start gap**, **End gap** and **Gap steps** fields. The default ST pulse duration is 100 µs for both pulses. The gap settings collectively define the sequence of gaps between the end of the first pulse and the start of the second pulse. The first and last gaps are always as set. RunSTAF fills in the intermediate values such that the increase between successive gap lengths is always by the same factor. For example, the default gap sequence (as shown in the above example) is 400, 566, 800, 1131, 1600, 2263, 3200, 4525, 6400, 9051 and 12800 µs. The relaxation phase analysis is based on the recovery of variable fluorescence between the first and second ST pulses.

See: **The relaxation phase (tau) fit**

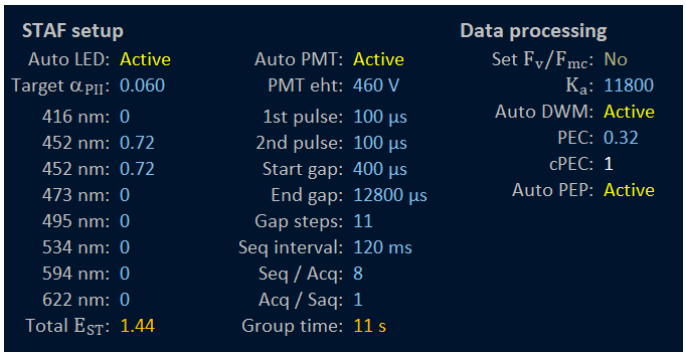

Figure 5.1: This crop from the home screen shows the default options. At this point, a LabSTAF unit has not attached.

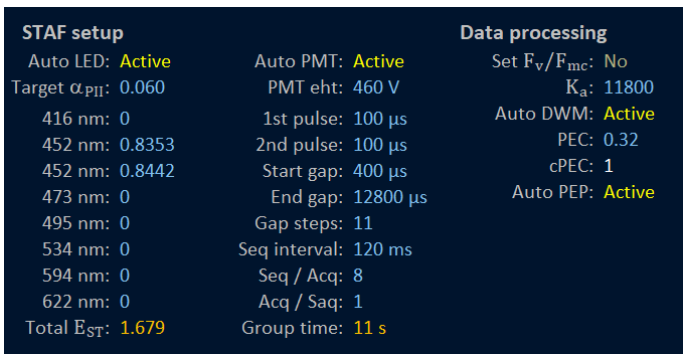

Figure 5.2: Once the LabSTAF unit has attached, the default MLED drive current for both of the 452 nm channels is set at 360 mA. The reported E_{ST} values are calculated from the calibration data stored within the LabSTAF unit.

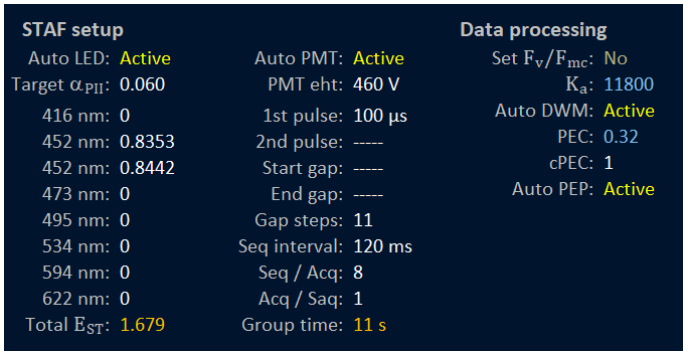

Figure 5.3: The first step within the automated setup is **Auto LED**. Before this step starts, the **2nd pulse**, **Start gap** and **End gap** values are deactivated. They remain inactive until the **Auto DWM** and **Auto PEP** steps have completed.

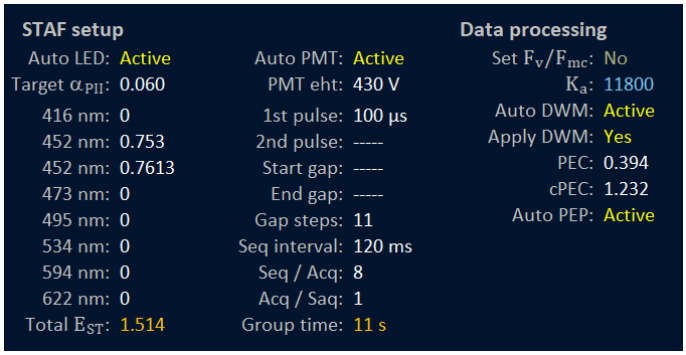

Figure 5.4: In this crop, the **Auto LED** step has completed, and the **452 nm** E_{ST} values have been adjusted to provide the **Target** α_{PII}. The **Auto DWM** function has also completed and the DWM-derived values for the **PEC** and **cPEC** have been set.

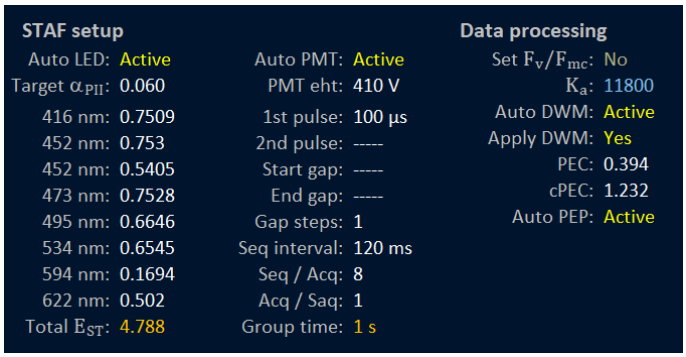

Figure 5.5: The E_{ST} values for all eight channels have been optimised for the PEP. Because the **452 nm** channels were the only ones set with a non-zero E_{ST} in Figure 5.4, the optimisation set is for PEP-bc.
See: The PEP protocols

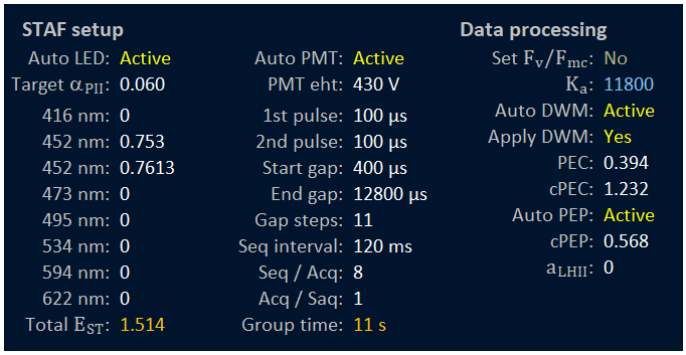

Figure 5.6: In this crop, the **Auto PEP** function has completed and a cPEP value has been set. The **2nd pulse**, **Start gap** and **End gap** fields have been reactivated and acquisition has started. At this point, there are no suitable data available to derive a value for a_{LHII}.

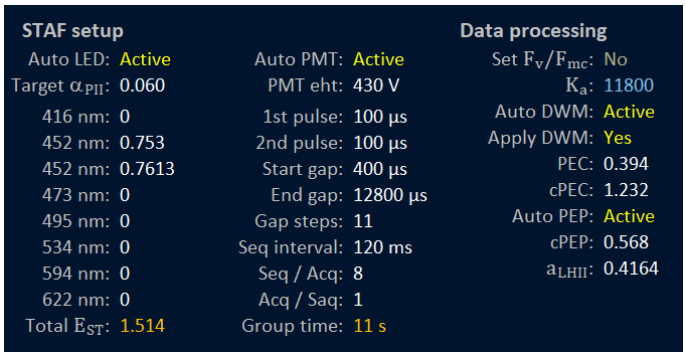

Figure 5.7: By this point, a number of dark Gaqs have completed and a value for a_{LHII} has been generated.

5.2 The Data processing section

Changes made within the Data processing section are immediately applied. The sample crops from the home screen shown within this subsection are from a saved file. Sample crops taken during acquisition are shown in the previous subsection.

5.2.1 Baseline fluorescence (F_b)

As noted elsewhere in this document, the fraction of F_o that does not originate from photochemically active PSII complexes is termed baseline fluorescence and is quantified as F_b. Baseline fluorescence introduces an error into the calculation of a number of fluorescence parameters, including a_{LHII} and JV_{PII}. RunSTAF includes a number of features that can be used to assess F_b. The Data processing section can be used to apply an appropriate correction, using the Set F_v/F_{mc} button and associated Value field (Figure 5.8).

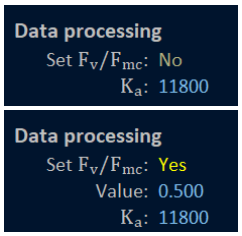

Figure 5.8: The **Set F_v/F_{mc}** option is set to **No** by default (upper crop). When set to **Yes** (lower crop) the **Value** field is used to set the set an assumed intrinsic value of F_v/F_m for photochemically active PSII complexes within the sample. If the value of F_v/F_m measured from the sample is higher than the set value, the set value is increased to the measured F_v/F_m.
See: **Derivation of F_b and F_{oc}'**

5.2.2 Package Effect Correction (PEC)

The PEC value can be the one generated by running the DWM or the one manually set by the user. Both options are shown within Figure 5.9.
See: **Applying the Package effect correction (PEC)**

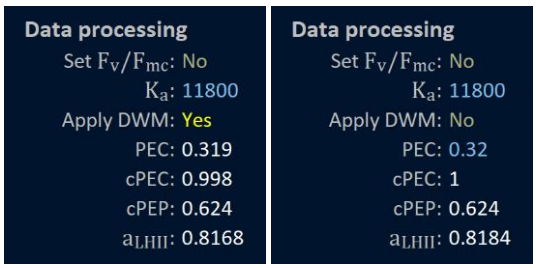

Figure 5.9: When **Apply DWM** is set to the default of **Yes** (left crop), the value for the Package Effect Correction (**PEC**) used is the one generated by running the automated Dual Waveband Measurement (DWM) step. When **Apply DWM** is set to **No** (right crop), the **PEC** field becomes editable. The default value is 0.32, as shown within this example.

5.2.3 The K_a constant

The K_a constant (the top field within Figure 5.10) can be set by the user. Calculated values of a_{LHII}, JV_{PII} and GO_{PII} are in direct proportion to the set value of $\mathbf{K_a}$. All Clipboard and csv functions that incorporate calculated values of JV_{PII} and GO_{PII} include a record of the applied value of $\mathbf{K_a}$. Values of a_{LHII}, JV_{PII} and GO_{PII} are not calculated unless a PEP is acquired using the **Auto PEP** function.
See: **Spectral correction**

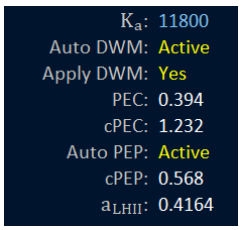

Figure 5.10: The $\mathbf{K_a}$ value can be set by the user at any point. An updated value is immediately applied to the calculation of a_{LHII}, JV_{PII} and GO_{PII}.

6 The home screen settings

This section provides a description of the settings available through the home screen within each of the acquisition modes.

6.1 Auto FLC mode setup

The Auto FLC mode is set by selecting **Settings → Acquisition mode → Auto FLC**

Figure 6.1 shows the **FLC setup** section of the home screen with all defaults set. The right side of the FLC setup shows the **E** values in orange, with units of µmol photons m^{-2} s^{-1}. These values are generated by the **High E**, **Steps** and **Push up** values entered in the left column. The set times for each steps (blue text) are seconds.

Most steps within the **Up**, **Dark** and **Down** columns can be skipped by setting the time to zero. The one exception is **Up 1**, which has a minimum value of **10** (seconds).

When the **Interlink off** button immediately above the **Dark** and **Down** labels is changed to **Interlink on**, changing the set time for one step will change all steps of the same value within the same column. For example, changing **Up 1** from **60** to **90** will also change **Up 4** through **Up 12** to **90** but will leave **Up 2** at **180**.

The FLC sequence starts by running through the **Up** column. A non-zero **Dark** period is implemented after the **Up** value at the same **Step**. The **Down** column is run in reverse order after the **Up** column and non-zero **Dark** values have all been implemented. The rP-E curve fit is applied to the **Up** data set.

In addition to the FLC steps, the **Run time** value includes the **Low time**, **Dark time**, **Auto DWM** and **Auto PEP** procedures.
See: **The Low E, Low time and Dark time fields** and **The data processing section**

The **Loop time** can be used to delay the start of the next FLC when **Loop FLC** is active.
See: **Loop FLC**

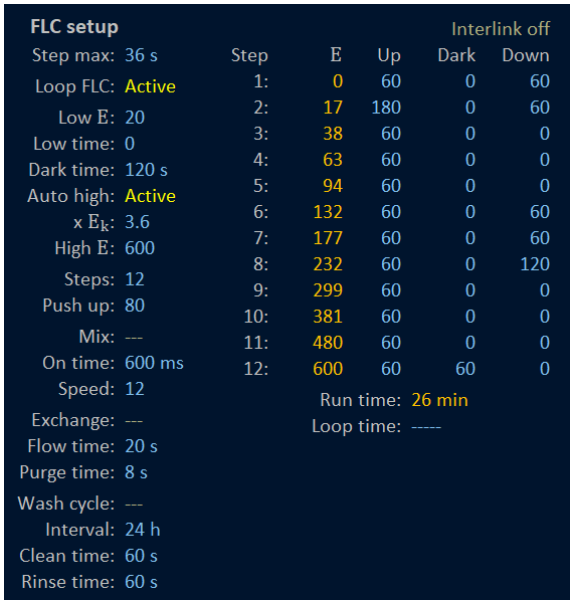

Figure 6.1: Screen crop from the home screen while the Auto FLC acquisition mode is active and all defaults values are set.

Figure 6.2 shows the order in which the programmable steps available while in Auto FLC mode are implemented. The starting point is the **Low time** (at the set value for **Low E**) followed by the **Dark time**. The **Low** step allows for reversal of downregulation. The **Dark** step allows for dark adaptation.
See: **The Stern-Volmer relationship, NPQ and NSV**

Running the **Low** and **Dark** steps first allows for the **Auto LED**, **Auto DWM** and **Auto PEP** steps to be run on a dark adapted sample.

If the Dual Single Turnover Pulse (DSP) sequence is set, it is not implemented until after the Auto PEP function has completed.

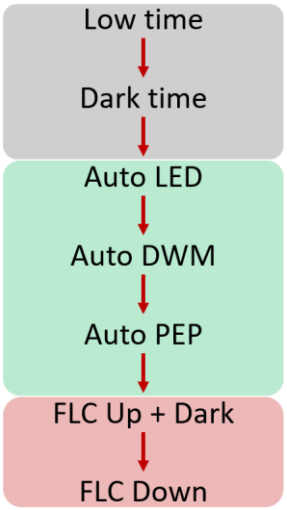

Figure 6.2: The order of implementation for the programmable steps available while in Auto FLC mode. The Auto PMT works continuously alongside these functions, to ensure that recorded ST data are always within the dynamic range of the PMT.

Table 1 provides a brief description of each element within the FLC setup. A more detailed description of each of the functions is provided in the following subsections.

Element	Definition
Step max:	defines how many Gaqs are used to define rP-E step data values
Loop FLC:	starts a new FLC after each FLC completes, when active
Low E:	photon irradiance for a pre-FLC low (light) step (µmol photons m^{-2} s^{-1})
Low time:	time at the Low E photon irradiance (seconds)
Dark time:	time in the dark after the Pre-FLC low (light) step (seconds)
Auto high:	optimises the **High E** value between successive FLCs when active
x E_k:	a factor used to generate the **High E** value when **Auto set** is active
High E:	highest actinic photon irradiance for the FLC (µmol photons m^{-2} s^{-1})
Steps:	number of steps for the FLC
Push up:	rate at which the photon irradiance increases between zero and **High E**
Mix:	injects air between FLC steps when active (flow-through unit required)
On time:	on time for the **Mix** (seconds)
Speed:	pump speed during the **Mix**
Exchange:	runs a sample exchange cycle when active
Flow time:	from the sample reservoir during an active **Exchange** cycle (seconds)
Purge time:	sample reservoir tube is cleared during and active **Exchange** cycle (seconds)
Wash cycle:	runs the programmed wash cycle when active
Interval:	time between successive wash cycles (hours)
Clean time:	using the cleaning fluid connected to the NO port of solenoid valve C (seconds)
Rinse time:	using the cleaning fluid connected to the NC port of solenoid valve C (seconds)

Table 6.1: Brief descriptions of all elements of the left column of **FLC setup**.

6.1.1 The Step max function

The **rP-E fit and step data** values are averages of values extracted from the last Gaqs at each **FLC Step**. The value of **Step max** defines how many Gaqs are used to generate each reported value. For example, if the **Group time** (shown under **STAF setup** on the home screen) is 11 s and the Step max value is 36 s, the last three Gaqs at each step will be included. Increasing the **Step max** value to 44 s would result in the last four Gaqs being included. By excluding the first Gaqs at each step, the calculated parameter values are usually pushed towards steady state. When the **Step max** value is changed, all rP-E step data values are recalculated immediately.

6.1.2 The Loop FLC function

If this function is active, FLCs are run continuously. If the **Exchange** function (below) is also active, the sample is exchanged between the end of one FLC and the start of the next. If the **Wash cycle** (below) is active, it runs before the sample **Exchange**. The FLC that has just finished is archived and a new data file is generated for the next FLC.

6.1.3 The Low E, Low time and Dark time fields

The **Low** E, **Low time** and **Dark time** fields can be used to implement low light pre-illumination and/or dark acclimation steps before **Auto DWM** and **Auto PEP** and the FLC steps. Either step can be skipped by setting the time to zero. Data acquired during the pre-FLC stage are logged within the RunSTAF data file and can be accessed through Clipboard functions (**Clipboard → Pre data** and **Clipboard → Pre traces**).

When the **Low** E is set to a very low value (typically below 20 µmol photons m^{-2} s^{-1}) the relationship between drive current and photon output becomes temperature dependent. To ensure that the actual output from the ALED is as close as possible to the requested value, and is accurately reported, a photodiode-monitored feedback loop has been incorporated. The same feedback loop is used to set low E values within the FLC steps or manual acquisition.

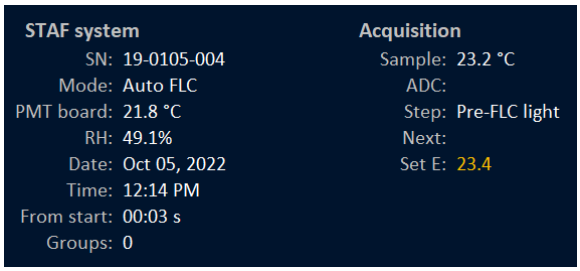

Figure 6.2A: In this example, the requested **Low** E value was set at **12** µmol photons m^{-2} s^{-1}. This was low enough to trigger the photodiode-monitored feedback loop to set the closest **Set** E value possible. The starting value was **23.4** µmol photons m^{-2} s^{-1}.

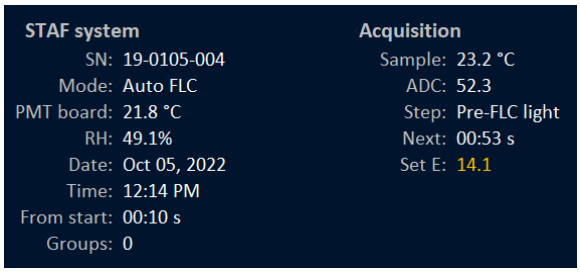

Figure 6.2B: After automated adjustment, the **Set** E value settled at **14.4** µmol photons m^{-2} s^{-1}.

6.1.4 Steps and Push up

The **Steps** field sets the number of **Up** steps for the FLC. If the number of **Steps** is set below **6**, the rP-E simulation is not drawn and RunSTAF does not attempt to fit an rP-E curve to the data. The user can add **Dark** and **Down** steps by setting non-zero values (seconds) within the appropriate field.

The **Push up** function determines the rate at which photon irradiance (E) increases through the FLC steps. Increasing the value pushes the distribution towards **High** E (see Figure 6.3). The distribution of Up steps through the FLC is one of a number of factors that could impact on the rP-E curve fit, including the value of $\mathrm{E_k}$. It follows that although there is no clear optimal value for the Push up

parameter, maintaining a consistent value may contribute to a consistent rP-E fit. In this context, it is important to note that the total duration of the Up phase of the FLC is likely to have a greater impact on the rP-E curve fit than either the number or distribution of Up steps.
See: **The rP-E data fit**

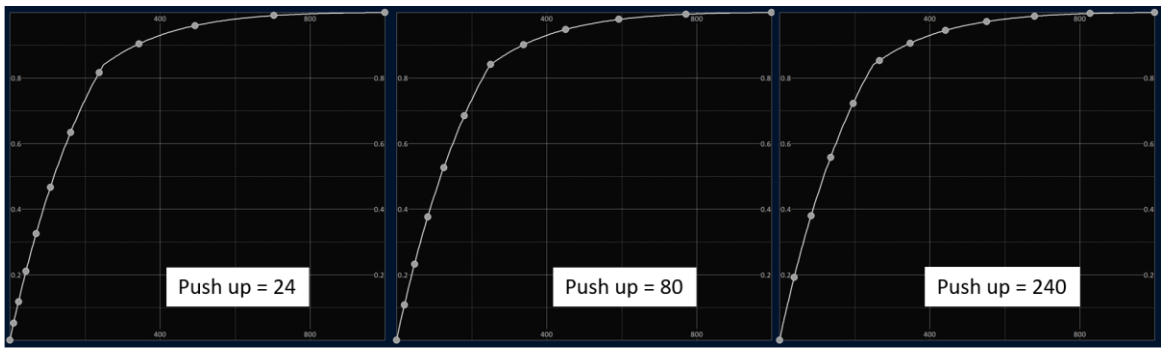

Figure 6.3: Screen crops showing the distribution of E values at different Push up settings. The values of **24** (left) and **240** (right) are the lowest and highest that can be set. The value of **80** (centre) is the default.

6.1.5 High E, Auto set and x E_k

When RunSTAF is launched, acquisition can be started as the result of the **Run acquisition on start-up** option being active or the Acquisition **start** button being pressed by the user. For the first FLC run, the set **High** $\mathbf{E}$ value is implemented. If the **Auto set** option is **Active**, the **High** $\mathbf{E}$ value for the second and subsequent FLCs is the product of the $\mathbf{E_k}$ from the rP-E fit to the previous FLC and the set value of **x** $\mathbf{E_k}$.

6.1.6 The Mix function

When **Mix** is **Active**, the peristaltic pump runs for the **On time** at the set **Speed** between successive FLC steps. The **Mix** function can be implemented with or without the solenoid unit being plumbed in and can be run with the flow-through unit or the flow-through stirrer unit. If the **Mix** function is **Active** with neither unit plumbed in, it will introduce a delay for the set **On time** between successive FLC steps.

6.1.7 The Exchange function

When **Active**, sample exchange is triggered at the end of a FLC. The solenoid unit and peristaltic pump must both be plumbed in for this function to operate correctly. There are two stages to the **Exchange** cycle. During the first stage, the peristaltic pump runs for the set **Flow time** with Solenoid A set to NC. This displaces the existing sample with a new sample. For the second stage, Solenoid A returns to NO and the peristaltic pump runs for the set **Purge time**. This clears all plumbing after the solenoid valve. The peristaltic pump is automatically set to the optimal speed while this function is running.
See: **LabSTAF hardware setup**

6.1.8 Wash cycle

When active, this function is triggered at the end of the first FLC to complete after the set **Interval** is reached. During the first stage of the cleaning cycle, set by the **Clean time**, Solenoids A and B are both set to the NC position. During the second stage of the cleaning cycle, set by the **Rinse time**, all three solenoids are set to the NC position. If the **Wash cycle** and **Exchange** functions are both active, the Wash cycle runs first. The peristaltic pump is automatically set to the maximum speed while this function is running.
See: **LabSTAF hardware setup**

6.2 Manual mode setup

The Manual mode is set by selecting **Settings → Acquisition mode → Manual**

When Manual mode is selected, the default **FLC setup** section for the Auto FLC mode is replaced with the **Manual settings** section, as shown in Figures 6.4 and 6.5.

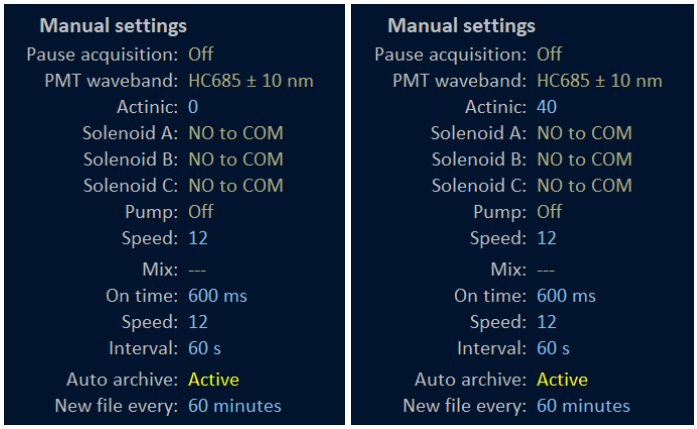

Figure 6.4: The **Manual settings** provides real time control over a range of LabSTAF system functions when the Manual mode is active. In this example, the **Actinic** light has been changed from zero (left) to 40 µmol photons m^{-2} s^{-1} (right).

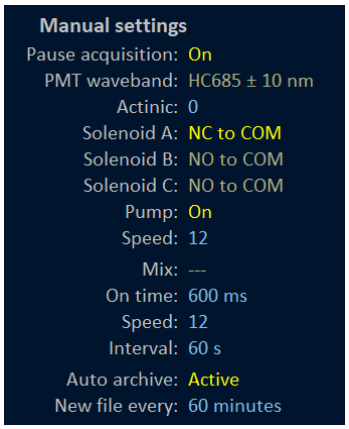

Figure 6.5: In this example, **Pause acquisition** has been activated, **Solenoid A** has been switched from NO to COM to **NC to COM** and the peristaltic **Pump** has been turned on at **Speed 12**. With the appropriate plumbing, this setup could be used for manual sample exchange.

Working through the list of **Manual settings**:

- **Pause acquisition** halts data input when turned **On** and resumes acquisition when turned Off
- **PMT waveband** manually exchanges the bandpass filter in front of the PMT between the default **HC685** and the optional **HC730**. Both filters are ± 10 nm Full Width-Half Max FWHM
- The **Actinic** field can be edited to set the required level of photon irradiance provided by the ALED with units of µmol photons m^{-2} s^{-1}
- **Solenoid A**, **B** or **C** switches between the default **NO to COM** (**Normally Open** to **Common**) and **NC to COM** (**Normally Closed** to **Common**) states
- **Pump** turns the peristaltic pump **On** and **Off**. The pump runs at the set **Speed** (1 – 16)
- **Mix** Runs the peristaltic pump when active. The pump runs for **On time** at the set **Speed** (1 – 16) and **Interval**
- **Auto archive** automatically archives data to a timestamped file when **Active**. The interval between files is set by the **New file every** value

7 Data access: Clipboard functions

The **Clipboard menu** provides options for accessing primary and processed data in a range of different formats.

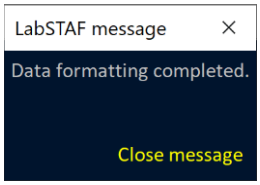

Figure 7.1: When a Clipboard function is run, the dialog shown below will open once the data array has been constructed. When this message is closed, the data are written to the Clipboard in a tab-delimited text format. This format is suitable for pasting directly into Excel and many other spreadsheet-based applications.

7.1 The Clipboard header

A Clipboard header is included with all Clipboard options.

	A	B	C	D	E	F	G	H	I	J	K	L
1	File path:	C:\Users...\Desktop\PEP import\221028-1530.rsf										
2												
3	STAF system			STAF setup						Temperatures at start		
4	LabSTAF:	21-2937-006		416 nm:	0		1st pulse:	100	µs	Sample:	27.8	°C
5	Mode:	Auto FLC		452 nm:	0.554		2nd pulse:	100	µs	System:	27.5	°C
6	Date:	Oct 28, 2022		452 nm:	0.554		Start gap:	400	µs			
7	Time:	15:30		473 nm:	0		End gap:	12800	µs			
8	Duration:	26:14 s		495 nm:	0		Gap steps:	11				
9	Acqs:	704		534 nm:	0		Seq interval:	120	ms			
10	Saqs:	704		594 nm:	0		Seq / Acq:	16				
11	Groups:	64		622 nm:	0		Acq / Saq:	1				
12							Group time:	22	s			
13												
14	File details											
15	Blank:	0										
16	Project:											
17	Reference:											
18	Run by:											
19	Note:											
20												
21	Data processing				Flat white coefficients				Imported PEP			
22	Set Fv/Fm:	0.5	(not applied)		MLED:	2.409			PEP SN:	19-0105-005		
23	Ka:	11800			ALED:	1.102			PEP file:	220326-0403		
24	PEC:	0.2715	(DWM value)		ESD:	1.203	(not applied)		PEP date:	Mar 26, 2022		
25	cPEC:	0.8486							PEP time:	220326-0403		
26	cPEP:	0.4576										
27	aLHII:	0.003734										

Figure 7.2: Sample Clipboard header. The Data processing, Flat white coefficients and Imported PEP sections are only included when relevant.

7.2 The Clipboard footer

The Clipboard footer is included by default but can be excluded be deselecting the option through the RunSTAF menu:

Clipboard → Include footer

130	LabSTAF SN:	19-0105-005													
131	Calibration date:	Mar 15 2022													
132															
133	PMT dynamic range				Fluorophore SU			PMT wavebands							
134	System °C:	20				Slope	ADC	Filter A:	HC685 ± 10						
135	LED mA:	160			0.48:	8.983	3466	Filter B:	HC730 ± 10						
136	PMT eht:	560			2.4:	9.083	16684	DW slope:	1.17						
137	PMT slope:	8.973			6.0:	8.96	40527								
138	Signal slope:	3833			12.0:	8.868	80751								
139															
140	LEDs		ALED calibration				MLED calibration								
141	MLED library:	MLED A	DAC	uA	EST			416 nm	452 nm	452 nm	473 nm	495 nm	534 nm	594 nm	622 nm
142	ALED type:	CXB1304 4000 K	154	0.013	5.5		80 mA:	0.174	0.1647	0.1667	0.1963	0.1422	0.1161	0.0211	0.0713
143	ALED window:	BG38/635 nm A	199	0.082	34.7		160 mA:	0.3959	0.3774	0.3746	0.4114	0.2807	0.2534	0.05	0.1587
144	ALED PADC slope:	0.0471	250	0.156	66.1		240 mA:	0.6019	0.5647	0.5655	0.5941	0.396	0.3731	0.0796	0.245
145	US_SQS/L constant:	2.36	345	0.29	122.9		320 mA:	0.7845	0.7464	0.7474	0.7685	0.4914	0.4798	0.1093	0.3293
146			385	0.346	146.6		400 mA:	0.9683	0.9203	0.92	0.9324	0.5817	0.5776	0.1395	0.4129
147			400	0.367	155.5		460 mA:	1.102	1.048	1.046	1.042	0.6463	0.653	0.1621	0.4721
148	Thermocouple		600	0.656	278										
149	TC slope:	0.038	800	0.946	400.8										
150	TC offset:	0	1000	1.238	524.6										
151			1400	1.818	770.3										
152	System response		2000	2.672	1132										
153	Decrease per °C:	0.39 %	4095	5.467	2317										

Figure 7.3: Example Clipboard footer. This provides a record of the calibration values used at the time the data within the file were acquired.
See: **LabSTAF calibration**

7.3 Clipboard → Pre data

Provides basic parameters from the Pre-FLC low (light) and dark Gaqs.

				F'	Fm'	Fq'/Fm'	AlphaPII'	SigmaPII'
Time (s)	Gaq	E	Fo	Fm	Fv/Fm	AlphaPII	SigmaPII	
26	1	20	136.6	242.2	0.4361	0.05607	3.471	
32	2	20	137.6	240.8	0.4287	0.0565	3.498	
38	3	20	135	235.3	0.4262	0.05716	3.539	
43	4	20	130.6	228.4	0.4283	0.05685	3.519	
50	5	20	125.9	222	0.4327	0.0561	3.473	
55	6	20	122.9	218.7	0.4381	0.05596	3.464	
62	7	0	85.85	199.4	0.5695	0.05542	3.431	
69	8	0	85.32	197.3	0.5675	0.05655	3.501	
74	9	0	88.12	204.4	0.5689	0.05644	3.494	

Figure 7.4: Sample Pre-FLC parameter data.

7.4 Clipboard → Pre traces

Provides basic parameters and trace data from the Pre-FLC low (light) and dark Gaqs.

Saq:	L 1	L 2	L 3	L 4	L 5	L 6	D 1	D 2
Time (s):	26	32	38	43	50	55	62	
F', Fo:	136.6	137.6	135	130.6	125.9	122.9	85.85	
Fm', Fm:	242.2	240.8	235.3	228.4	222	218.7	199.4	
AlphaPII', AlphaPII:	0.05607	0.0565	0.05716	0.05685	0.0561	0.05596	0.05542	0
SigmaPII', SigmaPII:	3.471	3.498	3.539	3.519	3.473	3.464	3.431	
		Traces						
	µs	L 1	L 2	L 3	L 4	L 5	L 6	D 1
	-22	87.6	87.59	87.57	87.58	87.57	87.58	
	-21	87.58	87.59	87.58	87.58	87.56	87.56	
	-20	87.6	87.59	87.58	87.57	87.56	87.57	
	-19	87.58	87.59	87.58	87.57	87.57	87.55	
	-18	87.59	87.58	87.58	87.56	87.57	87.56	
	-17	87.59	87.58	87.57	87.57	87.56	87.55	
	-16	87.58	87.58	87.57	87.56	87.56	87.56	
	-15	87.57	87.57	87.57	87.57	87.55	87.55	
	-14	87.58	87.57	87.57	87.55	87.56	87.55	
	-13	87.56	87.57	87.56	87.56	87.54	87.55	
	-12	87.57	87.57	87.56	87.55	87.55	87.55	
	-11	87.57	87.56	87.55	87.56	87.54	87.54	
	-10	87.57	87.57	87.57	87.54	87.55	87.54	
	-9	87.55	87.56	87.55	87.55	87.53	87.54	
	-8	87.57	87.57	87.56	87.55	87.54	87.54	
	-7	87.55	87.56	87.54	87.55	87.53	87.53	
	-6	87.55	87.55	87.57	87.54	87.53	87.54	
	-5	87.54	87.55	87.55	87.55	87.52	87.53	
	-4	87.55	87.54	87.56	87.53	87.52	87.52	
	-3	87.54	87.55	87.54	87.54	87.52	87.52	
	-2	87.55	87.54	87.56	87.53	87.53	87.52	
	-1	102.3	102.3	102.1	101.7	101.1	100.9	
	0	196.9	197.2	195.4	191.9	188.5	186.3	
	1	218	218.4	216	212.1	208.1	205.3	
	2	224.5	225	222.5	218.4	214	210.9	

Figure 7.5: Sample Pre-FLC parameter and trace data.

7.5 Clipboard → DWM data

The dataset copied to the Clipboard includes the trace data used to generate the DWM value. Either this value or a user-set value is used for Package Effect Correction (PEC). In the example shown below, the plot has been generated within Excel.

	A	B	C	D	E	F	G	H	I	J	K	L	M	N
1	File path:	C:\Users\PEP and SCS files\Chlorella vulgaris\201220-1632.rsf												
2														
3	LabSTAF:	20-0325-001		416 nm:	0		1st pulse:	100	µs	Sample:	21	°C		
4	Mode:	Auto FLC		452 nm:	0.8135		2nd pulse:	100	µs	System:	25.8	°C		
5	Date:	Dec 20, 2020		452 nm:	0.8525		Start gap:	200	µs					
6	Time:	16:32		473 nm:	0		End gap:	6400	µs					
7	Duration:	23:13 s		495 nm:	0		Gap steps:	6						
8	Acqs:	1392		534 nm:	0		Seq interval:	120	ms					
9	Saqs:	1392		594 nm:	0		Seq / Acq:	8						
10	Groups:	232		622 nm:	0		Acq / Saq:	1						
11							Group time:	6	s					
12														
13	Blank:	0												
14	Project:	Test with the stir unit												
15	Reference:	Chlorella vulgaris												
16	Run by:	KO												
17	Note:													
18														
19		W685				W730				W730/W685				
20		Fo	Fm	Fv	Fv/Fm	Fo	Fm	Fv	Fv/Fm	Fo	Fm	Fv	Fv/Fm	DWM
21	Rep 1:	80.19	164.5	84.35	0.5126	16.65	30.24	13.59	0.4494	0.2076	0.1838	0.1611	0.8766	0.2561
22	Rep 2:	80.73	164.7	84.01	0.51	17.51	30.5	12.99	0.426	0.2168	0.1851	0.1546	0.8353	0.2459
23	Rep 3:	81.8	165.5	83.66	0.5056	16.47	30.34	13.86	0.4569	0.2014	0.1833	0.1657	0.9037	0.2635
24	Mean:	80.91	164.9	84.01	0.5094	16.88	30.36	13.48	0.4441	0.2086	0.1841	0.1605	0.8717	0.2551
25	SE:	0.4722	0.2776	0.2003	0.00205	0.3186	0.07563	0.2568	0.00931	0.00449	0.00054	0.00321	0.01988	0.0051
26														
27			Traces											
28		µs	685 nm 1	685 nm 2	685 nm 3	730 nm 1	730 nm 2	730 nm 3						
29		1	80.95	80.77	80.94	16.58	17.49	16.54						
30		2	84.81	84.48	84.94	17.15	17.95	17.23						
31		3	87.58	87.34	87.92	17.73	18.57	17.69						
32		4	90.66	90.51	91.07	18.21	18.96	18.17						
33		5	93.48	93.42	94.08	18.8	19.41	18.8						
34		6	96.34	96.16	97.05	19.27	19.95	19.27						
35		7	99.62	99.4	100.1	19.63	20.38	19.68						
36		8	102.7	102.6	103.3	20.2	20.95	20.15						
37		9	105.3	105.7	106.3	20.68	21.44	20.81						
38		10	108.5	109	109.2	21.06	21.84	21.46						
39		11	111.5	111.8	112.2	21.65	22.14	21.6						
40		12	114.4	114.4	114.7	22.22	22.83	22.25						
41		13	117.1	117.2	117.8	22.53	23.16	22.68						
42		14	120.2	119.7	120.2	22.98	23.64	23.09						
43		15	122.2	122.7	123.1	23.44	24.01	23.53						
44		16	124.7	124.9	125.5	23.86	24.31	23.97						
45		17	127.2	127.4	127.8	24.25	24.78	24.21						

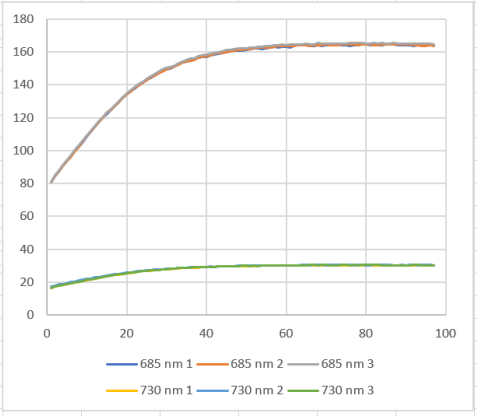

Figure 7.6: Sample DWM Clipboard data.
See: **Applying the Package Effect Correction (PEC)**

7.6 Clipboard → PEP data

The dataset copied to the Clipboard includes the trace data used to generate the **Fv** and **SigmaPII** values for each of the seven MLED wavebands. In the example shown below, the plots have been generated within Excel.

		Corrected values											
				Mean	Mean								
		Total EST	Peak nm	Fv	SigmaPII	Fv 1	Fv 2	Fv 3	SE	SigmaPII 1	SigmaPII 2	SigmaPII 3	SE
	416 nm:	1.65	414.8	79.46	3.099	81.55	79.05	77.77	1.11	3.047	3.133	3.115	0.02617
	452 nm:	1.42	447	79.78	3.267	80.68	79.55	79.09	0.4729	3.276	3.254	3.269	0.00644
	473 nm:	1.65	469.9	61.9	2.558	63.3	59.95	62.45	1.006	2.572	2.595	2.506	0.0268
	495 nm:	1.485	491.3	46.78	2.004	48.11	46.24	45.99	0.667	1.984	1.977	2.051	0.02356
	534 nm:	1.484	525.8	12.53	0.5363	13.73	13.84	10.02	1.253	0.6071	0.6073	0.3946	0.07086
	594 nm:	1.593	593.9	18.46	0.8573	19.01	21.56	14.81	1.969	0.9964	0.9911	0.5843	0.1365
	622 nm:	1.893	622.5	39.88	1.52	43.21	38.75	37.68	1.692	1.445	1.659	1.455	0.06986
	Mode:	PEP-bc											
		Uncorrected values											
		Fo	Fm	Fv	AlphaPII								
	452A + 416 nm:	113.4	247.2	133.9	0.05218								
		112.7	243.5	130.9	0.0527								
		112.1	241.5	129.4	0.05268								
	452A + 452B nm:	97.89	212.5	114.6	0.04653								
		97.2	210.2	113	0.04622								
		96.17	208.5	112.3	0.04644								
	452A + 473 nm:	101.7	220.6	118.8	0.04827								
		102	217.1	115.1	0.04828								
		99.76	216.6	116.8	0.04766								
	452A + 495 nm:	82.34	180.7	98.34	0.04014								
		82.32	178.5	96.18	0.03991								
		81.21	176.8	95.63	0.04052								
	452A + 452B + 534 nm:	105.2	228.8	123.6	0.05052								
		104.5	226.5	122.1	0.05022								
		105.7	224.7	118.9	0.04903								
	452A + 452B + 594 nm:	101.9	219.8	117.9	0.04826								
		101.1	217.8	116.7	0.04794								
		101.2	216.1	114.9	0.04745								
	452A + 452B + 622 nm:	115.8	250.8	135	0.05337								
		115.7	247	131.3	0.05407								
		115.4	245.6	130.1	0.05332								
			Traces										
		µs	416 nm 1	416 nm 2	416 nm 3	452 nm 1	452 nm 2	452 nm 3	473 nm 1	473 nm 2	473 nm 3	495 nm 1	495 nm 2	495 nm 3	534 nm 1	534 nm 2	534 nm 3
		1	114	112.8	112.8	97.59	97.06	96.47	101.7	100.8	100.6	82.22	82.13	81.63	106.1	105.4	105.1
		2	119.3	118.7	117.8	102.1	101.6	101.1	106.3	105.9	105	85.42	85.47	84.84	110.8	110.4	109.8
		3	123.5	122.6	122.1	105.3	104.5	104.2	109.7	108.9	108.4	87.76	87.34	87.22	114.8	114.1	113.8
		4	127.8	126.5	126.3	108.6	107.4	107.2	113.2	112.6	111.9	90.16	89.85	89.66	118.3	118	117.1
		5	131.6	131.1	130.5	111.8	111	110.4	116.7	115.7	115.1	92.62	92.27	91.44	122	121.9	120.8
		6	136.6	135.3	134.4	114.9	114.2	113.4	120.1	119.1	118.7	95.1	94.52	93.89	125.9	125.5	124.3

Figure 7.7: Sample PEP Clipboard data.

See: See: [Working with Photochemical Excitation Profiles (PEPs)]

7.7 Clipboard → SCS data

This function copies the Actinic LED (**ALED**) emission spectrum plus the **Fv** and **SigmaPII** absorption spectra at 1 nm resolution. In the example shown below, the plots have been generated within Excel.

nm	ALED	Fv	SigmaPII
380	0	0	0
381	0	8.837	0.06549
382	0	17.67	0.131
383	0	26.51	0.1965
384	0	35.35	0.262
385	0	44.18	0.3274
386	0	53.02	0.3929
387	0	61.86	0.4584
388	0.0011	70.7	0.5239
389	0.0012	79.53	0.5894
390	0.0013	88.37	0.6549
391	0	97.21	0.7204
392	0	106	0.7859
393	0	114.9	0.8514
394	0	123.7	0.9168
395	0	132.6	0.9823
396	0.001	141.4	1.048
397	0.001	150.2	1.113

Figure 7.8: Sample SCS Clipboard data.

See: [Using PEP data to apply spectral correction]

7.8 Clipboard → rP-E data

The dataset copied to the Clipboard includes JV_{PII} and GO_{PII} values generated using the Absorption method plus J_{PII} values generated using the Sigma method. In the example shown below, the data have been pasted into Excel and a data plot has been generated within Excel. The Gaq traces used to generate the rP-E values are also included within the output.

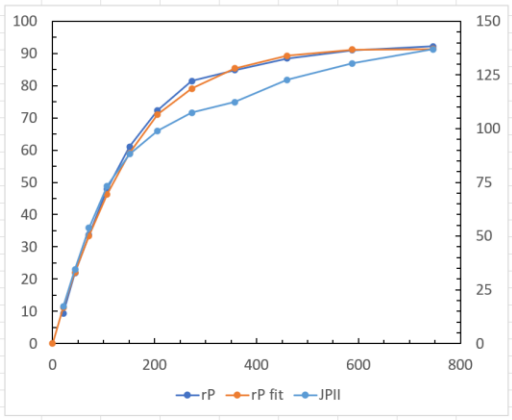

File details																				
Blank:	0																			
Project:	PEP and FLC tests with the stir unit																			
Reference:	Conticribra weissflogii																			
Run by:	KO																			
Note:	Pre-diluted 36 h before																			
Data processing					Flat white coefficients															
Set Fv/Fm:	0.5723	(not applied)			MLED:	1.73														
Ka:	11800				ALED:	1.037														
PEC:	0.32	(user defined)																		
cPEC:	1																			
cPEP:	0.5998																			
aLHII:	0.4885																			
rPE fit																				
Alpha:	0.5614																			
Beta:	0.05062																			
Ek:	196	µmol photons / m² / s																		
EkBeta:	459	µmol photons / m² / s																		
rPm:	91.65																			
JVPIIm:	44.78	µmol photons / m³ / s																		
GOPIIm:	40.3	mmol O2 / m³ / h																		
		Up																		
								Fo	Fm	Fv	Fv/Fm	Fv/Fmc						AlphaPII	Si
	E	Fb	rP	rP fit	JVPII	GOPII	JPII	F'	Fm'	Fq'	Fq'/Fm'	Fq'/Fmc'	Fv'/Fmc'	Fq'/Fv'	EkS	Ekt'	Ekt	AlphaPII'	Si
	0	0		0				39.39	91.76	52.37	0.5707	0.5707	0.5707		263			0.05479	
	21	0	9.4	11.2	4.593	4.134	17.22	44.88	93.8	48.92	0.5215	0.5215	0.5761	0.9053	195	89	90	0.05059	
	44	0	21.9	22.1	10.72	9.645	34.55	46.86	93.3	46.44	0.4978	0.4978	0.5748	0.866	568	150	151	0.05063	
	71	0	33.7	33.4	16.48	14.84	53.75	48.59	92.87	44.28	0.4768	0.4768	0.5737	0.8312	583	185	186	0.05086	
	107	0	48	46.3	23.45	21.11	73.32	51.81	94.17	42.35	0.4498	0.4498	0.577	0.7795	474	205	207	0.04909	
	151	0	61.1	59.1	29.84	26.85	88.24	56.85	95.42	38.58	0.4043	0.4043	0.5803	0.6967	292	196	199	0.04684	
	206	0	72.4	71.1	35.38	31.84	99.01	61.64	95.01	33.37	0.3512	0.3512	0.5792	0.6063	212	187	190	0.04426	
	273	0	81.5	79.1	39.83	35.85	107.4	64.45	91.89	27.43	0.2986	0.2986	0.571	0.5228	272	185	185	0.04202	
	357	0	84.8	85.4	41.44	37.3	112.3	60.87	79.86	18.99	0.2378	0.2378	0.5364	0.4434	415	185	174	0.03962	
	460	0	88.5	89.3	43.23	38.91	122.7	49.87	61.75	11.87	0.1923	0.1923	0.4722	0.4072	595	211	175	0.03658	
	588	0	91	91.2	44.46	40.01	130.4	40.71	48.16	7.452	0.1547	0.1547	0.411	0.3765	234	243	175	0.03289	
	746	0	92.2	91.4	45.06	40.55	136.9	34.19	39.01	4.821	0.1236	0.1236	0.3611	0.3423	762	273	173	0.02995	
		Gaq parameters																	
	From linear regression																		
Base:		35.83	35.83	35.83	35.83	35.89	35.89	35.89	35.89	35.89	35.89	35.89	35.89	35.89	35.89	35.97	35.96	35.95	
F', Fo:		40.1	40.16	40.22	40.19	46.15	46.76	46.59	46.36	46.27	46.1	46.06	45.88	45.71	45.68	54.83	48.03	47.27	
Fm', Fm:		89.25	89.29	89.43	89.25	92.64	94.69	94.76	94.12	93.99	93.61	93.55	93.1	92.64	92.54	101.4	93.55	91.81	
	From rho fit																		
F', Fo:		39.3	39.36	39.42	39.39	45.71	46.31	45.29	45.28	45.19	45.02	45.09	44.91	44.85	44.71	53.18	46.9	46.82	
Fm', Fm:		91.65	91.69	91.83	91.66	93.25	95.32	95.7	95.05	94.92	94.55	94.48	94.03	93.57	93.46	101.4	94.17	92.43	

Figure 7.9: Sample rP-E Clipboard data.

7.9 Clipboard → Relaxation phase data

RunSTAF provides three options for accessing relaxation phase data, as detailed below.
See: **The relaxation phase (tau) fit**

7.9.1 Clipboard → Relaxation phase data → Parameters

The dataset copied to the Clipboard includes time-constants and amplitudes for the Fast and Slow phases for each of the three fitting methods used within RunSTAF to fit the relaxation kinetics (Fv, Rho and Dimer). Values for all parameters are calculated for every group within the file.

		Delta								Tau							
	Grp	FvF	RhoF	DimerF	FvS	RhoS	DimerS	E	Grp	FvF	RhoF	DimerF	FvS	RhoS	DimerS	E	
	1	0.8768	0.7347	0.7357	0.1232	0.2653	0.2643	0	1	1169	1251	1211	15024	9691	18224	0	
	2	0.8922	0.7146	0.7232	0.1078	0.2854	0.2768	0	2	1164	1251	1251	24411	8197	13957	0	
	3	0.872	0.7472	0.7414	0.128	0.2528	0.2586	0	3	1108	1251	1251	24624	12891	21424	0	
	4	0.8902	0.7366	0.7251	0.1098	0.2634	0.2749	0	4	1129	1251	1251	24624	9691	13957	0	
	5	0.8749	0.7482	0.7414	0.1251	0.2518	0.2586	0	5	1101	1251	1231	24624	11824	19291	0	
	6	0.8922	0.7347	0.7395	0.1078	0.2653	0.2605	0	6	1136	1251	1248	21744	9691	19291	0	
	7	0.8518	0.729	0.7414	0.1482	0.271	0.2586	0	7	1088	1251	1241	10149	8624	17157	0	
	8	0.896	0.751	0.7386	0.104	0.249	0.2614	0	8	1131	1251	1225	24624	11824	23557	0	
	9	0.872	0.7645	0.7318	0.128	0.2355	0.2682	0	9	1108	1251	1201	24624	15557	20357	0	
	10	0.8998	0.7213	0.7261	0.1002	0.2787	0.2739	0	10	1169	1251	1251	21424	8240	13957	0	
	11	0.7174	0.7328	0.6714	0.2826	0.2672	0.3286	10	11	910.6	1221	1067	4987	9701	12336	10	
	12	0.7453	0.6992	0.6685	0.2547	0.3008	0.3315	10	12	973.1	1128	1041	7184	10096	12677	10	
	13	0.8086	0.7558	0.7146	0.1914	0.2442	0.2854	10	13	1029	1151	1076	22491	24624	22491	10	
	14	0.823	0.7818	0.7338	0.177	0.2182	0.2662	10	14	1082	1209	1136	17051	21424	18757	10	
	15	0.8307	0.7808	0.7338	0.1693	0.2192	0.2662	10	15	1109	1224	1139	23237	24624	20251	10	
	16	0.8278	0.7587	0.7482	0.1722	0.2413	0.2518	10	16	1093	1211	1191	21424	17157	23877	10	

Figure 7.10: A selection from the Clipboard output generated using the **Parameters** option for relaxation phase data.

7.9.2 Clipboard → Relaxation phase data → Alternating fits

The screenshot in Figure 7.11 show a selection from the Clipboard output within Excel.

µs	0	200	400	800	1600	3200	6400
Fv 1	1	0.9192	0.7508	0.5263	0.3322	0.1657	0.08168
µs	0	200	400	800	1600	3200	6400
Rho 1	1	0.942	0.81	0.612	0.418	0.246	0.148
µs	0	200	400	800	1600	3200	6400
Dimer 1	1	0.9371	0.8025	0.6096	0.4274	0.2794	0.193
µs	0	200	400	800	1600	3200	6400
Fv 2	1	0.9164	0.7556	0.5165	0.3216	0.1628	0.0842
µs	0	200	400	800	1600	3200	6400
Rho 2	1	0.942	0.822	0.614	0.424	0.24	0.146
µs	0	200	400	800	1600	3200	6400
Dimer 2	1	0.9371	0.8146	0.6157	0.4426	0.2739	0.1873
µs	0	200	400	800	1600	3200	6400
Fv 3	1	0.9228	0.7423	0.519	0.3213	0.1549	0.1131
µs	0	200	400	800	1600	3200	6400
Rho 3	1	0.944	0.81	0.616	0.424	0.236	0.176
µs	0	200	400	800	1600	3200	6400
Dimer 3	1	0.9418	0.8025	0.6188	0.4449	0.2685	0.208
µs	0	200	400	800	1600	3200	6400
Fv 4	1	0.915	0.7488	0.5202	0.3041	0.1521	0.09461
µs	0	200	400	800	1600	3200	6400
Rho 4	1	0.942	0.816	0.624	0.412	0.232	0.154
µs	0	200	400	800	1600	3200	6400
Dimer 4	1	0.9371	0.8106	0.625	0.4382	0.2698	0.1864
µs	0	200	400	800	1600	3200	6400
Fv 5	1	0.9157	0.736	0.5159	0.3193	0.1579	0.1046
µs	0	200	400	800	1600	3200	6400
Rho 5	1	0.94	0.808	0.614	0.42	0.234	0.168
µs	0	200	400	800	1600	3200	6400
Dimer 5	1	0.9371	0.7985	0.6126	0.4382	0.2658	0.2009
µs	0	200	400	800	1600	3200	6400
Fv 6	1	0.9129	0.7435	0.5216	0.3027	0.1605	0.08182
µs	0	200	400	800	1600	3200	6400
Rho 6	1	0.94	0.816	0.624	0.404	0.248	0.148
µs	0	200	400	800	1600	3200	6400
Dimer 6	1	0.9371	0.8065	0.625	0.4274	0.2822	0.1959

Figure 7.11: A selection from the Clipboard output generated using the **Alternating fits** option for relaxation phase data.

7.9.3 Clipboard → Relaxation phase data → Blocks of fits

This function separated the three fits (Fv, Rho and Dimer) into separate blocks.

E	µs	0	200	400	800	1600	3200	6400
0	Fv 1	1	0.9192	0.7508	0.5263	0.3322	0.1657	0.08168
0	Fv 2	1	0.9164	0.7556	0.5165	0.3216	0.1628	0.0842
0	Fv 3	1	0.9228	0.7423	0.519	0.3213	0.1549	0.1131
0	Fv 4	1	0.915	0.7488	0.5202	0.3041	0.1521	0.09461
0	Fv 5	1	0.9157	0.736	0.5159	0.3193	0.1579	0.1046
0	Fv 6	1	0.9129	0.7435	0.5216	0.3027	0.1605	0.08182
0	Fv 7	1	0.9154	0.738	0.5131	0.3181	0.1652	0.07731
0	Fv 8	1	0.9076	0.7382	0.5218	0.3117	0.1346	0.09554
0	Fv 9	1	0.9057	0.7405	0.5273	0.3156	0.1674	0.1034
0	Fv 10	1	0.9095	0.7419	0.5174	0.3302	0.1449	0.07858
10	Fv 11	1	0.8881	0.7155	0.5117	0.3468	0.165	0.07968
10	Fv 12	1	0.8981	0.7318	0.5221	0.3676	0.1859	0.1062
10	Fv 13	1	0.8991	0.7297	0.5432	0.3485	0.1991	0.1517
10	Fv 14	1	0.9037	0.742	0.5377	0.35	0.1964	0.1212
10	Fv 15	1	0.9055	0.7492	0.5524	0.3438	0.2008	0.1325
10	Fv 16	1	0.9053	0.7434	0.541	0.3539	0.1937	0.131

E	µs	0	200	400	800	1600	3200	6400
0	Rho 1	1	0.942	0.81	0.612	0.418	0.246	0.148
0	Rho 2	1	0.942	0.822	0.614	0.424	0.24	0.146
0	Rho 3	1	0.944	0.81	0.616	0.424	0.236	0.176
0	Rho 4	1	0.942	0.816	0.624	0.412	0.232	0.154
0	Rho 5	1	0.94	0.808	0.614	0.42	0.234	0.168
0	Rho 6	1	0.94	0.816	0.624	0.404	0.248	0.148
0	Rho 7	1	0.942	0.81	0.61	0.416	0.244	0.138
0	Rho 8	1	0.934	0.81	0.622	0.422	0.222	0.168
0	Rho 9	1	0.932	0.812	0.606	0.414	0.25	0.166
0	Rho 10	1	0.938	0.814	0.62	0.426	0.23	0.142
10	Rho 11	1	0.916	0.782	0.606	0.434	0.244	0.142
10	Rho 12	1	0.92	0.78	0.592	0.44	0.258	0.162
10	Rho 13	1	0.918	0.774	0.606	0.408	0.26	0.198
10	Rho 14	1	0.914	0.778	0.6	0.406	0.248	0.166
10	Rho 15	1	0.92	0.784	0.6	0.412	0.256	0.172
10	Rho 16	1	0.924	0.782	0.61	0.414	0.258	0.172

E	µs	0	200	400	800	1600	3200	6400
0	Dimer 1	1	0.9371	0.8025	0.6096	0.4274	0.2794	0.193
0	Dimer 2	1	0.9371	0.8146	0.6157	0.4426	0.2739	0.1873
0	Dimer 3	1	0.9418	0.8025	0.6188	0.4449	0.2685	0.208
0	Dimer 4	1	0.9371	0.8106	0.625	0.4382	0.2698	0.1864
0	Dimer 5	1	0.9371	0.7985	0.6126	0.4382	0.2658	0.2009
0	Dimer 6	1	0.9371	0.8065	0.625	0.4274	0.2822	0.1959
0	Dimer 7	1	0.9371	0.7985	0.6096	0.436	0.278	0.1809
0	Dimer 8	1	0.9277	0.7985	0.6219	0.4426	0.2698	0.2165
0	Dimer 9	1	0.9277	0.8025	0.6065	0.436	0.2865	0.1999
0	Dimer 10	1	0.9324	0.8065	0.625	0.4426	0.2632	0.1892
10	Dimer 11	1	0.9099	0.7756	0.6066	0.4481	0.2851	0.1975
10	Dimer 12	1	0.9142	0.7754	0.5942	0.4494	0.287	0.2003
10	Dimer 13	1	0.9139	0.7725	0.6094	0.4159	0.2846	0.2231
10	Dimer 14	1	0.9141	0.7771	0.6048	0.4188	0.2735	0.1916
10	Dimer 15	1	0.9191	0.7793	0.604	0.4198	0.2791	0.1952
10	Dimer 16	1	0.9188	0.782	0.6135	0.4253	0.2758	0.1964

Figure 7.12: A selection from the Clipboard output generated using the **Blocks of fits option** for relaxation phase data.

7.10 Clipboard → Saq parameters or Clipboard → Acq parameters

This copies values for a wide range of derived and primary parameters to the Clipboard. The headers of each column match with the **Plot selection** labels on the data screen.

	x-axis				Rho fit parameters								Dimer fit parameters		
					Rho	sRho	AlphaPII	sAlphaPII	SigmaPII	sSigmaPII			dRho		
	Gap (µs)	Time (s)	Saq	E	Rho'	sRho'	AlphaPII'	sAlphaPII'	SigmaPII'	sSigmaPII'	SE	sSE	dRho'	[oo]	[oc]
	400	192	1	0	0.321	0.009779	0.06349	0.04921	5.731	4.442	0.000427	0.000335	0.5678	1	0
	566	192	2	0	0.3356	0.01231	0.06471	0.05429	5.84	4.899	0.000357	0.0004	0.5929	1	0
	800	192	3	0	0.265	0.0162	0.06436	0.05351	5.809	4.829	0.000399	0.000413	0.5053	1	0
	1131	192	4	0	0.3185	0.01828	0.06238	0.05605	5.63	5.059	0.000378	0.000341	0.5844	1	0
	1600	192	5	0	0.3237	0.1183	0.06102	0.05709	5.507	5.153	0.000337	0.000422	0.5825	1	0
	2263	192	6	0	0.2908	0.06676	0.06304	0.05637	5.689	5.088	0.000349	0.000342	0.5342	1	0
	3200	192	7	0	0.2621	0.05302	0.06314	0.05599	5.698	5.053	0.000409	0.00034	0.524	1	0

											Primary fluorescence values					
		dAlphaPII	sdAlphaPII	dSigmaPII	sdSigmaPII			Fb			Fo	sF	Fm	sFm	Fv	
[cc]	s[oo]	s[oc]	s[cc]	dAlphaPII'	sdAlphaPII'	dSigmaPII'	sdSigmaPII'	dSE	sdSE	Fb'	Fo'	Fv'	F'	sF'	Fm'	
0	0.06827	0.3892	0.5425	0.06261	0.03857	5.65	3.481	0.00047	0.000341	0	0.3944	0.37	0.3955	0.632	0.7644	
0	0.119	0.4545	0.4265	0.0638	0.04298	5.758	3.879	0.000395	0.000418	0	0.3928	0.3655	0.3922	0.5945	0.7582	
0	0.2051	0.4976	0.2973	0.06384	0.04546	5.762	4.103	0.000439	0.000451	0	0.3941	0.369	0.3874	0.5654	0.763	
0	0.29	0.4986	0.2114	0.06188	0.04792	5.585	4.325	0.000393	0.000408	0	0.3935	0.3675	0.399	0.5355	0.7611	
0	0.3801	0.474	0.1459	0.06053	0.04968	5.463	4.484	0.000325	0.000436	0	0.3947	0.3707	0.4013	0.5114	0.7653	
0	0.4577	0.4385	0.1038	0.06241	0.05063	5.633	4.569	0.000344	0.000405	0	0.3941	0.3691	0.3965	0.4937	0.7632	
0	0.5405	0.39	0.06948	0.06314	0.05212	5.698	4.704	0.000421	0.000469	0	0.3942	0.3694	0.3954	0.4744	0.7636	

			Relaxation phase parameters					Derived fluorescence parameters							
sFq	DeltaF	DeltaS	TauF	TauS		Fv/Fm	Fv/Fmc								
sFm'	Fq'	sFq'	DeltaF'	DeltaS'	TauF'	TauS'	Taut'	Fq'/Fm'	Fq'/Fmc'	Fv'/Fmc'	Fq'/Fv'	Ekt'	Ekt	JVPII	JPII
0.7535	0.3689	0.1215	0.8576	0.1424	810	11749		0.4826	0.4826	0.484					
0.7542	0.366	0.1597	0.8576	0.1424	810	11749		0.4827	0.4827	0.482					
0.7715	0.3756	0.2061	0.8576	0.1424	810	11749		0.4923	0.4923	0.4836					
0.7787	0.3621	0.2431	0.8576	0.1424	810	11749		0.4757	0.4757	0.4829					
0.7862	0.364	0.2748	0.8576	0.1424	810	11749		0.4756	0.4756	0.4843					
0.7946	0.3668	0.301	0.8576	0.1424	810	11749		0.4805	0.4805	0.4836					
0.8	0.3682	0.3257	0.8576	0.1424	810	11749		0.4822	0.4822	0.4837					

		Linear regression					STAF setup								Temperatures(°C)	
NPQ	NSV	Qi	Qo	QoSE	Qm	QmSE	PMT eht	416 nm	452 nm	452 nm	473 nm	495 nm	534 nm	594 nm	622 nm	Sample	System
0.001009	1.066	0.3687	0.7809	0.008023	1.13	0.004415	550	0	0	0	0	0	0	0	0	27.81	27.5
0.009099	1.075	0.3687	0.7751	0.007782	1.117	0.003275	550	0	0	0	0	0	0	0	0	27.81	27.5
0.00276	1.068	0.3687	0.7783	0.008065	1.126	0.003835	550	0	0	0	0	0	0	0	0	27.81	27.5
0.00536	1.071	0.3687	0.7804	0.006689	1.128	0.003898	550	0	0	0	0	0	0	0	0	27.81	27.5
-0.00026	1.065	0.3687	0.7793	0.006077	1.119	0.003067	550	0	0	0	0	0	0	0	0	27.81	27.5
0.002523	1.068	0.3687	0.7794	0.006689	1.127	0.003653	550	0	0	0	0	0	0	0	0	27.81	27.5
0.002086	1.067	0.3687	0.7824	0.008391	1.126	0.003415	550	0	0	0	0	0	0	0	0	27.81	27.5

Figure 7.13: Sample Saq parameters or Acq parameters Clipboard data.

7.11 Clipboard → Saq traces or Clipboard → Acq traces

The main purpose of this function is to copy the primary Saq or Acq trace data to the Clipboard. Above the trace data, a range of calculated parameters are provided in a vertical format, as shown in the left screenshot below. The trace data include the first 20 µs of acquisition, which provides access to the instrument signal offset. The timescale (the µs column in the right screenshot below) shows the first 22 µs as negative values. This range is the 20 µs of instrument signal offset plus the 2 µs between triggering the first ST pulse and $t = 0$ for the first ST pulse. Because these are primary data, the instrument signal offset has not been subtracted from the Saq values as it normally is.

23		Saq	1	2	3	4
24		E	0	0	0	0
25	Gap Index:	1	2	3	4	5
26	Gap (µs):	200	400	800	1600	3200
27	Reps:	1	1	1	1	1
28		From linear regression				
29	Base:	35.83	35.83	35.83	35.83	35.83
30	F', Fo:	40.1	40.06	39.95	40.14	40.18
31	Fm', Fm:	89.37	88.53	89.64	89.23	89.4
32	sF', sF:	74.41	63.76	55.51	49.52	45.77
33	sFm', sFm:	85.5	86.07	88.87	91.14	92.88
34		From rho fit				
35	F', Fo:	39.3	39.01	39.63	39.34	39.38
36	Fm', Fm:	91.77	91.28	91.75	91.63	91.8
37	Fq', Fv:	52.47	52.27	52.12	52.29	52.42
38	Rho', Rho:	0.3733	0.3708	0.3924	0.3767	0.377
39	AlphaPII', AlphaPII:	0.05447	0.05496	0.05471	0.05443	0.05445
40	SigmaPII', SigmaPII:	2.701	2.725	2.712	2.698	2.7
41	SE:	0.01669	0.0196	0.01767	0.016	0.0158
42	sF', sF:	74.02	62.68	53.61	47.8	44.67
43	sFm', sFm:	85.5	85.72	88.87	91.14	93.5
44	sFq', sFq:	11.48	23.05	35.27	43.34	48.83
45	sRho', sRho:	0.08738	0.07599	0.0495	0.1794	0.2909
46	sAlphaPII', sAlphaPII:	0.04255	0.04632	0.04648	0.04858	0.05067
47	sSigmaPII', sSigmaPII:	2.11	2.297	2.304	2.408	2.512
48	sSE:	0.00593	0.01038	0.00775	0.0103	0.01099
49		From dimer fit				
50	dRhoPII:	0.6781	0.6617	0.7141	0.68	0.6829
51	AlphaPII', AlphaPII:	0.05393	0.0543	0.05427	0.05399	0.05402
52	SigmaPII', SigmaPII:	2.674	2.692	2.691	2.677	2.678
53	[oo]:	1	1	1	1	1
54	SE:	0.0422	0.04404	0.03796	0.04292	0.04317
55	sAlphaPII', sAlphaPII:	0.03011	0.03536	0.03812	0.04319	0.04615
56	sSigmaPII', sSigmaPII:	1.493	1.753	1.89	2.141	2.288
57	s[oo]:	0.03072	0.142	0.3369	0.5425	0.6867
58	s[oc]:	0.2929	0.4721	0.4884	0.3887	0.2843
59	s[cc]:	0.6764	0.3858	0.1748	0.06879	0.02905
60	sSE:	0.00795	0.01064	0.03446	0.01733	0.01786
61		Derived				
62	Fq'/Fmc', Fv/Fmc:	0.5717	0.5726	0.568	0.5707	0.571
63	sFq'/Fmc', sFq/Fmc:	0.1343	0.2688	0.3968	0.4755	0.5222
64	aLHII:	0.8101	0.8101	0.8101	0.8101	0.8101
65	Fv'/Fmc':	0.572	0.5707	0.572	0.5717	0.5721
66	Fq'/Fv':					
67	Ekt':					
68	Ekt:					
69	JVPII:					
70	JPII:					
71	NPQ:	0.0012	0.00658	0.00138	0.00272	0.00086
72	NSV:	0.7481	0.7522	0.7483	0.7493	0.7479
73						
74		µs	Saq 1	Saq 2	Saq 3	Saq 4
75		-22	35.83	35.83	35.82	35.82
76		-21	35.83	35.83	35.83	35.83
77		-20	35.83	35.83	35.82	35.83
78		-19	35.82	35.83	35.83	35.83

73						
74		µs	Saq 1	Saq 2	Saq 3	Saq 4
75		-22	35.83	35.83	35.82	35.82
76		-21	35.83	35.83	35.83	35.83
77		-20	35.83	35.83	35.82	35.83
78		-19	35.82	35.83	35.83	35.83
79		-18	35.82	35.83	35.82	35.82
80		-17	35.82	35.82	35.83	35.83
81		-16	35.82	35.82	35.82	35.82
82		-15	35.82	35.83	35.83	35.83
83		-14	35.83	35.82	35.82	35.82
84		-13	35.81	35.82	35.82	35.82
85		-12	35.82	35.82	35.82	35.82
86		-11	35.81	35.82	35.83	35.82
87		-10	35.82	35.82	35.82	35.82
88		-9	35.82	35.82	35.82	35.82
89		-8	35.82	35.82	35.82	35.81
90		-7	35.81	35.82	35.82	35.82
91		-6	35.81	35.81	35.81	35.81
92		-5	35.81	35.82	35.82	35.82
93		-4	35.81	35.81	35.81	35.81
94		-3	35.81	35.81	35.82	35.81
95		-2	35.81	35.81	35.81	35.81
96		-1	39.58	39.6	39.58	39.59
97		0	68.69	68.67	68.57	68.68
98		1	75.37	75.34	75.26	75.41
99		2	77.4	77.32	77.26	77.42
100		3	79.01	78.94	78.9	79.05
101		4	80.69	80.61	80.6	80.74
102		5	82.39	82.33	82.34	82.46
103		6	84.22	84.1	84.13	84.16
104		7	86.02	85.88	85.95	85.96
105		8	87.83	87.68	87.8	87.81
106		9	89.61	89.51	89.65	89.6
107		10	91.45	91.25	91.53	91.41
108		11	93.23	93.12	93.33	93.2
109		12	94.95	94.83	95.19	94.97
110		13	96.8	96.54	96.93	96.69
111		14	98.47	98.2	98.6	98.37
112		15	100.1	99.96	100.3	100.1
113		16	101.7	101.5	101.9	101.6
114		17	103.2	103	103.4	103.2
115		18	104.8	104.5	105	104.7
116		19	106.1	105.9	106.4	106
117		20	107.5	107.3	107.7	107.5
118		21	108.8	108.5	109.1	108.8
119		22	110	109.8	110.3	109.9
120		23	111.2	110.9	111.5	111.1
121		24	112.3	112.1	112.6	112.2
122		25	113.4	113.2	113.7	113.3
123		26	114.4	114.1	114.7	114.3
124		27	115.3	115	115.6	115.2
125		28	116.2	115.9	116.4	116
126		29	117	116.7	117.2	116.9

↓...

Figure 7.14: Sample Saq or Acq Clipboard data. See: ST data acquisition

7.12 Clipboard → Saq trace fits or Clipboard → Acq trace fits (Rho)

Each ST trace is accompanied by the RunSTAF-generated Rho fit (Fit 1, Fit 2…) and an associated column showing the accumulation of closed RCIIs through the ST trace (C 1, C 2…).

Set Fv/Fm:	0.5	(not applied)														
Ka:	11800															
PEC:	0.32	(user defined value)														
Saq:	1			2			3			4			5			
E:	0			0			0			0			0			
Gap Index:	1			2			3			4			5			
Gap (µs):	200			400			800			1600			3200			
F', Fo:	14.39			14.33			14.35			14.45			14.31			
Fm', Fm:	32.87			32.51			32.68			32.57			32.69			
Rho', Rho:	0.3328			0.35			0.3434			0.3538			0.3329			
AlphaPII', AlphaPII:	0.05501			0.05612			0.0556			0.05505			0.05528			
SigmaPII', SigmaPII:	2.697			2.752			2.726			2.699			2.711			
sF', sF:	27.12			23.23			20.25			18.01			16.41			
sFm', sFm:	30.74			30.75			31.59			32.3			33.4			
sRho', sRho:	0.07926			0.01493			0.1026			0.2376			0.2206			
sAlphaPII', sAlphaPII:	0.04126			0.0436			0.04586			0.0492			0.05034			
sSigmaPII', sSigmaPII:	2.023			2.138			2.249			2.413			2.469			
	Saq 1	Fit 1	C 1	Saq 2	Fit 2	C 2	Saq 3	Fit 3	C 3	Saq 4	Fit 4	C 4	Saq 5	Fit 5	C 5	
0		14.39	0		14.33	0		14.35	0		14.45	0		14.31	0	
1	15.16	15.08	0.05501	15.12	15	0.05612	15.08	15.03	0.0556	15.13	15.11	0.05505	15.06	15	0.05528	
2	15.81	15.77	0.108	15.73	15.68	0.1102	15.74	15.71	0.1091	15.77	15.77	0.1081	15.72	15.69	0.1085	
3	16.43	16.46	0.1589	16.34	16.36	0.1621	16.32	16.39	0.1606	16.35	16.42	0.1591	16.38	16.37	0.1596	
4	17.15	17.14	0.2077	17.05	17.03	0.212	16.95	17.07	0.21	16.99	17.08	0.2082	17.02	17.06	0.2087	
5	17.75	17.82	0.2545	17.67	17.7	0.2597	17.61	17.74	0.2573	17.58	17.74	0.2552	17.68	17.73	0.2557	
6	18.34	18.49	0.2993	18.33	18.37	0.3054	18.32	18.41	0.3026	18.24	18.38	0.3003	18.32	18.4	0.3007	
7	19.02	19.15	0.3421	19.02	19.03	0.3491	19	19.07	0.3459	18.97	19.03	0.3434	18.93	19.07	0.3436	
8	19.68	19.8	0.383	19.65	19.68	0.3907	19.67	19.72	0.3872	19.62	19.66	0.3845	19.6	19.72	0.3846	
9	20.34	20.44	0.4219	20.3	20.31	0.4303	20.3	20.36	0.4265	20.28	20.29	0.4238	20.26	20.36	0.4236	
10	21.07	21.07	0.4589	20.87	20.94	0.468	20.97	20.99	0.4638	20.93	20.9	0.4611	20.95	20.98	0.4607	

Figure 7.15: Sample Saq or Acq rho trace fits Clipboard data.

7.13 Clipboard → Saq trace fits or Clipboard → Acq trace fits (dimer)

Each ST trace is accompanied by the RunSTAF-generated Dimer fit and concentration curves for the three dimer forms: the [oo], [oc] and [cc] labels correspond to the fractions of dimers within the sample in the open-open, open-closed and closed-closed states, respectively.

Set Fv/Fm:	0.5	(not applied)													
Ka:	11800														
PEC:	0.32	(user defined value)													
Saq:	1					2					3				
E:	0					0					0				
Gap Index:	1					2					3				
Gap (µs):	200					400					800				
dRho', dRho:	0.6041					0.6275					0.6275				
F', Fo:	14.39					14.33					14.35				
Fm', Fm:	32.87					32.51					32.68				
AlphaPII', AlphaPII:	0.05435					0.05545					0.05504				
SigmaPII', SigmaPII:	2.665					2.719					2.699				
sF', sF:	27.12					23.23					20.25				
sFm', sFm:	30.74					30.75					31.59				
sAlphaPII', sAlphaPII:	0.03044					0.03433					0.03822				
sSigmaPII', sSigmaPII:	1.492					1.684					1.874				
	Saq 1	Fit 1	[oo] 1	[oc] 1	[cc] 1	Saq 2	Fit 2	[oo] 2	[oc] 2	[cc] 2	Saq 3	Fit 3	[oo] 3	[oc] 3	[cc] 3	
0		14.39	1	0	0		14.33	1	0	0		14.35	1	0	0	
1	15.16	14.96	0.8913	0.1087	0	15.12	14.87	0.8891	0.1109	0	15.08	14.89	0.8899	0.1101	0	
2	15.81	15.58	0.7944	0.1971	0.008464	15.73	15.48	0.7905	0.2005	0.008961	15.74	15.5	0.7919	0.1992	0.00883	
3	16.43	16.24	0.7081	0.2681	0.02381	16.34	16.13	0.7028	0.272	0.02516	16.32	16.15	0.7048	0.2704	0.02481	
4	17.15	16.92	0.6311	0.3242	0.04469	17.05	16.8	0.6249	0.328	0.04714	16.95	16.82	0.6272	0.3263	0.0465	
5	17.75	17.61	0.5625	0.3676	0.06994	17.67	17.49	0.5556	0.3708	0.07364	17.61	17.52	0.5581	0.3692	0.07268	
6	18.34	18.31	0.5014	0.4001	0.09856	18.33	18.2	0.494	0.4024	0.1036	18.32	18.22	0.4967	0.401	0.1023	
7	19.02	19.01	0.4469	0.4234	0.1297	19.02	18.9	0.4392	0.4247	0.1361	19	18.92	0.442	0.4235	0.1345	
8	19.68	19.7	0.3983	0.439	0.1627	19.65	19.59	0.3905	0.4391	0.1704	19.67	19.61	0.3933	0.4382	0.1684	
9	20.34	20.38	0.355	0.4481	0.1969	20.3	20.28	0.3472	0.4469	0.2059	20.3	20.3	0.35	0.4464	0.2036	
10	21.07	21.04	0.3164	0.4518	0.2318	20.87	20.95	0.3087	0.4493	0.242	20.97	20.97	0.3115	0.4491	0.2394	

Figure 7.16: Sample Saq or Acq dimer trace fits Clipboard data.

8 Data access: CSV functions

The CSV files functions provide access to the primary data and processed values in the most widely accessible format. All functions can be accessed through **File → CSV files**. The CSV output written to file is simultaneously copied to the Clipboard in a tab-delimited format. This format is suitable for pasting into Excel and a number of other spreadsheet-based programs.

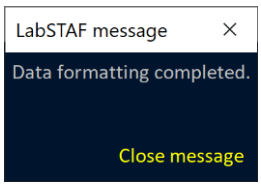

Figure 8.1: This message is shown in the top left corner of the screen when any CSV file function is used. This indicates that the CSV output has been copied to the Clipboard.

Although CSV is widely taken as an abbreviation for 'Comma Separated Values', this document uses the more general definition of 'Character Separated Values'. This is because RunSTAF allows the (default) comma separator to be replaced with a tab or semicolon. These alternatives can be accessed through:

File → CSV files → Field separator for CSV output.

A tab is always used to separate data fields with the Clipboard output, independently of the option selected for the CSV output. This allows for pasting directly from the Clipboard into Excel.

8.1 Folder-based files and Individual files

The **Folder-based DWM file**, **Folder-based PEP file**, **Folder-based rP-E file** and **Folder-based Saq file** options build a single CSV file by extracting data across all files within the selected folder. The **Individual rP-E files** and **Individual Saq files** options create a CSV file for each RunSTAF data file within the folder.

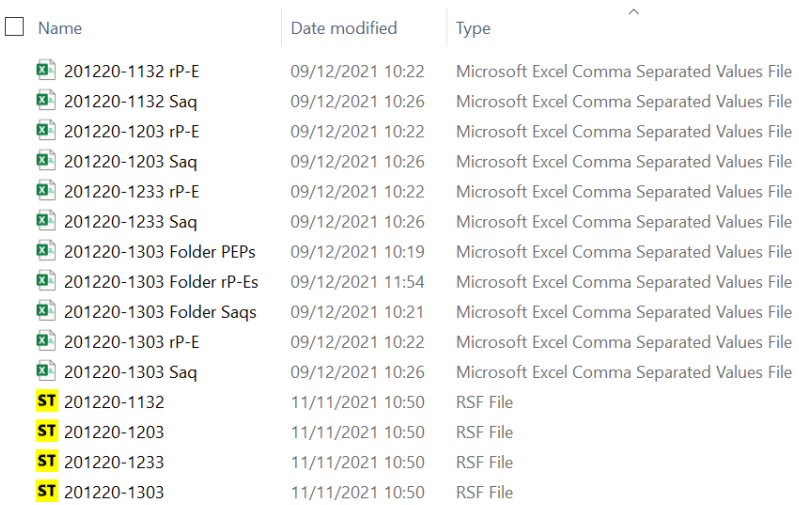

Name	Date modified	Type
201220-1132 rP-E	09/12/2021 10:22	Microsoft Excel Comma Separated Values File
201220-1132 Saq	09/12/2021 10:26	Microsoft Excel Comma Separated Values File
201220-1203 rP-E	09/12/2021 10:22	Microsoft Excel Comma Separated Values File
201220-1203 Saq	09/12/2021 10:26	Microsoft Excel Comma Separated Values File
201220-1233 rP-E	09/12/2021 10:22	Microsoft Excel Comma Separated Values File
201220-1233 Saq	09/12/2021 10:26	Microsoft Excel Comma Separated Values File
201220-1303 Folder PEPs	09/12/2021 10:19	Microsoft Excel Comma Separated Values File
201220-1303 Folder rP-Es	09/12/2021 11:54	Microsoft Excel Comma Separated Values File
201220-1303 Folder Saqs	09/12/2021 10:21	Microsoft Excel Comma Separated Values File
201220-1303 rP-E	09/12/2021 10:22	Microsoft Excel Comma Separated Values File
201220-1303 Saq	09/12/2021 10:26	Microsoft Excel Comma Separated Values File
201220-1132	11/11/2021 10:50	RSF File
201220-1203	11/11/2021 10:50	RSF File
201220-1233	11/11/2021 10:50	RSF File
201220-1303	11/11/2021 10:50	RSF File

Figure 8.2: Screenshot of folder with four original RunSTAF data files plus their csv derivatives. The naming of these files is fully automated.

The first lines of all folder-based files provide the **Project** and **Run by** fields from the first file in the folder. The **Reference** and **Note** fields from each data file are shown to the right of the main data output block of the CSV output.

8.1.1 Example of a Folder-based DWM file…

	A	B	C	D	E	F	G	H	I	J	K	L	M	N	O	P	Q
1	First file:	C:\Users\Projects\STAFES\Data\201220-210104 PEP stir unit and cultures B\A Conticribra weissflogii\201220-1132.rsf															
2																	
3	Project:	PEP and FLC tests with the stir unit															
4	Run by:	KO															
5																	
6															Mean values		
7							MLED output during data acquisition								W685		
8	Index	SN	DW slope	Date	Time	Seconds	416 nm	452 nm	452 nm	473 nm	495 nm	534 nm	594 nm	622 nm	Fo	Fm	Fv
9	1	20-0325-001	1.59	Dec-20	11:32	0	0	0.9683	1.014	0	0	0	0	0	432.7	1046	613.1
10	2	20-0325-001	1.59	Dec-20	12:03	1868	0	0.9831	1.029	0	0	0	0	0	426.5	999.3	572.9
11	3	20-0325-001	1.59	Dec-20	12:33	3642	0	0.9855	1.032	0	0	0	0	0	440.2	1024	583.5
12	4	20-0325-001	1.59	Dec-20	13:03	5419	0	0.9855	1.032	0	0	0	0	0	451.2	1052	600.3
13	5	20-0325-001	1.59	Dec-20	13:32	7192	0	0.9831	1.029	0	0	0	0	0	463.6	1068	604
14	6	20-0325-001	1.59	Dec-20	14:02	8991	0	0.9806	1.029	0	0	0	0	0	480.2	1093	612.8
15	7	20-0325-001	1.59	Dec-20	14:35	10956	0	0.9978	1.047	0	0	0	0	0	502.3	1143	640.6
16	8	20-0325-001	1.59	Dec-20	15:07	12864	0	0.9978	1.047	0	0	0	0	0	513.1	1158	644.7
17																	

→…

R	S	T	U	V	W	X	Y	Z	AA	AB	AC	AD	AE	AF	AG	AH
											SE values					
	W730				W730/W685						W685				W730	
Fv/Fm	Fo	Fm	Fv	Fv/Fm	Fo	Fm	Fv	Fv/Fm	PEC	cPEC	Fo	Fm	Fv	Fv/Fm	Fo	Fm
0.5863	103.6	233.5	129.9	0.5565	0.2394	0.2233	0.2119	0.9491	0.337	1.053	0.6453	1.694	1.065	0.00013	0.5647	0.3489
0.5733	101.2	223.4	122.2	0.5469	0.2374	0.2236	0.2133	0.954	0.3391	1.06	2.81	1.98	4.776	0.00366	0.1611	0.4642
0.57	103.7	230.3	126.6	0.5498	0.2354	0.2249	0.217	0.9647	0.345	1.078	2.465	2.572	0.9475	0.00145	0.7698	0.3235
0.5709	106.7	235	128.3	0.546	0.2365	0.2235	0.2137	0.9563	0.3398	1.062	0.9473	2.24	1.311	0.00014	0.5082	0.3191
0.5657	110.1	239.6	129.5	0.5404	0.2375	0.2244	0.2144	0.9552	0.3408	1.065	2.407	2.962	2.265	0.00171	0.3945	0.1425
0.5607	114.5	246.1	131.6	0.5347	0.2385	0.2251	0.2147	0.9537	0.3414	1.067	1.328	2.764	3.515	0.00194	0.3117	0.4613
0.5605	119.9	257.9	138	0.535	0.2388	0.2257	0.2154	0.9545	0.3425	1.07	0.8986	1.855	0.9606	0.00009	0.2055	0.3872
0.5568	123.9	264.1	140.2	0.5309	0.2414	0.2281	0.2174	0.9533	0.3457	1.08	1.098	0.522	1.237	0.00098	0.3912	0.07177

→…

AI	AJ	AK	AL	AM	AN	AO	AP	AQ	AR
		W730/W685							
Fv	Fv/Fm	Fo	Fm	Fv	Fv/Fm	PEC	cPEC	Reference	Note
0.2227	0.00176	0.00123	0.00048	0.00058	0.00287	0.00092	0.00289	Conticribra weissflogii	Pre-diluted 36 h before
0.3031	0.00022	0.00192	0.00004	0.00127	0.00575	0.00202	0.00632	Conticribra weissflogii	Pre-diluted 36 h before
0.9361	0.00362	0.00048	0.00068	0.00155	0.00403	0.00246	0.0077	Conticribra weissflogii	Pre-diluted 36 h before
0.4937	0.00203	0.00066	0.00058	0.00129	0.00356	0.00204	0.00639	Conticribra weissflogii	Pre-diluted 36 h before
0.5186	0.00188	0.00171	0.00075	0.00166	0.00576	0.00264	0.00824	Conticribra weissflogii	Pre-diluted 36 h before
0.6641	0.00183	0.00118	0.00091	0.00214	0.00606	0.00341	0.01065	Conticribra weissflogii	Pre-diluted 36 h before
0.1909	0.00018	0.00071	0.00062	0.00057	0.00037	0.0009	0.00283	Conticribra weissflogii	Pre-diluted 36 h before
0.4136	0.00152	0.00113	0.00007	0.00076	0.0036	0.00121	0.00378	Conticribra weissflogii	Pre-diluted 36 h before

Figure 8.3: Example of a folder-based DWM file comprising eight files.

8.1.2 Example of a Folder-based PEP file…

The included plots were generated within Excel. The **ALED normalized values** are the MLED waveband values of F_v and σ_{PII} normalized to the ALED values. For example, an ALED normalized σ_{PII} value of 2.0 would simply mean that the σ_{PII} for that waveband is twice as high as the ALED σ_{PII}.

First file:	C:\Desktop\Ek test files\201220-1132.rsf																
SN:	20-0325-001				Project:	PEP and FLC tests with the stir unit											
Start date:	Dec 20 2020				Run by:	KO											
			Mean values														
			Fv								Sigma						
		Actual nm	414.8	447	469.9	491.3	525.8	593.9	622.5	414.8	447	469.9	491.3	525.8	593.9	622.5	
	Date	Time	416 nm	452 nm	473 nm	495 nm	534 nm	594 nm	622 nm	416 nm	452 nm	473 nm	495 nm	534 nm	594 nm	622 nm	
	Dec-20	11:32	300.5	325.6	249.9	219.8	173.2	104.6	163.2	2.227	2.874	2.146	2.093	0.9146	0.5306	0.6946	
	Dec-20	12:03	277.3	301.7	229.8	199.8	160.1	93.28	141.2	2.225	2.889	2.155	2.062	0.886	0.4521	0.6804	
	Dec-20	12:33	281.2	308.5	231.3	205.4	163.1	65.6	143.8	2.233	2.885	2.147	2.105	0.8871	0.5012	0.6714	
	Dec-20	13:03	291.5	313	236.4	208.5	165.2	75.23	156.1	2.236	2.895	2.142	2.098	0.8888	0.4605	0.673	
	Dec-20	13:32	295.8	316.2	241.7	207.5	167	79.71	170.5	2.241	2.903	2.121	2.103	0.9014	0.4674	0.6903	
	Dec-20	14:02	299	320.4	241.6	210.5	169.5	84.06	168.7	2.25	2.91	2.156	2.09	0.9096	0.4923	0.7094	

→

ALED normalized values															
Fv							Sigma							File details	
414.8	447	469.9	491.3	525.8	593.9	622.5	414.8	447	469.9	491.3	525.8	593.9	622.5		
416 nm	452 nm	473 nm	495 nm	534 nm	594 nm	622 nm	416 nm	452 nm	473 nm	495 nm	534 nm	594 nm	622 nm	Reference	Note
1.471	1.594	1.224	1.076	0.8479	0.512	0.799	1.466	1.892	1.413	1.378	0.6022	0.3494	0.4574	C. weissflogii	Pre-diluted 36 h
1.482	1.612	1.228	1.068	0.8555	0.4986	0.7547	1.489	1.934	1.442	1.38	0.593	0.3026	0.4554	C. weissflogii	Pre-diluted 36 h
1.52	1.667	1.25	1.11	0.8817	0.3545	0.7772	1.481	1.914	1.424	1.396	0.5885	0.3324	0.4454	C. weissflogii	Pre-diluted 36 h
1.533	1.646	1.243	1.096	0.869	0.3957	0.8209	1.49	1.93	1.428	1.398	0.5924	0.307	0.4487	C. weissflogii	Pre-diluted 36 h
1.528	1.634	1.249	1.072	0.8632	0.4119	0.8809	1.489	1.929	1.409	1.397	0.599	0.3106	0.4588	C. weissflogii	Pre-diluted 36 h
1.525	1.634	1.232	1.074	0.8645	0.4287	0.8604	1.483	1.917	1.421	1.377	0.5993	0.3244	0.4674	C. weissflogii	Pre-diluted 36 h

Figure 8.4: Example of a folder-based PEP file comprising six files.

8.1.3 Example of a Folder-based rP-E file…

The folder-based rP-E file provides a synopsis for each file in the folder.

	A	B	C	D	E	F	G	H	I	J	K	L	M
1	First file:	C:\Desktop\Ek test files\201220-1132.rsf											
2													
3	SN:	20-0325-001			Project:	PEP and FLC tests with the stir unit							
4	Start date:	Dec 20 2020			Run by:	KO							
5													
6							rP-E values						
7		Date	Time	Seconds	Minutes	PEC	High E	Alpha	Ek	Beta	EkBeta	rPm	JVPIIm
8		Dec-20	11:32	0	0	0.3376	600	0.5214	167	0.02651	950	75.51	64.01
9		Dec-20	12:03	1868	31.13	0.3397	666	0.5625	187	0.07209	313	84.39	71.35
10		Dec-20	12:33	3642	60.7	0.3422	746	0.5615	196	0.05063	459	91.65	79.7
11		Dec-20	13:03	5419	90.32	0.3373	883	0.5591	211	0.05265	451	97.89	86.78
12		Dec-20	13:32	7192	119.9	0.3379	983	0.5468	236	0.0719	376	103.6	93.76
13		Dec-20	14:02	8991	149.9	0.34	1011	0.5497	245	0.05946	539	109.1	103.7
14													

→…

	N	O	P	Q	R	S	T	U	V	W	X	Y	Z
		Dark (Step 1 Up) values								Details			
	GOPIIm	Fo	Fm	Fv/Fm	Fv/Fmc	AlphaPII	SigmaPII	Rho	Tau	Sample °C	System °C	Reference	Note
	57.61	39.43	94.16	0.5812	0.5812	0.05238	2.642	0.3729	3460	18.7	22.9	C. weissflogii	Pre-diluted 36 h
	64.22	38.48	89.94	0.5722	0.5722	0.05448	2.708	0.3688	3867	19	23.7	C. weissflogii	Pre-diluted 36 h
	71.73	39.29	91.88	0.5723	0.5723	0.05479	2.716	0.3725	3420	19.5	24.7	C. weissflogii	Pre-diluted 36 h
	78.1	40.43	93.92	0.5695	0.5695	0.055	2.727	0.3836	4976	19.9	25.6	C. weissflogii	Pre-diluted 36 h
	84.38	41.21	95.69	0.5694	0.5694	0.05509	2.738	0.3753	5504	20.2	25.4	C. weissflogii	Pre-diluted 36 h
	93.29	42.53	97.38	0.5633	0.5633	0.05531	2.752	0.3913	6128	20.6	25.8	C. weissflogii	Pre-diluted 36 h

Figure 8.5: Example of a folder-based rP-E file comprising six files.

8.1.4 Example of a Folder-based Saq file…

This copies values for a wide range of derived and primary parameters to the Clipboard. The headers of each column match with the **Plot selection** labels on the data screen.

	A	B	C	D	E	F	G	H	I	J	K	L	M
1	First file:	C:\Desktop\Cvulgaris\211023-1023.rsf											
2													
3	SN:	19-0105-006			Project:	N-limited grown							
4	Start date:	Oct 23 2021			Run by:	ABC							
5													
6													
7		x-axis				Rho fit parameters							
8		Gap (µs)	Time (s)	Saq	E	Rho	sRho	AlphaPII	sAlphaPII	SigmaPII	sSigmaPII	SE	sSE
9	Oct 23 2021	200	0	1	0	0.1351	0.03258	0.05201	0.02688	2.984	1.542	0.05957	0.02338
10	Time: 10:23	400	0	2	0	0.1352	0.02344	0.05238	0.0437	3.005	2.507	0.05271	0.03182
11	Sample: 23°C	800	0	3	0	0.2116	0.01005	0.05282	0.04766	3.03	2.734	0.07899	0.04303
12	System: 25.8°C	1600	0	4	0	0.1368	0.1432	0.05263	0.04877	3.019	2.798	0.05614	0.07342
13		3200	0	5	0	0.1354	0.09427	0.05218	0.04797	2.993	2.752	0.05977	0.0633
14		6400	0	6	0	0.1342	0.01851	0.05193	0.04624	2.979	2.653	0.06001	0.05338

→…

Figure 8.6: Leftmost columns from a folder-based Saq file.

8.2 Auto archive report line

Activated through **File → csv files → Auto archive report line**

This function generates a simple summary CSV file each time a RunSTAF data file is completed. The default comma used to separate adjacent values can be switched to a tab or semicolon.

Accessed through F**ile → CSV files →Field separator for CSV output**

The report line CSV has the same filename as the associated RunSTAF data file.

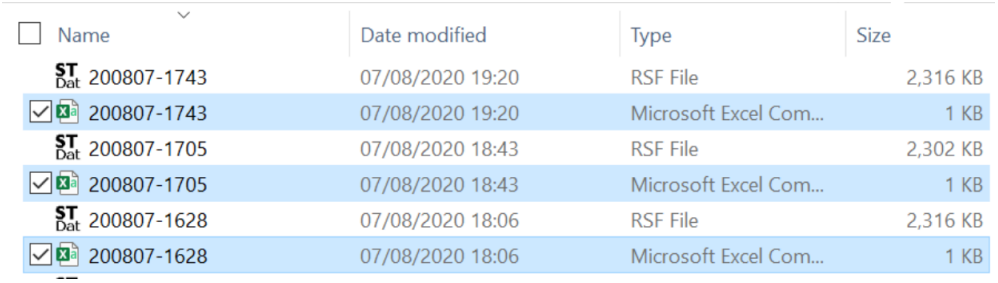

Name	Date modified	Type	Size
200807-1743	07/08/2020 19:20	RSF File	2,316 KB
200807-1743	07/08/2020 19:20	Microsoft Excel Com...	1 KB
200807-1705	07/08/2020 18:43	RSF File	2,302 KB
200807-1705	07/08/2020 18:43	Microsoft Excel Com...	1 KB
200807-1628	07/08/2020 18:06	RSF File	2,316 KB
200807-1628	07/08/2020 18:06	Microsoft Excel Com...	1 KB

Figure 8.7: Screenshot of folder containing standard RunSTAF binary files and associated report line CSV files

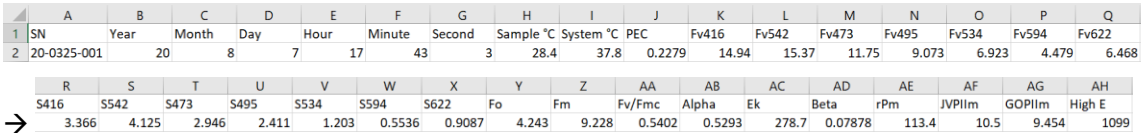

	A	B	C	D	E	F	G	H	I	J	K	L	M	N	O	P	Q
1	SN	Year	Month	Day	Hour	Minute	Second	Sample °C	System °C	PEC	Fv416	Fv542	Fv473	Fv495	Fv534	Fv594	Fv622
2	20-0325-001	20	8	7	17	43	3	28.4	37.8	0.2279	14.94	15.37	11.75	9.073	6.923	4.479	6.468

	R	S	T	U	V	W	X	Y	Z	AA	AB	AC	AD	AE	AF	AG	AH
	S416	S542	S473	S495	S534	S594	S622	Fo	Fm	Fv/Fmc	Alpha	Ek	Beta	rPm	JVPIIm	GOPIIm	High E
→	3.366	4.125	2.946	2.411	1.203	0.5536	0.9087	4.243	9.228	0.5402	0.5293	278.7	0.07878	113.4	10.5	9.454	1099

Figure 8.8: Example Auto archive report line file.

9 Data access: COM port output

There are currently three COM port data streams supported by RunSTAF. All three output data in CSV format.

- SPAR sensor output at programmed intervals
- FLC steps at the completion of each FLC in a repeating sequence
- Saq data at the completion of each Group during acquisition

The SPAR sensor COM output always has the same configuration. The FLC steps and Saq Group outputs include a wide range of formatting options.

9.1 COM port configuration

The COM port settings for data output are always as shown below. These values are automatically set by RunSTAF.

Baud rate:	115200
Byte size:	8
Parity:	NONE
Stop bits:	1
Flow control:	NONE

9.2 Finding the COM port

The number of the COM port for data output (SPAR sensor, FLC steps or Saq groups) must be set by the user and must be between 1 and 64. It is possible to set the same COM port for more than one data stream. Device Manager provides a list of connected COM ports, as shown in Figure 9.1.

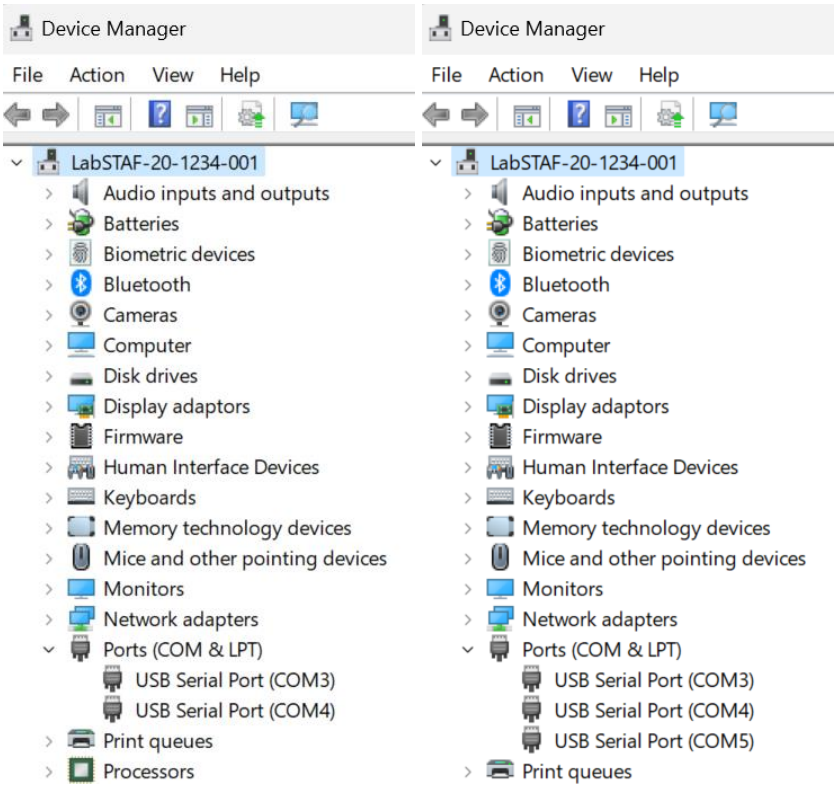

Figure 9.1: The COM port number for data output can be found using Device Manager. In this example, the left screen crop shows a LabSTAF attached to **COM3** and **COM4**. The right screen crop shows the COM output port as **COM5**.

9.3 SPAR sensor COM and CSV file output

SPAR sensor data can be output in CSV format through the defined COM port and/or written to a local file in CSV format. The COM port number for SPAR data output needs to be set through the SPAR sensor screen. This can be reached through the menu bar command:

Settings → View SPAR sensor screen

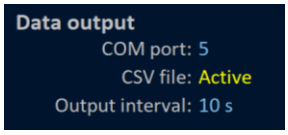

Figure 9.2: Screen crop from the **SPAR sensor screen** showing **COM port 5** set for output and the **CSV file Active**. The **Output interval** defines the output frequency for both the **COM port** and writing to the local **CSV file**.

9.3.1 SPAR sensor COM port output

Output term	Structure
Start flag (6 characters)	***SPAR** + **carriage return**
Date and time stamps (14 characters)	**yymmdd,hhmmss,**
SN of the SPAR sensor (12 characters)	**xx-xxxx-xxx,**
Lambda offset	**unsigned integer,**
Lambda multiplier	**floating point** + **carriage return**
Integration time (µs)	**unsigned integer,**
Internal temperature (°C)	**floating point,**
Orientation of the SPAR sensor (±°)	**signed integer,**
Photon irradiance between 380 and 660 nm (µmol photons m^{-2} s^{-1})	**floating point,**
Baseline to subtract from each data point	**unsigned integer** + **carriage return**
192 raw data values (no comma after last value)	**four digit unsigned integer,…**
End flag (4 characters)	***END**

Table 9.1: The structure of the SPAR sensor COM port CSV output.

9.3.2 SPAR sensor sample COM port output

Figure 9.3 provides an example of the SPAR sensor COM output.

```
*SPAR
221018,170010,22-1234-001,321,2.30
12500,30.8,+015,30.0,392
0424,0426,0418,0424,0415,0414,0424,0418,0423,0418,0415,0421,0424,0431,0447,0463,0494,0527,0547,058
3,0609,0637,0672,0701,0726,0742,0739,0767,0761,0773,0815,0868,0922,0989,1074,1239,1367,1517,1577,16
01,1646,1660,1650,1642,1587,1564,1548,1481,1475,1487,1537,1602,1654,1687,1770,1805,1858,1923,1927,1
975,1998,2002,1998,2028,2019,2003,1996,1986,1962,1915,1878,1810,1802,1795,1735,1727,1679,1643,1591,
1568,1546,1515,1514,1509,1508,1535,1569,1567,1566,1582,1564,1580,1583,1591,1598,1593,1611,1620,159
6,1613,1598,1571,1558,1524,1558,1515,1504,1508,1479,1477,1494,1476,1484,1454,1435,1435,1420,1407,14
26,1428,1428,1431,1420,1427,1403,1402,1387,1391,1388,1388,1352,1342,1326,1317,1302,1306,1310,1315,1
292,1320,1286,1284,1264,1244,1230,1215,1206,1219,1206,1231,1236,1230,1226,1215,1202,1196,1181,1171,
1157,1148,1122,1091,1035,1037,1023,1020,1038,1039,1046,1039,1028,1039,1025,1025,1026,1001,0993,095
4,0910,0894,0868,0840,0836,0827,0840,0844,0836,0863,0856,0873,0874,0874
*END
```

Figure 9.3: Sample SPAR sensor COM output.

9.3.3 Processing of SPAR sensor COM output

The CSV format provides compatibility with a range of data handling platforms. The example below provides an Excel™ template that incorporates the simple steps required to generate a normalised plot of the SPAR data.

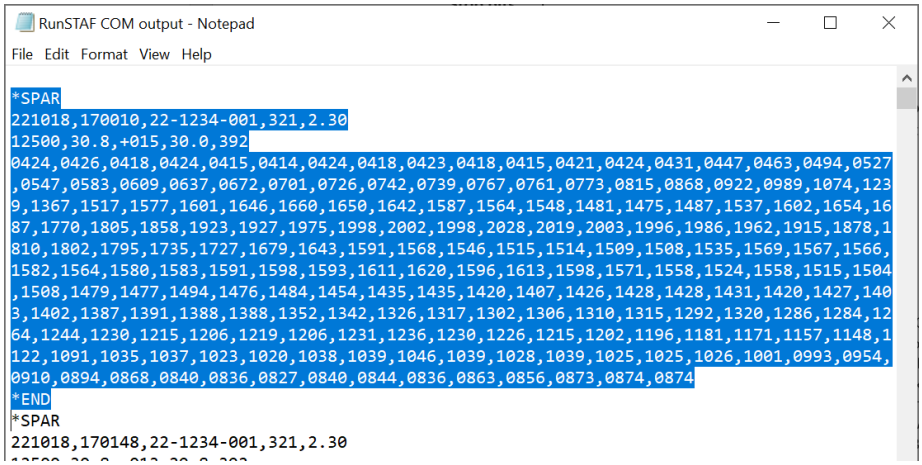

Figure 9.4: For this example, the COM data stream from the SPAR sensor was written to a txt file through the Windows Notepad application. This screen crop shows the output from a single scan highlighted for copying.

The copied data were be pasted into Excel™ using the Text Import Wizard:

Home → Paste → Use Text Import Wizard…

The screen crops below show the correct selections for importing the SPAR data…

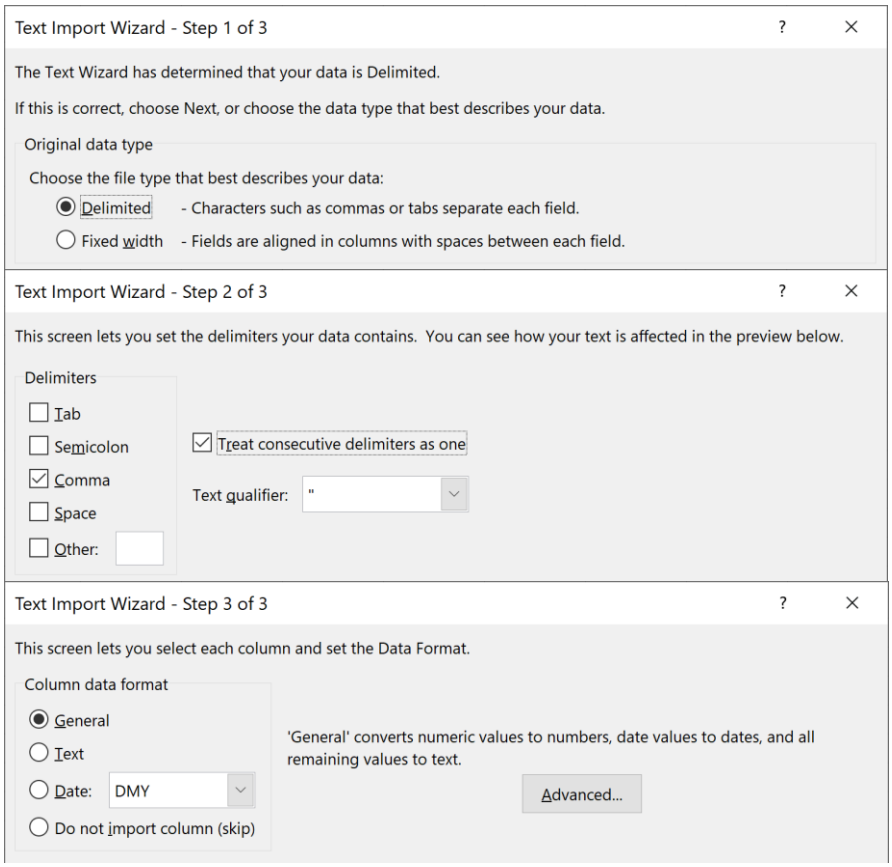

Figure 9.5: The three Steps required to import SPAR sensor CSV text using the Excel™ Text Import Wizard.

The screen crop in Figure 9.6 shows the SPAR data pasted into Excel™ using the Wizard.

	A	B	C	D	E	F	G	H	I
1	*SPAR								
2	221018	170010	22-1234-0(	321	2.3				
3	12500	30.8	15	30	392				
4	424	426	418	424	415	414	424	418	423
5	*END								

Figure 9.6: Screen crop showing the SPAR sensor COM output text pasted into Excel™ using the Text Import Wizard. Line 4 contains the 192 raw data values.

The next screen crop, in Figure 9.7, shows the additions to the worksheet to build a template.

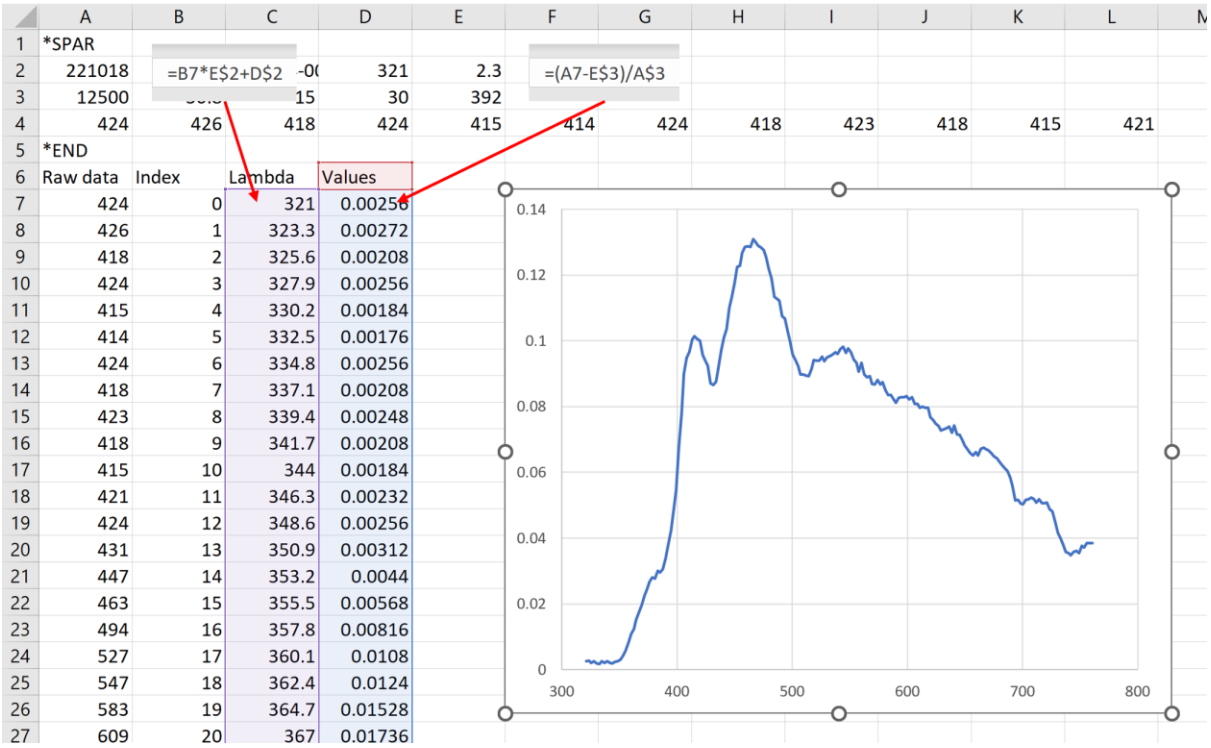

	A	B	C	D	E	F	G	H	I	J	K	L
1	*SPAR											
2	221018			321	2.3							
3	12500		15	30	392							
4	424	426	418	424	415	414	424	418	423	418	415	421
5	*END											
6	Raw data	Index	Lambda	Values								
7	424	0	321	0.00256								
8	426	1	323.3	0.00272								
9	418	2	325.6	0.00208								
10	424	3	327.9	0.00256								
11	415	4	330.2	0.00184								
12	414	5	332.5	0.00176								
13	424	6	334.8	0.00256								
14	418	7	337.1	0.00208								
15	423	8	339.4	0.00248								
16	418	9	341.7	0.00208								
17	415	10	344	0.00184								
18	421	11	346.3	0.00232								
19	424	12	348.6	0.00256								
20	431	13	350.9	0.00312								
21	447	14	353.2	0.0044								
22	463	15	355.5	0.00568								
23	494	16	357.8	0.00816								
24	527	17	360.1	0.0108								
25	547	18	362.4	0.0124								
26	583	19	364.7	0.01528								
27	609	20	367	0.01736								

Figure 9.7: Screen crop incorporating the steps required to generate a plot from the SPAR sensor COM output.

To generate the plot:

- The raw data values have been copied from **Cells A4:GJ4** and transposed to **Cells A7:A198** (pasted into **Cell A7** using the **Transpose** option)
- The Index column has been generated in **Column B** as a series running from **0** to **191** (against the 192 raw data values)
- The formula in **Cell C7** generates the first **Lambda** value
- The formula in **Cell C7** has been extended through the entire **Lambda** column (**Cells C7:C198**)
- The formula in **Cell C7** subtracts the baseline (**Cell E3**) and normalises the raw data value to the integration time (**Cell A3**)
- The formula in **Cell D7** has been extended through the entire **Values** column (**Cells D7:D198**)

The line plot within Figure 9.7 shows **Values** against **Lambda**. The **Lambda** range is from **321** nm to **760.3** nm. Because the SPAR COM output always has the same structure, pasting an alternative block into **Cell A1** will generate a new plot that is baseline corrected and normalized to the integration time.

9.3.4 SPAR sensor CSV file structure

SPAR sensor CSV files are automatically written to this location:

C:\Users\...\Documents\CT-RunSTAF\SPAR\CSV files

The file name is formed from the serial number of the SPAR sensor without dashes plus a six digit date stamp (yymmdd). For example:

221234001-221016.csv

If the **CSV file** option is **Active**, a new file is automatically started each day. The file structure of the header is shown in Table 9.2.

Output term	Symbol	Sample output
SN of the SPAR sensor	---	22-1234-001
Last calibration	---	Sep 02 2022
The baseline offset	**BO**	390
The baseline slope (ms)	**BSms**	0.1285
The baseline slope (°C)	**BSdc**	0.014
Lambda offset (nm)	---	321
Lambda multiplier	---	0.23
Photon multiplier	---	1.2

Table 9.2: The structure of each of the terms within the header of the SPAR sensor CSV file.

Each SPAR acquisition is then added as a single line. The structure is shown in Table 9.3.

Output	Symbol	Format	Sample
Date	---	yymmdd	221006
Time	---	hhmmss	204915
Integration time (µs)	**IT**	integer	6250
Internal temperature (°C)	**DC**	floating point	32.1
Angle (±°)	---	signed integer	89
Photon irradiance (E) as µmol photons m^{-2} s^{-1}	---	floating point	57.4
Baseline	**BS**	integer	391
192 raw data values (Spectral output..)	---	integer	2024

Table 9.3: The structure of each acquisition within the PAR sensor CSV file.

The PEP-based spectral corrections within RunSTAF cover the spectral range between 380 nm and 660 nm. Other applications may require isolation of a different subset of the total SPAR range. For example, the widely applied definition of Photosynthetically Active Radiation (PAR) runs between 400 nm and 700 nm. To provide flexibility, the SPAR output covers the spectral range from 320 nm to 760.3 nm.

The SPAR COM and CSV file outputs both include a baseline value with each scan. This value is generated using the formulae below.

Slope = BSms + BSms x BSdc x ([DC x 10] – 300)

BS = (IT / 1000) x Slope + BO

Where all required terms within the formulae are provided within the **Symbol** columns of Tables 9.2 and 9.3.

9.3.5 Processing of SPAR sensor CSV files

This section runs through the simple steps required to generate a normalised plot of the SPAR data.

The screen crop below is from a SPAR sensor CSV file opened in Excel™. This is the **CSV** worksheet.

	A	B	C	D	E	F	G	H	I	J	K
1	SN:	22-1234-001									
2	Last calibration:	Oct 18 2022									
3	Baseline offfset:	390									
4	Baseline slope (ms):	0.1285									
5	Baseline slope (°C):	0.014									
6	Lambda offset:	321									
7	Lambda multiplier:	2.3									
8	Photon multiplier:	1.2									
9											
10	Date	Time	µs	°C	°Angle	E	Baseline	Spectral output...			
11	221018	150716	6250	32.1	15	57.4	391	432	431	426	438
12	221018	150720	6250	32.2	15	56.5	391	429	431	426	431
13	221018	150724	6250	32.1	15	58.2	391	431	431	424	431
14	221018	150744	6250	32.2	16	56.5	391	434	431	427	437

Figure 9.8: A screen crop from the **CSV** worksheet in this example.

The next screen crop shows a second worksheet, which has been used to process the CSV values. This is the **DATA** worksheet.

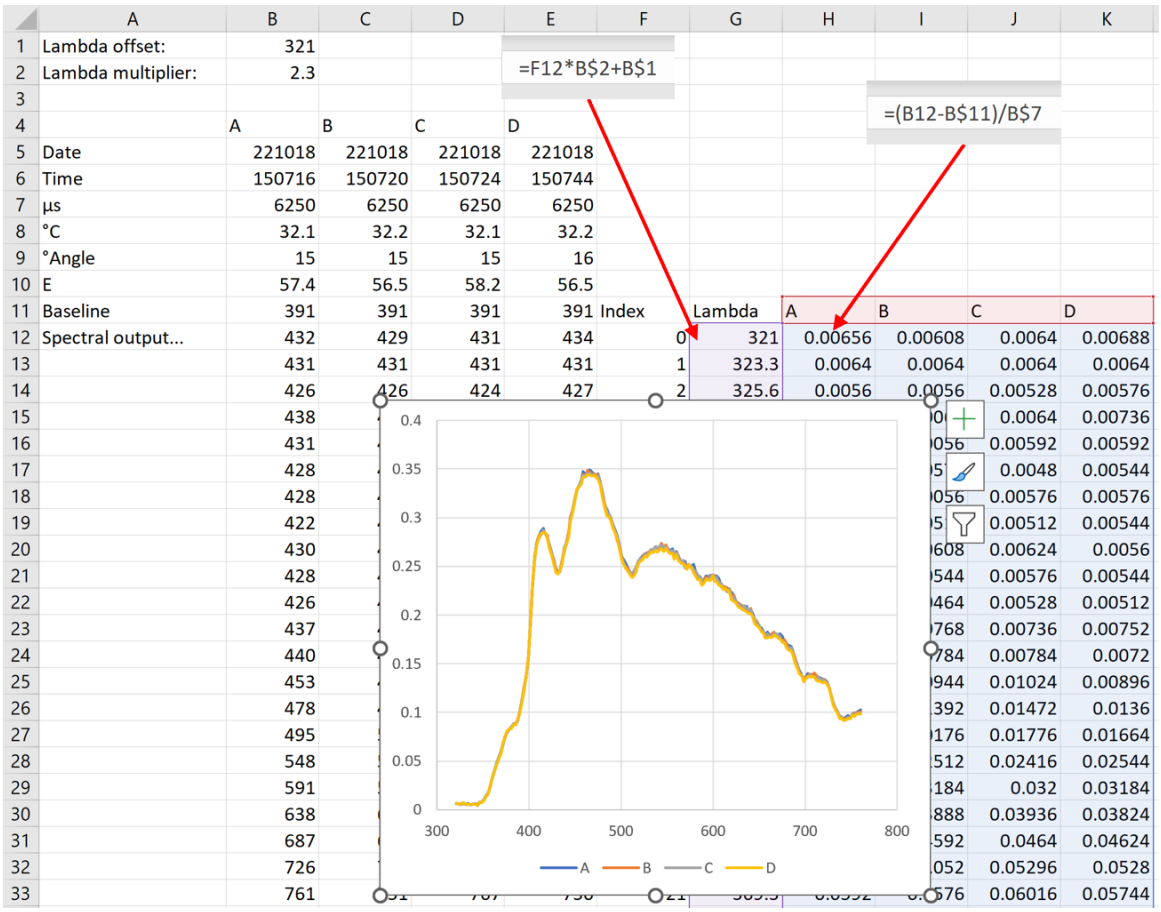

	A	B	C	D	E	F	G	H	I	J	K
1	Lambda offset:	321									
2	Lambda multiplier:	2.3									
3											
4		A	B	C	D						
5	Date	221018	221018	221018	221018						
6	Time	150716	150720	150724	150744						
7	µs	6250	6250	6250	6250						
8	°C	32.1	32.2	32.1	32.2						
9	°Angle	15	15	15	16						
10	E	57.4	56.5	58.2	56.5						
11	Baseline	391	391	391	391	Index	Lambda	A	B	C	D
12	Spectral output...	432	429	431	434	0	321	0.00656	0.00608	0.0064	0.00688
13		431	431	431	431	1	323.3	0.0064	0.0064	0.0064	0.0064
14		426	426	424	427	2	325.6	0.0056	0.0056	0.00528	0.00576
15		438								0.0064	0.00736
16		431								0.00592	0.00592
17		428								0.0048	0.00544
18		428								0.00576	0.00576
19		422								0.00512	0.00544
20		430								0.00624	0.0056
21		428								0.00576	0.00544
22		426								0.00528	0.00512
23		437								0.00736	0.00752
24		440								0.00784	0.0072
25		453								0.01024	0.00896
26		478								0.01472	0.0136
27		495								0.01776	0.01664
28		548								0.02416	0.02544
29		591								0.032	0.03184
30		638								0.03936	0.03824
31		687								0.0464	0.04624
32		726								0.05296	0.0528
33		761								0.06016	0.05744

Figure 9.10: A screen crop from the **DATA** worksheet in this example.

- The first four scans from the CSV worksheet (**CSV → Cells A11:GQ14**) have been transposed to the DATA worksheet (pasted into **DATA → Cell B5**)
- **CSV → Cells A10:H10** have also been transposed to the DATA worksheet (pasted into **DATA → Cell A5**)

- **CSV → Cells A6:B7** have been copied and pasted into **DATA → Cell A1**

On the **DATA** worksheet:

- The four scans have been labelled as **A**, **B**, **C** and **D**
- The **Index** column contains values of **0** to **191**
- The formula in **Cell G12** generates the Lambda value for the first data point
- The formula in **Cell G12** has been extended through to **Cell G203**
- The formula in **Cell H12** subtracts the baseline and normalises the raw data value to the integration time
- The formula in **Cell H12** has been extended through to **Cell K203** to cover all raw data values

The line plot within Figure 9.10 shows all four spectra.

9.4 The COM port data screen

The COM port data screen can be accessed through:

Settings → View COM port data screen

Figure 9.11 shows all default selections for the FLC steps and Saq groups output. The **COM port** has been set to **5** for both output streams.

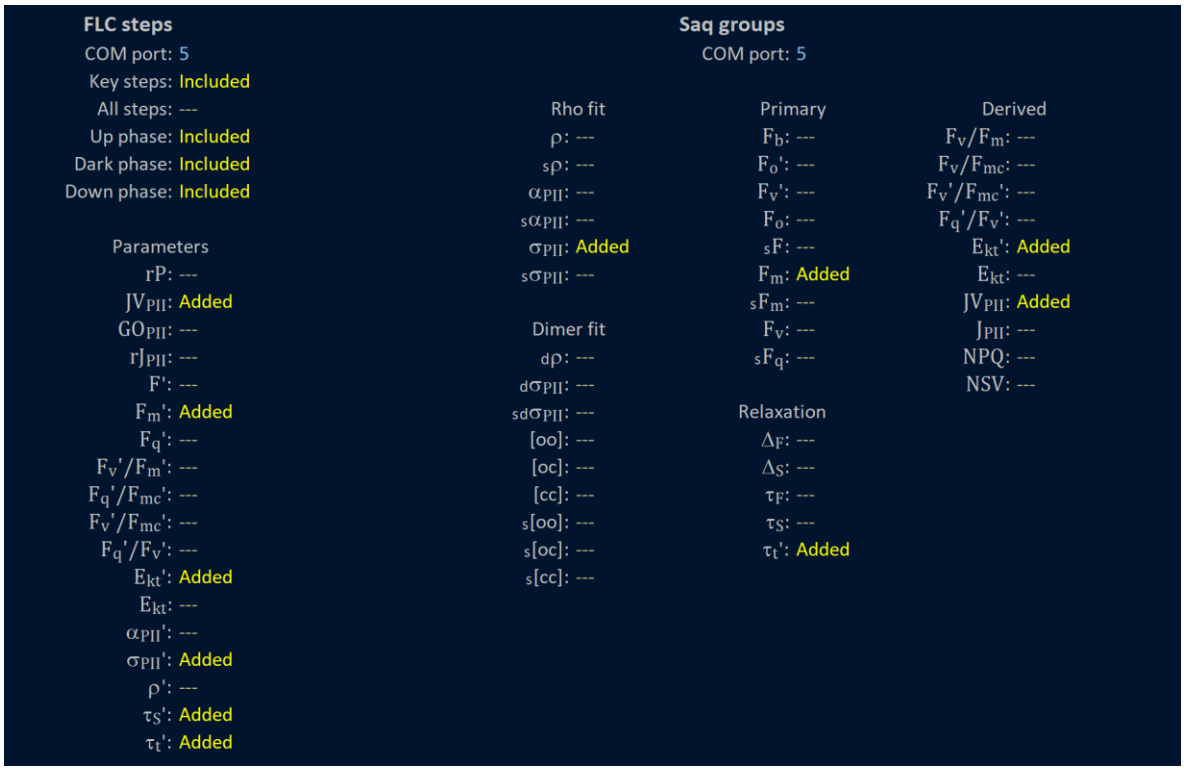

Figure 9.11: Crop from the COM port data screen showing the options for the **FLC steps** and **Saq groups**

9.5 FLC steps COM output

The **Key steps** and **All steps** options cannot be **Included** together. The Structure of the **Key steps** output is shown in Table 9.4. The **Up phase**, **Dark phase** and **Down phase** are only valid if the **All steps** option is **Included**. The structure of the **All steps** output is shown in Table 9.5. All **Added** fields under **Parameters** are **Included** for all steps within **Key steps** or **All steps**. Table 9.6 provides a list of the single character code prefix for each **Added** parameter.

Output term	Structure
Start flag (11 characters)	***FLC STEPS** plus **carriage return**
Date and time stamps (14 characters)	**yymmdd,hhmmss,**
SN of the SPAR sensor (12 characters)	**xx-xxxx-xxx,**
The values of α, E_k and P_m from the rP-E fit	**floating point, unsigned integer, floating point** plus **carriage return**
Up dark flag (8 characters)	**Up dark** plus **carriage return**
Selected **Parameters** data stream	**Variable length**
Up Ek flag (6 characters) = first step after Ek	**Up Ek** plus **carriage return**
Selected **Parameters** data stream	**Variable length**
Up last flag (8 characters)	**Up last** plus **carriage return**
Selected **Parameters** data stream	**Variable length**
Dark last flag (10 characters)	**Dark last** plus **carriage return**
Selected **Parameters** data stream	**Variable length**
Down dark flag (10 characters)	**Down dark** plus **carriage return**
Selected **Parameters** data stream	**Variable length**
End flag (4 characters)	***END**

Table 9.4: FLC steps COM port output structure (Key steps).

Output term	Structure
Start flag (11 characters)	***FLC STEPS** plus **carriage return**
Date and time stamps (14 characters)	**yymmdd,hhmmss,**
SN of the SPAR sensor (12 characters)	**xx-xxxx-xxx,**
The values of α, E_k and P_m from the rP-E fit	**floating point, unsigned integer, floating point** plus **carriage return**
Up flag (3 characters) if the Up phase is present	**Up plus carriage return**
Selected **Parameters** data stream	**Variable length**
Dark flag (5 characters) if the Dark phase is present	**Dark** plus **carriage return**
Selected **Parameters** data stream	**Variable length**
Down flag (5 characters) if the Down phase is present	**Down** plus **carriage return**
Selected **Parameters** data stream	**Variable length**
End flag (4 characters)	***END**

Table 9.5: FLC steps COM port output structure (All steps).

Code	Parameter	Format
a	rP	FLOAT
b	JV_{PII}	FLOAT
c	GO_{PII}	FLOAT
d	rJ_{PII}	FLOAT
e	F_o or F'	FLOAT
f	F_m or F_m'	FLOAT
g	F_v or F_v'	FLOAT
h	F_v/ F_m or F_q'/ F_m'	FLOAT
i	F_v/ F_{mc} or F_q'/ F_{mc}'	FLOAT

Code	Parameter	Format
j	F_v'/ F_{mc}'	FLOAT
k	F_q'/ F_v'	FLOAT
l	E_{kt}'	UINT
m	E_{kt}	UINT
n	α_{PII} or α_{PII}'	FLOAT
o	σ_{PII} or σ_{PII}'	FLOAT
p	ρ or ρ'	FLOAT
q	τ_S or τ_S'	UINT
r	τ_t'	UINT

Table 9.6: The output codes used to define each parameter within the FLC steps COM output. The terms in the **Parameter** columns match up with the step data parameters on the Auto FLC home screen.

Figures 9.12 and 9.13 provide sample FLC steps COM output with **Key steps** and **All steps** set as **Included**, respectively. Each line of parameters starts with the step number, the actinic light level (E) at that step in µmol photons m^{-2} s^{-1} and the length of the step in seconds. The **Added** parameters are then listed in sequence, with each parameter starting with the single character codes listed in Table 9.6.

```
*FLC STEPS
221022,142956,19-0105-004
0.360,189,54.83
Up dark
1,0,60,b0,f17.97,l,o3.928,q24421,r
Up Ek
8,242,60,b13.58,f19.18,l177.9,o3.482,q7664,r4670
Up last
12,633,60,b15.28,f13.49,l196.7,o2.814,q8475,r5226
Dark last
12,633,60,b,f15.18,l,o4.034,q11056,r
Down dark
1,0,60,b,f20.4,l,o4.547,q9691,r
*END
```

Figure 9.12: Sample FLC steps COM output with **Key steps** set to **Included**.

```
*FLC STEPS
221022,140157,19-0105-004
0.365,176,54.19
Up
1,0,60,b0,f18.52,l,o4.026,q33275,r
2,17,180,b1.83,f22.23,l58.73,o4.291,q8891,r11202
3,39,60,b3.648,f23.11,l83.35,o4.283,q6555,r7908
4,64,60,b5.696,f23.8,l104.5,o4.207,q13872,r6423
5,96,60,b7.929,f24,l122.1,o4.012,q10245,r5764
6,134,60,b9.949,f22.66,l139.9,o3.874,q8443,r5209
7,181,60,b11.84,f20.71,l159.8,o3.66,q8688,r4827
8,237,60,b13.45,f19.28,l172,o3.506,q5808,r4682
9,306,60,b14.52,f17.57,l180.8,o3.268,q6949,r4778
10,390,60,b15.12,f15.97,l186.8,o3.092,q2021,r4887
11,492,60,b15.36,f14.73,l189.9,o2.888,q8859,r5148
12,617,60,b15.32,f13.68,l192.4,o2.625,q13744,r5590
Dark
12,617,60,b,f15.32,l,o4.02,q10117,r
Down
1,0,60,b,f20.31,l,o4.578,q11312,r
2,17,60,b1.916,f20.2,l182,o4.252,q5723,r3648
6,134,60,b10.03,f20.14,l174,o3.628,q9179,r4472
7,181,60,b11.52,f18.11,l182.1,o3.403,q11077,r4554
8,237,120,b12.58,f16.7,l180.8,o3.349,q4176,r4663
*END
```

Figure 9.13: Sample FLC steps COM output with **All steps** set to **Included**. The **Up phase**, **Dark phase** and **Down phase** are all **Included**.

9.6 Saq groups COM output

The Saq groups options are shown in Figure 9.11. Table 9.7 shows the structure of the Saq groups COM output. Table 9.8 provides a list of the single character code prefix for each **Added** parameter.

Output term	Structure
Start flag (9 characters)	***SAQ GRP** plus **carriage return**
Date and time stamps (14 characters)	**yymmdd,hhmmss,**
SN of the SPAR sensor (12 characters)	**xx-xxxx-xxx,**
The actinic light level (E) for this group	**unsigned integer** plus **carriage return**
Selected **Parameters** data stream for each Saq within the group	**Variable length**
End flag (4 characters)	***END**

Table 9.7: Saq group COM port output structure.

Code	Parameter	Format
a	ρ or ρ'	FLOAT
b	sρ or sρ'	FLOAT
c	α_{PII} or α_{PII}'	FLOAT
d	sα_{PII} or sα_{PII}'	FLOAT
e	σ_{PII} or σ_{PII}'	FLOAT
f	sσ_{PII} or sσ_{PII}'	FLOAT
g	dρ or dρ'	FLOAT
h	dσ_{PII} or dσ_{PII}'	FLOAT
i	sdσ_{PII} or sdσ_{PII}'	FLOAT
j	[oo]	FLOAT
k	[oc]	FLOAT
l	[cc]	FLOAT
m	s[oo]	FLOAT
n	s[oc]	FLOAT
o	s[cc]	FLOAT
p	F_b or F_b'	FLOAT
q	F_o'	FLOAT
r	F_v'	FLOAT
s	F_o or F'	FLOAT
t	sF or sF'	FLOAT

Code	Parameter	Format
u	F_m or F_m'	FLOAT
v	sF_m or sF_m'	FLOAT
w	F_v or F_q'	FLOAT
x	sF_q or sF_q'	FLOAT
y	Δ_F or Δ_F'	FLOAT
z	Δ_S or Δ_S'	FLOAT
A	τ_F or τ_F'	UINT
B	τ_S or τ_S'	UINT
C	τ_t'	UINT
D	F_v/ F_m or F_q'/ F_m'	FLOAT
E	F_v/ F_{mc} or F_q'/ F_{mc}'	FLOAT
F	F_v'/ F_{mc}'	FLOAT
G	F_q'/ F_v'	FLOAT
H	E_{kt}'	UINT
I	E_{kt}	UINT
J	JV_{PII}	FLOAT
K	J_{PII}	FLOAT
L	NPQ	FLOAT
M	NSV	FLOAT

Table 9.8: The field codes used within the Saq groups csv output. The terms in the **Parameter** columns match up with the data plot parameters.

Figures 9.14 and 9.15 provide sample Saq groups COM output for a dark group and light group, respectively. Each line of parameters starts with the Saq number within the data file and the gap length in µs. The **Added** parameters are then listed in sequence, with each parameter starting with the single character codes listed in Table 9.8.

```
*SAQ GRP
221022,124133,19-0105-004,0
12,400,e4.229,u21.83,C,H,J
13,566,e4.377,u21.68,C,H,J
14,800,e4.451,u21.68,C,H,J
15,1131,e4.239,u21.73,C,H,J
16,1600,e4.439,u21.67,C,H,J
17,2263,e4.353,u21.7,C,H,J
18,3200,e4.352,u21.73,C,H,J
19,4525,e4.357,u21.73,C,H,J
20,6400,e4.253,u21.78,C,H,J
21,9051,e4.269,u21.79,C,H,J
22,12800,e4.284,u21.74,C,H,J
*END
```

Figure 9.14: Sample Saq groups COM output from a sample in the dark.

```
*SAQ GRP
221022,124710,19-0105-004,18
34,400,e4.091,u23.07,C13883,H51.92,J1.817
35,566,e4.128,u23.08,C14532,H49.15,J1.8
36,800,e4.173,u23.08,C13747,H51.39,J1.814
37,1131,e4.101,u23.11,C14215,H50.58,J1.811
38,1600,e4.071,u23.14,C14706,H49.25,J1.803
39,2263,e4.141,u23.1,C15065,H47.26,J1.788
40,3200,e4.095,u23.15,C14785,H48.69,J1.801
41,4525,e4.099,u23.17,C14299,H50.31,J1.812
42,6400,e4.093,u23.16,C14959,H48.16,J1.797
43,9051,e4.131,u23.15,C13780,H51.8,J1.82
44,12800,e4.083,u23.17,C14989,H48.18,J1.798
*END
```

Figure 9.15: Sample Saq groups COM output from a sample in the light at 18 µmol photons m^{-2} s^{-1}.

10 Data processing within RunSTAF

10.1 ST data acquisition

The default RunSTAF ST pulse is 100 µs. Data acquisition is always at 1 MHz. Acquisition starts 20 µs before the ST pulse is triggered, to provide a signal offset, and runs through to the end of the pulse. If a second ST pulse is included within a Seq, data are also acquired for the entire duration of this pulse. No data are acquired during the gap between the first and second ST pulses. The second ST pulse starts immediately after the set gap. The Dual ST Pulse (DSP) is defined as the combination of first ST pulse, gap and second ST pulse (Figure 10.1). The interval between the end of one DSP and the start of the next is the sequence interval. By default, the sequence interval is 120 ms.

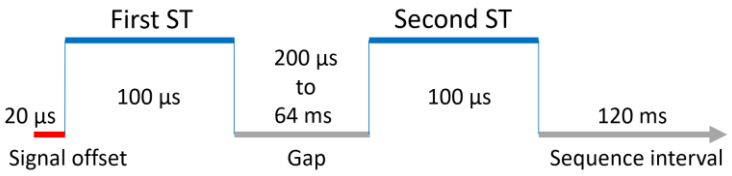

Figure 10.1: The structure of a typical Dual ST Pulse (DSP) sequence plus the signal offset and sequence interval.

Although the first ST pulse is always triggered 20 µs into the sequence, it takes approximately 3 µs after this trigger for the MLEDs to get to full output. Table 10.1 shows typical MLED output data for the first 4 µs after the ST pulse is triggered. The second ST pulse rise kinetic shows the same profile.

t (µs)	ST fit t (µs)	delivery	sum
1	-1	<< 1%	<< 1%
2	0	30%	30%
3	1	80%	110%
4+	2+	100%	-

Table 10.1: All curve fitting functions within RunSTAF use an offset of 2 µs. Working from the values presented here, this means that at *t* = 1 µs for the ST fit, the sample will have received 110% of the photons delivered over 1 µs once stable output is reached (from 4 µs onwards). This 110% value is the sum of 80% delivered between *t* = 0 and *t* = 1 and 30% between *t* = -1 and *t* = 0 on the ST fit scale.

10.2 The Rho ST curve fit

The ST curve fitting procedure within RunSTAF is centred around Equations 10.1 and 10.2 (Kolber, Prášil and Falkowski, 1998).

$$C_t = C_{t-1} + C_{t=1} \cdot (1 - C_{t-1})/(1 - C_{t-1} \cdot \rho) \qquad \text{Equation 10.1}$$

$$\mathrm{F}_t = \mathrm{F}_\mathrm{o} + \mathrm{F}_\mathrm{v} \cdot C_t \cdot (1 - \rho)/(1 - C_t \cdot \rho) \qquad \text{Equation 10.2}$$

Where F_t is the fluorescence intensity at time t, C_t is the fraction of RCII in the closed state at time t, ρ (Rho) accounts for connectivity between RCIIs, and $\mathrm{F}_\mathrm{v} = \mathrm{F}_\mathrm{m} - \mathrm{F}_\mathrm{o}$. It is assumed that $C = 0$ at $t = 0$. During the fitting process, $C_{t=1}$, ρ, F_o and F_m are all allowed to float. Adjacent values of t are always 1 µs apart (1 MHz acquisition). The connectivity parameter ρ accounts for the transfer of photons between PSII complexes.
See: **Deconstructing Rho**

The value of $C_{t=1}$ provides the initial rate at which PSII centres are closed during a ST pulse (α_{PII}). For the LabSTAF system, α_{PII} is defined by $C_{t=1}$ (the proportion of PSII complexes closed during the first microsecond of the ST pulse). The units for α_{PII} are photons PSII^{-1} $\mu\mathrm{s}^{-1}$.

The value of σ_{PII} can be generated using Equation 10.3.

$$\sigma_{\mathrm{PII}} = \alpha_{\mathrm{PII}} \cdot 100/\mathrm{E}_{\mathrm{ST}} \qquad \text{Equation 10.3}$$

Where E_{ST} has units of photons nm^{-2} (100 µs)$^{-1}$. This provides a value for σ_{PII} with units of nm^2 PSII^{-1}.

Although Equations 10.1 and 10.2 use terminology appropriate to a dark-adapted sample, these equations can also be applied to a light-adapted sample. This is because the term C within these equations is always set to zero at t = 0 under ambient light, even though a proportion of the RCII within the sample are closed at t = 0. The reason for this is that Equations 10.1 and 10.2 only track the closure of RCII that are open at t = 0 and implicitly assume that the proportion of RCII held in the closed state by the actinic light remains constant throughout the ST pulse. Equations 10.4 and 10.5 provide the light-adapted versions of Equations 10.1 and 10.2.

$$C_t = C_{t-1} + C_{t=1} \cdot (1 - C_{t-1})/(1 - C_{t-1} \cdot \rho') \qquad \text{Equation 10.4}$$

$$F_t' = F' + F_q' \cdot C_t \cdot (1 - \rho')/(1 - C_t \cdot \rho') \qquad \text{Equation 10.5}$$

10.3 The Dimer ST curve fit

It is now widely accepted that photochemically active PSII complexes form structural dimers within thylakoid membranes (e.g., Nield and Barber, 2006; Watanabe et al. 2009; Umena et al. 2011) and it seems likely that this dimerization can at least partially account for the connectivity defined by ρ and ρ'. The dimer curve fit incorporated within RunSTAF makes the following basic assumptions:

- All functional PSII reaction centres are incorporated within dimeric complexes and the two RCIIs within each dimer effectively share a single light harvesting system
- PSII dimer complexes are completely isolated from each other, preventing the transfer of photons from one dimer to another

With these assumptions in place, Equations 10.6A to 10.6D can be used to fit a dark ST curve:

$$[oo]_t = [oo]_{t-1} - [oo]_{t-1} \cdot C_{t=1} \qquad \text{Equation 10.6A}$$

$$[oc]_t = [oc]_{t-1} + [oo]_{t-1} \cdot C_{t=1} \qquad \text{Equation 10.6B}$$

$$[oc]_t = [oc]_{t-1} - [oc]_{t-1} \cdot C_{t=1} \cdot 0.5/(1 - 0.5 \cdot \rho) \qquad \text{Equation 10.6C}$$

$$[cc]_t = [cc]_{t-1} + [oc]_{t-1} \cdot C_{t=1} \cdot 0.5/(1 - 0.5 \cdot \rho) \qquad \text{Equation 10.6D}$$

Within Equations 10.7A-C, ooF, ocF, and ccF are the relative fluorescence intensities from [oo], [oc], and [cc] dimers, respectively. Because the RCIIs within each dimer are assumed to share a single light harvesting system, ρ is theoretically equal to ϕ_{PII}.

$$ooF = [oo] \cdot F_o \qquad \text{Equation 10.7A}$$

$$ocF = [oc] \cdot (F_o + F_v \cdot 0.5 \cdot [1 - \rho]/[1 - 0.5 \cdot \rho]) \qquad \text{Equation 10.7B}$$

$$ccF = [cc] \cdot F_m \qquad \text{Equation 10.7C}$$

For the second ST curve in a dual ST sequence and measurements from light-adapted samples, the Dimer fit requires initial (t = 0) values for [oo], [oc] and [cc]. These values are estimated by assuming that [cc] equals unity at the asymptote of the ST fit (F_m or F_m').

It is worth noting that the Dimer fit is more sensitive to heterogeneity than the Rho fit. Mainly for this reason, the Dimer fit is only used to generate parameters that directly relate to this fitting process (within the **Dimer fit parameters** section of the data screen). All other parameters that have dependence on a ST curve fit (within the **Rho fit parameters**, **Primary fluorescence values**, **Relaxation phase parameters** and **Derived fluorescence parameters** sections) are derived using the Rho fit.

10.4 The rP-E data fit

The rP-E curve is a variant of the established photosynthesis – photon irradiance (P-E) response curve. The 'P' in P-E is generally taken to represent mass-specific photosynthesis (normalised to chlorophyll *a*, for example). In contrast, the rP-E curve plots relative photosynthesis (rP). The 'E' in P-E or rP-E is always incident photon irradiance. Although values of rP are reported on a unitless scale within RunSTAF, they are actually calculated as the product of E and $\mathrm{F_q'/F_{mc}'}$. This generates units of µmol photons m^{-2} s^{-1}.

There are three basic parameters derived from all P-E curve fits: α, $\mathrm{E_k}$, and $\mathrm{P_m}$. The value of α is the initial slope of the relationship between P and E. $\mathrm{E_k}$ is an inflection point along the P-E curve which is often described as the light saturation parameter (Platt and Gallegos, 1980). $\mathrm{P_m}$ is the maximum rate of photosynthesis.

A range of models have been used to generate a fit to rP-E and other P-E curves (see Silsbe and Kromkamp, 2012 and references therein). There are two phases to the rP-E fitting process incorporated within RunSTAF: the alpha phase and the beta phase. The fitting process is based around minimisation of the sum of squares (SS) of the difference between actual and fit values. The mean of the actual values at each E level are used for the fit.

The alpha phase of the rP-E fit uses the Webb model (Webb et al. 1974) to generate values for α and $\mathrm{E_k}$. The value of $\mathrm{F_q'/F_{mc}'}$ used to generate each rP-E value is calculated using Equation 10.8.

$$\frac{\mathrm{F_{q\prime}}}{\mathrm{F_{mc\prime}}} = \alpha \cdot \mathrm{E_k} \cdot \left(1 - e^{-\mathrm{E}/\mathrm{E_k}}\right) \cdot \mathrm{E}^{-1} \qquad \text{Equation 10.8}$$

It follows that α is theoretically equal to $\mathrm{F_v/F_{mc}}$ and that $\mathrm{E_k}$ is the point on the rP-E curve at which the value of $\mathrm{F_q'/F_{mc}'}$ is 63.2% of $\mathrm{F_v/F_{mc}}$. The screenshot in Figure 10.2 shows the alpha phase fit to a complete rP-E curve.

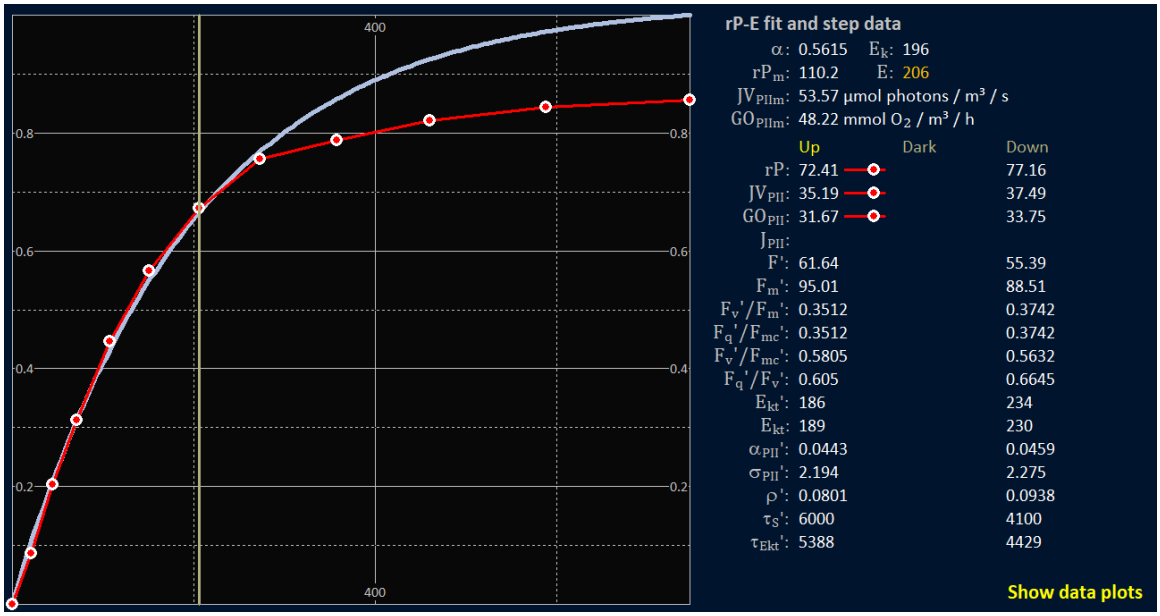

Figure 10.2: rP-E curve fit with the beta phase blocked such that the (solid light blue) rP-E fit line is defined by Equation 10.10. The sample is cultured cells of *Conticribra weissflogii*.

The beta phase is generated using Equation 10.9. The beta phase is only applied to points after the $\mathrm{E_k}$ value generated by the alpha phase. Consequently, the values of α and $\mathrm{E_k}$ are not affected by addition of the beta phase.

$$\frac{\mathrm{F_{q\prime}}}{\mathrm{F_{mc\prime}}} = \left(\alpha \cdot \mathrm{E_k} \cdot \left[1 - e^{-\mathrm{E}/\mathrm{E_k}}\right] - \beta \cdot \mathrm{E_{k\beta}} \cdot \left[1 - e^{-\mathrm{E}/\mathrm{E_{k\beta}}}\right]\right) \cdot \mathrm{E}^{-1} \qquad \text{Equation 10.9}$$

The screenshot in Figure 10.3 shows the same fit with the beta phase added. As noted elsewhere in this document, calculated values of JV_{PII} and GO_{PII} scale with rP. Consequently, P-E curves for these three parameters have the same shape.

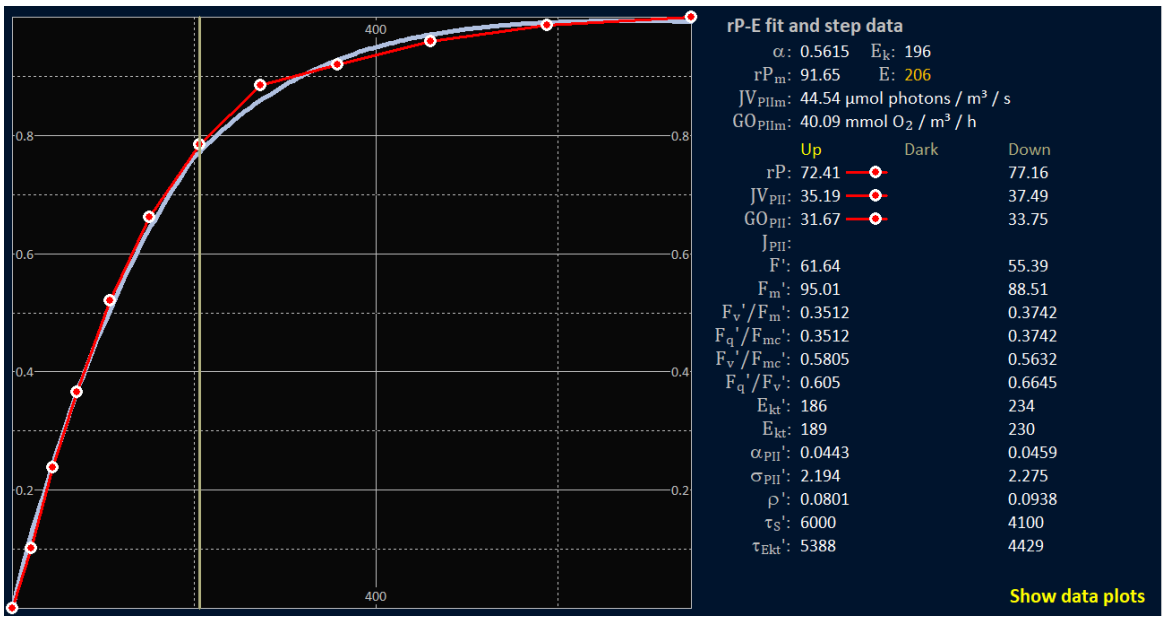

Figure 10.3: rP-E curve fit with the beta phase applied such that the (solid light blue) rP-E fit line is defined by Equation 10.9.

10.5 Fitting a Dual ST Pulse (DSP) sequence

The screenshot in Figure 10.4 shows a dual ST pulse Saq from a dark-adapted sample. The gap applied between the first and second ST pulses in this example was 200 µs. The small orange numbers in the bottom right corner of each ST plot defines the number of points incorporated within the Rho and Dimer fits. The first ST pulse fit was to the first 68 points. Over the last part of the curve, there is a clear decrease in fluorescence which was excluded from the fit. The second ST pulse was fit to all 96 available points.

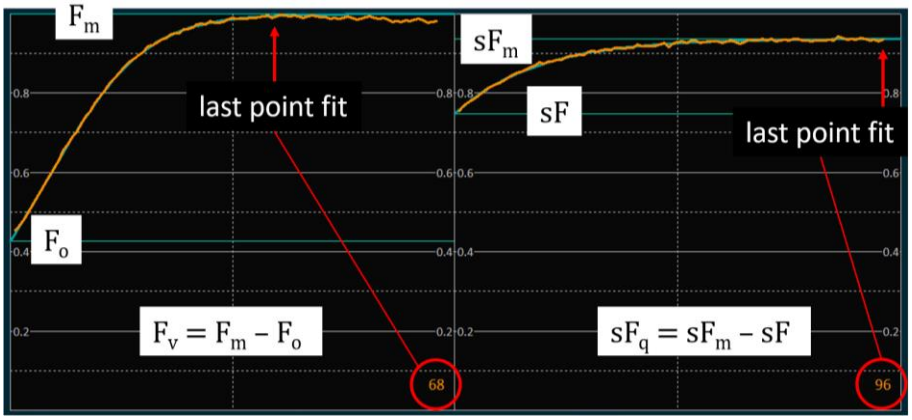

Figure 10.4: Crop from a screenshot of the data screen showing a dual ST pulse. The gap between the first and second ST pulse was 200 µs.

The observed decrease in fluorescence towards the end of the first ST pulse tends to be most evident when the ratio of variable fluorescence to total fluorescence is relatively high (above approximately 0.5). The decrease in fluorescence towards the end of the first ST pulse is correlated with an absorption change centred at 515 nm (Witt, 1971) which tracks the rapid formation of an electric field across the thylakoid membrane ($\Delta\psi$) as most of the RCIIs within the interrogated volume undergo charge separation within the timeframe of the ST pulse. To minimise the impact of this electric field-dependent quenching on the Rho curve fit, the part of the algorithm that determines the number of points to be fit incorporates initial estimates of F_v/F_m or F_q'/F_m' for the

first ST pulse and sF_q/sF_m or sF_q'/sF_m' for the second ST pulse. These values are generated by a simple algorithm that applies linear regression to the first and last few points of each ST curve.

Within the example provided by Figure 10.4, the first ST pulse is fit to 68 points because the initial estimate of F_v/F_m was high (approximately 0.57). The second ST pulse is fit to all 96 points because the initial value of sF_q/sF_m was much lower (approximately 0.2). The overall result is consistent with the extent of the electric field-dependent quenching at the end of the first ST pulse being increased by charge separation during the second ST pulse. As a result, sF_m is significantly lower than F_m.

The dual ST pulse shown in Figure 10.4 was extracted from the group of six dual ST pulse acquisitions shown in Figure 10.5. This group covers a range of gaps between 200 and 6400 µs. Working through the gaps from shortest to longest, there is a consistent increase in sF_m, relative to F_m. At 200 µs, sF_m is noticeably lower than F_m. By 1600 µs, sF_m is very close to F_m and by 6400 µs sF_m is slightly higher than F_m. The relative increase in sF_m is consistent with neutralisation of the electric field-dependent quenching between the end of the first ST pulse and the start of the second ST pulse with a time-constant of around 1 ms (Witt, 1971; Johnson and Ruban, 2014). In addition, the increase in sF_m to a point that is higher than F_m can be at least partly attributed to transient reduction of plastoquinone to semi-plastoquinone and semi-plastoquinone to plastoquinol as closed RCIIs are reopened through the transfer of electrons from reduced Q_A (Vernotte, Etienne and Briantais, 1979).

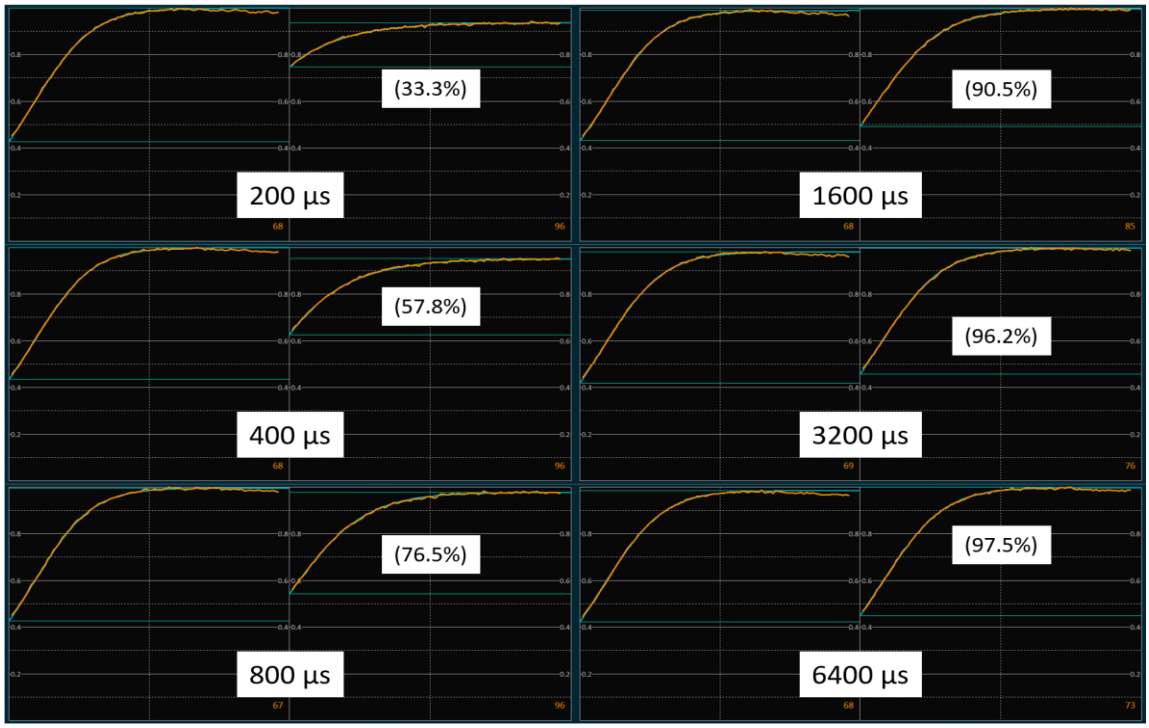

Figure 10.5: Composite of crops from screenshots of the data screen showing curves from a complete dual ST pulse Set. The target sample was dark adapted. The times shown are the gaps between first and second ST pulses. The numbers within brackets are % recovery of variable fluorescence between the first and second ST pulse.

For comparison, Figure 10.6 shows a group from the same sample under actinic illumination of 1000 µmol photons m^{-2} s^{-1}. Recovery of variable fluorescence is broadly in line with the dark group shown above. One important difference is that the electric field-dependent quenching evident in the dark group is not evident within this group. It is also worth noting that sF_m is very slightly higher than F_m with gaps of between 1600 and 6400 µs. This is consistent with short-lived formation of plastoquinol as this relatively small pool of RCIIs reopen within the gap.

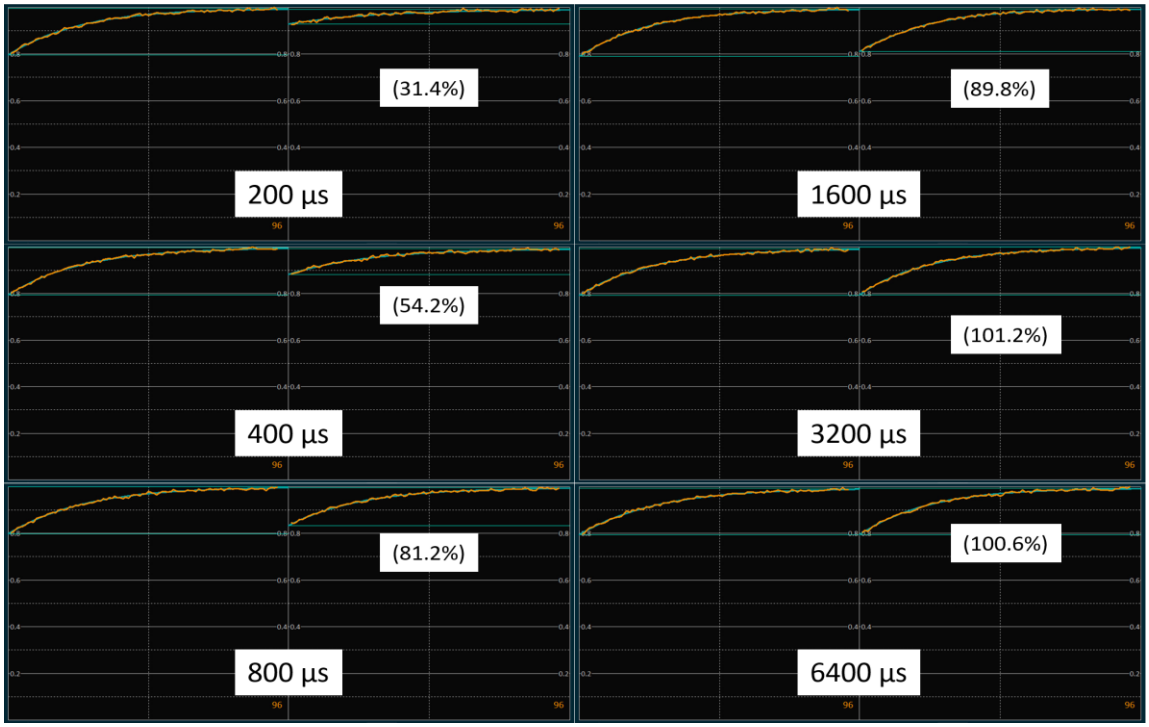

Figure 10.6: Composite of crops from screenshots of the data screen showing curves from a complete dual ST pulse Set. The sample was under actinic illumination of 1000 µmol photons m^{-2} s^{-1}. The times shown are the gaps between the first and second ST pulses. The numbers within brackets are % recovery of variable fluorescence between the first and second ST pulse.

10.6 The relaxation phase (tau) fit

Three relaxation phase fits are generated by RunSTAF: **Fv**, **Rho** and **Dimer**. All three fits incorporate fast and slow components, as shown in Figure 10.10. The **Fv** fit tracks the recovery of variable fluorescence during the gap between the first and second ST pulses as $1 - sF_q/F_v$ for a dark measurement or $1 - sF_q'/F_q'$ under actinic light. The **Rho** and **Dimer** relaxation phase fits track the reopening of RCIIs (decrease in the proportion of RCIIs in the closed state) during the gap between the first and second ST pulses using the Rho and Dimer models, respectively. All three fits incorporate Equation 10.10 within the fitting procedure. The fitting process minimises the sum of squares between F_t and the measured value.

$$F_t = F_v \cdot \left(\Delta_F \cdot e^{-\frac{t}{\tau_F}} + \Delta_S \cdot e^{-\frac{t}{\tau_S}}\right) \qquad \text{Equation 10.10}$$

Where the subscripts F and S refer to the fast and slow components of the relaxation phase. The F_v in Equation 10.10 is appropriate for a dark-adapted sample. For a light-adapted sample, F_q' is used in place of F_v. The total amplitude of the recovery phase ($\Delta_F + \Delta_S$) is fixed at unity.

It is assumed that the fast component is dominated by the reopening of RCIIs with plastoquinone or semi-plastoquinone bound at the Q_B site at the end of the first ST pulse while the slow component is dominated by the reopening of RCIIs with an empty Q_B site at the end of the first ST pulse. Δ_F and Δ_S are the proportions of the total amplitude of the relaxation phase attributable to the fast and slow components, respectively, while τ_F and τ_S are the time-constants for the fast and slow components of the relaxation phase, respectively.

Figures 10.7, 10.8 and 10.9 all show relaxation phase curves of 12800 µs (upper panel of each figure) and the Dual ST Pulses (DSPs) at the 400 µs gap point (lower panel of each figure) from the same sample. The curves within Figure 10.7 were generated when the sample was in the dark-adapted

state. The curves in Figures 10.8 and 10.9 were generated when the actinic light level was 109 and 384 µmol photons m^{-2} s^{-1}, respectively.

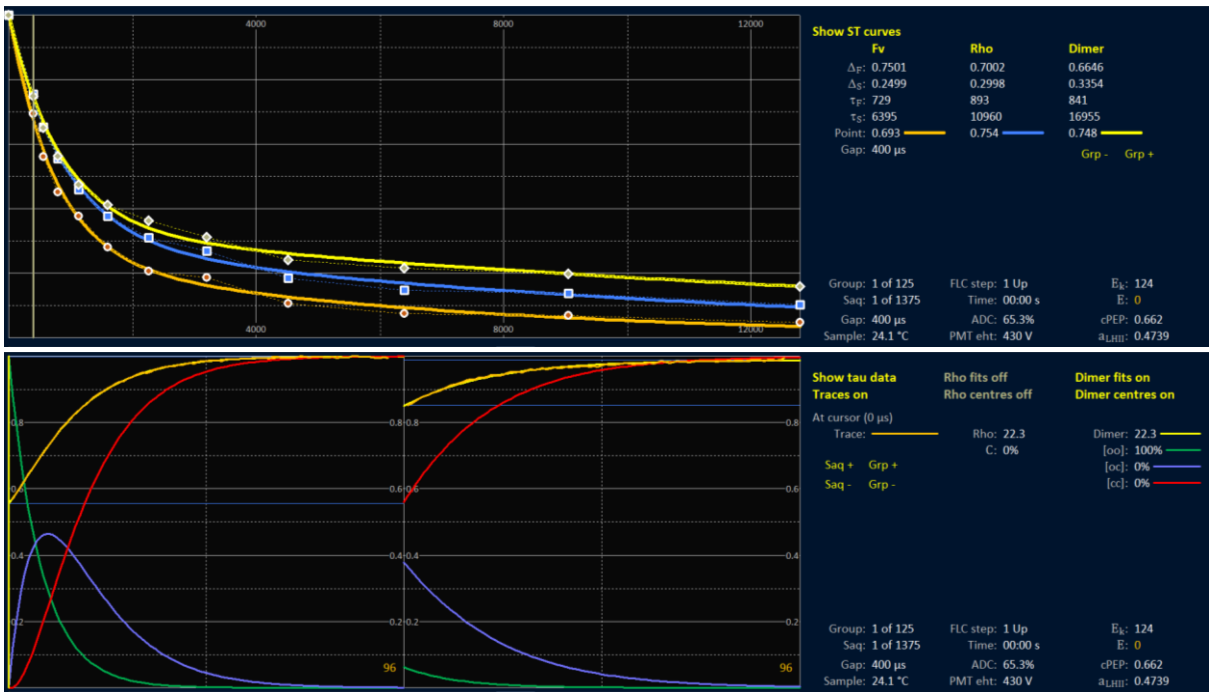

Figure 10.7: The upper panel shows the three relaxation phase (tau) curves generated by a dark-adapted sample. The lower panel shows the Dual ST Pulses at the 400 µs gap. Selection of the 400 µs point is indicated by the vertical yellow line in the upper panel.

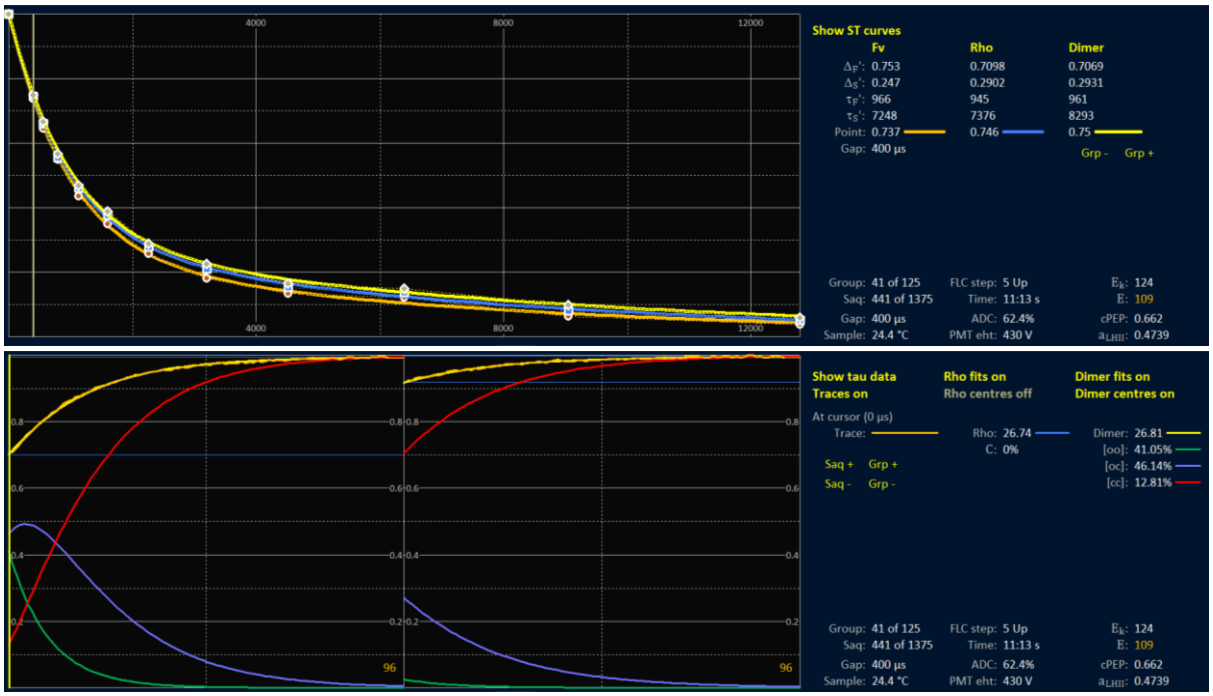

Figure 10.8: The upper panel shows the three relaxation phase (tau) curves generated by a sample under an actinic photon irradiance of 109 µmol photons m^{-2} s^{-1}. The lower panel shows the DSPs at the 400 µs gap.

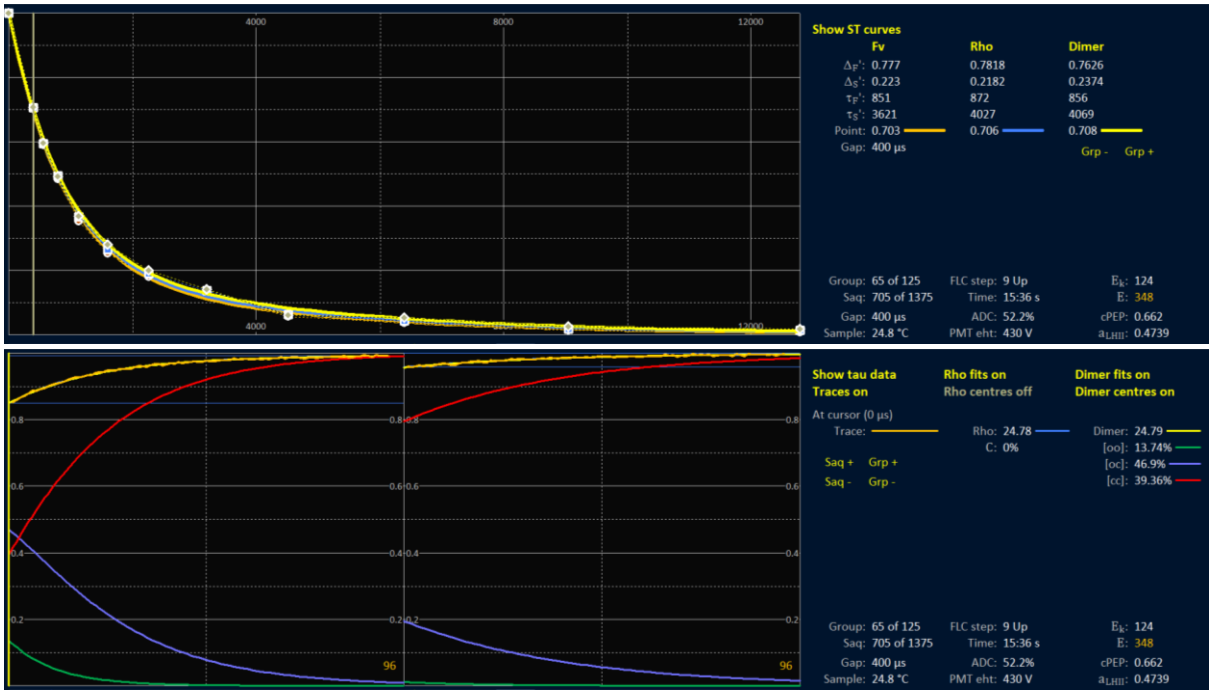

Figure 10.9: The upper panel shows the three relaxation phase (tau) curves generated by a sample under an actinic photon irradiance of 348 µmol photons m^{-2} s^{-1}. The lower panel shows the Dual ST Pulses at the 400 µs gap.

In the dark-adapted state, the separation of curves is usually as shown in Figure 10.7: the **Rho** and **Dimer** curves are above the **Fv** curve all the way through while the **Dimer** fit curve starts out with the **Rho** curve fit and then runs above it. The differences between the three curves can be explained in terms of connectivity among PSII complexes. Because the **Fv** curve is based purely on the recovery of variable fluorescence, connectivity among PSII complexes will result in the first PSII complexes that reopen having a connectivity-enhanced value of σ_{PII} which increases the level of photochemical quenching of fluorescence per PSII. Importantly, the **Fv** curve is reporting the recovery of photochemical capacity, rather than the reopening of PSII complexes. In contrast, the **Rho** and **Dimer** curves track the reopening of PSII complexes, using the appropriate model of connectivity. With the **Rho** curve, connectivity is defined by the value of ρ (0.281 in this example). With the **Dimer** curve, connectivity is defined by the proportion of dimers in the oo state at the start of the first ST pulse ([oo] = 100% in this example).

The actinic photon irradiance of 109 µmol photons m^{-2} s^{-1} in Figure 10.8 is very close to the E_k for this sample (124 µmol photons m^{-2} s^{-1}). Clearly, the curves are much closer to each other than in the dark-adapted state (Figure 10.7). This indicates that, at around E_k, connectivity has much less of an impact on the relationship between the recovery of PSII photochemical capacity, as tracked by the **Fv** curve, and the proportion of PSII complexes in the open state, as tracked by the **Rho** and **Dimer** curves. For the **Rho** curve, the value of ρ' is 0.051. For the **Dimer** curve, the value of [oo] is 41.05%.

The actinic photon irradiance of 348 µmol photons m^{-2} s^{-1} in Figure 10.9 is slightly more than three times the E_k for this sample and the JV_{PII} for this group is actually higher than the JV_{PIIm} calculated from the rP-E fit (23.78 compared to 20.65). In other words, the actinic light level applied in Figure 10.8 is saturating. Clearly, the relaxation phase curves in the upper panel are now very close to each other. In terms of measured connectivity, the value of ρ' for the **Rho** curve is down to 0.009 and the [oo] for the **Dimer** curve is at 13.74%.

Looked at together, these curves indicate that connectivity between PSII complexes may improve light use efficiency at sub-saturating actinic light levels, but that this impact of connectivity is low by E_k and close to non-existent at saturating light levels.

Because the **Fv** curve tracks the recovery of PSII photochemical capacity, rather than the proportion of PSII complexes in the open state, it aligns well with the Absorption method and its lack of reliance on any assessment of connectivity to calculate JV_{PII}. In contrast, the Sigma method requires an assessment of the actual proportion of PSII complexes in the open state to calculate JV_{PII}. The relaxation phase data presented here strongly suggest that the impact of connectivity on the relationship between variable fluorescence and the proportion of PSII complexes in the open state may need to be factored in at low actinic light levels but has a much lower impact by E_k and is largely irrelevant at saturating light.

10.7 Derivation of transient E_k (E_{kt}')

In addition to the single rP-E value of E_k, RunSTAF incorporates an algorithm to generate values for E_k from individual Saqs under actinic illumination. This subsection outlines the derivation of these values.

The rP-E curve fit incorporated within RunSTAF (Equations 10.8 and 10.9) sets α as the maximum PSII photochemical efficiency. As already noted earlier within this section, a perfect match between the rP-E fit and the actual data would generate a value for α equal to F_v/F_{mc} and E_k would be the point on the rP-E curve at which PSII photochemical efficiency (F_q'/F_{mc}') is 63.2% of F_v/F_{mc}.

Equation 10.11 shows PSII photochemical efficiency under actinic illumination (F_q'/F_{mc}') as the product of the maximum PSII photochemical efficiency at the point of measurement (F_v'/F_{mc}') and the PSII photochemical factor (F_q'/F_v').

$$\frac{F_{q\prime}}{F_{mc\prime}} = \frac{F_{v\prime}}{F_{mc\prime}} \cdot \frac{F_{q\prime}}{F_{v\prime}} \qquad \text{Equation 10.11}$$

Equation 10.12 is derived from Equation 10.8. The F_q'/F_{mc}' term within Equation 10.8 has been replaced with the right-hand side of Equation 10.11 and α has been replaced with F_v/F_{mc}.

$$\frac{F_{v\prime}}{F_{mc\prime}} \cdot \frac{F_{q\prime}}{F_{v\prime}} = \frac{F_v}{F_{mc}} \cdot E_k \cdot \left(1 - e^{-E/E_k}\right) \cdot E^{-1} \qquad \text{Equation 10.12}$$

Within Equation 10.13, the F_v'/F_{mc}' on the left-hand side and the F_v/F_{mc} on the right-hand side of Equation 10.12 have been excluded (discussed below).

$$\frac{F_{q\prime}}{F_{v\prime}} = E_k \cdot \left(1 - e^{-E/E_k}\right) \cdot E^{-1} \qquad \text{Equation 10.13}$$

The value of E_k within Equation 10.13 defines the point at which F_q'/F_v' is expected to have a value of 0.632 (63.2% of the maximum value). To distinguish the E_k derived from an rP-E curve fit from the E_k in Equation 10.13, Equation 10.14 uses the term E_{kt}' to define this 'transient' E_k value, which is specific to the actinic photon irradiance (E) and F_q'/F_v' at the point of measurement. The term includes a 'prime' because it is derived from a point measurement under actinic illumination.

$$\frac{F_{q\prime}}{F_{v\prime}} = E_{kt}' \cdot \left(1 - e^{-\frac{E}{E_{kt}'}}\right) \cdot E^{-1} \qquad \text{Equation 10.14}$$

Even though E_{kt}' is the only unknown within Equation 10.14, it is not possible to solve for this parameter. To get around this, a Look Up Table (LUT) has been generated from iteratively derived values for E_{kt}' at each of 63 set values for F_q'/F_v' of between 0.08 and 0.96. With this LUT, it is possible to use Equation 10.14 to estimate E_{kt}' from a measurement made at any value of E. The exclusion of F_v'/F_{mc}' and F_v/F_{mc} between Equations 10.12 and 10.13, which is carried through to Equation 10.14, means that the calculated value of E_{kt}' is only valid for the F_v'/F_{mc}' at the point of measurement. However, the value of E_{kt}' is inversely proportional to F_v'/F_{mc}', which makes it straightforward to compare values of E_{kt}' within and between FLC steps.

A plot of the LUT values is shown in Figure 10.10. This plot shows that the sensitivity of E_{kt}'/E declines with F_q'/F_v'. The LUT values have been integrated within RunSTAF and are used to automatically generate E_{kt}' values from measured values of F_q'/F_v' and the set value of E.

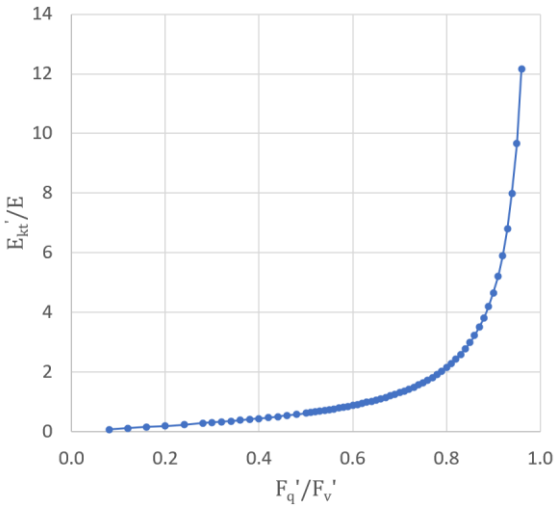

Figure 10.10: Plot of values from a Look Up Table (LUT) that has been compiled to allow for the derivation of E_{kt}' from values of F_q'/F_v' measured at a set value of E. The LUT values have been integrated within RunSTAF to facilitate real time calculation of E_{kt}'.

Figure 10.11 provides a sample home screen data plot of σ_{PII}' and F_m' plus the three parameters discussed within this subsection, so far: F_v'/F_{mc}', F_q'/F_v' and E_{kt}'.

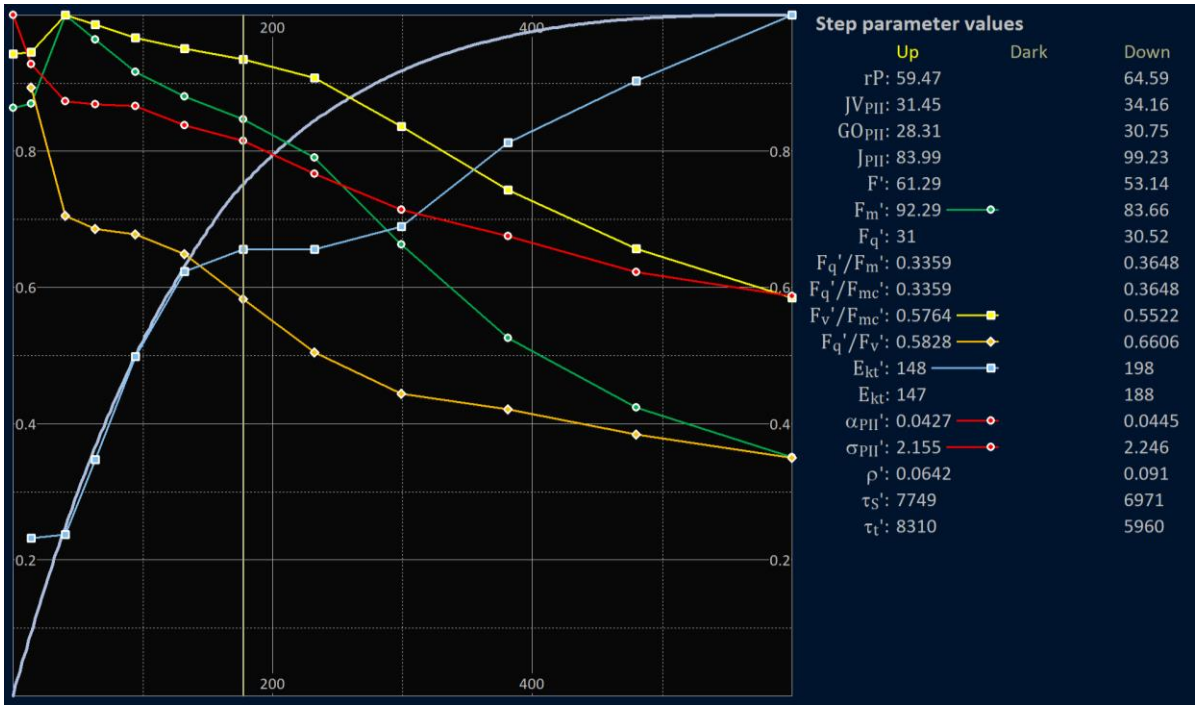

Figure 10.11: Crop from the RunSTAF home screen showing rP-E step data for the parameters discussed within this section, so far. The sample was low light-grown cultured cells of *Conticribra weissflogii*.

Some notable features of the data presented in Figure 10.11 are:

- There are steep drops in $\sigma_{PII}^{(')}$ between Up 1 and 2 and between Up 2 and Up 3
- There is a steep drop in F_q'/F_v' between Up 2 and 3
- The value of F_q'/F_v' at the nearest point to E_k is within 8% of the expected value (0.5828 compared to the expected 0.632)
- The E_{kt}' closest to E_k is within 11% of E_k (148 against 167 µmol photons m^{-2} s^{-1})
- A decrease in F_m' after E_k is matched to an increase in E_{kt}'

The plot in Figure 10.12 shows the complete datasets used to generate the values in Figure 10.11. The much higher temporal resolution within Figure 10.12 provides a more detailed overview than the FLC-level data within Figure 10.11. For example, it is clear that the drop from σ_{PII} to σ_{PII}' between Up 1 and 2 is dominated by a very sharp drop at the start of Up 2, followed by a slow, partial recovery over the remainder of the step.

Figure 10.12 includes a plot of E_{kt} (E_{kt}' without the prime), which is calculated using Equation 10.15.

$$E_{kt} = E_{kt}' \cdot \frac{F_v'}{F_{mc}'} \Big/ \frac{F_v}{F_{mc}} \qquad \text{Equation 10.15}$$

This parameter provides an estimate of what E_{kt}' would be in the absence of downregulation. In this example, E_{kt}' and E_{kt} are very close to each other up to the E_k plateau, between Up 6 and Up 8, after which they diverge as downregulation increases and F_v'/F_{mc}' decreases. The E_{kt} trace indicates that without downregulation, E_{kt}' would have stayed very close to E_k instead of increasing.

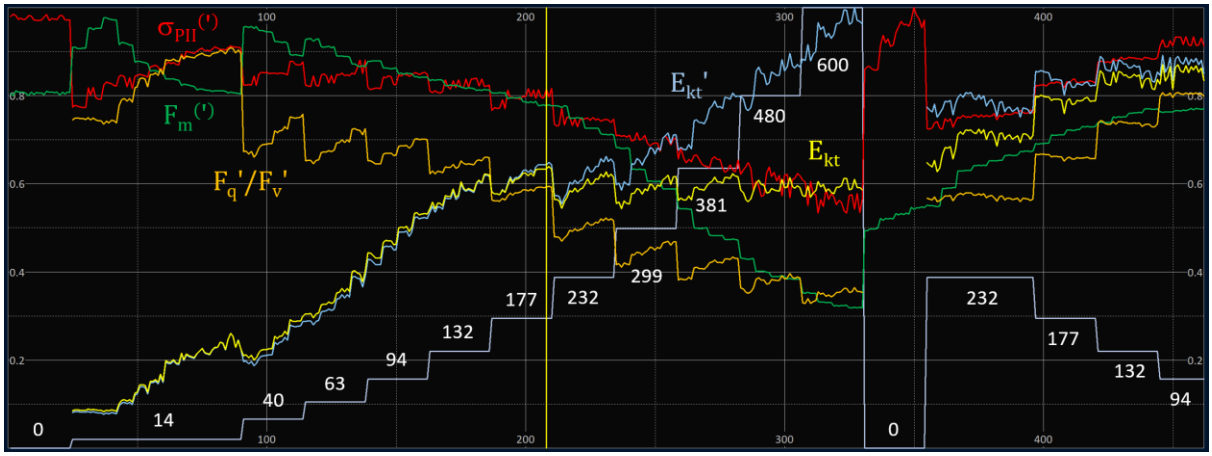

Figure 10.12: Crop from the data screen showing the complete dataset from the FLC shown in Figure 10.11. The stepped line is incident photon irradiance (E). The E values are shown at each step. The vertical yellow line marks the FLC step that is closest to E_k.

10.8 Derivation of τ_t'

Equation 10.16 provides a theoretical relationship between E_{kt}' and the reciprocal of the product of σ_{PII}' and τ_t'.

$$E_{kt}' = 1/(\sigma_{PII}' \cdot \tau_t') \qquad \text{Equation 10.16}$$

Where the τ_t' parameter is a time-constant for the reopening of PSII complexes that were closed by constant actinic illumination. In contrast, the DSP-derived τ_F' and τ_S' mainly track the reopening of RCIIs closed by the first ST pulse in the DSP sequence. This important difference between the two approaches to the derivation of 'tau' under actinic illumination is discussed in more detail later within this section.

Figure 10.13 shows data plots of the three parameters within Equation 10.16, plus τ_S' and F_v'/F_{mc}'. As already noted, there is a significant and steady increase in the value of E_{kt}' between Up 2 and E_k. Although this increase may be at least partly linked to activation of carbon assimilation, the rapid 20% drop from σ_{PII} to σ_{PII}' between Up 1 and 2 does not easily fit with this as a complete explanation.

Equation 10.17 shows σ_{PII}' as the product of σ_{LHII} and F_v'/F_{mc}'. We can consider that the sharp drop in σ_{PII}' may be linked to a drop in either parameter, or some combination of the two.

$$\sigma_{PII}' = \sigma_{LHII} \cdot \frac{F_v'}{F_{mc}'} \qquad \text{Equation 10.17}$$

The value of F_v'/F_{mc}' actually increases above the dark value of F_v/F_{mc} at the start of Up 2, before falling slowly back to end up close to the dark F_v/F_{mc}. Similarly, while a decrease in σ_{LHII} would normally be expected to result in a decrease in F_{mc}', F_{mc}' actually increased by nearly 20% during the first part of Up 2, before falling back (Figure 10.12).

As proposed earlier within this section, the rapid drop in σ_{PII}' at the start of Up 2 may indicate that the sample includes a sub-population of PSII complexes that have a significantly larger σ_{PII} than the overall population. To fully account for the initial 20% drop in σ_{PII}', matched with an F_q'/F_v' of 0.75, (Figure 10.12) the proposed sub-population of PSII complexes would need to have a dark σ_{PII} value that is roughly 1.6 times higher than the overall population.

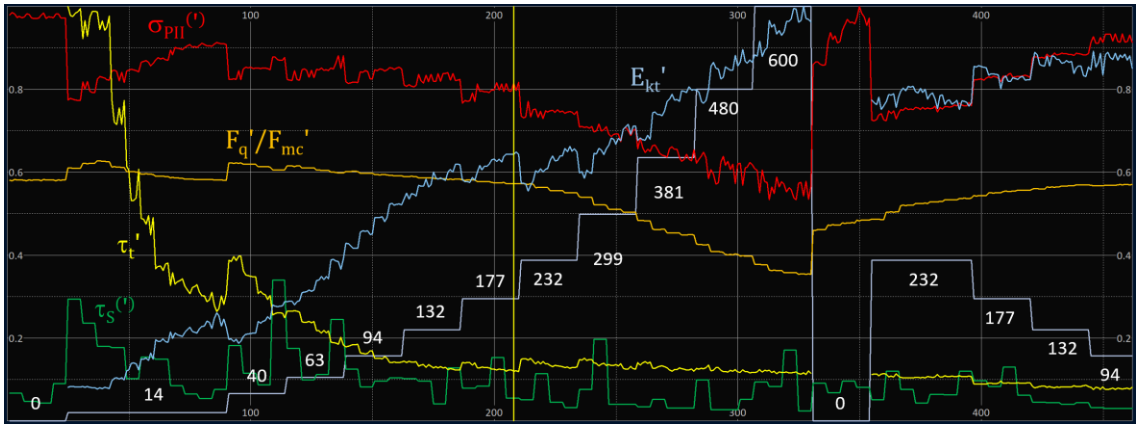

Figure 10.13: Crop from the data screen showing plots from the same dataset as shown in Figure 10.12. The vertical yellow line marks the end of the FLC step that is closest to E_k. The parameter values within the yellow boxes are from a Saq close to the end of this step.

One possible explanation for the required 1.6 fold higher value for σ_{PII} is that the sample includes a sub-population of PSII dimers with only one photochemically active RCII. To test the likelihood of this 'dimer explanation', we can use Equation 10.2 to quantify the expected increase in σ_{PII} when one of the RCIIs within a dimer is closed. This equation is valid because any change in F_t resulting from a change in C_t is theoretically proportional to a parallel change in σ_{PII}.

For the theoretical dimer complex, we can approximate the assumption of perfect connectivity within the dimer by making the value of ρ in Equation 10.2 equal to F_v/F_m. With both RCII within the dimer open, C_t within Equation 10.2 is zero. For one RCII open and the other closed, C_t becomes 0.5. For the example in Figures 10.13 and 10.14, F_o was 39.43, F_v was 54.73 and F_v/F_m was 0.58. Plugging these values into Equation 10.2 gives a 1.49 times increase in F_t (and σ_{PII}) when one of the RCIIs within the dimer is closed, which is very close to the required value of 1.6.

This potential form of heterogeneity is important because of the impact it has on the value of E_{kt}'. Because the putative sub-population of PSII complexes with the larger σ_{PII} values will close more easily, the decrease in F_q'/F_v' between Up 1 and 2 is larger than would be expected for a population of monomeric, fully disconnected PSII complexes. The knock-on effect is that E_{kt}' is lower than it would be without this heterogeneity. Moving through the Up steps, the observed increase in E_{kt}' can be at least partly attributed to the increase in the proportion of closed PSII complexes that have the lower value of σ_{PII} offsetting the sub-population of PSII complexes with the larger value of σ_{PII}.

To summarise the apparent impact of σ_{PII} heterogeneity on the value of E_{kt}':

- At the start of Up 2, the combination of 14 µmol photons m^{-2} s^{-1} actinic photon irradiance and an F_q'/F_v' of 0.75 generates an E_{kt}' value of 20 µmol photons m^{-2} s^{-1} from the LUT in Figure 10.12
- By the end of Up 2, F_q'/F_v' has increased to 0.9, which generates an E_{kt}' value of 65 µmol photons m^{-2} s^{-1}

- The decrease in σ_{PII} observed between Up 1 (dark) and Up 2 is consistent with the presence of a sub-population of PSII complexes (open at Up 1 and closed at Up 2) with approximately 1.6 times the σ_{PII} of the overall population
- Using Equation 10.18 to adjust E_{kt}' generates a revised value of 104 µmol photons m^{-2} s^{-1}

Although the revised value of E_{kt}' is only 62% of the FLC-derived E_k, it is notable that the unrevised value of E_{kt}' is still increasing at the end of Up 2 and continues to increase up to 153 µmol photons m^{-2} s^{-1} by Up 7 (the closest to E_k), which is within 8% of E_k. It seems reasonable to conclude that this slow increase in E_{kt}' reflects an increase in the requirement for electrons derived from PSII photochemistry driven by activation of carbon assimilation.

10.9 Comparing τ_S' with τ_t'

A comparison between τ_S' and τ_t' is valid because both time-constants are dominated by the re-opening of closed PSII complexes with an empty Q_B-binding site. The most significant difference between the two is that while τ_S' predominantly tracks the re-opening of PSII complexes that were closed through the application of a ST pulse, τ_t' is effectively monitoring the rate at which PSII complexes re-open under continuous actinic illumination. It follows that a sub-population of PSII complexes with larger values of σ_{PII}' will push τ_t' values higher than values for τ_S', simply because these complexes are more likely to be closed at steady state.

Looking at the example in Figure 10.13, the values of τ_t' at the start of Up 2 are approximately five times higher than the values of τ_S'. This difference decreases over the course of Up 2, such that τ_t' is roughly three time the value of τ_S' by the end of the step. By E_k, values of τ_t' are within a factor of two of the τ_S' values. This factor stays within the same range until the end of the Up phase and through the Down phase.

10.10 Deriving a value for E_k from σ_{PII} and τ

In addition to the single value of E_k from the rP-E curve fit and the transient E_{kt}' values derived from ambient light ST measurements, RunSTAF incorporates a third method for deriving E_k at each step through a FLC. This derivation couples values of E_k that originate from the DSP-derived 'tau' values with a temporal resolution comparable to the transient E_{kt}' analysis.

Equation 10.18 incorporates the same basic relationship as Equation 10.16.

$$E_k = 1/(\sigma_{PII} \cdot \tau) \qquad \text{Equation 10.18}$$

The E_k within Equation 10.18 is consistent with the E_k derived from Equation 10.8, in that it assumes an exponential decay in the fraction of PSII complexes that are in the open state between darkness (the Up 1 step under the FLC protocol) and E_k. It follows that the PSII photochemical efficiency at E_k is 63.2% of the dark value. The σ_{PII} within Equation 10.18 is derived using the Rho ST curve fit (Equations 10.1, 10.2 and 10.3).

Equation 10.10, which is central to the DSP-based relaxation phase (tau) fit, includes two values of τ. While the value of τ_F is generally taken to reflect the reopening of closed PSII complexes with a PQ or $PQ^{\cdot-}$ bound at the Q_B site, the value of τ_S is largely defined by the reopening of closed PSII complexes with an empty Q_B site. Closed PSII complexes with a PQ or $PQ^{\cdot-}$ bound at the Q_B site generally open an order of magnitude faster than closed PSII complexes with an empty Q_B site. Consequently, the τ in Equation 10.18 is largely defined by τ_S. Equation 10.19 incorporates this modification.

$$E_{kS} = 1/(\sigma_{PII} \cdot \tau_S) \qquad \text{Equation 10.19}$$

Where E_{kS} is specific to the point at which $\sigma_{PII}^{(')}$ and $\tau_S^{(')}$ were derived. As an example, the Up 1 (dark) value of σ_{PII} in Figure 10.14 was 2.716 nm^2 $PSII^{-1}$ and the τ_S' value at this step was 2219 ms. A

spectral correction is required to generate the Value of E_{kS} in Equation 10.19. The appropriate value for this correction is provided by the ratio of the MLED and ALED flat white coefficients. In this case, the MLED coefficient is 1.73 and the ALED coefficient is 1.037. Feeding the required values into Equation 10.19 generates an E_{kS} of 264 µmol photons m^{-2} s^{-1}. This compares to an E_k from the standard rP-E curve fit of 196 µmol photons m^{-2} s^{-1}, making E_{kS} some 35% higher.

The inset to Figure 10.14 shows a drop between σ_{PII} at Up 1 (dark) and σ_{PII}' at Up 2 (21 µmol photons m^{-2} s^{-1}) from 2.716 to 2.508 nm^2 $PSII^{-1}$. The value of τ_S' at Up 2 is 5669 ms. Plugging the Up 2 values of both σ_{PII}' and τ_S' into Equation 10.19 produces an E_{kS} of 195 µmol photons m^{-2} s^{-1}, which is within 0.5% of the rP-E E_k value.

The closest Up E value to the rP-E E_k is at Up 7 (206 µmol photons m^{-2} s^{-1}). Plugging the σ_{PII}' and τ_S' values from this step into Equation 10.19 produces an E_{kS} of 213 µmol photons m^{-2} s^{-1}, which is within 9% of the rP-E E_k value.

Although the three E_{kS} values generated for this example are all close to the rP-E E_k, this is not always the case. For example, the E_{kS} values from the other FLC steps within this file are between 195 and 762 µmol photons m^{-2} s^{-1}. The main factor contributing to this wide range of values is the difficulty with generating a consistent value for τ_S[1].

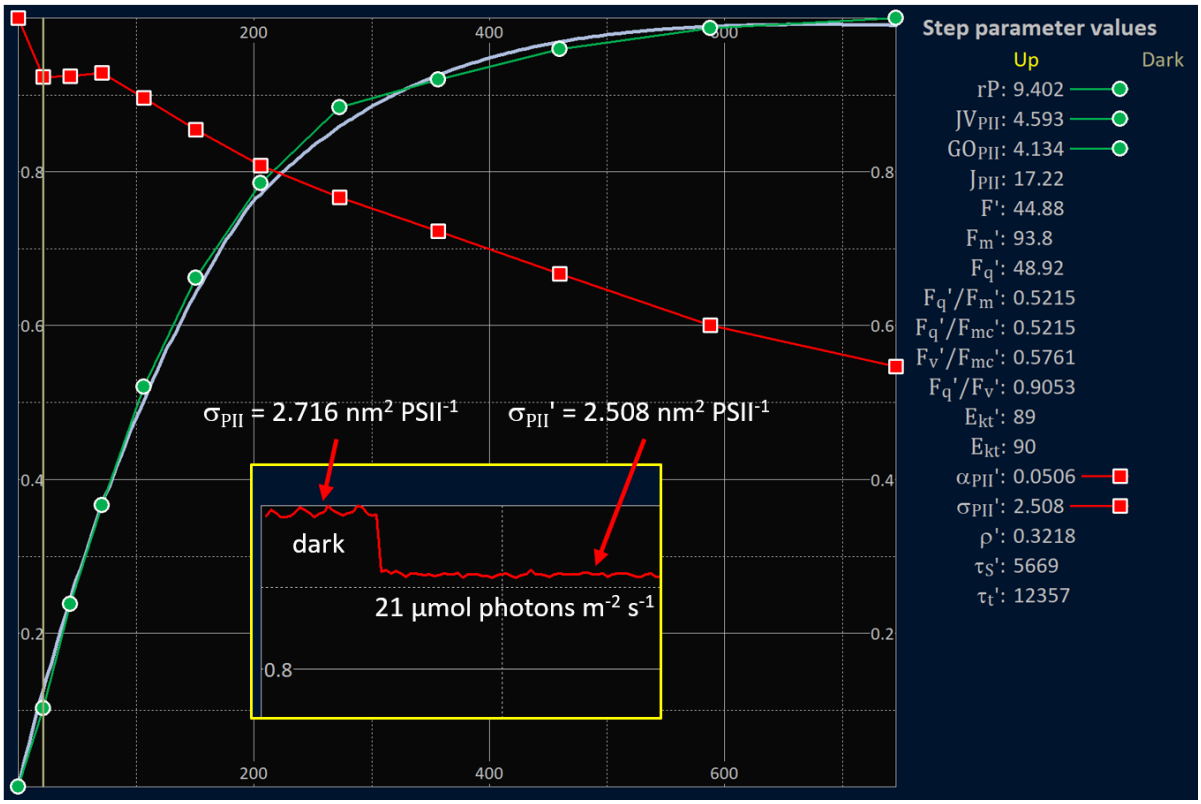

Figure 10.14: Crop from the RunSTAF home screen showing the rP-E curve fit and σ_{PII}[1] step data. These sample was low light-grown cultured cells of *Conticribra weissflogii*. The inset is a crop from the data screen showing the complete set of σ_{PII}[1] values for the Up 1 and Up 2 steps of the FLC.

E_{kS} values are not currently presented on the home screen and E_{kS} is not included as a parameter on the data screen. However, E_{kS} values are output with the Clipboard rP-E data.
See: **Clipboard → rP-E data**

10.11 Derivation of F_b and F_{oc}'

The fraction of F_o that does not originate from photochemically active PSII complexes is termed baseline fluorescence (F_b) and the fraction that does is termed baseline corrected F_o (F_{oc}). Equation 10.20 can be used to derive a value for F_b.

$$F_b = F_m - \frac{F_v}{(F_v/F_{mc})} \qquad \text{Equation 10.20}$$

Where F_v/F_{mc} is the assumed 'intrinsic' value for photochemically active PSII complexes within the sample. When running in Auto FLC mode, the values of F_o and F_m used within Equation 10.20 are from step Up 1 of the FLC. In Manual mode, F_b is only calculated if acquisition starts with the actinic light turned off. If this is the case, the values of F_o and F_m from the last Gaq acquired before the actinic light is turned on are used.

Within a study conducted by Boatman, Geider and Oxborough (2019), an assumed intrinsic value for F_v/F_{mc} of 0.518 generated a good match between STAF-generated estimates of GO_{PII} and more direct estimation of GO_{PII} using a Clark-type O_2 electrode. Although a value of 0.518 is unlikely to be appropriate in every circumstance, these data imply that it may be possible to extrapolate from a relatively small number of direct measurements of GO_{PII} across a much wider dataset of STAF-derived values.

Figure 10.15 is a crop from the home screen showing the processing controls for derivation of F_b and parameters within RunSTAF. The baseline correction (subtraction of F_b from $F_o^{(\prime)}$) can be turned on and off at any point. All affected parameters are automatically recalculated to reflect the current settings. The remainder of this subsection outlines on approach to test if baseline correction is required for a specific dataset, based on the calculation of F_o'.

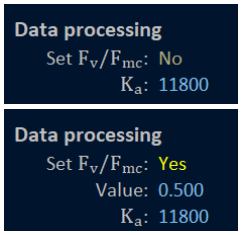

Figure 10.15: The F_b-relevant controls and parameters within **Data processing**. The **Set F_v/F_{mc}** option turns F_b processing on (**Yes**) and off (**No**). When set to **Yes**, the **Value** field sets the assumed intrinsic value of F_v/F_m. In this example, a value of 0.5 has been set.

Within RunSTAF, Equation 10.21 (Oxborough and Baker, 1997) is used to derive the value of F_{oc}' required to calculate F_q'/F_v' and NSV. Because Equation 10.22 includes baseline corrected values (F_{oc} and F_{mc}) the value of F_{oc}' generated is dependent on the value of F_b generated by Equation 10.21.

$$F_{oc}' = \frac{F_{oc}}{(F_v/F_{mc})+(F_{oc}/F_{mc}\prime)} \qquad \text{Equation 10.21}$$

Values of F_o' reported by RunSTAF are generated by adding back the relevant value of F_b. It is important to note that this value of F_o' is not the same as generated when F_b is set to zero for the F_{oc}, F_{mc} and F_{mc}' values in Equation 10.21.

The derived value of F_b is one of the plottable parameters listed under **Primary fluorescence values** on the data screen. Figure 10.16 shows plots of F_b, F_o', F_o plus F' and F_m plus F_m', with and without baseline correction. All parameters within both plots are on the same y-scale.

The F_o plus F' and F_m plus F_m' plots are not affected by F_b. Consequently, the only plots that are different between the upper and lower panels are F_b and F_o'. The F_o' values are calculated as F_{oc}' + F_b to allow for direct comparison with the F_o plus F' and F_m plus F_m' values. The red circles highlight Dark 12, which sits between Up 12 and the first Down step (Down 8). In the upper panel, where **Set F_v/F_{mc}** is set to **No**, there is a clear gap between the measured F_o data (yellow line) and the F_o values calculated using Equation 10.21 (purple line). In the lower panel, baseline correction has been implemented by setting **Set F_v/F_{mc}** to **Yes** and the **Value** to **0.518**. This has brought the measured and calculated F_o values much closer to each other. The match between measured and calculated values of F_o at Down 1 (the very last step within the plots in Figure 10.17) is good within both panels. Taken together, these results are consistent with Equations 10.20 and 10.21 because the downregulation responsible for the separation of measured and calculated values of F_o at Dark 12 has almost completely reversed by Down 1. It follows that baseline correction has a significant impact at Dark

12 (where there is clear evidence of downregulation), but virtually no impact at Down 1 (where downregulation has reversed).

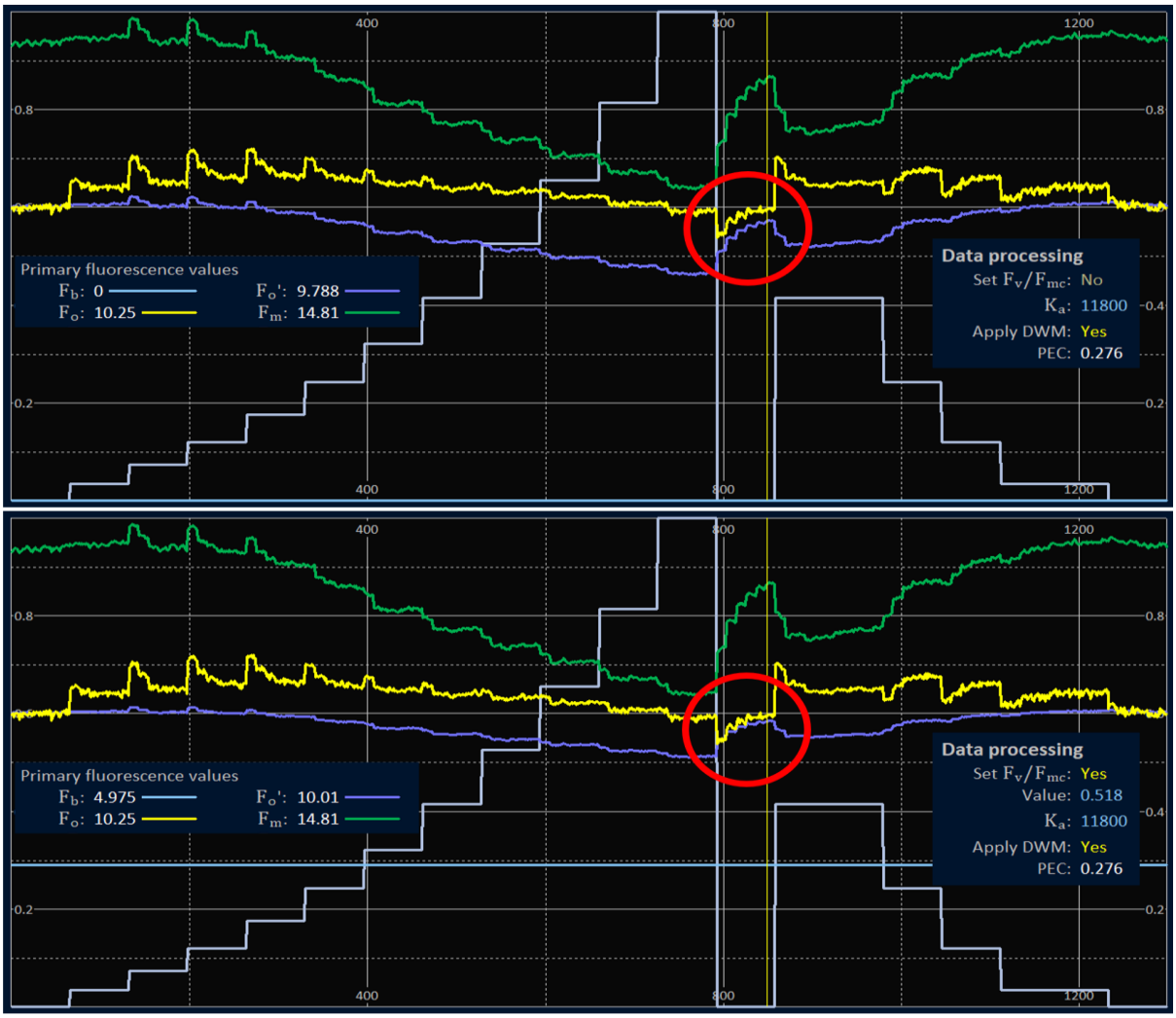

Figure 10.17: Plots of the **Primary fluorescence values** from the first ST pulse through an entire FLC with the **Set F_v/F_{mc}** option set to **No** (upper panel) and **Yes** with Value set to **0.518** (lower panel). The red circles highlight Dark 12, which is located between Up 12 and Down 8. The sample was low light-grown cultured cells of *Conticribra weissflogii*.

10.12 Folder-based file version and data updates

The structure of RunSTAF data files allows for the refitting of primary data. RunSTAF includes a number of functions for refitting and/or reprocessing data across all files within a selected folder. When one of these functions is selected, the process starts with a standard **Open** file folder, as shown in Figure 10.18.

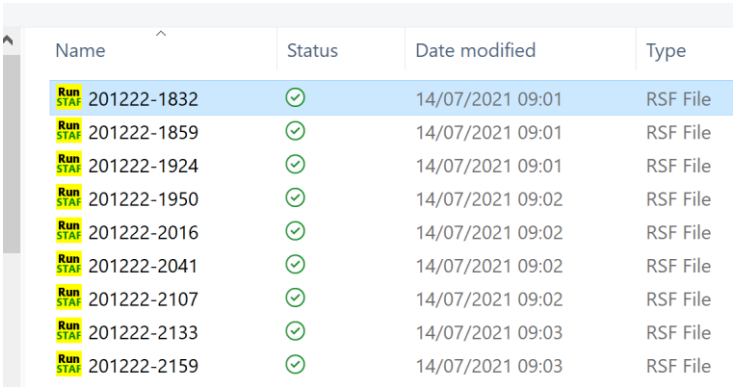

Figure 10.18: Crop from the File Explorer folder that is launched when one of the folder-based functions for refitting and/or reprocessing of data is selected from the menu bar. Double clicking on any file within the folder sets off a refit and/or reprocessing of data across all files within the same folder.

While the refitting and/or reprocessing it being implemented, progress is reported through a dialog located in the top left corner of the screen, as shown in Figure 10.19.

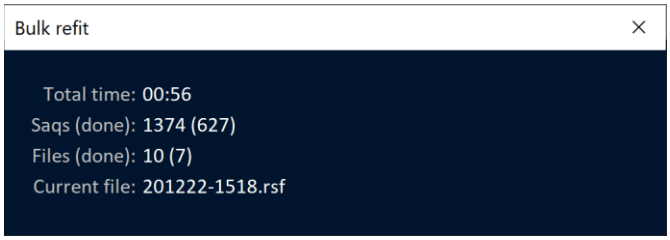

Figure 10.19: The Bulk refit dialog while the bulk refitting process is underway.

While the refit is running, you may see a **Bulk refit (not responding)** message within the dialog title bar. Despite this message, data processing will normally continue in the background and you should be able to see the list of files being updated through the **Date modified** field within File Explorer. Once the refit has finished, RunSTAF will open a message dialog, as shown in Figure 10.20**.**

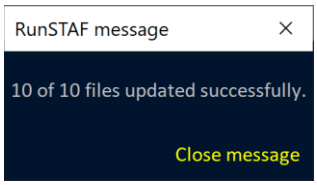

Figure 10.20: A message dialog is opened once refitting and/or reprocessing of all files within the selected folder has completed.

10.12.1 Update the file version (and refit data)

File → Run a folder-based version update

This function updates all files within the selected folder to the current format. If any of the curve fits are out of date, they will be refit during this process. Each file can take anywhere from less than a second to tens of seconds, depending on the level of processing required.

10.12.2 K_a update

File → Folder-based data updates → Run a folder-based Ka update

The value of K_a stored within a data file is applied to the calculation of all K_a-dependent parameters on the fly. In some studies, the optimum value of K_a may only become available after data have been acquired. This function allows K_a to be changed across all files within a folder in a single step. When run, the value of K_a currently set on the home screen under **Data processing** is written to all files within the selected folder. This process normally only takes a few seconds to complete.
See: **Derivation of K_a**

10.12.3 PEC update

File → Folder-based data updates → Run a folder-based PEC update

The user-defined or DWC-generated PEC value is used to generate the cPEC value used to apply a package effect correction to a_{LHII}. This function allows the PEC value from one file to be copied to all files within the selected folder. This function automatically sets the **Apply DWM** parameter as inactive.
See: **Applying the Package Effect Correction (PEC)**

10.12.4 PEP update

File → Folder-based data updates → Run a folder-based PEP update

In situations where a high level of signal averaging is required (under extreme oligotrophic conditions, for example) the time required to run a PEP may compromise the temporal resolution of a continuous series of FLCs. This function allows the PEP from one file to be copied to all files within the selected folder. Although the expectation is that the donor and acceptor files for the PEP will have been generated using the same LabSTAF unit. However, this function does allow for the input of PEP data collected from a different LabSTAF unit. If this is done, the PEP will automatically be reconfigured using the scs data for the file into which the PEP data are being imported.
See: **Spectral correction**

Figure 10.22: If PEP data are imported from another file, the donor file details are shown on the home screen of the modified files.

10.12.5 ESD update

File → Folder-based data updates → Run a folder-based ESD update

This function allows the ESD embedded within the current RunSTAF file to be copied to all files within the selected folder.
See: **Working with External Spectral Data**

10.12.6 Blank update

File → Folder-based data updates → Run a folder-based Blank update

A blank is often generated after a series of measurements has been run. This function allows a single blank value to be applied to all files within a folder, in a single step. When run, the **Blank** value currently set on the home screen under **File details** is written to all files within the selected folder. This process normally only takes a few seconds to complete.

10.12.7 Fv/Fmc update

File → Folder-based data updates → Run a folder-based Fv/Fmc update

This function applies the currently selected **Set F_v/F_{mc}** state (**Yes** or **No**) to all files within the selected folder. If the **Set F_v/F_{mc}** state is **Yes**, the set **Value** of F_v/F_{mc} is applied.

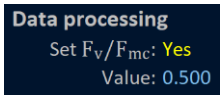

Figure 10.23: The **Set F_v/F_{mc}** and **Value** fields applied to all files within a folder when the **Run a folder-based Fv/Fmc update** is selected.

10.12.8 Calibration update

File → Folder-based data updates → Run a folder-based calibration update

This is the most complex of the folder-based options for the refitting and/or reprocessing of data. This function may be required to update recently acquired data if an instrument recalibration shows relevant changes from the previous calibration. The first step in implementing the calibration update is to generate a calibration file for the LabSTAF system with the updated calibration data installed. To do this, attach the LabSTAF unit and select:

Settings → Factory → Save calibration data

This should generate the LabSTAF message shown in Figure 10.24.

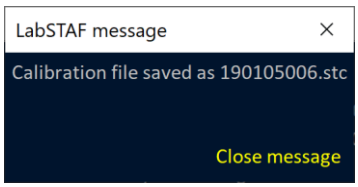

Figure 10.24: This message shows that a calibration file for the STAF unit with SN 19-0105-006 has been generated within the **Calibration files** folder. This file is required to update data that were acquired using this unit.

In addition to the newly created stc file, the update requires that the spectral correction spectra (scs) file is also present within the calibration files folder. The path for this folder is:

C:\Users\User\Documents\CT-RunSTAF\Calibration files

The screen crop in Figure 10.25 shows that both files required to update files collected using the STAF system with SN 19-0105-006 are present.

Name	Status	Date modified	Type	Size
190105004.stc	✓	03/09/2021 12:20	STC File	1 KB
190105005.scs	✓	29/11/2020 16:08	SCS File	9 KB
190105006.scs	✓	20/09/2021 16:04	SCS File	9 KB
190105006.stc	✓	19/09/2021 16:38	STC File	1 KB
200325001.scs	✓	29/10/2020 17:24	SCS File	9 KB
200787006.scs	✓	29/10/2020 17:24	SCS File	9 KB

Figure 10.25: Screen crop from the **Calibration files** folder. The scs and stc files for the STAF unit with SN 19-0105-006 are highlighted.

The calibration update reverses the original processing of primary data that was applied at the point of acquisition and then reprocesses the data using the updated calibration data within the stc file. The data from the scs file are also incorporated within the file at this stage. The updated primary data are then run through a ST refit at the Saq level.
See: **LabSTAF calibration**

11 Generating values of J_{PII} and JV_{PII}

The combination of LabSTAF hardware and RunSTAF software allows for measurement of J_{PII} and JV_{PII} using the so-called Sigma and Absorption methods, respectively. Because the spectral output of the LEDs used for ST measurements (MLEDs) is very different from the spectral output of the LED providing actinic illumination (ALED) a spectral correction step is required for both parameters. In the case of JV_{PII}, correction is also required for the package effect.

This section covers some basic concepts underlying the Sigma and Absorption algorithms. The application of Package Effect Correction (PEC) and the Photochemical Excitation Profile (PEP) for spectral correction and are covered in Sections 12 and 13.
See: **Applying the Package Effect Correction (PEC)** and **Spectral correction**

Under the assumption that every photon used to drive PSII photochemistry results in the transfer of an electron from water to the plastoquinone pool and that every O_2 released reflects the transfer of four electrons, JV_{PII} can be directly converted to Gross Oxygen release (GO_{PII}) with SI units of mol O_2 m^{-3} s^{-1}. While GO_{PII} can be derived from JV_{PII} with a high level of confidence, processes operating within phytoplankton can uncouple PhytoPP from JV_{PII} and GO_{PII} (Geider and MacIntyre, 2002; Behrenfeld et al., 2004; Halsey et al., 2010; Suggett et al., 2010; Lawrenz et al., 2013). It follows that while JV_{PII} provides an upper limit for PhytoPP, the true value of PhytoPP can be significantly lower.

The value of JV_{PII} generated by STAF-based analysis is the product of the rate at which photons are absorbed by the PSII light harvesting system per unit volume and the proportion of absorbed photons used to drive PSII photochemistry. This value is defined as the PSII photochemical flux per unit volume because it is directly proportional to the absorption cross section of PSII photochemistry provided by all PSII complexes within each unit volume of ocean.

11.1 Absorption cross sections

An absorption cross section is linked to an absorption process. There are two processes intrinsic to PSII photochemical flux that are dependent on the absorption of photons: formation of an excited state within the PSII pigment matrix (PSII light harvesting, LHII) and PSII photochemistry (PII). Within this document, the absorption cross sections for these processes are defined by the terms σ_{LHII} and σ_{PII}, respectively, with SI units of m^2 $PSII^{-1}$. Clearly, a photon can only result in PSII photochemistry after being absorbed. It follows that σ_{LHII} is always larger than σ_{PII} and that the relationship between σ_{LHII} and σ_{PII} is defined by the proportion of absorbed photons that ultimately result in PSII photochemistry. The absorption process is illustrated by Figure 11.1.

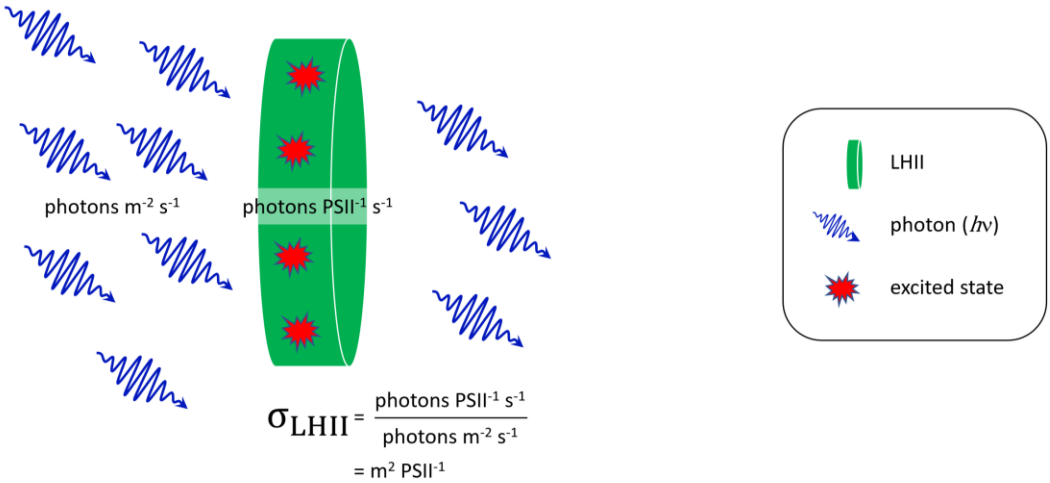

Figure 11.1: The absorption cross section of PSII light harvesting. A proportion of incident photons are absorbed and generate excited states within the pigment matrix.

At the simplest level, PSII photochemistry competes directly with two other processes operating within the PSII complex: the loss of excited states through thermal dissipation (DII) and the emission of photons as fluorescence (FII).

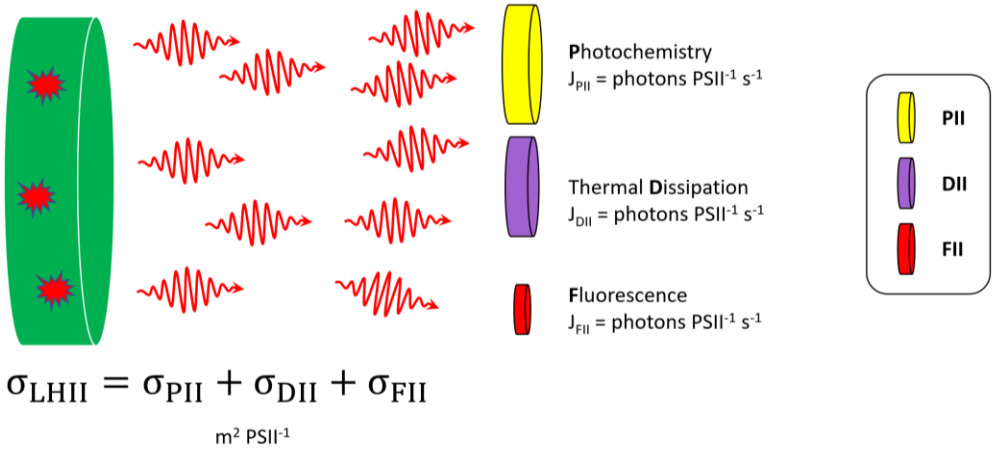

Figure 11.2: The excited states generated within the pigment matrix of the PSII light harvesting system through the absorption of incident photons are energetically equivalent to red photons, even if the absorbed photons that generated the excited states were of shorter wavelength (higher energy). Individual excited states are lost through photochemistry, thermal dissipation or the emission of photons as fluorescence.

The relationships between these processes can be defined by a series of simple equations. As a starting point, Equation 11.1 defines σ_{LHII} as the sum of the absorption cross sections for the three processes that are in direct competition with each other for photon-induced excited states.

$$\sigma_{LHII} = \sigma_{PII} + \sigma_{DII} + \sigma_{FII} \qquad \text{Equation 11.1}$$

The probability that an excited state will be quenched through a particular process is defined by the yield for that process. In turn, the yield for each process can be defined by the rate-constants for the three competing processes, as shown in Equations 11.2A, B and C.

$$\phi_{PII} = \frac{k_{PII}}{k_{PII}+k_{DII}+k_{FII}} \qquad \text{Equation 11.2A}$$

$$\phi_{DII} = \frac{k_{DII}}{k_{PII}+k_{DII}+k_{FII}} \qquad \text{Equation 11.2B}$$

$$\phi_{FII} = \frac{k_{FII}}{k_{PII}+k_{DII}+k_{FII}} \qquad \text{Equation 11.2C}$$

Where ϕ_{PII}, ϕ_{DII} and ϕ_{FII} are all dimensionless. The sum of the yields for all three processes must be unity (Equation 11.3) since they collectively account for the fate of all photon-induced excited states.

$$\phi_{PII} + \phi_{DII} + \phi_{FII} = 1 \qquad \text{Equation 11.3}$$

Equation 11.4 illustrates an important consequence of the relationships defined by Equations 11.1 and 11.3. This equation simply states that the absorption cross section of PSII photochemistry is equal to the product of the absorption cross section for PSII light harvesting and the probability that the absorption of a photon by the PSII light harvesting system will result in PSII photochemistry.

$$\sigma_{PII} = \sigma_{LHII} \cdot \phi_{PII} \qquad \text{Equation 11.4}$$

Values for two of the three parameters within Equation 11.4 can be generated directly from STAF data. A value for σ_{PII} can be generated using the equations provided by Kolber, Prášil and Falkowski (1998) and a value for ϕ_{PII} can be generated from F_{oc} and F_{mc} using Equation 11.5.

$$\phi_{PII} = \frac{F_v}{F_{mc}} \qquad \text{Equation 11.5}$$

Where $F_v = F_{mc} - F_{oc}$.
See: **The Rho ST curve fit** and **Glossary of terms**

11.2 PSII photochemical flux (J_{PII} and JV_{PII})

As already noted, PSII photochemical flux is dependent on the absorption cross section for PSII photochemistry. This can be defined by a single PSII or all PSII complexes suspended within a unit volume of medium.

Equation 11.6 provides a simple expression for the relationship between J_{PII} and JV_{PII}.

$$JV_{PII} = J_{PII} \cdot [PSII] \qquad \text{Equation 11.6}$$

Where $[PSII]$ is the concentration of photochemically active PSII complexes, with units of PSII m^{-3}.

In the dark-adapted state, the absorption cross section of PSII photochemistry provided by a single PSII is defined by σ_{PII} (units of m^2 $PSII^{-1}$). In the case of all PSII complexes within a m^3 of medium, the absorption cross section of PSII photochemistry is defined by the absorption coefficient, a_{PII} (units of m^2 m^{-3} = m^{-1}).

Within an illuminated sample containing multiple PSII complexes, some will be in the open state while others are in the closed state. The PSII photochemical flux for a single PSII complex in the open state is provided by Equation 11.7.

$$J_{PII} = \sigma_{PII} \cdot E \qquad \text{Equation 11.7}$$

Where E is photon irradiance with SI units of photons m^{-2} s^{-1}.

Equation 11.8 generates an average photochemical flux through each PSII (open or closed) within an illuminated sample.

$$J_{PII} = \sigma_{PII}' \cdot \frac{F_q'}{F_v'} \cdot E \qquad \text{Equation 11.8}$$

Where J_{PII} is PSII photochemical flux, $F_q' = F_m' - F'$ and $F_v' = F_m' - F_o'$.

Within this equation, σ_{PII}' denotes the absorption cross section of PSII photochemistry of each open PSII complex within the sample and F_q'/F_v' provides a baseline-independent estimate of the proportion of PSII complexes within the sample that are in the open state at the point of measurement. The relationship between the proportion of PSII complexes in the open state and F_q'/F_v' is 1:1 for a homogeneous population of PSII complexes with zero connectivity. Connectivity and σ_{PII} heterogeneity introduce a deviation from a 1:1 relationship, particularly at high values for F_q'/F_v' (where a high proportion of PSII complexes are in the open state).

An alternative approach to the derivation of J_{PII} begins by using Equation 11.9 to generate a value for σ_{LHII}.

$$\sigma_{LHII} = \sigma_{PII} \cdot \frac{F_{mc}}{F_v} \qquad \text{Equation 11.9}$$

Under the assumption that σ_{LHII} doesn't change between the dark and light-adapted states, the value of σ_{LHII} can be used to generate Equation 11.10.

$$J_{PII} = \sigma_{LHII} \cdot \frac{F_q'}{F_{mc}'} \cdot E \qquad \text{Equation 11.10}$$

With this approach, we are using a STAF measurement from a dark-adapted sample to generate a value for σ_{LHII} and then using a STAF measurement from the same sample under actinic light to

quantify PSII photochemical efficiency (F_q'/F_{mc}'). This approach is largely insensitive to connectivity but remains sensitive to σ_{PII} heterogeneity.

The PSII photochemical flux for all PSII complexes within a unit volume of water can be calculated using Equation 11.11.

$$JV_{PII} = a_{LHII} \cdot \frac{F_{q'}}{F_{mc'}} \cdot E \qquad \text{Equation 11.11}$$

This approach is similar to Equation 11.10 in the sense that we are using a STAF measurement from a dark-adapted sample to quantify PSII light harvesting (in this case, for all PSII complexes within a unit volume of water) and the same measurement under actinic light to define the average efficiency at which harvested photons are used to drive PSII photochemistry. This approach is largely insensitive to both connectivity and heterogeneity.

We can define two routes for generating a value for a_{LHII}. The first route (Equation 11.12) incorporates the right hand side of Equation 11.9.

$$a_{LHII} = \sigma_{PII} \cdot \frac{F_{mc}}{F_v} \cdot [PSII] \qquad \text{Equation 11.12}$$

The second route for generating a value for a_{LHII} is illustrated by Equation 11.13 (Oxborough et al. 2012).

$$a_{LHII} = K_a \cdot \frac{F_{mc} \cdot F_{oc}}{F_v} \qquad \text{Equation 11.13}$$

Where K_a is an instrument-type specific constant, with units of m^{-1}.
See: **Derivation of K_a**

As an alternative to Equation 11.11, Equation 11.14 can be derived from the relationship defined by Equation 11.6 and the right hand side of Equation 11.8.

$$JV_{PII} = \sigma_{PII}' \cdot \frac{F_{q'}}{F_{v'}} \cdot [PSII] \cdot E \qquad \text{Equation 11.14}$$

It follows that Equations 11.11 to 11.14 provide three routes to JV_{PII}:

- Equation 11.11 combined with Equation 11.12
- Equation 11.11 combined with Equation 11.13
- Equation 11.14

Equations 11.12 and 11.14 include $[PSII]$. A value for this parameter can be derived using Equation 11.15 (Oxborough et al. 2012).

$$[PSII] = K_a \cdot \frac{F_{oc}}{\sigma_{PII}} \qquad \text{Equation 11.15}$$

Substituting the right hand side of Equation 11.15 for the $[PSII]$ in Equation 11.12 generates Equation 11.16, which simplifies to Equation 11.13.

$$a_{LHII} = \sigma_{PII} \cdot \frac{F_{mc}}{F_v} \cdot K_a \cdot \frac{F_{oc}}{\sigma_{PII}} \qquad \text{Equation 11.16}$$

Substituting the right hand side of Equation 11.15 for $[PSII]$ within Equation 11.14 generates Equation 11.17. This serves to emphasise the inclusion of both σ_{PII} and σ_{PII}' with this approach.

$$JV_{PII} = \sigma_{PII}' \cdot \frac{F_{q'}}{F_{v'}} \cdot K_a \cdot \frac{F_{oc}}{\sigma_{PII}} \cdot E \qquad \text{Equation 11.17}$$

Consequently, we can now define two approaches to the calculation of JV_{PII}:

- The **Sigma method** which uses Equation 11.14
- The **Absorption method** which uses Equation 11.11

Figure 11.3 summarises the different approaches to the calculation of JV_{PII} incorporated within the Sigma and Absorption methods.

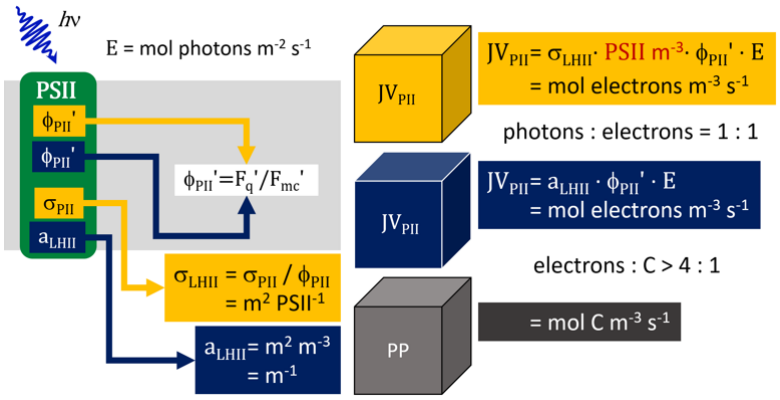

Figure 11.3: Schematic showing that while the Sigma method can provide J_{PII} (electrons $PSII^{-1}$ s^{-1}) from STAF data alone, it cannot be used to generate values of JV_{PII} (mol electrons m^{-3} s^{-1}) without additional input. In contrast, the Absorption method can provide JV_{PII} from STAF data alone.

To select the best method for use in any specific situation, the following points are worth considering:

1. Values of F_o, F_m, F' and F_m' can be measured at higher precision than values of σ_{PII} and σ_{PII}'
2. Values of F_o, F_m and σ_{PII} can be measured at higher precision than values of F', F_m' and σ_{PII}'
3. F_o, F_m, F' and F_m' are all sensitive to baseline fluorescence
4. σ_{PII} and σ_{PII}' are insensitive to baseline fluorescence
5. F_{oc}, F_{mc}, F_c' and F_{mc}' are insensitive to heterogeneity within the sample
6. σ_{PII} and σ_{PII}' are sensitive to heterogeneity within the sample

The precision issue raised by Points 1 and 2 is most obvious when photon irradiance is increased to levels that saturate photosynthesis. This can decrease the amplitude of F_q' to the point where a reliable value of σ_{PII}' can no longer be generated.

With the Absorption method, baseline fluorescence (Points 3 and 4) increases the value of a_{LHII} and decreases the value of F_q'/F_m' (Oxborough et al. 2012). With the Sigma method, baseline fluorescence increases the value of [PSII] generated by Equation 11.14 in proportion to the increase in a_{LHII}.

Within Equation 11.14, the value of F_q'/F_v' is nominally independent of baseline fluorescence. However, if the required value of F_o' is generated using the method provided by Oxborough and Baker (1997), baseline fluorescence can decrease the calculated value of F_q'/F_v'. It should be noted that the baseline fluorescence-induced decrease in F_q'/F_v' is always lower than the baseline fluorescence-induced decrease in F_q'/F_m' and approaches zero with samples that exhibit low levels of downregulation.

An obvious potential form of heterogeneity within a sample (points 5 and 6) is the combining of phytoplankton species with differing σ_{PII} values within the waveband(s) used for the ST measurements. Providing the ST pulse is bright enough to ensure that F_m or F_m' is reached for all species within a sample, this type of heterogeneity does not generate errors with the Absorption method (Equation 11.11). This is because the values of F_{oc}, F_{mc}, F_c' and F_{mc}' are additive and, as a result, both a_{LHII} and F_q'/F_{mc}' are unaffected by heterogeneity. Conversely, this type of heterogeneity can generate an error with the Sigma method (Equation 11.14) because the σ_{PII} value generated from adding multiple curves together and applying a single Rho fit is likely to generate sizeable errors.
See: **Spectral correction**

11.3 Scaling of JV_{PII} and GO_{PII} values to FLC-derived rP data

As noted elsewhere within this document, the relative photosynthesis (rP) data values scale directly to values of JV_{PII} and GO_{PII}, such that all three parameters remain in constant proportion to each other with changes in incident photon irradiance. Because rP is the product of F_q'/F_{mc}' and E, we can link rP and JV_{PII} by substituting rP for the product of F_q'/F_{mc}' and E within Equation 11.11 to generate Equation 11.18.

$$JV_{PII} = a_{LHII} \cdot rP \qquad \text{Equation 11.18}$$

Within RunSTAF, values of GO_{PII} are always JV_{PII} divided by four.

11.4 Derivation of K_a

The current default K_a value for LabSTAF is the same as used with the FastOcean FRRf and the fluorescence values have been scaled to match with FastOcean through a series of comparative measurements from natural samples. It is worth noting that K_a only affects the calculated values of a_{LHII}, JV_{PII} and GO_{PII} and that any change in the set value of K_a is immediately applied to existing data. A function has been incorporated within RunSTAF to allow for a folder-based update of K_a across files…

File → Folder-based updates → Run a folder-based Ka update

A derivation procedure for K_a was originally provided by Oxborough et al. (2012). Within this manuscript, the term K_R was used in place of K_a. The only difference between K_R and K_a is that the former is only applicable to a single fluorometer while the latter can be used with any fluorometers built to the same specification. This difference is illustrated by Equations 11.19 and 11.20.

$$K_R = [PSII] \cdot \frac{\sigma_{PII}}{F_{oc}} \cdot E_{ST} \qquad \text{Equation 11.19}$$

$$K_a = [PSII] \cdot \frac{\sigma_{PII}}{F_{oc}} \qquad \text{Equation 11.20}$$

The E_{ST} term incorporated within Equation 11.18 is required for systems where the primary fluorescence data are not scaled to MLED output. Equation 11.19, which omits the E_{ST} term, is applicable to LabSTAF because fluorescence values reported by RunSTAF are automatically corrected for MLED output. The reported units for E_{ST} are photons nm^{-2} $(100\ \mu s)^{-1}$. A value of 1.0 photons nm^{-2} $(100\ \mu s)^{-1}$ is equal to 16 603 µmol photons m^{-2} s^{-1}.

The accuracy of K_a derived using Equation 11.19 is dependent on σ_{PII} and F_{oc} scaling together. As already noted, the fluorescence signal and σ_{PII} have different sensitivities to baseline fluorescence and sample heterogeneity. It follows that the most accurate values for K_a from Equation 11.19 are likely to come from single species cultures with high values of F_v/F_m.

Within Equations 11.19 and 11.20, the value of [PSII] is derived using the flash-O_2 method described by Boatman, Geider and Oxborough (2019). Equation 11.21 provides an alternative for deriving K_a. Within this equation, JV_{PII} is derived from direct measurement of O_2 release.

$$K_a = JV_{PII} \,/\, \left(\frac{F_{mc} \cdot F_{oc}}{F_v} \cdot \frac{F_q'}{F_{mc}'} \cdot E\right) \qquad \text{Equation 11.21}$$

From a purely practical point of view, it is much easier to derive K_a using Equation 11.21 than 11.20. One option is to derive the saturated rate of rP from a FLC (calculated as the product of F_q'/F_{mc}' and E) and measure O_2 release at the same E using a spectrally matched actinic light source. Measuring at saturation is advantageous because although the value of F_q'/F_{mc}' decreases with E, overall accuracy is improved through having the highest rate of O_2 evolution.

12 Applying the Package Effect Correction (PEC)

When using the Absorption method to derive values for JV_{PII}, measurement accuracy is highly dependent on there being a consistent ratio between photons used to drive photochemistry and photons emitted as fluorescence (i.e., the ratio between JV_{PII} and JV_{FII} must be consistent). The package effect can have a significant impact on this ratio.

The package effect is largely a consequence of the high concentration of chlorophyll *a* and other light-absorbing pigments within phytoplankton cells. To put this in context, while the concentration of chlorophyll *a* within the open ocean is often below 0.1 mg m^{-3}, the concentration within phytoplankton cells is approximately a million times higher than this, at 0.1 kg m^{-3} (calculated from data within Montagnes et al. 1994). It follows that while sea water with phytoplankton cells suspended within it can be considered optically thin, the localized volume within each phytoplankton cell is optically very thick (see Boatman, Geider and Oxborough, 2019 and references therein).

Within LabSTAF, fluorescence emission is normally defined by a 685 nm bandpass filter in front of the PMT. Because this is very close to the emission peak from PSII within phytoplankton cells (around 683 nm) the proportion of the fluorescence signal coming from PSII is maximised. On the downside, the red absorption peak of chlorophyll *a* is Stokes shifted by only 2-3 nm from the emission peak and, consequently, reabsorption of fluorescence is also very close to the maximum. The probability of reabsorption is dependent on the size and optical characteristics of the cell plus the concentration of chlorophyll within the cell. At one end of the scale, reabsorption within a small cell with a simple cell wall is likely to be at the low end of the scale (low package effect) while reabsorption within, for example, a large haptophyte surrounded by coccoliths will be much higher (high package effect). The images within Figures 12.1 to 12.3 illustrate this phenomenon.

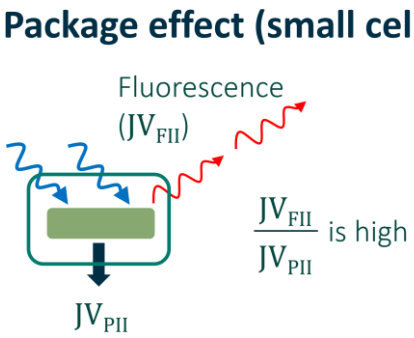

Figure 12.1: With a simple small cell, a high proportion of the photons emitted as fluorescence make it out of the cell. Consequently, the measured ratio of JV_{FII} to JV_{PII} is at the higher end of possible values.

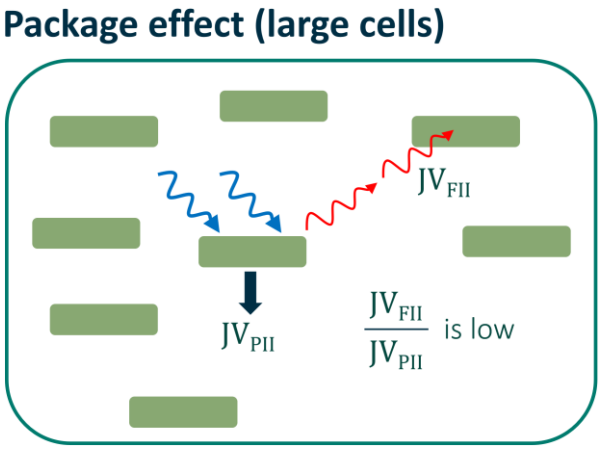

Figure 12.2: With increasing size and changes in optical characteristics, the proportion of photons emitted as fluorescence that make it out of the cell decreases due to reabsorption. Consequently, the measured ratio of JV_{FII} to JV_{PII} becomes lower.

Package effect correction

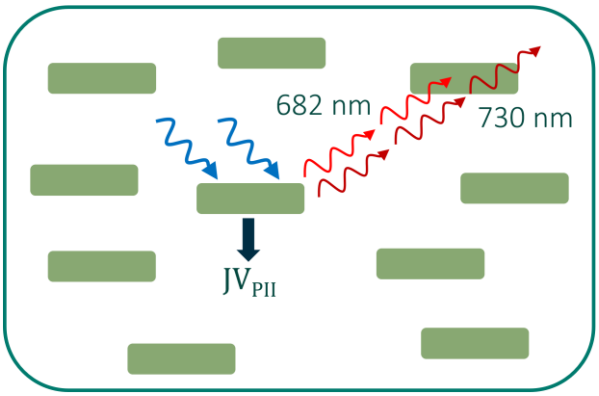

Figure 12.3: Fluorescence emission is much higher at 682 nm than at 730 nm. However, reabsorption of fluorescence at 682 nm, relative to 730 nm, is orders of magnitude higher still. It follows that the 730 nm : 682 nm emission ratio can provide a correction for the package effect.

In addition to the 685 nm bandpass filter that is normally used to define fluorescence emission, LabSTAF incorporates a 730 nm bandpass filter. Both filters are ±10 nm Full Width-Half Max FWHM. A linear actuator is used to switch between these two filters as the Dual Waveband Measurement (DWM) is run. Three reps of 685 and 730 nm measurements are made and stored within the RunSTAF data file. These primary data are available through:

Clipboard → DWM data

The number of sequences averaged within each rep ($n\text{Seq}_{DWM}$) is defined by Equation 12.1.

$$n\text{Seq}_{DWM} = (\text{Seq} / \text{Acq}) \times (\text{Acq} / \text{Saq}) \times 2 \qquad \text{Equation 12.1}$$

Where **Seq / Acq** and **Acq / Saq** are as set under **STAF setup** on the home screen.
See: **Pre-FLC changes in STAF setup**

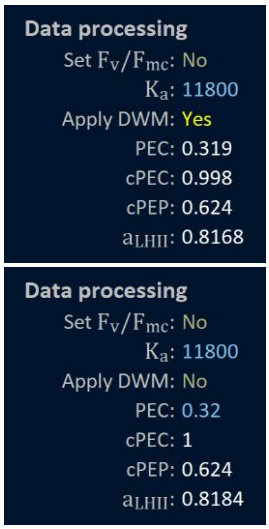

Figure 12.4: If the **Apply DWM** option is set to **Yes**, the DWM-derived value of the Package Effect Correction (**PEC**) is applied to values of JV_{PII} and GO_{PII}. If the **Apply DWM** option is set to **No**, the value of **PEC** is set to the default of **0.32** and can be edited. A change to the value of **PEC** is reflected in the value of **cPEC** and is automatically applied to a_{LHII} and (as a consequence) all values of JV_{PII}.

If the default PEC value of 0.32 is applied, the cPEC value is 1.0 and there is no package effect correction applied. If the PEC value is other than 0.32, the value of cPEC is simply the set value divided by the default. For example, a PEC value of 0.16 would generate a cPEC value of 0.5. The package effect corrected value of a_{LHII} is the non-corrected value multiplied by the value of cPEC.

13 Spectral correction

13.1 Working with Photochemical Excitation Profiles (PEPs)

The two PEPs reported by RunSTAF incorporate seven F_v or σ_{PII} values generated by the application of different combinations of MLED channels. The F_v PEP values are on the SU scale while the σ_{PII} PEP values have reported units of nm^2 $PSII^{-1}$. In theory, a completely homogeneous population of PSII complexes would generate identical normalized F_v PEP and σ_{PII} PEP values. In practice, although many samples show a close match between normalized F_v PEP and σ_{PII} PEP values, PSII heterogeneity can generate very subtle to highly dramatic differences between the two.

The main value of PEPs is to facilitate spectral correction of a_{LHII}, J_{PII} and JV_{PII}. The F_v PEP values from different PSII sub-populations within a sample are additive. Consequently, PSII heterogeneity does not introduce an obvious error when incorporating F_v PEP data within spectral corrections. In contrast, σ_{PII} PEP values from PSII sub-populations within a sample do not combine in a way that allows them to be used for spectral correction.

13.1.1 Excitation wavebands for the PEP

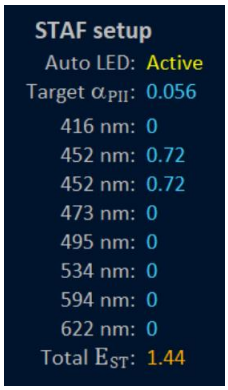

Figure 13.1: The labelling of the eight LabSTAF MLED channels within LabSTAF is as shown in this screenshot crop from the RunSTAF home screen. As part of the LabSTAF calibration, the emission spectra for all eight MLED channels and the ALED channel are recorded from within the sample chamber and stored at 1 nm resolution within the SCS calibration file for the attached LabSTAF. The two 452 nm channels are combined into a single waveband. PEP data are processed using the wavelength of the measured emission peak for each MLED waveband in preference to the channel name values.

Figures 13.2 shows a completed PEP, cropped from the home screen. The numbers in brackets within the key below the plots show the effectiveness of the selected MLED waveband in generating values of F_v and σ_{PII}, relative to the ALED. In this case, the 495 nm waveband has been selected. This waveband generates an F_v value that is 7.6% higher and a value for σ_{PII} that is 37.8% higher than the ALED reference.

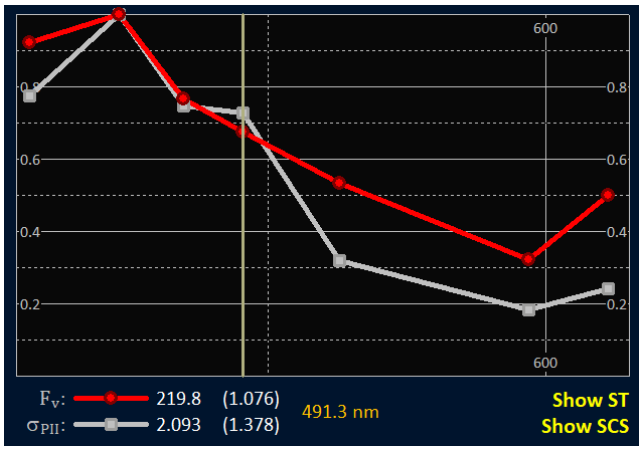

Figure 13.2: A completed PEP recorded from cultured cells of *Conticribra weissflogii* with the **Show SCS** option inactive. The 491.3 nm label in orange text defines the central wavelength for the 495 nm waveband, as measured during calibration.

Figure 13.3 shows the Spectral Correction Spectra (SCS) output generated from the PEP within Figure 13.2. The **Flat white coefficients** within Figure 13.3 define the relative photon yield of the selected MLED combination and the ALED in generating F_v, in comparison to a theoretical light source that provides a spectrally flat output between 380 and 660 nm.

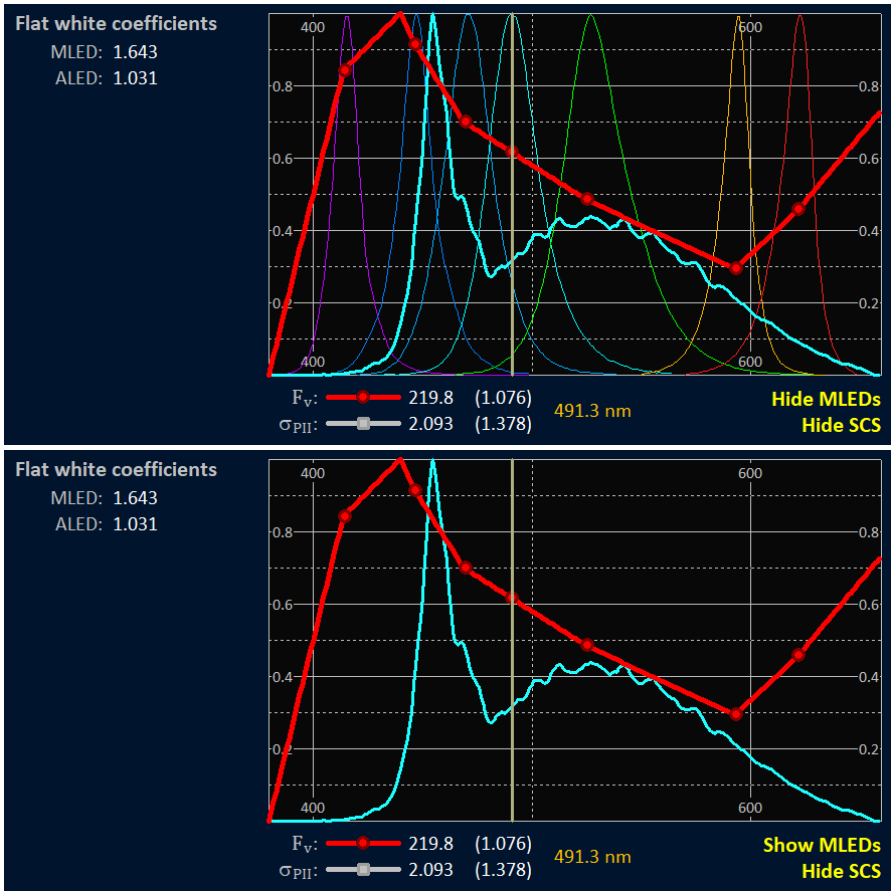

Figure 13.3: A completed PEP recorded from cultured cells of the diatom *Conticribra weissflogii* with the **Show SCS** option active. The extrapolations to virtual points (at 380 nm, 440 nm and 660 nm) within these plots are discussed within this section.

The MLED spectra have been hidden in the lower plot, by pressing the **Hide MLEDs** button.

13.1.2 The PEP protocols

The reliability of F_v and σ_{PII} PEP values is dependent on a high proportion of the photochemically active RCIIs being closed by application of the ST pulse. Importantly, in this respect, the σ_{PII} values for diatoms, dinoflagellates, green algae and haptophytes tend to be much lower between 500 and 590 nm than they are between 435 and 470 nm. For example, σ_{PII} values at 590 nm are typically around 25% of values at 435 and 450 nm. It follows that you need to deliver approximately four times as many photons from measuring LEDs at 590 nm, compared to 450 nm, in order to close the same proportion of RCIIs within the same timeframe.

Gorbunov et al. (2020) recently described a STAF-based method for physiological and taxonomic analysis of phytoplankton communities. Within this study, a mini-FIRe fluorometer was used to provide ST pulses from six measuring LED wavebands centred at 435, 450, 470, 500, 530 and 590 nm. All measurements were made using single wavebands and spectral analysis was limited to waveband-specific values of σ_{PII}. ST pulse saturation at 530 and 590 nm was achieved through a combination of higher photon irradiances and longer ST pulses than were used with the shorter wavebands (150 µs for the 530 and 590 nm wavebands, compared with 80 µs for the 435 and 450 nm wavebands).

In contrast to the approach employed by Gorbunov et al. (2020), the PEP function incorporated within RunSTAF achieves the required level of ST pulse saturation by running different combinations of LED wavebands. With this approach, the same pulse duration is used for all LED waveband combinations. Table 13.1 compares the maximum photon irradiances that can be provided by the LED wavebands incorporated within LabSTAF with the nearest equivalent wavebands used by Gorbunov et al. (2020).

Waveband central λ (nm)	Maximum photon irradiance (typical) µmol photons m^{-2} s^{-1} [photons nm^{-2} $(100\ \mu s)^{-1}$] { Single waveband}	Gorbunov et al. (2020) µmol photons m^{-2} s^{-1}
416	13,851 [0.834] { 15 }	20,000 – 25,000 for each waveband between 435 and 505 nm
452 x 2	34,047 [2.051] { 10 }	
473	16,574 [0.998] { 10 }	
495	10,142 [0.611] { 20 }	
534	9267 [0.558] { 40 }	40,000 – 60,000 for the 530 and 590 nm wavebands
594	2500 [0.151] { 300 }	
622	8206 [0.494] { 40 }	NA

Table 13.1: The maximum photon irradiance provided by the measuring LED wavebands incorporated within LabSTAF and the system used by Gorbunov et al. (2020). The LabSTAF 452 nm photon irradiance is the sum of both channels. A LabSTAF currently includes 40 LEDs (five LEDs per channel). The **Single waveband** values within curly braces indicate approximately how many LEDs would be required to saturate the sample shown in Figure 13.3, if each waveband were applied individually.

The numbers in curly brackets (the **Single waveband** values) indicate how many LEDs of each waveband would be required to saturate the sample shown in Figure 13.3 (as an example) if each waveband was applied individually. Even without the 594 nm channel (which alone would require 300 LEDs) the total number required would still be over three times higher than the 40 LEDs currently integrated within LabSTAF, at 135. Incorporation of this number of LEDs would severely compromise the optical arrangement and more than double the overall power requirement of LabSTAF. The combined waveband approach incorporated within RunSTAF effectively circumvents this problem.

As already noted, Gorbunov et al. (2020) used the parameter σ_{PII} to provide the spectral information required for physiological and taxonomic analysis of phytoplankton communities. In contrast, RunSTAF generates PEPs derived from both σ_{PII} and F_v. The expectation is that the F_v and σ_{PII} PEPs recorded from spectrally homogeneous samples will be closely matched in terms of quantitative accuracy, with F_v providing a marginally higher level of precision. As already noted within this section, spectral heterogeneity within a sample does not impact on the quantitative accuracy of F_v PEPs, providing ST pulse saturation is reached. Conversely, σ_{PII} PEPs lose quantitative accuracy as spectral heterogeneity increases, even if ST pulse saturation is attained. This is true for both the single waveband approach employed by Gorbunov et al. (2020) and the combined waveband approach incorporated within RunSTAF. It follows that divergence between F_v and σ_{PII} PEPs provides the potential for qualitative assessment of heterogeneity within samples.

There are currently two protocol options, within RunSTAF, for generating PEPs. The default option is run if the two 452 nm MLED channels are the only ones set with a non-zero value under **STAF setup**. This option (**PEP-bc**) is optimised for samples that are dominated by phytoplankton incorporating chlorophylls *b* or *c* as the main light harvesting pigments.

The second option (**PEP-cy**) is run for any other combination of MLED channels (other than just the two 452 nm channels) and is primarily intended for samples that are dominated by cyanobacteria incorporating phycobilins as the main light harvesting pigments. Table 13.2 shows the LED combinations at each step of the PEP within the PEP-bc and PEP-cy protocols.

Step	PEP-bc active channels (nm)	Reps	PEP-cy active channels (nm)	Reps
1	1st 452 nm + 416 nm	1	534 nm + 622 nm + 416 nm	1
2	1st 452 nm + 2nd 452 nm	1	534 nm + 622 nm + 2nd 452 nm	1
3	1st 452 nm + 473 nm	1	534 nm + 622 nm + 473 nm	1
4	1st 452 nm + 495 nm	1	534 nm + 622 nm + 495 nm	1
5	1st 452 nm + 2nd 452 nm + 534 nm	2	534 nm + 622 nm	1
6	1st 452 nm + 2nd 452 nm + 594 nm	4	534 nm + 622 nm + 594 nm	3
7	1st 452 nm + 2nd 452 nm + 622 nm	2	622 nm	4

Table 13.2: The waveband combinations used for the **PEP-bc** and **PEP-cy** functions implemented through RunSTAF. The system cycles through all steps repeatedly until the programmed level of signal averaging has been reached. The **Reps** columns show the repeats at each step. These are implemented to improve the signal to noise of wavebands that generally have low σ_{PII} and/or low photon output. Typically, each loop through all seven steps takes approximately 1.4 s.

The PEP function generates three reps of seven waveband combinations. With the default settings, RunSTAF cycles through all seven waveband combinations at approximately 0.6 Hz. The number of Seqs averaged per PEP rep (Seq_{PEP}) is defined by Equation 13.1.

$$Seq_{PEP} = (Seq / Acq) \times (Acq / Saq) \qquad \text{Equation 13.1}$$

Where (Seq / Acq) and (Acq / Saq) are as set under **STAF setup** on the home screen. From experience, this approach to signal averaging generates highly reproducible PEP data.

While PEP-bc is running, the 1st 452 nm channel is as set by the Auto LED function while the 2nd 452 nm channel is attenuated to 72% of the Auto LED value. The 416 nm and 473 nm channels are both set as close as possible to the E_{ST} output for the 1st 452 nm channel. The remaining channels (534 nm, 594 nm and 622 nm) are set to maximum output. While PEP-cy is running, all seven MLED channels used are set to maximum output.

A central feature of the PEP method is the determination of waveband-specific values for photon yield of F_v, and waveband-specific σ_{PII} values. This is achieved by combining different wavebands to reach saturation during the application of ST pulses and then deconvolving the measured values as described below. For the PEP-bc option, the 452 nm waveband is incorporated within all seven waveband combinations. Because σ_{PII} is high at 452 nm for the four major eukaryotic phytoplankton groups, its incorporation provides saturation with all waveband combinations within PEP-bc. Step 2 of PEP-bc in Table 13.2 provides direct 452 nm-specific values of the photon yield of F_v, and σ_{PII}. Values of these parameters for the other wavebands are then calculated as the difference between the 452 nm-specific values and the values measured using the waveband combinations listed in the PEP-bc column of Table 13.2.

Automated optimisation of MLED intensity is incorporated within the PEP procedure. With PEP-cy, achieving saturation is more challenging than with PEP-bc and may require a manual increase in the duration of the ST pulse from the default of 100 µs.

13.1.3 Checking PEP saturation

Figure 13.4 provides two example PEP plots from a freshwater chlorophyte (*Chlorella vulgaris*) and a freshwater cyanobacterium (*Anabaena* sp.). Although there is a reasonable match between the F_v and σ_{PII} traces within each example, there are also some highly reproducible differences.

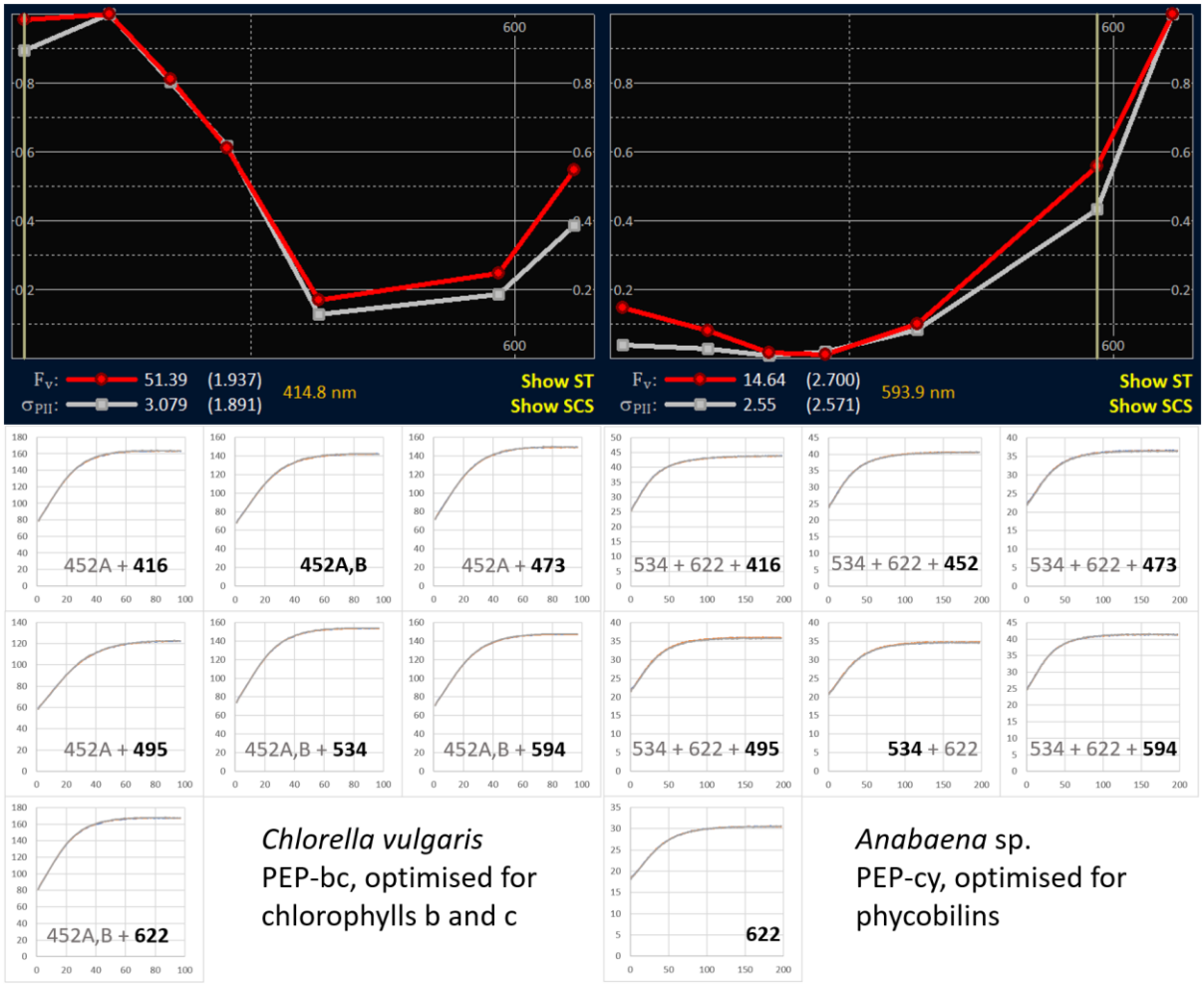

Figure 13.4: Sample PEPs optimised for chlorophylls *b* and *c* (PEP-bc) or for phycobilins (PEP-cy). The waveband evaluated by each ST pulse is shown in bold. Each ST plot includes three traces.

Also included within Figure 13.4 are the ST traces generated by the PEP protocol. These data are not shown within RunSTAF but can be accessed through the **Clipboard →PEP data** option on the RunSTAF menu. The ST traces all show good saturation for all waveband combinations. For *Anabaena* sp., the ST pulse duration has been increased from the default of 100 µs to 200 µs to ensure good saturation. Each of the ST plots includes three traces.

13.2 How heterogeneity affects the relationship between F_v PEP and σ_{PII} PEP data

Figure 13.5 shows five PEP screen crops from each of three different phytoplankton cultures. The F_v and σ_{PII} values are both plotted on a scale that goes from zero to one. For spectra with all values greater than zero, points are normalized to the highest value. A heterogeneous sample can generate negative values for σ_{PII} PEPs. In such cases, the entire range of measured values is rescaled to between zero and one.

The PEPs in the first set (Figure 13.5, **A1** – **A5**) were recorded from samples of *C. vulgaris* (CCAP 211/11B), using the PEP-bc protocol. In all cases, all points shown within the F_v and σ_{PII} PEPs are greater than zero and the highest values are at the 452 nm waveband. Although the F_v and σ_{PII} PEPs are closely matched overall, it is worth noting that the normalised σ_{PII} values are consistently lower than normalized values for F_v at 416 nm and 622 nm.

As already noted, F_v and σ_{PII} measured from a homogeneous population of PSII complexes should track each other closely across all wavebands. However, there is scope for F_v and σ_{PII} to diverge where some form of PSII heterogeneity exists within the sample. One well documented type of PSII

heterogeneity within the four major eukaryotic phytoplankton groups is the division between PSIIα and PSIIβ (Andrée, Weis and Krieger, 1998; Black, Brearley and Horton, 1986; Guenther and Melis, 1990; de Marchin et al. 2014). PSIIβ are less numerous than PSIIα, have a much smaller light harvesting complex and a higher ratio of chlorophyll *a* to chlorophyll *b*. In combination, these characteristics have the potential to account for the divergence between F_v and σ_{PII} at the 416 nm and 622 nm wavebands. Within the proposed model, the reported F_v at each waveband is the sum of the signals from PSIIα and PSIIβ. In contrast, σ_{PII} is much lower for PSIIβ than PSIIα, because the PSIIβ light harvesting complex is much smaller than the PSIIα light harvesting complex. As a consequence, the measured values of σ_{PII} for PSIIα plus PSIIβ are lower than for PSIIα alone. Because PSIIβ have a higher chlorophyll *a* to chlorophyll *b* ratio than PSIIα, the PSIIβ-dependent decrease in σ_{PII} is more evident at the 416 nm and 622 nm wavebands because absorption by chlorophyll *a* relative to chlorophyll *b* is highest at these points.

The PEPs in the second set (Figure 13.5, **B1** – **B5**) were recorded from samples of *Anabaena* sp. (CCAP 1403/13A), using PEP-cy. As with the *C. vulgaris* set, all points within the F_v and σ_{PII} PEPs are greater than zero. The F_v and σ_{PII} PEPs are both normalized to the 622 nm waveband.

Within all of the *Anabaena* sp. plots, the normalized values of F_v are consistently higher than the normalized values of σ_{PII} values at the 416 nm, 452 nm, 534 nm and 594 nm wavebands. The PSII light harvesting system within *Anabaena* sp. comprises a relatively small compliment of chlorophylls *a* within each PSII core complex plus phycocyanin and allophycocyanin within phycobilisomes. It follows that the heterogeneity causing divergence between F_v and σ_{PII} values at 416 nm and 452 nm may simply be between PSII complexes that are energetically connected to phycobilisomes and PSII complexes that are not. Within this model the phycobilisome-connected PSII complexes would generate much higher σ_{PII} and F_v in the red (594 nm and 622 nm) than in the blue (416 nm and 452 nm). Conversely, σ_{PII} and F_v would both be higher in the blue than in the red for phycobilisome-disconnected PSII complexes. Because F_v is additive, the phycobilisome-disconnected PSII complexes increase the overall signal within the blue but do not contribute significantly within the red. In contrast, the phycobilisome-connected and disconnected PSII complexes would have very similar σ_{PII} values within the blue while σ_{PII} values within the red would be almost entirely attributable to the phycobilisome-connected PSII complexes. As a consequence, the σ_{PII} PEP is likely to be representative of the phycobilisome-connected PSII complexes while the F_v PEP provides a more accurate assessment of the complete PSII population within the sample.

The PEPs in the third set (Figure 13.5, **C1** – **C5**) were recorded from samples of a marine dinoflagellate, *Alexandrium catenella* (CCAP 1119/17), using the PEP-bc protocol. Of the three examples, this one shows the greatest divergence between the normalized F_v and σ_{PII} values. As with *C. vulgaris*, the highest values for F_v and σ_{PII} are at the 452 nm waveband and both PEPs are normalised to this point. As with both *C. vulgaris* and *Anabaena* sp., the normalized σ_{PII} value is lower than F_v at the 416 nm waveband. The PEP-bc protocol was used for this set because *A. catenella* incorporates chlorophyll *c* as a PSII light harvesting pigment. Because the PEP-bc protocol was used, any PSII complexes within the sample that rely on longer wavelength light harvesting pigments, such as phycocyanin and allophycocyanin, are unlikely to have been saturated. This could be an issue here because the greatest divergence between F_v and σ_{PII} occurs at the three longest wavebands. This divergence at the three longest wavebands may indicate that the samples used were contaminated with cryptophytes and/or cyanobacteria or that the cells of *A. catenella* incorporate cyanobacteria cells as symbionts (e.g., Nakayama et al. 2019).

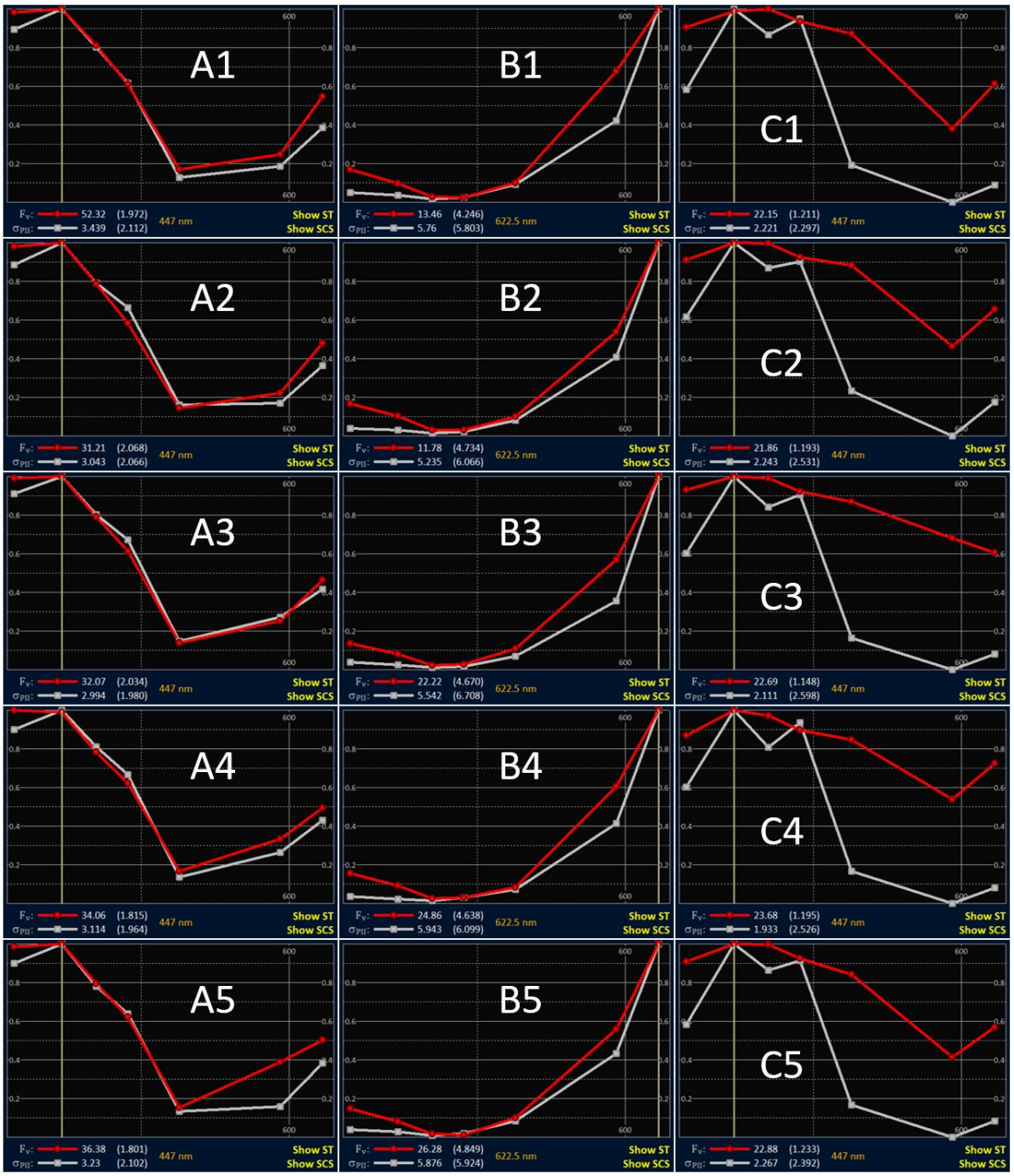

Figure 13.5: Sets of five PEPs from three phytoplankton species. **A1** – **A5** are from *Chlorella vulgaris*. **B1** – **B5** are from *Anabaena* sp. **C1** – **C5** are from *Alexandrium catenella*.

Figure 13.6 shows PEP examples from a range of additional single-species lab cultures. Examples **A** to **E** within Figure 13.6 are all diatoms. Both the F_v and σ_{PII} PEPs for **A**, **B** and **C** are very similar to each other in shape and significantly different from the non-diatom examples provided by **F** to **J**. The σ_{PII} PEPs for **D** and **E** show a slightly different shape to **A**, **B** and **C** in that the 495 nm channel is relatively high and the 534 nm channel is relatively low. The 416 nm channel is also noticeably lower for **E**. Within **D** and **E**, there are clearer gaps between the F_v and σ_{PII} PEPs than are evident within **A**, **B** and **C**. This may indicate the presence of one or more additional species within these cultures. It is noticeable that the relative shapes of the F_v and σ_{PII} PEPs in the example for the large diatom, *C. granii* (**E**) is similar to the dinoflagellate, *A. catenella* (**J**).

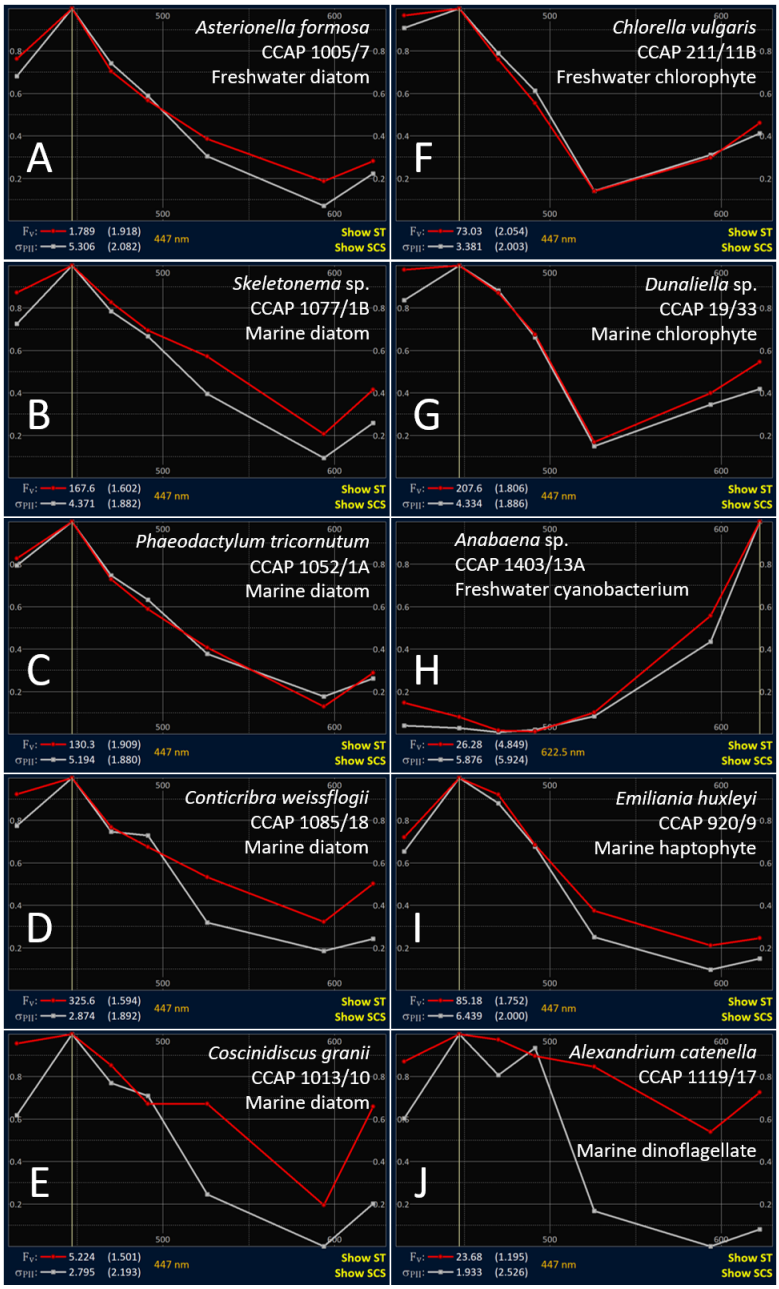

Figure 13.6: Representative PEPs for each of ten phytoplankton species. All samples are from cultures grown at 15 °C on a 16h/8h day/night cycle. Incident photon irradiance (white light) was 50 µmol photons m^{-2} s^{-1} for **A** to **E** and **I**, 120 µmol photons m^{-2} s^{-1} for **F** and **G** and 80 µmol photons m^{-2} s^{-1} for **H** and **J**.

Most of the σ_{PII} PEP data within Figure 13.6 are consistent with the spectra presented by Gorbunov et al. (2020). The two notable differences are the *C. granii* and *A. catenella* cultures (**E** and **J**). As already noted, it is possible that these cultures are contaminated by at least one additional species with a significantly different spectral profile.

Although the examples presented within Figures 13.6 provide a very limited dataset, it seems reasonable to conclude that combining F_v PEP data and σ_{PII} PEP data is likely to add significantly to the information provided by either data set alone.

13.2.1 Using PEP data to apply spectral correction

Within RunSTAF, spectral correction is applied between 380 nm and 660 nm. This requires extrapolation beyond the spectral range of the PEP at each end. Figure 13.7 shows the extrapolations made to extend the PEPs for the ten species shown in Figure 13.6.

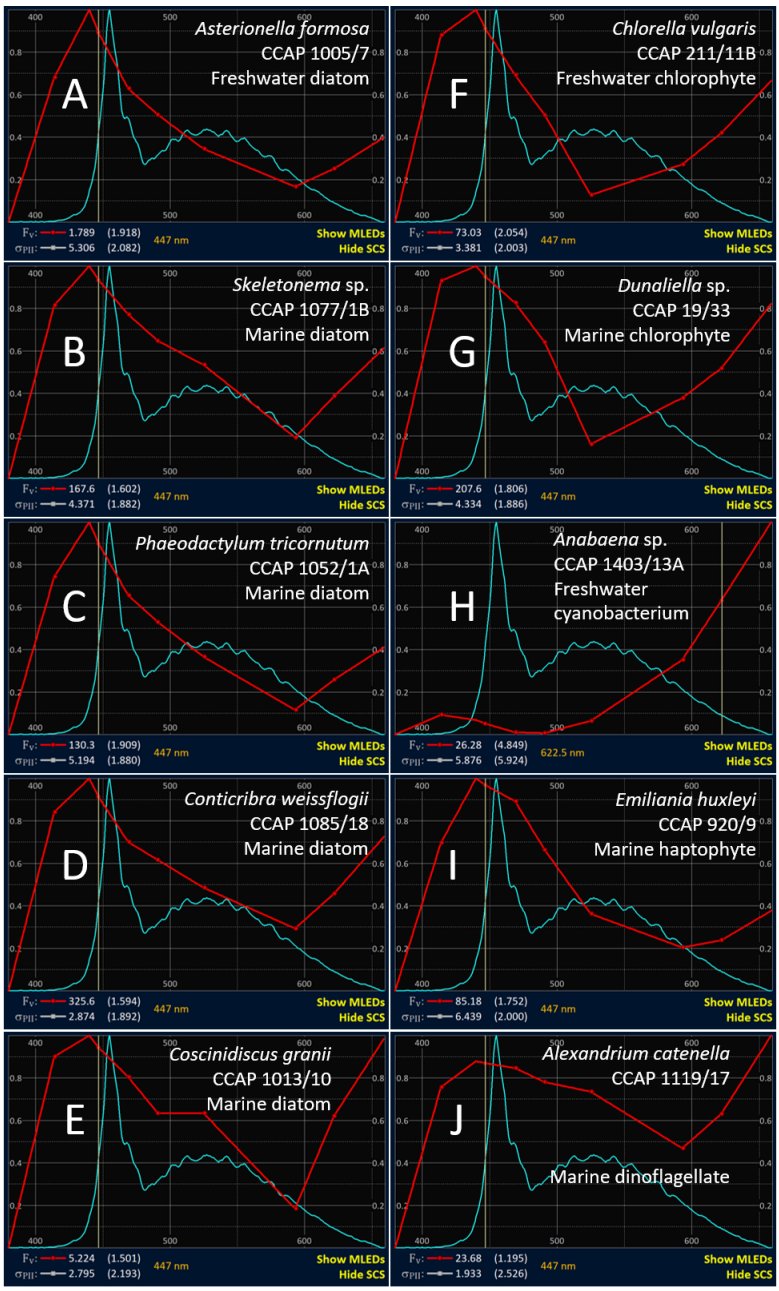

Figure 13.7: Representative PEP data plots with Spectral Correction Spectra (**SCS**) activated. All examples are the same as presented within Figure 13.6.

To complete the extended PEP spectral range required for the automated application of spectral correction, the following extrapolations are applied to the F_v PEP:

1. A straight line is applied between the 416 nm waveband point and zero at 380 nm
2. The slope of the line between the 473 nm waveband point and the 452 nm waveband point is extrapolated to 440 nm (the absorption peak of chlorophyll *a* within this region)
3. A straight line connection is applied between the derived 440 nm point and the measured 416 nm point
4. A straight line connection is applied between the measured 622 nm data point and 660 nm, such that the value at 660 nm is 160% of the value at 622 nm

Extrapolation 1 has minimal impact on spectral correction, simply because the ALED emits very little between 380 and 416 nm. The other three extrapolations have a small impact on the spectral correction.

These extrapolations are based on comparisons made between PEP data and higher resolution Fluorescence Excitation Spectra (FES). Figure 13.8 provides some comparisons between FES data generated from four phytoplankton species during the study by Silsbe et al. (2015) and RunSTAF-generated extended PEP data. The paired species within each plot have been selected to provide the best available match of light harvesting pigments. In examples **A**, **B** and **C**, the main PSII light harvesting pigments are chlorophyll *a* and chlorophyll *c*. In example **D**, both species incorporate chlorophyll *a* and chlorophyll *b*.

In assessing the differences between the spectra within each plot, it is important to note that while the F_v data used to generate the extended PEP plots are exclusively from functional PSII complexes, the F_m data used to generate the FES plots potentially include fluorescence from photoinactivated PSII and other sources.

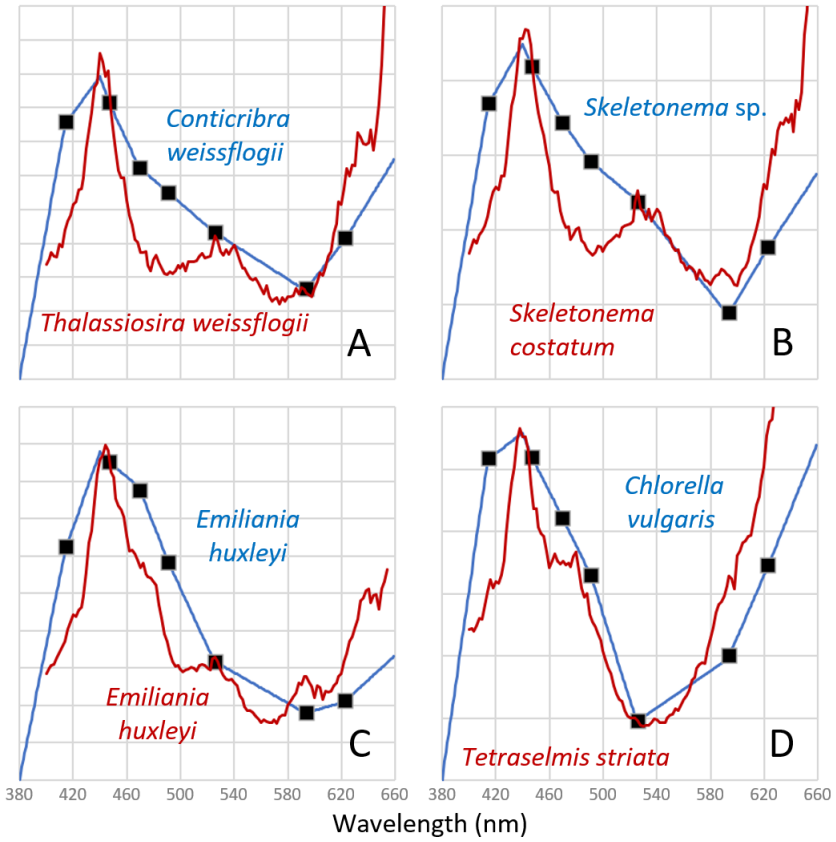

Figure 13.8: The Fluorescence Excitation Spectra (FES) traces are from Silsbe et al. (2015). The extended F_v PEPs are from RunSTAF.

It is possible that the default implementation of spectral correction will be modified in future, as more data become available. The logging of primary STAF data within RunSTAF files makes it possible to rapidly apply spectral updates across large datasets.

13.2.2 Derivation of PEP values

As already noted, the values of F_v and σ_{PII} for each waveband within each PEP are calculated through simple subtraction. For the PEP-bc protocol in Table 13.2, Step 2 (the 452 nm only waveband) provides the subtracted value for the other six wavebands. An intensity correction is applied to the subtracted 452 nm value for Steps 1, 3 and 4 (the 416 nm, 473 and 495 nm wavebands, respectively) to account for the use of only one of the two 452 nm channels. For the PEP-cy values, Step 5 (the 534 nm plus 622 nm wavebands) provide the subtracted value for Steps 1,

2, 3, 4 and 6 (wavebands 416 nm, 452 nm, 473 nm, 495 nm and 594 nm, respectively). Step 7 then provides the subtracted value for the 534 waveband.

As an alternative to the simple subtraction of F_v and σ_{PII} values derived from the ST curve fits, it is feasible to subtract one curve from another and apply a fit to the difference. The data in Figure 13.9 provide an example of how this could work.

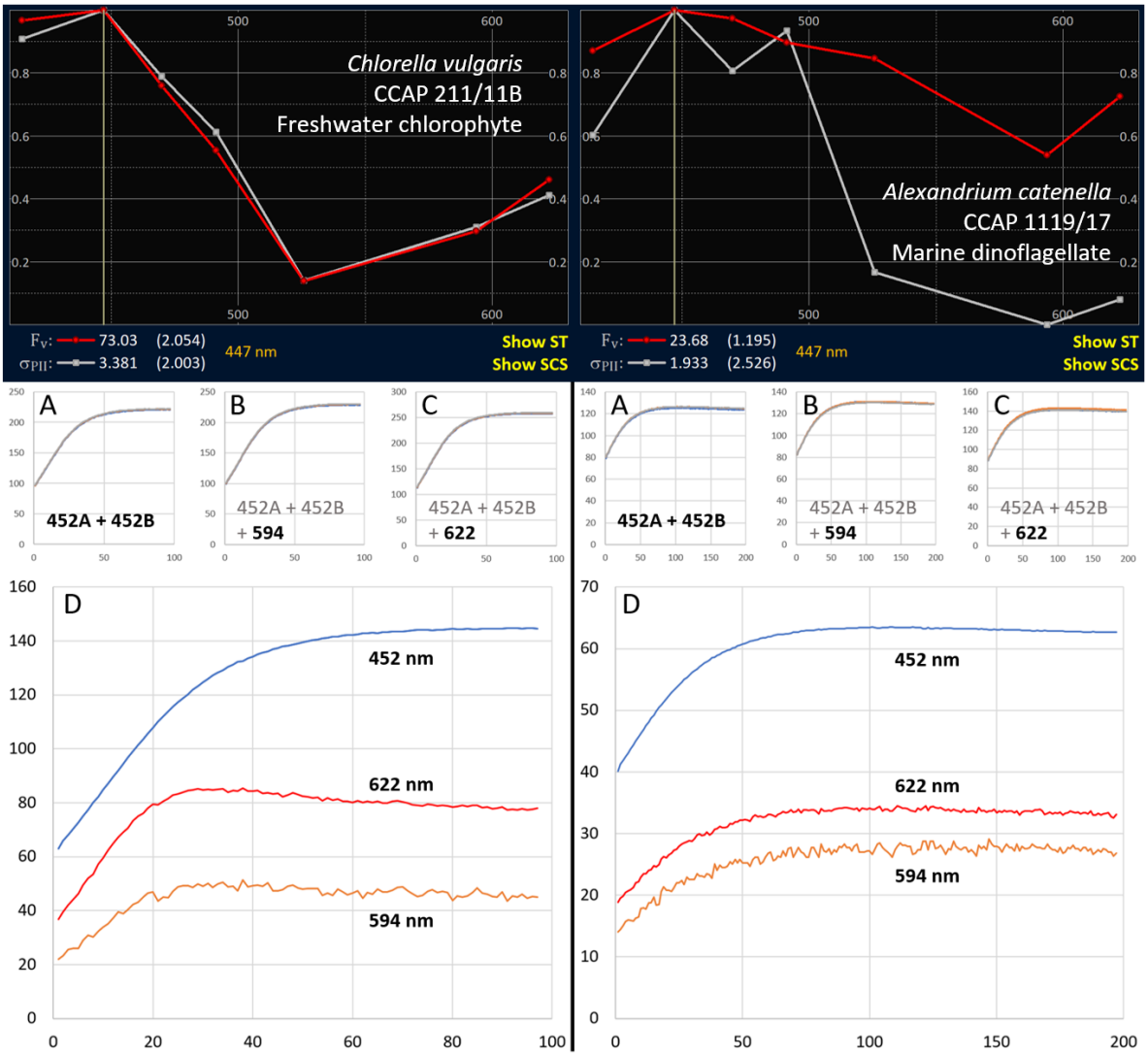

Figure 13.9: PEP data from cultured cells of *C. vulgaris* (left) and *A. catenella* (right) acquired using PEP-bc. The ST traces within **A**, **B** and **C** for each culture are the three reps used for evaluation of the 452 nm, 594 nm and 622 nm wavebands. The ST traces within **D** for each culture show average traces for **A** (**452 nm**), **B** minus **A** (**594 nm**) and **C** minus **A** (**622 nm**) normalized to the appropriate E_{ST} value.

Plots **A**, **B** and **C** of Figure 13.9 show the three ST trace reps for the 452 nm, 594 nm and 622 nm waveband evaluations for the two cultures. Note that these are the primary data incorporated within the Clipboard output and are not normalized to E_{ST} values. In all cases, the noise level is low enough and the degree of saturation high enough to be confident of the σ_{PII}, F_o and F_m values derived from the fits.

The traces in the **D** plots of Figure 13.9 are derived from the average of the three reps in each of **A**, **B** and **C** and are all normalized to the appropriate E_{ST} values. The **452 nm** trace is simply the average of the three reps in **A** normalized to E_{ST} values from the 452A plus 452B channels. The **594 nm** and **622 nm** traces are the average of the traces in **B** or **C** respectively minus the average of **A**, normalized to E_{ST} values for the 594 or 622 channel, respectively.

For *C. vulgaris*, the highest fluorescence values within the normalized 594 nm and 622 nm traces are at around 30 µs. In both cases, these values are approximately 8% higher than the end point of each trace. If these high point values were taken as F_m, the values of F_v would be assessed as 10 to 20% higher than the values calculated in the normal way. In contrast to the normalized 594 nm and 622 nm traces within **D** of *C. vulgaris*, the equivalent traces for *A. catenella* show a similar 'shape' to the 452 nm trace.

The simplest interpretation of the 594 nm and 622 nm traces within plots **D** for both cultures is that they quantify the increase in fluorescence induced by addition of the 594 or 622 channel, respectively, to the 452A and 452B channels. In the case of *C. vulgaris*, this is almost certainly not the case. A more likely explanation is that the rise to the 30 µs peak seen in both traces is due to connectivity between PSII complexes, such that addition of the 594 nm or 622 nm waveband increases the rate at which the 452 nm waveband closes RCII during the early part of the curve.

In contrast to the example of *C. vulgaris*, where the F_v and σ_{PII} PEPs are closely matched through the entire range, the F_v and σ_{PII} PEPs from *A. catenella* diverge widely within the spectral range that incorporates the 594 nm and 622 nm traces. Earlier in this section, this divergence was attributed to the presence of two sub-populations of PSII complexes within the sample that are spectrally very different from each other: the assumption being that one sub-population is intrinsic to *A. catenella* and the other to a separate symbiotic or contaminating species. This explanation is supported by the similarity of the shape of all three ST traces in the **D** plot for *A. catenella* which is most easily understood in the context of a lack of connectivity between one sub-population of PSII complexes that dominates absorption at 452 nm and a second sub-population of PSII complexes dominating absorption at 594 nm and 622 nm.

14 Working with External Spectral Data (ESD)

14.1 Using ESD from a third party spectrometer

Spectral correction between the LabSTAF MLEDs and ALED is applied to the relevant STAF parameters by default. This correction incorporates SCS-based processing of the sample-specific Photochemical Excitation Profile (PEP). RunSTAF also includes functions to allow ESD to be used for spectral correction, in place of the ALED spectrum. The ESD can be read in directly, from a connected Spectral PAR (SPAR) sensor or indirectly, through an imported ESD file. The first example presented here involves formatting and applying a selection of spectra collected from a photosynthetron using a third party spectrometer (OtO Photonics, Model SE2030-010-DUV5). Spectra were collected at sub-nm resolution, directly from the lamp and behind chambers 1 to 6 (Figure 14.6).

The first step of formatting involved putting together a spreadsheet of the data required to generate the ESD files. The example in Figure 14.1 shows the wavelength values in column A and the seven sets of emission spectra in columns B to H. These values are scaled as relative photon flux. To visualise the spectral data within the spreadsheet, the max value from each column has been found (cells B1 to H1) and the all values within each column have been normalized to the maximum value within that column. The normalized (plotted) values are in columns K to Q.

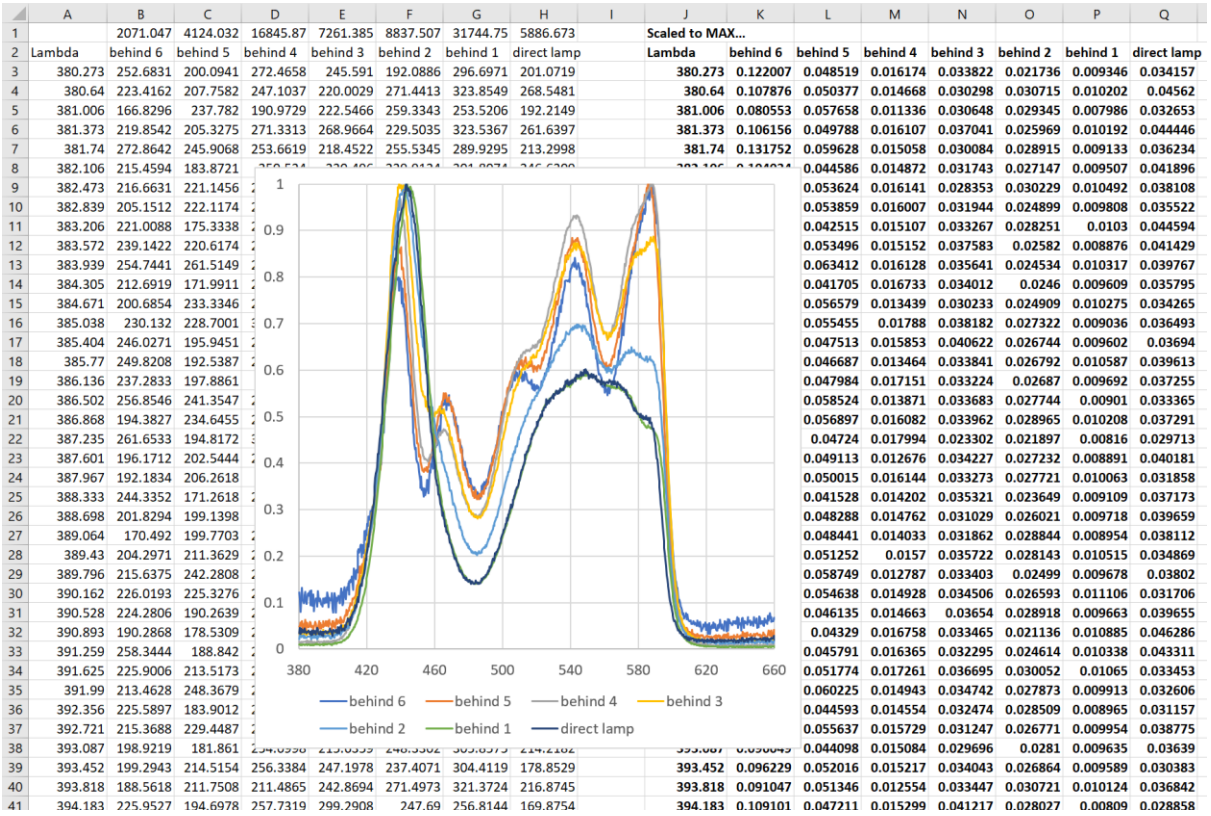

	A	B	C	D	E	F	G	H	I	J	K	L	M	N	O	P	Q
1		2071.047	4124.032	16845.87	7261.385	8837.507	31744.75	5886.673		Scaled to MAX...							
2	Lambda	behind 6	behind 5	behind 4	behind 3	behind 2	behind 1	direct lamp		Lambda	behind 6	behind 5	behind 4	behind 3	behind 2	behind 1	direct lamp
3	380.273	252.6831	200.0941	272.4658	245.591	192.0886	296.6971	201.0719		380.273	0.122007	0.048519	0.016174	0.033822	0.021736	0.009346	0.034157
4	380.64	223.4162	207.7582	247.1037	220.0029	271.4413	323.8549	268.5481		380.64	0.107876	0.050377	0.014668	0.030298	0.030715	0.010202	0.04562
5	381.006	166.8296	237.782	190.9729	222.5466	259.3343	253.5206	192.2149		381.006	0.080553	0.057658	0.011336	0.030648	0.029345	0.007986	0.032653
6	381.373	219.8542	205.3275	271.3313	268.9664	229.5035	323.5367	261.6397		381.373	0.106156	0.049788	0.016107	0.037041	0.025969	0.010192	0.044446
7	381.74	272.8642	245.9068	253.6619	218.4522	255.5345	289.9295	213.2998		381.74	0.131752	0.059628	0.015058	0.030084	0.028915	0.009133	0.036234
8	382.106	215.4594	183.8721									0.044586	0.014872	0.031743	0.027147	0.009507	0.041896
9	382.473	216.6631	221.1456									0.053624	0.016141	0.028353	0.030229	0.010492	0.038108
10	382.839	205.1512	222.1174									0.053859	0.016007	0.031944	0.024899	0.009808	0.035522
11	383.206	221.0088	175.3338									0.042515	0.015107	0.033267	0.028251	0.0103	0.044594
12	383.572	239.1422	220.6174									0.053496	0.015152	0.037583	0.02582	0.008876	0.041429
13	383.939	254.7441	261.5149									0.063412	0.016128	0.035641	0.024534	0.010317	0.039767
14	384.305	212.6919	171.9911									0.041705	0.016733	0.034012	0.0246	0.009609	0.035795
15	384.671	200.6854	233.3346									0.056579	0.013439	0.030233	0.024909	0.010275	0.034265
16	385.038	230.132	228.7001									0.055455	0.01788	0.038182	0.027322	0.009036	0.036493
17	385.404	246.0271	195.9451									0.047513	0.015853	0.040622	0.026744	0.009602	0.03694
18	385.77	249.8208	192.5387									0.046687	0.013464	0.033841	0.026792	0.010587	0.039613
19	386.136	237.2833	197.8861									0.047984	0.017151	0.033224	0.02687	0.009692	0.037255
20	386.502	256.8546	241.3547									0.058524	0.013871	0.033683	0.027744	0.00901	0.033365
21	386.868	194.3827	234.6455									0.056897	0.016082	0.033962	0.028965	0.010208	0.037291
22	387.235	261.6533	194.8172									0.04724	0.017994	0.023302	0.021897	0.00816	0.029713
23	387.601	196.1712	202.5444									0.049113	0.012676	0.034227	0.027232	0.008891	0.040181
24	387.967	192.1834	206.2618									0.050015	0.016144	0.033273	0.027721	0.010063	0.031858
25	388.333	244.3352	171.2618									0.041528	0.014202	0.035321	0.023649	0.009109	0.037173
26	388.698	201.8294	199.1398									0.048288	0.014762	0.031029	0.026021	0.009718	0.039659
27	389.064	170.492	199.7703									0.048441	0.014033	0.031862	0.028844	0.008954	0.038112
28	389.43	204.2971	211.3629									0.051252	0.0157	0.035722	0.028143	0.010515	0.034869
29	389.796	215.6375	242.2808									0.058749	0.012787	0.033403	0.02499	0.009678	0.03802
30	390.162	226.0193	225.3276									0.054638	0.014928	0.034506	0.026593	0.011106	0.031706
31	390.528	224.2806	190.2639									0.046135	0.014663	0.03654	0.028918	0.009663	0.039655
32	390.893	190.2868	178.5309									0.04329	0.016758	0.033465	0.021136	0.010885	0.046286
33	391.259	258.3444	188.842									0.045791	0.016365	0.032295	0.024614	0.010338	0.043311
34	391.625	225.9006	213.5173									0.051774	0.017261	0.036695	0.030052	0.01065	0.033453
35	391.99	213.4628	248.3679									0.060225	0.014943	0.034742	0.027873	0.009913	0.032606
36	392.356	225.5897	183.9012									0.044593	0.014554	0.032474	0.028509	0.008965	0.031157
37	392.721	215.3688	229.4487									0.055637	0.015729	0.031247	0.026771	0.009954	0.038775
38	393.087	198.9219	181.861									0.044098	0.015084	0.029696	0.0281	0.009635	0.03639
39	393.452	199.2943	214.5154	256.3384	247.1978	237.4071	304.4119	178.8529		393.452	0.096229	0.052016	0.015217	0.034043	0.026864	0.009589	0.030383
40	393.818	188.5618	211.7508	211.4865	242.8694	271.4973	321.3724	216.8745		393.818	0.091047	0.051346	0.012554	0.033447	0.030721	0.010124	0.036842
41	394.183	225.9527	194.6978	257.7319	299.2908	247.69	256.8144	169.8754		394.183	0.109101	0.047211	0.015299	0.041217	0.028027	0.00809	0.028858

Figure 14.1: Spreadsheet (Excel) of the spectral data used for this example.

The second step is to copy and paste the values into a text editor in tab-delimited format. The values must cover the SCS spectral range of 380 nm to 660 nm. The formatting rules are:

- The first line must include the column titles and the first title must be **Lambda**
- There can be a maximum of 12 data columns, each with a unique column title
- The lambda values must include at least one point at each nm between 380 and 660 nm

Figure 14.2 shows the selected cells within the spreadsheet. Either the unscaled (columns A to H) or the **Scaled to MAX…** (columns J to Q) values can be used.

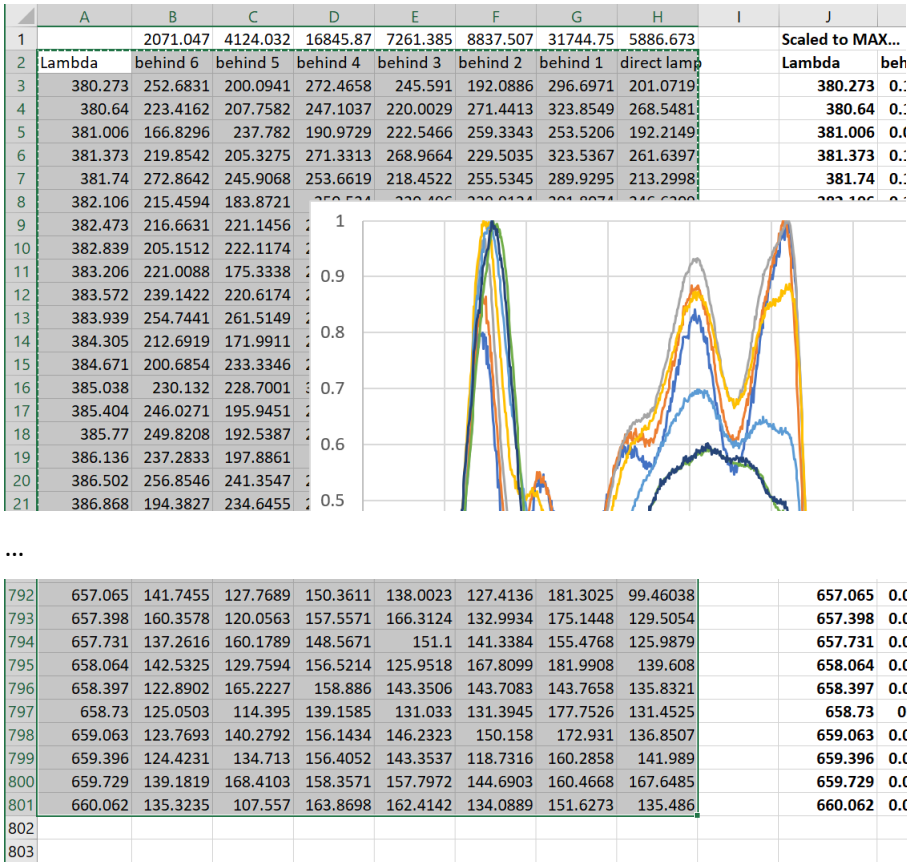

	A	B	C	D	E	F	G	H	I	J
1		2071.047	4124.032	16845.87	7261.385	8837.507	31744.75	5886.673		Scaled to MAX...
2	Lambda	behind 6	behind 5	behind 4	behind 3	behind 2	behind 1	direct lamp		Lambda beh
3	380.273	252.6831	200.0941	272.4658	245.591	192.0886	296.6971	201.0719		380.273 0.
4	380.64	223.4162	207.7582	247.1037	220.0029	271.4413	323.8549	268.5481		380.64 0.
5	381.006	166.8296	237.782	190.9729	222.5466	259.3343	253.5206	192.2149		381.006 0.
6	381.373	219.8542	205.3275	271.3313	268.9664	229.5035	323.5367	261.6397		381.373 0.
7	381.74	272.8642	245.9068	253.6619	218.4522	255.5345	289.9295	213.2998		381.74 0.
8	382.106	215.4594	183.8721							
9	382.473	216.6631	221.1456							
10	382.839	205.1512	222.1174							
11	383.206	221.0088	175.3338							
12	383.572	239.1422	220.6174							
13	383.939	254.7441	261.5149							
14	384.305	212.6919	171.9911							
15	384.671	200.6854	233.3346							
16	385.038	230.132	228.7001							
17	385.404	246.0271	195.9451							
18	385.77	249.8208	192.5387							
19	386.136	237.2833	197.8861							
20	386.502	256.8546	241.3547							
21	386.868	194.3827	234.6455							

...

792	657.065	141.7455	127.7689	150.3611	138.0023	127.4136	181.3025	99.46038		657.065 0.0
793	657.398	160.3578	120.0563	157.5571	166.3124	132.9934	175.1448	129.5054		657.398 0.0
794	657.731	137.2616	160.1789	148.5671	151.1	141.3384	155.4768	125.9879		657.731 0.0
795	658.064	142.5325	129.7594	156.5214	125.9518	167.8099	181.9908	139.608		658.064 0.0
796	658.397	122.8902	165.2227	158.886	143.3506	143.7083	143.7658	135.8321		658.397 0.0
797	658.73	125.0503	114.395	139.1585	131.033	131.3945	177.7526	131.4525		658.73 0
798	659.063	123.7693	140.2792	156.1434	146.2323	150.158	172.931	136.8507		659.063 0.0
799	659.396	124.4231	134.713	156.4052	143.3537	118.7316	160.2858	141.989		659.396 0.0
800	659.729	139.1819	168.4103	158.3571	157.7972	144.6903	160.4668	167.6485		659.729 0.0
801	660.062	135.3235	107.557	163.8698	162.4142	134.0889	151.6273	135.486		660.062 0.0
802										
803										

Figure 14.3 shows the values copied from Excel pasted into Notepad, ready for saving.

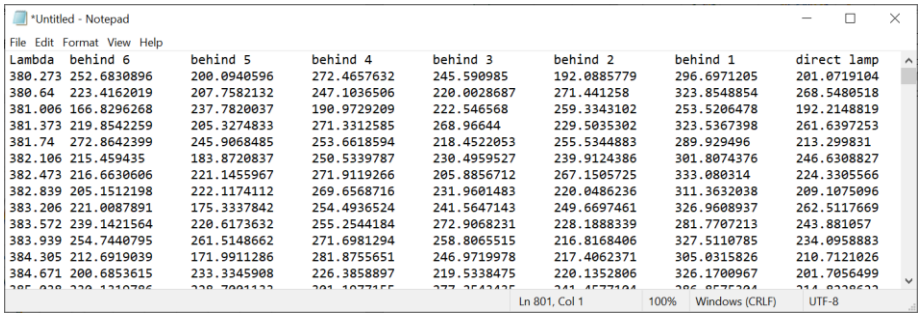

*Untitled - Notepad

File Edit Format View Help

Lambda	behind 6	behind 5	behind 4	behind 3	behind 2	behind 1	direct lamp
380.273	252.6830896	200.0940596	272.4657632	245.590985	192.0885779	296.6971205	201.0719104
380.64	223.4162019	207.7582132	247.1036506	220.0028687	271.441258	323.8548854	268.5480518
381.006	166.8296268	237.7820037	190.9729209	222.546568	259.3343102	253.5206478	192.2148819
381.373	219.8542259	205.3274833	271.3312585	268.96644	229.5035302	323.5367398	261.6397253
381.74	272.8642399	245.9068485	253.6618594	218.4522053	255.5344883	289.929496	213.299831
382.106	215.459435	183.8720837	250.5339787	230.4959527	239.9124386	301.8074376	246.6308827
382.473	216.6630606	221.1455967	271.9119266	205.8856712	267.1505725	333.080314	224.3305566
382.839	205.1512198	222.1174112	269.6568716	231.9601483	220.0486236	311.3632038	209.1075096
383.206	221.0087891	175.3337842	254.4936524	241.5647143	249.6697461	326.9608937	262.5117669
383.572	239.1421564	220.6173632	255.2544184	272.9068231	228.1888339	281.7707213	243.881057
383.939	254.7440795	261.5148662	271.6981294	258.8065515	216.8168406	327.5110785	234.0958883
384.305	212.6919039	171.9911286	281.8755651	246.9719978	217.4062371	305.0315826	210.7121026
384.671	200.6853615	233.3345908	226.3858897	219.5338475	220.1352806	326.1700967	201.7056499

Ln 801, Col 1 100% Windows (CRLF) UTF-8

Figure 14.3: The values pasted into Notepad.

The next step is to generate ESD files that RunSTAF can import. Go to:

Settings → Factory → Build ESD files

Open the Notepad file created within the previous step. The dialog shown in Figure 14.4 should show in the top left corner of the screen.

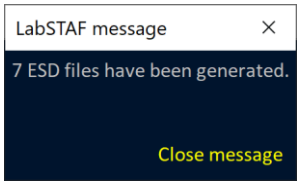

Figure 14.4: A message with this format should show when the **Build ESD files** function is implemented. The seven ESD files (in this example) are located within the same folder as the file Notepad file used to generate them.

Figure 14.5 shows the list of ESD files generated by the **Build ESD files** function. The filenames are constructed from the name of the Notepad file (**ESD data**) plus a space-dash-space (**-**) plus the text entry from the first row of each column within the Notepad file (**behind 6**, for example).

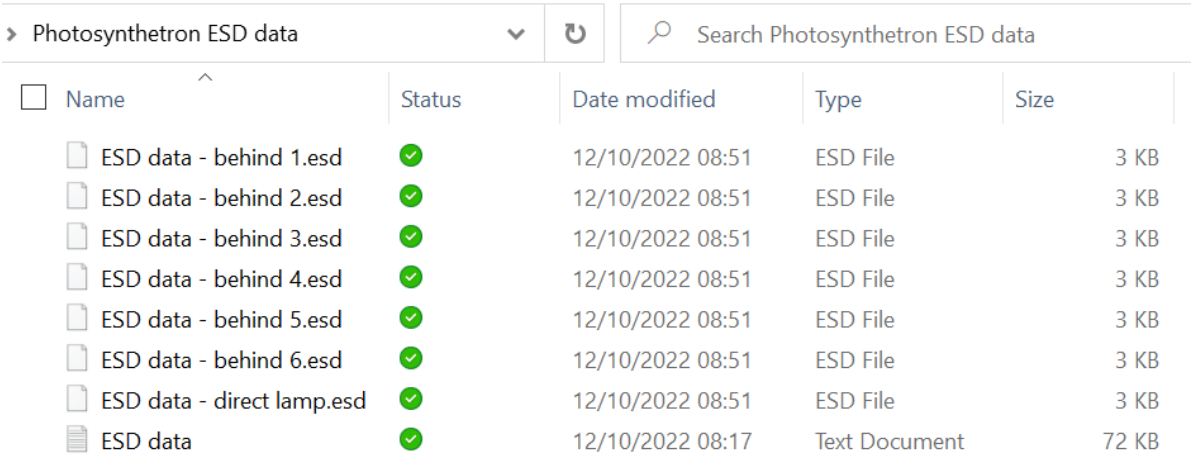

Figure 14.5: The folder containing all ESD files generated, within the example, by the **Build ESD files** function within RunSTAF.

This example is from a work package conducted as part of the JERICO-S3 programme:

www.jerico-ri.eu/projects/jerico-s3

The water samples used was collected from a depth of 20 m from the oligotrophic Eastern Mediterranean during October, 2021. Figure 14.6 shows the general arrangement of the photosynthetron sample chambers in this example. A complete description of the experimental work will be included within the JERICO-S3 report.

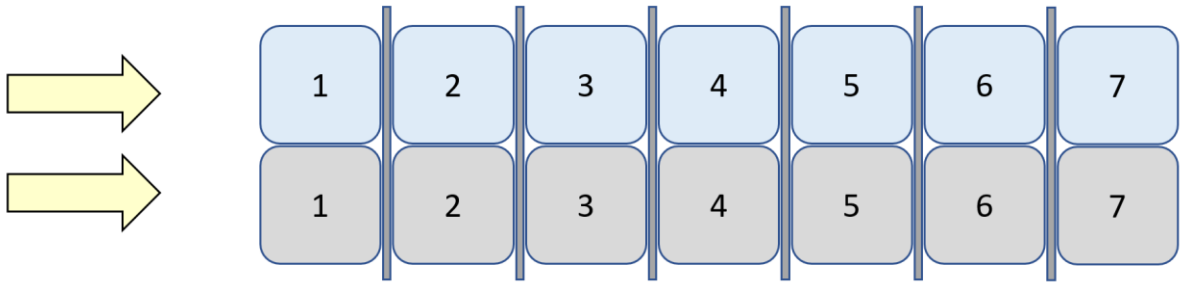

Figure 14.6: General arrangement of the sample chambers within the photosynthetron used for this application example. The bars between chambers are Neutral Density (ND) filters. Attenuation of light through the walls of the sample chamber, the sample and the ND filters was not spectrally neutral (see Figure 14.1). The light blue set of chambers contained ^{14}C-spiked samples. The grey set of chambers contained un-spiked samples from the same source and are spectrally and intensity matched to the ^{14}C-spiked chamber at the same position.

Sub-samples were transferred from the un-spiked chambers to a LabSTAF at specific time points during the photosynthetron incubations. The main reason for running the LabSTAF samples as sub-samples from the photosynthetron was to generate values of JV_{PII} (as µmol electrons m^{-3} s^{-1}) and carbon assimilation (as µmol C m^{-3} s^{-1}) to provide electron per carbon values ($\Phi_{e,C}$). While spectral matching between the MLEDs and ALED within the LabSTAF is fully automated within RunSTAF, matching the photosynthetron-derived carbon assimilation values with the LabSTAF-derived JV_{PII} values requires spectral matching between the actinic light sources. This is achieved by replacing the ALED spectrum within the RunSTAF spectral correction procedure with the ESD from the photosynthetron chamber that each LabSTAF sub-sample was taken from.

Figure 14.7 shows a crop of the SCS data from the home screen of one of the RunSTAF data files. The sample was taken from the un-spiked chamber 5 of the photosynthetron setup. The required ESD file required to apply the spectral correction is:

ESD data – behind 4.esd

This file was pulled into the RunSTAF data file using:

File → Import ESD from file

Within the example shown in Figure 14.7, the ALED flat white coefficient is almost exactly 10% higher than the ESD flat white coefficient. Switching to the ESD has a proportional impact on a_{LHII}, JV_{PII} and J_{PII}.

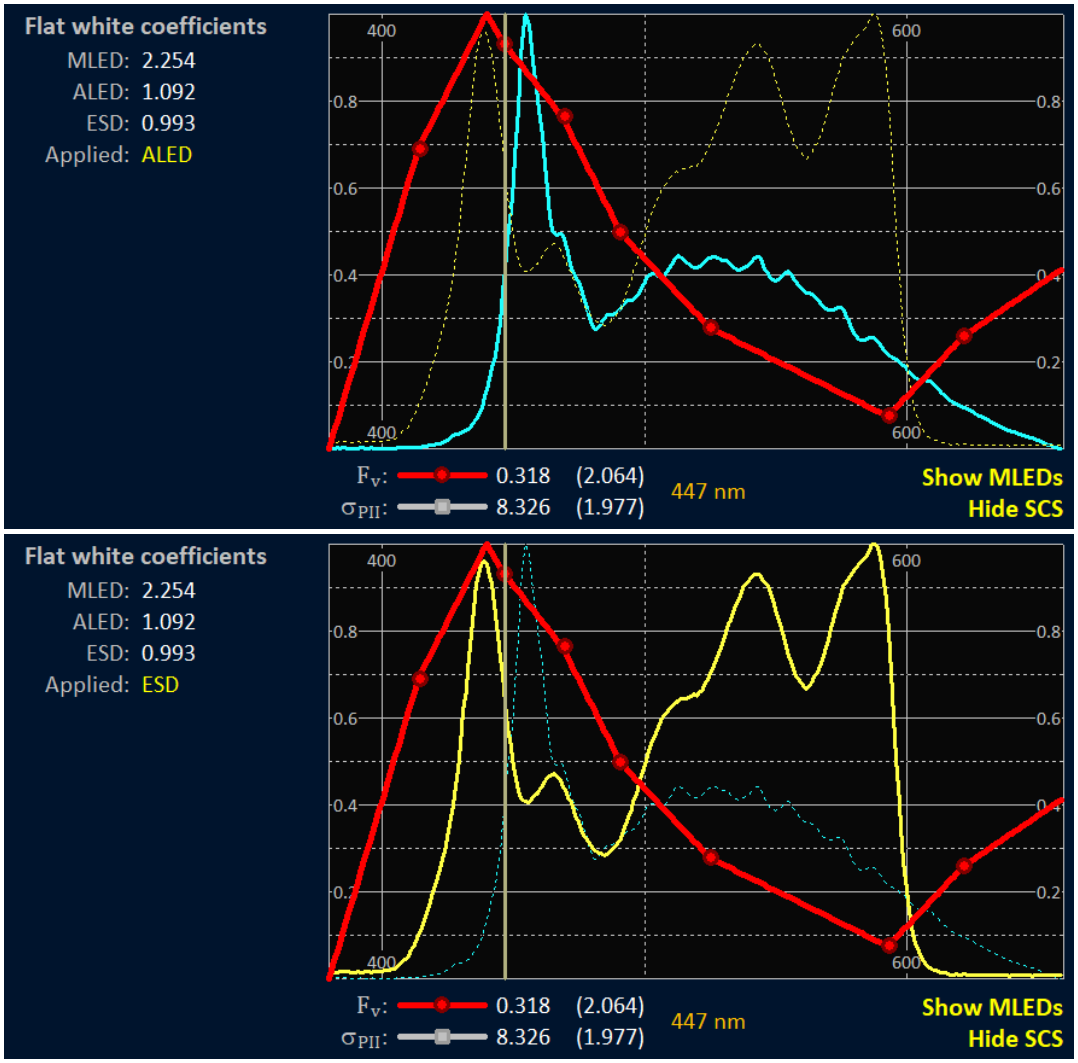

Figure 14.7: Screen crops showing the switch from ALED-based to ESD-based spectral correction.

14.2 Applying an ESD from a Spectral PAR (SPAR) sensor

A SPAR sensor can be connected to RunSTAF through the COM port of most Windows 10 or Windows 11-based computers. Data from the connected SPAR sensor can be read into an existing RunSTAF data file or saved in the ESD file format for integration with an existing RunSTAF data file. See: **Using a SPAR sensor with LabSTAF and RunSTAF**

15 Non-standard experimental procedures

This section covers experimental procedures that are not covered in earlier sections. The use of scintillation vials inside the sample chamber of a LabSTAF unit is described in section 15.1, while section 15.2 briefly outlines the 'dual incubation method' for simultaneous measurements of JV_{PII} and ^{14}C fixation (which utilises scintillation vials). Section 15.3 describes a protocol which allows the continuous implementation of the pre-FLC functions without running the usual multi-step FLC protocol.

15.1 Using scintillation vials

The integrated sample chamber within LabSTAF provides a number of practical advantages and contributes significantly to the ability to work at very low biomass. However, the minimum sample volume of 10 mL can sometimes be an issue. Also, making a series of short measurements from a large number of discrete samples can be impractical with this arrangement.

In situations where automated sample exchange and/or sample stirring are not required, scintillation vials can be used to overcome both of the above issues. To date, three readily available sizes of scintillation vials have been tested. These are listed in Table 15.1.

Part number	Height (mm)	OD (mm)	Volume (mL)
11547733	68	19	12
11553522	73	21	16
11563522	88	23	24

Table 15.1: Scintillation vials tested with LabSTAF. The supplier for all three is Fisher Scientific (Lab Equipment and Lab Supplies | Fisher Scientific).

15.1.1 Index matching

To minimise signal degradation, the space between the wall of the sample chamber and the scintillation vial should be filled with de-ionised water. This effectively blocks reflection between the surfaces of the sample chamber and vial and minimises refractive index-based changes in the shape of the MLED and ALED outputs.

15.1.2 The potential impact of using vials on key STAF parameters

Figure 15.1 provides sample ST plots for each of five concentrations of *Chlorella vulgaris* (freshwater), covering more than three orders of magnitude. This range was used to assess potential changes in optical characteristics when each of the three scintillation vials was used to hold the sample. In all cases, the scintillation vial containing the sample was centred horizontally within the sample chamber and was touching the bottom of the chamber. The space between the vial and the wall of the chamber was always filled with de-ionised water. The values of F_v/F_m and σ_{PII} reported within each ST trace in Figure 15.1 are specific to that trace.

Figure 15.2 provides plots of three parameters that are important for this assessment: σ_{PII}, F_m and F_v/F_m. In all cases, the sample chamber values are on the x-axis and the scintillation vials values on the y-axis. A single point for each of the five concentrations (**A** - **E**) shown in Figure 15.1 are included for all three parameters. Each data point is the average of 12 Saq-level values. Each Saq was generated from the number of Acqs shown in the legend to Figure 15.1. The values of all points within these graphs, plus Standard Deviations (SDs), are provided in Tables 15.2, 15.3 and 15.4.

Part (**i**) of Figure 15.2 show plots of σ_{PII} values. This parameter allows for a direct assessment of potential attenuation of the MLED light when the sample is placed within one of the scintillation vials. Although most of the points are below the red 1:1 line, all are within one SD and most

scintillation vial values are within 2% of the chamber values (see Table 15.5). Overall, these data indicate that attenuation of MLED output by any of the scintillation vials is minimal.

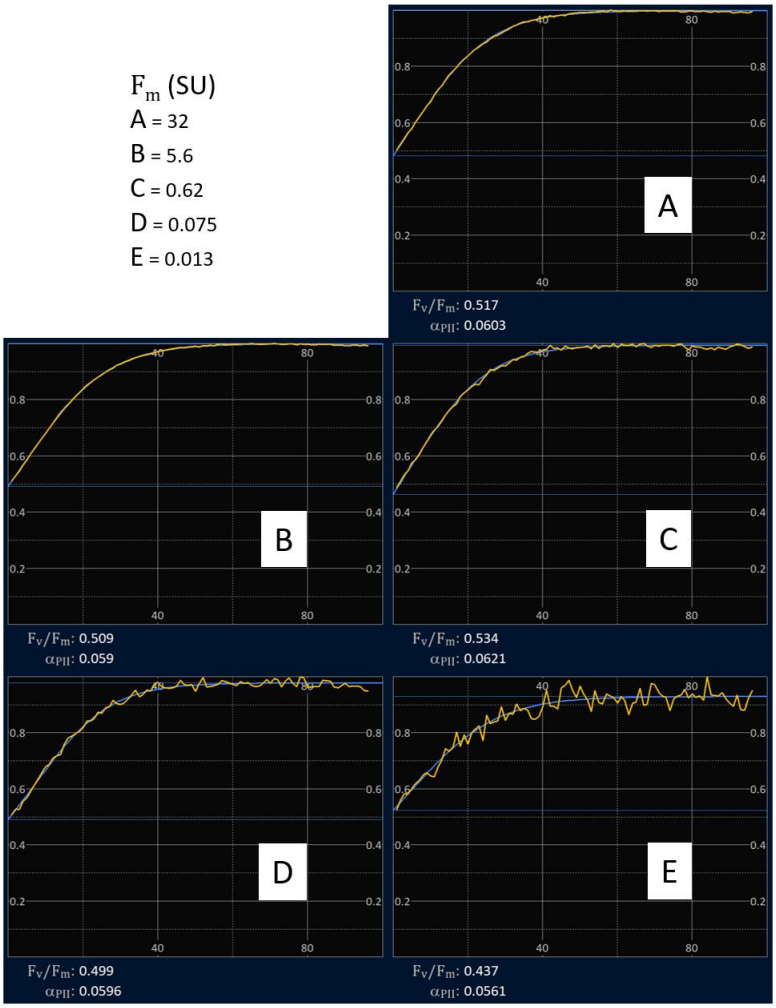

Figure 15.1: Sample Saq ST traces from the five concentrations of *C. vulgaris* cells. The F_m values provided in the key approximate to mg chlorophyll *a* m^{-3}. **A** and **B** are the average of 24 Acqs, **C** is the average of 32 Acqs, **D** and **E** are the average of 48 Acqs. All five traces shown were recorded from a sample in the Small scintillation vial.

Parts **ii** and **iii** of Figure 15.2 shows plots of F_m. Lower values for F_m from the scintillation vial measurements could result from attenuation of the MLED output reaching the interrogated volume and/or attenuation of emitted fluorescence reaching the PMT. The data presented within Part **ii** are on a double log plot and, as a consequence, would hide any subtle attenuation of signal. Part **iii** provides a linear plot of values from concentrations **B** to **E**. These data are consistent with minimal attenuation of MLED output or emitted fluorescence.

Parts **iv** and **v** of Figure 15.2 show plots of F_v/F_m. Part **iv** shows values from all five concentrations, while part **v** shows values from concentrations **A** to **D**, with a smaller range of axis values. The most obvious feature of these plots is that most points are above the 1:1 red line. That is to say, the values of F_v/F_m are generally higher when the sample is placed within one of the scintillation vials. The difference between scintillation vial and chamber values increases with decreasing cell density. At the lowest cell density (**E**), the differences between scintillation vial and chamber values is greater than the SD (Tables 15.4 and 15.7). The most likely basis for these differences is the scattering of MLED light towards the PMT. A series of blank measurements made with de-ionised water produced chamber-based values of between approximately 0.001 and 0.002 and scintillation vial-based values of between approximately 0.0005 and 0.0001 on the SU scale.

Overall, these data indicate that making dark measurements from samples within scintillation vials, in particular under high biomass laboratory conditions, doesn't give rise to significant bias in the acquired parameters due to optical issues.

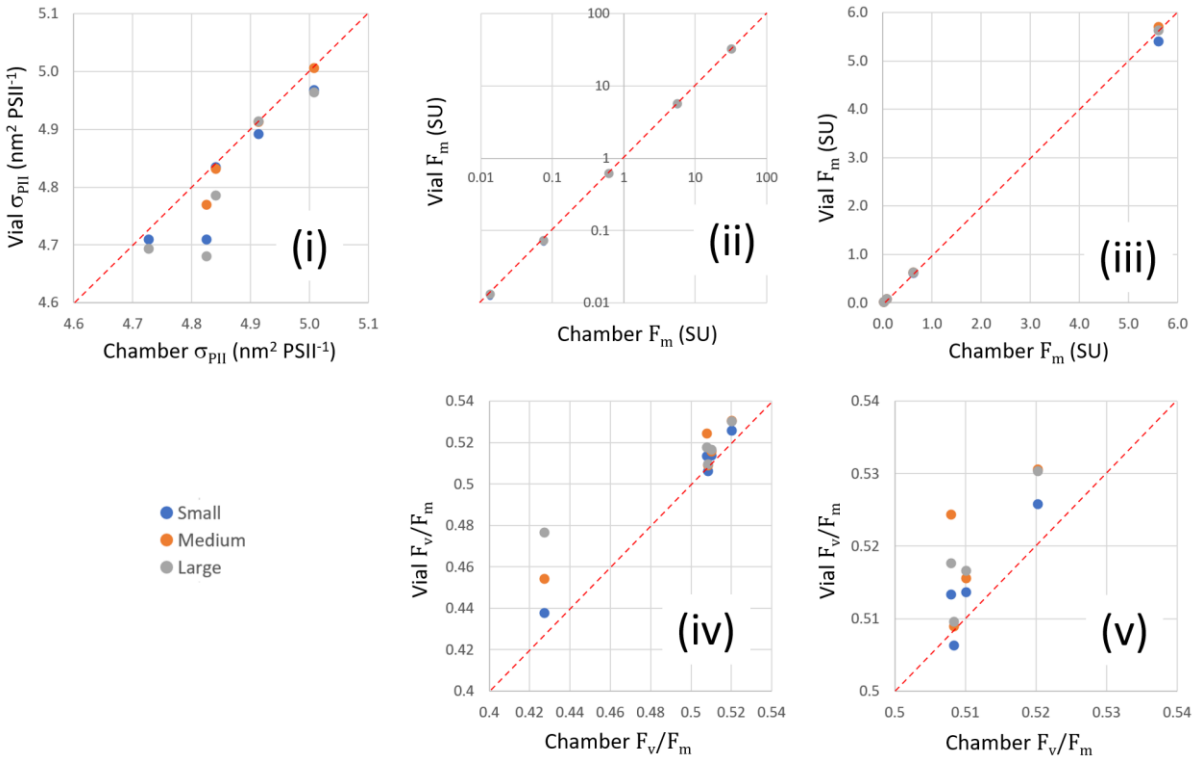

Figure 15.2: Values for σ_{PII}, F_m and F_v/F_m from cultured cells of *Chlorella vulgaris* (freshwater chlorophyte), at a range of dilutions with MilliQ, as shown in Figure 15.1. The x-axis values were measured from the sample within the sample chamber. The y-axis values are from the same sample, measured from within one of the three scintillation vial sizes. Each point is an average of 12 values. Point values with Standard Deviations are provided in Tables 15.1, 15.2 and 15.3. Percentage deviation values are shown within Tables 15.4, 15.5 and 15.6.

σ_{PII}	Chamber	Small	Medium	Large
A (*SD*)	5.008 (*0.0372*)	4.968 (*0.03358*)	5.006 (*0..0291*)	4.964 (*0.0465*)
B (*SD*)	4.913 (*0.0306*)	4.892 (*0.0304*)	4.913 (*.03077*)	4.913 (*0.0468*)
C (*SD*)	4.841 (*0.0544*)	4.835 (*0.0610*)	4.832 (*0.0853*)	4.785 (*0.0697*)
D (*SD*)	4.825 (*0.1040*)	4.710 (*0.1736*)	4.769 (*0.0892*)	4.681 (*0.1231*)
E (*SD*)	4.727 (*0.4783*)	4.710 (*0.5746*)	4.254 (*0.4276*)	4.693 (*0.3413*)

Table 15.2: Values of σ_{PII} at each of the five concentrations of *C. vulgaris* used for this assessment.

F_m	Chamber	Small	Medium	Large
A (*SD*)	31.979 (*0.1893*)	31.969 (*0.0303*)	32.613 (*0.0885*)	32.540 (*0.0995*)
B (*SD*)	5.608 (*0.0937*)	5.407 (*0.0784*)	5.706 (*0.1386*)	5.625 (*0.0574*)
C (*SD*)	0.617 (*0.0119*)	0.610 (*0.0114*)	0.623 (*0.0160*)	0.619 (*0.0176*)
D (*SD*)	0.075 (*0.0038*)	0.068 (*0.0054*)	0.072 (*0.0042*)	0.073 (*0.0047*)
E (*SD*)	0.013 (*0.0018*)	0.012 (*0.0012*)	0.013 (*0.0014*)	0.013 (*0.0026*)

Table 15.3: Values of F_m at each of the five concentrations of *C. vulgaris* used for this assessment.

F_v/F_m	Chamber	Small	Medium	Large
A (*SD*)	0.508 (*0.0034*)	0.506 (*0.0065*)	0.509 (*0.0042*)	0.510 (*0.0031*)
B (*SD*)	0.510 (*0.0061*)	0.514 (*0.0041*)	0.516 (0.0037)	0.517 (*0.0049*)
C (*SD*)	0.520 (*0.0046*)	0.526 (*0.0037*)	0.531 (*0.0056*)	0.530 (*0.0074*)
D (*SD*)	0.508 (*0.0080*)	0.513 (*0.0110*)	0.524 (*0.0117*)	0.518 (*0.0123*)
E (*SD*)	0.427 (*0.0261*)	0.438 (*0.0253*)	0.454 (*0.0214*)	0.477 (*0.0263*)

Table 15.4: Values of F_v/F_m at each of the five concentrations of *C. vulgaris* used for this assessment.

σ_{PII}	Small	Medium	Large
A	-0.80%	-0.04%	-0.87%
B	-0.44%	-0.01%	0.00%
C	-0.11%	-0.18%	-1.14%
D	-2.40%	-1.16%	-2.99%
E	-0.36%	-10.00%	-0.71%

Table 15.5: Deviation of σ_{PII} values measured within the **Small**, **Medium** and **Large** scintillation vials, compared to values measured within the sample chamber.

F_m	Small	Medium	Large
A	-0.03%	1.98%	1.75%
B	-3.58%	1.74%	0.31%
C	-1.11%	0.87%	0.25%
D	-9.64%	-4.45%	-3.22%
E	-10.38%	-4.96%	-1.68%

Table 15.6: Deviation of F_m values measured within the **Small**, **Medium** and **Large** scintillation vials, compared to values measured within the sample chamber.

F_v/F_m	Small	Medium	Large
A	-0.41%	0.11%	0.23%
B	0.70%	1.07%	1.27%
C	1.06%	1.99%	1.93%
D	1.06%	3.22%	1.90%
E	2.40%	6.23%	11.48%

Table 15.7: Deviation of F_v/F_m values measured within the **Small**, **Medium** and **Large** scintillation vials, compared to values measured within the sample chamber.

15.2 The dual incubation method (^{14}C-fixation + STAF)

Parallel measurements of JV_{PII} and ^{14}C-fixation are required to understand the factors controlling the variable ratio between these two metrics. To date, methodological inconsistencies, including differences in incubation lengths and light quality, have greatly inhibited practical assessment of electron to carbon ratios ($\Phi_{e,C}$). The image in Figure 15.3 shows a LabSTAF unit being used to run a 'dual incubation' measurement of JV_{PII} and ^{14}C-fixation. This measurement is facilitated by the relatively large sample chamber incorporated within LabSTAF (25 mm ID and 56 mm height). The ^{14}C-spiked sample is contained within a scintillation vial (23 mm OD). In addition to providing a single actinic light source for both measurements, this arrangement allows STAF measurements to be made over the entire ^{14}C incubation period.

The data plots within Figure 15.4 are from a set of dual incubations performed with natural phytoplankton assemblages in the North Atlantic Ocean. In this specific example, two LabSTAF units were used to incubate ^{14}C-spiked samples sequentially at six light levels, with each incubation lasting for 30 minutes. The approach allowed for the construction of P-E curves for both metrics (JV_{PII} and C-fixation) plus the derived conversion factor $\Phi_{e,C}$, which ranged from around five to slightly above seven. The magnitude and range of $\Phi_{e,C}$ observed in this example is smaller than observed in previous experiments, where STAF-assessed and ^{14}C-assessed rates were measured in parallel, rather than simultaneously.

Figure 15.3: The large sample chamber within LabSTAF allows a scintillation vial to be used to facilitate parallel measurement of JV_{PII} and ^{14}C-fixation using a single actinic light source (dual incubation).

Clearly, a much larger set of dual incubation experiments, under a range of environmental conditions, are required to fully characterize the magnitude and variability of $\Phi_{e,C}$ in the oceans. However, removing the methodological bias which significantly limited previous intercomparisons of the two techniques (e.g. Lawrence et al., 2011) is an important step towards the goal of being able to model $\Phi_{e,C}$ with sufficient accuracy to utilize STAF measurements for accurate estimates of PhytoPP.

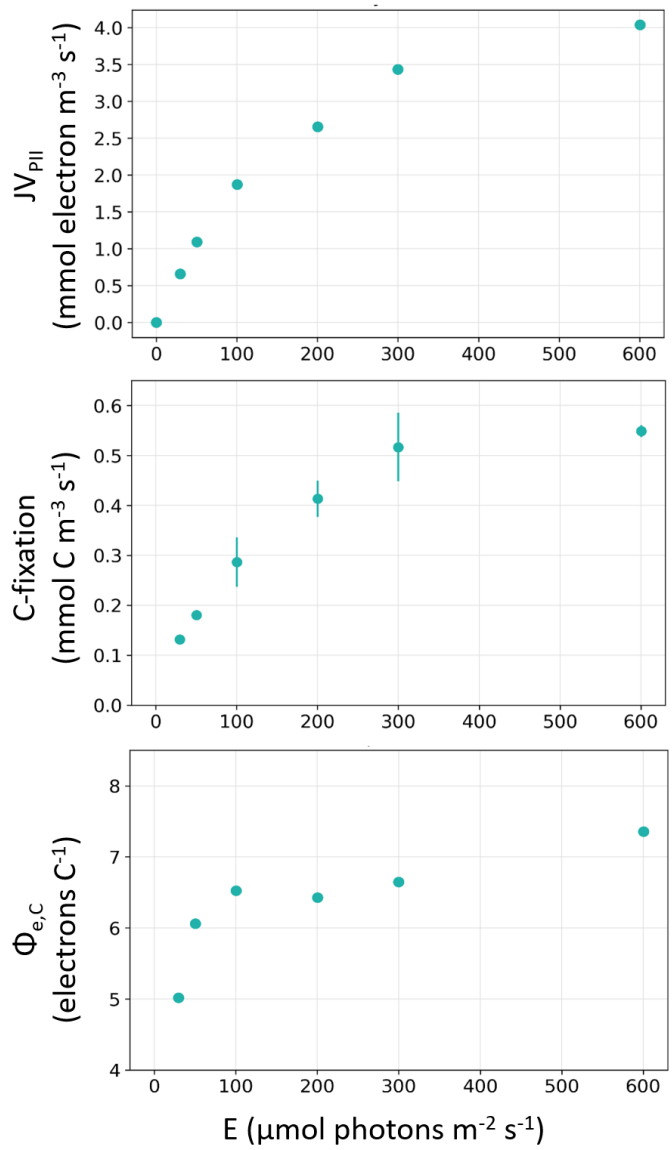

Figure 15.4: Data acquired using a LabSTAF-based dual incubation method.

15.3 Using the Pre-FLC functions without the FLC

A single or repeating protocol incorporating Pre-FLC functions can be run with only one or two FLC steps, instead of a full FLC. The example shown below illustrates how this feature can be used track potential changes in the PEP at high temporal resolution.

The FLC setup in Figure 15.5 has a single **Up** step of 60 s dark. The starting sample is a mixture of cultured cells of *Chlorella vulgaris* and *Anabaena* sp. The same sample was present within the sample chamber for the entire 12 h of acquisition and the stir unit was used throughout. The sample temperature was maintained at a constant 29.3 °C.

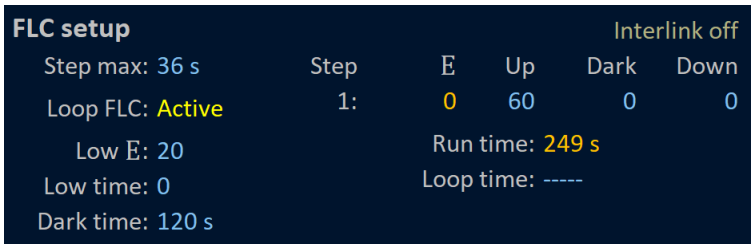

Figure 15.5: A single step FLC setup as part of a repeating protocol. In addition to the settings shown here, the **Auto DWM** and **Auto PEP** functions are both active. RunSTAF has calculated a total **Run time** of **249 s**.

Figure 15.6 shows the PEPs from the first and last measurement cycles of a 12 h repeating sequence.

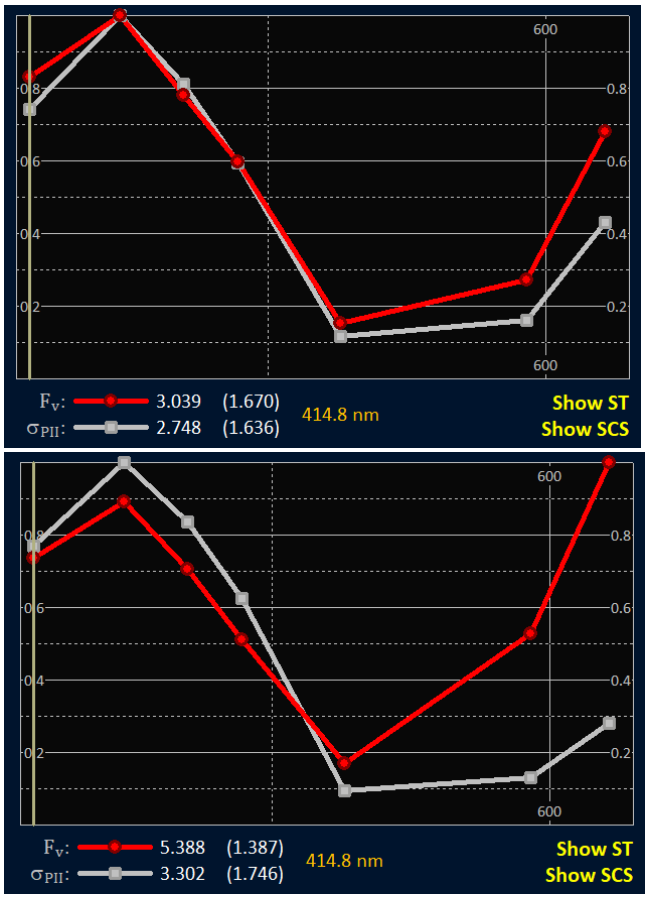

Figure 15.6: Screen crops showing the first and last PEPs from a 12 h repeating sequence, as defined by the settings in Figure 15.3. The difference between the F_v and σ_{PII} PEPS for the first measurement cycle is typical for a mixed population of *C. vulgaris* and *Anabaena* sp.. The last measurement is typical for cultured cells of *C. vulgaris* alone.

The F_v PEPs from Figure 15.6 are plotted in the SCS format within Figure 15.7.

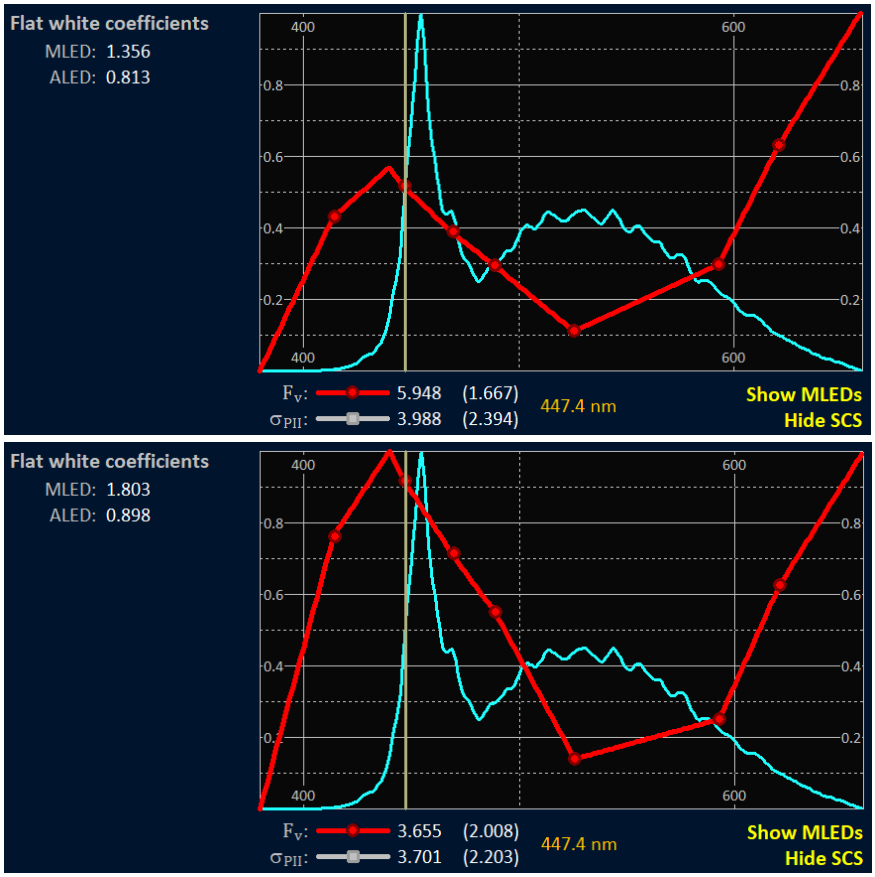

Figure 15.7: Screen crops of the F_v PEPs from Figure 15.6 plotted in the **SCS** format. The most obvious change between the first (upper) and last (lower) F_v PEPs is the increase in the relative height of the peak at 440 nm. Note the increase in the **MLED** and **ALED Flat white coefficients** between the first and last PEPs of the 12 h experiment.

Figure 15.8 shows plots of the change in all seven F_v PEP wavebands over the 12 h sequence. The steady decrease in the 594 nm and 622 nm wavebands is clearly steeper than for the other bands, resulting in the relative increase in the blue peak of the F_v PEP in Figure 15.7.

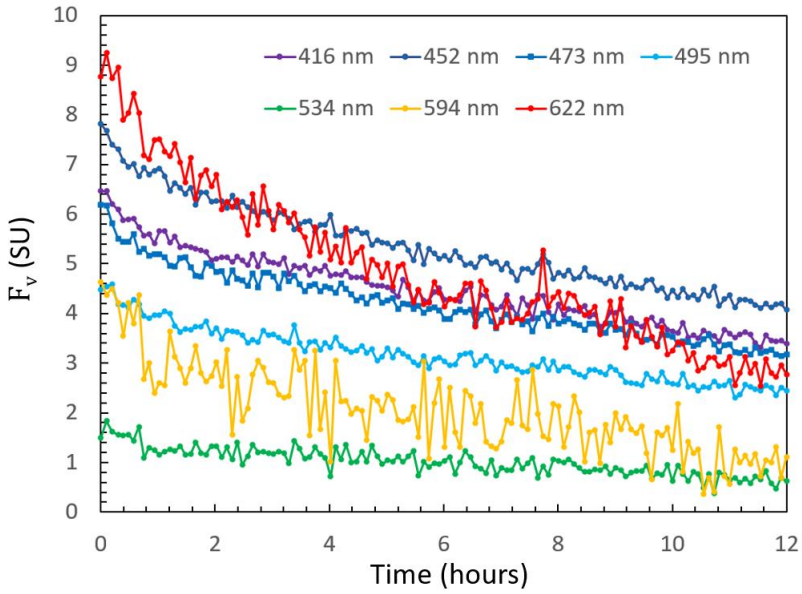

Figure 15.8: Plots of the change in all seven F_v PEP wavebands over the 12 h sequence. These values were extracted from the RunSTAF data files using the Folder-based PEP file function:

File → CSV files → Folder-based PEP file

The data presented within Figures 15.6, 15.7 and 15.8 may reflect a loss of the fluorescence signal from *Anabaena* sp. cells over the 12 h of the experiment and serve as a simple proof-of-concept of how high-resolution PEP data acquired in this way could serve to track changes in phytoplankton species composition.

16 Connectivity and heterogeneity

The impact of heterogeneity on STAF data has been raised within earlier sections of this document.
See: **Derivation of τ_t'** and **How heterogeneity affects the relationship between F_v PEP and σ_{PII} PEP data**

This chapter provides two additional examples to illustrate why it is important to consider connectivity and heterogeneity in the analysis of STAF data. The first subsection covers the rho parameter and how well, or badly, different models of connectivity account for the kinetics of the increase in fluorescence during an ST pulse. The second subsection examines evidence, from analysis of DSP data, that the connectivity arising from dimerization of PSII provides photoprotection.

16.1 Deconstructing rho

Equations 16.1 to 16.4 were originally presented by Kolber et al. (1998) and are very widely used to fit ST data curves. The rho parameter within these equations (ρ and ρ') is required to account for connectivity among PSII complexes and has the potential to provide qualitative information about the nature of connectivity between PSII complexes and/or the degree of PSII heterogeneity within a sample.

Equations 16.1 and 16.2 are valid for a dark-adapted sample and assume that all photochemically active RCIIs are in the open state at $t = 0$. Equations 16.3 and 16.4 are valid for a light-adapted sample where a proportion of the photochemically active RCIIs within the sample are in the closed state.

$$C_t = C_{t-1} + C_{t=1} \cdot (1 - C_{t-1})/(1 - C_{t-1} \cdot \rho) \qquad \text{Equation 16.1}$$

$$\mathrm{F}_t = \mathrm{F_o} + \mathrm{F_v} \cdot C_t \cdot (1 - \rho)/(1 - C_t \cdot \rho) \qquad \text{Equation 16.2}$$

$$C_t = C_{t-1} + C_{t=1} \cdot (1 - C_{t-1})/(1 - C_{t-1} \cdot \rho') \qquad \text{Equation 16.3}$$

$$\mathrm{F'}_t = \mathrm{F'} + \mathrm{F_q}' \cdot C_t \cdot (1 - \rho')/(1 - C_t \cdot \rho') \qquad \text{Equation 16.4}$$

Where t = time since the start of the ST pulse (µs) and C_t is the proportion of centres that were open at $t = 0$ that are closed at t. As a consequence, C is 0 at $t = 0$ in both the dark-adapted and light-adapted states, even though a proportion of the photochemically active RCII within the sample are in the closed state under ambient light.

Within a completely homogeneous population of perfectly or imperfectly connected PSII complexes, ρ can be defined as the probability of a photon absorbed by a PSII complex with a closed RCII being transferred to a PSII complex with an open RCII and then used to drive PSII photochemistry. Figure 16.1 shows ST pulse data from dark-adapted cultured cells of *Chlorella vulgaris*. Both Rho and Dimer fits are also included.

Although there is a close visual match between the ST data and either fit within Figure 16.1., the Rho fit provides a closer overall match than the Dimer fit. In this example, the closer match provided by the Rho fit is evident over the first 10 µs or so (see inset to Figure 16.1). Because the value of F_v/F_m is high, RunSTAF has limited the Rho ST fit to the first 76 points to limit the possible impact of electric field-dependent quenching.
See: **Fitting a Dual ST Pulse (DSP) sequence**

Within a theoretical model incorporating zero connectivity among RCII, the value of ρ in Equations 16.1 and 16.2 is zero and the values of α_{PII} and σ_{PII} derived from the fit are unchanged as C_t increases. At the other end of the scale, perfect connectivity among RCII (i.e. all RCII within the interrogated volume have equal access to a single light harvesting pigment matrix) generates a value of ρ equal to ϕ_{PII} and values of α_{PII} and σ_{PII} that increase with C_t. The curves in Figure 16.3 show the original ST curve and Rho fit from Figure 16.1 (**A**), the fit with zero connectivity among RCII (**B**) and the fit with perfect connectivity among RCII (**C**). For both **B** and **C**, the values of F_o and F_m were fixed

at the values generated by the Rho ST fit in **A**. The perfect connectivity in **C** was set by using the value of F_v/F_m from **A** as a proxy for ϕ_{PII}.

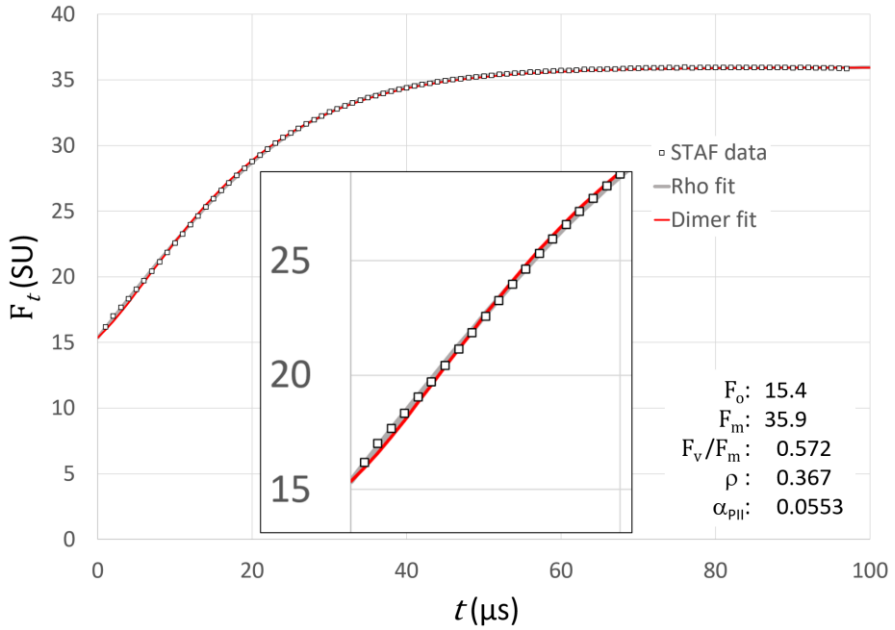

Figure 16.1: An example Saq ST curve recorded from cultured cells of *C. vulgaris*. The Rho fit was made using Equations 16.1 and 16.2. The Dimer fit was made using Equations 10.7 and 10.8. The first 76 points were incorporated within both fits (t = 1 to t = 76). The inset provides an exploded view of the first points.

See: **The Rho ST curve fit** and **The Dimer ST curve fit**

Setting the value of ρ to zero is equivalent to the 'separate package' or 'puddle' model while setting ρ as ϕ_{PII} is equivalent to the 'matrix' or 'lake' model of PSII connectivity (e.g. Butler et al. 1983; Kramer et al. 2004). Looking at the three fits within Figure 16.2, it is clear that a good fit to the entire ST curve is only achieved by allowing the value of ρ to assume an intermediate value during the iterative fitting process.

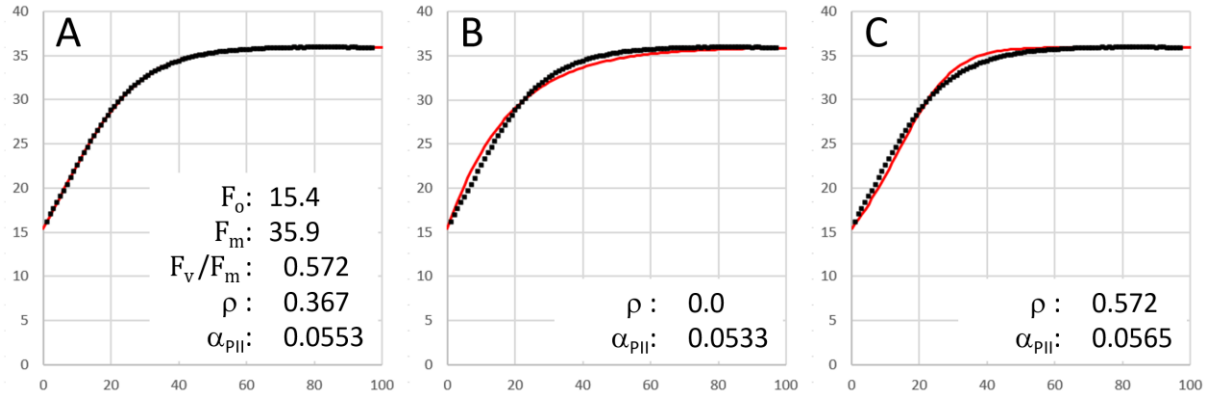

Figure 16.2: Rho ST curve fits to the same ST data as presented in Figure 16.1. The fit in **A** is identical to Figure 16.1 (F_o, F_m, ρ and $C_{t=1}$ were all allowed to float in Equations 16.1 and 16.2). For the CT fits in **B** and **C**, only $C_{t=1}$ was allowed to float. The value of ρ was fixed as zero in **B** and 0.572 in **C** (the value of F_v/F_m derived from the fit in **A**). As with Figure 16.1, the x-axes values are t (µs) and the y-axes values are F_t (SU).

16.1.1 Estimating the proportion of PSII complexes in the open state

From Equations 16.2 and 16.4, it is clear that the relationship between F_t and C_t in the dark-adapted state and F_t' and C_t in the light-adapted state are dependent on the values of ρ and ρ', respectively. One situation where the impact of ρ' on the relationship between F_t' and C_t has practical relevance is when using fluorescence to estimate the proportion of the total pool of photochemically active PSII complexes in the open state at t = 0, defined here by the term $[Q_A]$. It follows that the proportion of the total pool of photochemically active PSII complexes in the closed state is provided by $1 - [Q_A]$.

A value for $[Q_A]$ is required when using the Sigma method to calculate J_{PII} (Equation 11.8) or JV_{PII} (Equation 11.14). Within both equations, this value is provided by F_q'/F_v'. A value for $[Q_A]$ is not required when using the Absorption method to calculate JV_{PII} (Equation 11.11).

Equations 16.5 and 16.6 can be used to calculate a value for $[Q_A]$ from a dark-adapted sample or a sample under actinic illumination, respectively, for any value of ρ or ρ'. Equation 16.5 can be used to quantify $[Q_A]$ at any point within a ST pulse applied to a dark-adapted sample. Equation 16.6 can be used to calculate $[Q_A]$ at the start of a ST pulse ($t = 0$) applied to a sample under actinic illumination.

$$[Q_A] = 1 - (F - F_o)/[(1 - \rho) \cdot (F_m - F_o) + \rho \cdot (F - F_o)] \qquad \text{Equation 16.5}$$

$$[Q_A] = 1 - (F' - F_o')/[(1 - \rho') \cdot (F_m' - F_o') + \rho' \cdot (F' - F_o')] \qquad \text{Equation 16.6}$$

Setting the value of ρ' in Equation 16.6 to zero makes the right hand side exactly equivalent to F_q'/F_v'. In other words, using F_q'/F_v' to estimate $[Q_A]$ is effectively assuming zero connectivity among PSII complexes and is consistent with the separate package or puddle model of connectivity (Baker and Oxborough, 2004). The parameter F_q'/F_v' is mathematically equivalent to the widely used parameter, qP. At the other end of the connectivity scale, the parameter qL provides an estimate of $[Q_A]$ assuming the matrix or lake model of connectivity (Kramer et al. 2004). Substituting $1 - F_o'/F_m'$ for ρ' (as a proxy for ϕ_{PII}) in Equation 16.6 makes the right hand side equivalent to qL. Equations 16.7A and 16.7B (Kramer et al. 2004) provide equivalent options for the calculation of qL.

$$qL = 1 - (1/F_o' - 1/F')/(1/F_o' - 1/F_m') \qquad \text{Equation 16.7A}$$

$$qL = qP \cdot F_o'/F' \qquad \text{Equation 16.7B}$$

The curves in Figure 16.3 were generated using three different values of ρ within the dark-adapted equivalent of Equation 16.7A. The F_q/F_v term on the x-axis is the dark-adapted equivalent of the F_q'/F_v' term within Equations 11.8 and 11.14. The values of F_o and F_m required to generate these curves were taken from the ST fit in Figure 16.1. Setting ρ as zero has generated a set of qP-based values while setting ρ as $1 - F_o/F_m$ (as a proxy for ϕ_{PII}) has generated a set of qL-based values. These two sets of values provide the theoretical extremes for the relationship between F_q/F_v and the value of $[Q_A]$. The third curve in Figure 16.3 uses the value of ρ from the ST fit in Figure 16.1 and, by definition, provides the most appropriate values of $[Q_A]$ for the homogeneous, imperfect level of connectivity that is intrinsic to the Rho ST model.

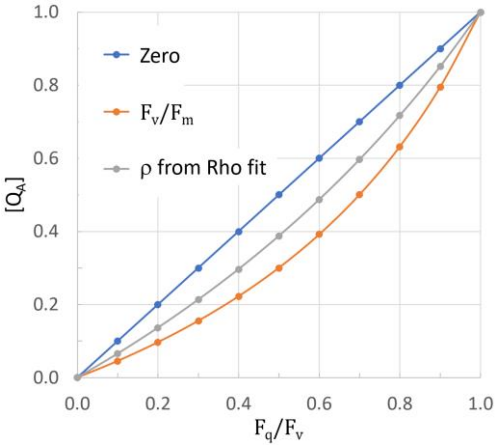

Figure 16.3: Data illustrating the relationship between F_q/F_v and values of ρ defined by qP, qL and the ST fit value. The ST curve in Figure 16.1 was used as the starting point for generating the theoretical values plotted. Data points were generated by initially setting F_q equal to F_o and then increasing the value in steps of 10% of F_v up to F_m.

16.1.2 The relationship between ρ and the yield of PSII photochemistry

The ST curves in Figure 16.4 are all derived from the single ST curve in Figure 16.1. Each curve within Figure 16.4 begins at the stated time within the original curve. The red fits are to the actual data points (Saq fits) and the green fits are to the Rho ST fit points (Rho fits). So, for example, the $t = 5$ µs Saq curve in Figure 16.4 is a fit to the Saq ST curve points in Figure 16.1 between $t = 5$ µs and $t = 76$

µs. These points are mapped to between $t = 0$ and $t = 71$ µs for the new fit. The $t = 5$ µs Rho curve in Figure 16.4 is a fit to the Rho ST fit points from Figure 16.1 between $t = 5$ µs and $t = 76$ µs. As with the Saq fit, these points have been mapped to between $t = 0$ and $t = 71$ µs for the fit.

As already noted, the value of C in Equations 16.1 and 16.2 is always zero at $t = 0$. This means that, for all curves in Figure 16.4, the value of C only tracks the closure of RCIIs that were in the open state at $t = 0$.

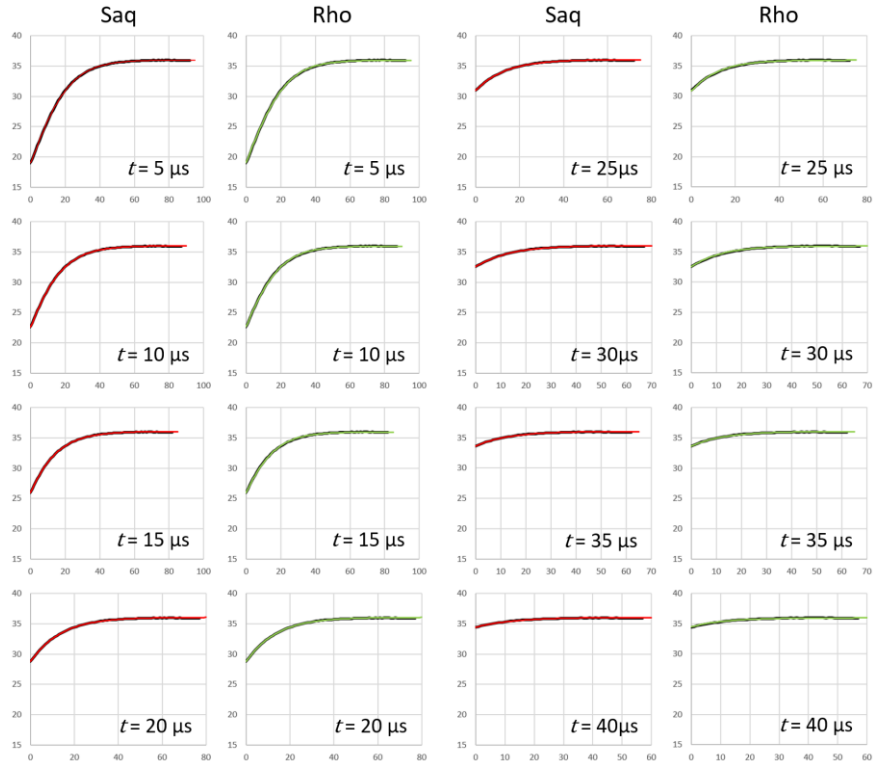

Figure 16.4: ST curve fits to subsets of the ST curve in Figure 16.1. The timestamps on each plot defines the points cropped from the initial ST curve. The red curves within the Saq columns are fits to the remaining raw data points. The green curves within the Rho column are fits to the equivalent section of the Rho ST curve fit from Figure 16.1. The x-axes are all t (µs). The y-axes are all F_t (SU).

The data presented within Figure 16.5 are derived from the Saq and Rho curve fits in Figure 16.4. The plots within **A** show how ρ changes as the starting point for the fit is increased from $t = 0$ to $t =$ 40 µs. Within **B**, the same ρ values are plotted against F_q/F_m. The Rho plot shows a linear relationship between these values while the Saq plot deviates significantly from a linear relationship. The plots within **C** show how the differences in ρ derived from the Rho and Saq data impact on the derived values of σ_{PII}.

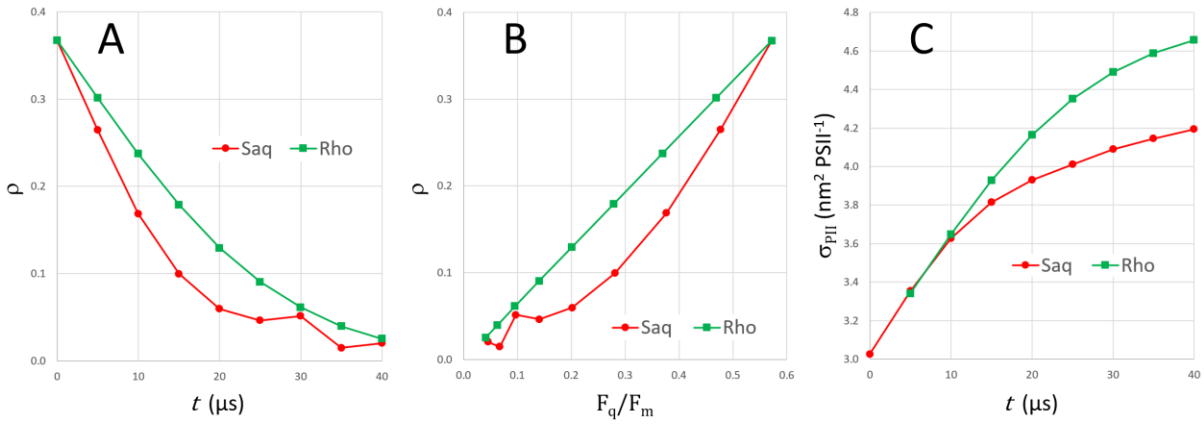

Figure 16.5: Data derived from the curve fits in Figures 16.1 and 16.2. Saq data and Rho fit data were derived for the entire curve with the starting point set between $t = 0$ and $t = 40$ µs. **A** shows ρ changing with t. **B** shows the relationship between ρ and F_v'/F_m'. **C** shows the change in σ_{PII}, derived from the curve fits.

Figure 16.6 provides additional examples of ρ plotted against F_q/F_m from Saq and Rho data fits. Example **A** is derived from a dark-adapted sample. As such, these values are directly comparable with those in Figure 16.5 **B**. Examples B and C within Figure 16.6 are from samples adapted to actinic light at the values shown.

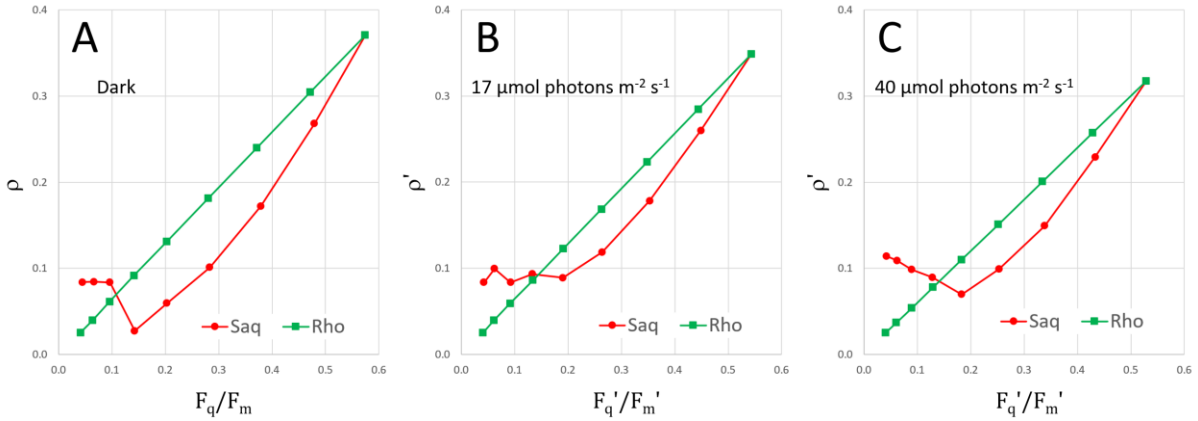

Figure 16.6: Data derived from fits to ST curves using the same fitting process as used for the example in Figure 16.4. Example **A** was dark adapted. Samples **B** and **C** were adapted to the actinic light levels shown.

When viewed in isolation, the non-linearity of the Saq plots in Figure 16.6 could perhaps be written off as a measurement artefact. However, the FLC-derived data presented within Figure 16.7 provide eight examples of a broadly similar relationship between ρ' and F_q'/F_m' with increasing incident photon irradiance. In all eight examples, the decrease in ρ' with increasing actinic light levels is faster than the concurrent decrease in F_q'/F_m'.

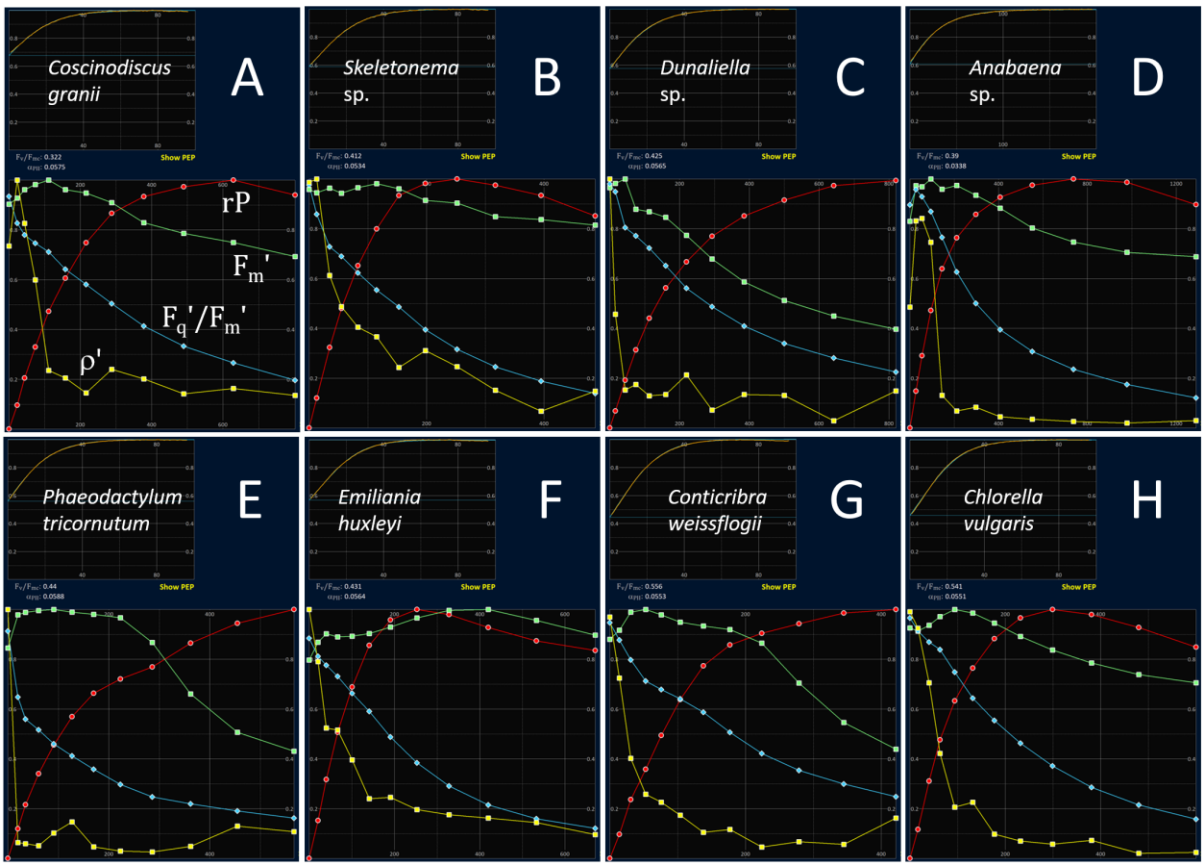

Figure 16.7: Screen shot crops of FLC-derived sample data from cultured cells of the species shown within each crop. The x-axis is incident photon irradiance with units of µmol photons m^{-2} s^{-1}. The ST curve shown within

each crop is the first dark-adapted Saq within each dataset. The plot colours code the same parameters within each crop: Red = rP, Green = F_m', Teal = F_q'/F_m' and Yellow = ρ', as labelled in **A**.

The plots of F_m' within the examples in Figure 16.7 track non-photochemical quenching due to downregulation. In some examples, most notably **B** and **F**, there is very little change in F_m' during the FLC. At the other end of the scale, the plots in **C**, **E** and **G** show very significant quenching of F_m', starting at around E_k.

The homogeneous model defined by Equations 16.1 to 16.4 doesn't distinguish between changes in ρ' and F_q'/F_m' driven by the accumulation of closed RCIIs or by downregulation. It follows that the model defined by 16.1 to 16.4, while generally providing a convincing fit, can only approximate the underlying mechanism.

16.1.3 Heterogeneity induced by dimerization of PSII

As already noted, it seems likely that dimerization of PSII could be responsible for a high proportion of the connectivity defined by ρ.
See: **The Dimer ST curve fit**

While the Rho fit assumes a homogeneous, imperfect level of connectivity among PSII complexes, the Dimer fit makes three basic assumptions: that the two RCIIs within the dimer are perfectly connected, that there is no connectivity among dimers and that all dimers are in the oo state (both RCIIs open) at $t = 0$. Another difference between the Rho and Dimer fits is that while the Rho fit does not quantify the proportion of RCII that are open at $t = 0$ in the light-adapted state, the relative proportions of oo, oc and cc dimers at $t = 0$ are fixed through extrapolation from the dark-adapted fit.

Because of the additional constraints imposed by the Dimer fit, Standard Error (SE) values for the Dimer fit tend to be higher than for the Rho fit. One feature that is commonly observed is a higher level of sigmoidicity in the early part of a Dimer fit to a dark-adapted sample, compared to either the Rho fit or the actual ST data points (e.g., Figure 16.1). Given the constraints incorporated within the Dimer fit, it is not too surprising that some deviation is observed between the fit and the actual trace. For example, heterogeneity introduced by the combination of PSIIα and PSIIβ is not incorporated within the algorithm.
See: **How heterogeneity affects the relationship between F_v PEP and σ_{PII} PEP data**

Figure 16.8 provides an example of how dimerization changes the relationship between F_q/F_v and ρ.

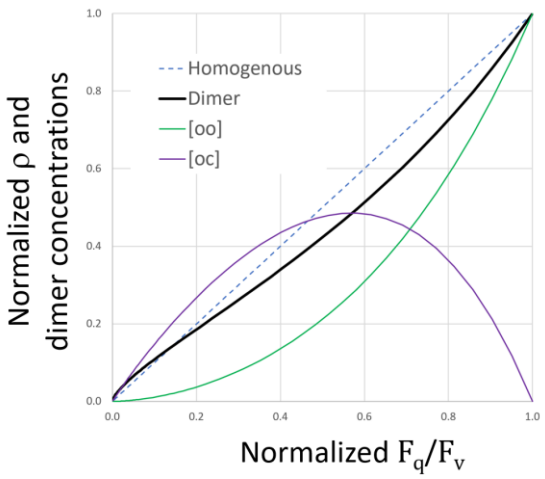

Figure 16.8: Normalized values of F_q/F_v and ρ generated from the dark-adapted ST curve example shown in Figure 16.1. **Homogeneous** shows the linear relationship between F_q/F_v and ρ that is intrinsic to the Rho fit. **Dimer** shows the overall level of ρ generated as **[oo]** and **[oc]** change with F_q/F_v. Data have been normalized to the $t = 0$ value for each parameter.

Because the Dimer fit assumes perfect connectivity within each dimer and zero connectivity among dimers, the normalized value of ρ at any point within Figure 16.8 is provided by Equation 16.8.

$$\text{Normalized } \rho = \frac{[oo]}{[oo]+[oc]\cdot 0.5/(1-0.5\cdot\rho)} \qquad \text{Equation 16.8}$$

Tracking the change in normalized ρ values through the ST curve (from right to left along the x-axis), the shape is defined by a first order decay in [oo] accompanied by an increase in [oc] driven by closure of one of the two open RCIIs within an [oo] dimer and an decrease in [oc] driven by closure of the remaining open RCII. These changes generate the 'S' shape of the Dimer curve and may at least partly explain the Saq relationships between F_q/F_v and ρ in **B** of Figure 16.5 and **A** of Figure 16.6 and between F_q'/F_v' and ρ' in **B** and **C** of Figure 16.6.

16.2 DSP-derived evidence that dimerization of PSII is photoprotective

One consistent and surprising observation from application of the DSP method is a rapid, transient decrease in $\sigma_{PII}{}'$ such that the second ST pulse value, $s\sigma_{PII}{}'$, is as much as 50% lower than the first ST pulse value (Figure 16.9). The 'recovery' time from this decrease is hundreds of µs to low ms and detailed analysis of the kinetics of this recovery (Figure 16.10) strongly support the idea of connectivity among PSII complexes being largely, if not entirely, limited to dimerization.

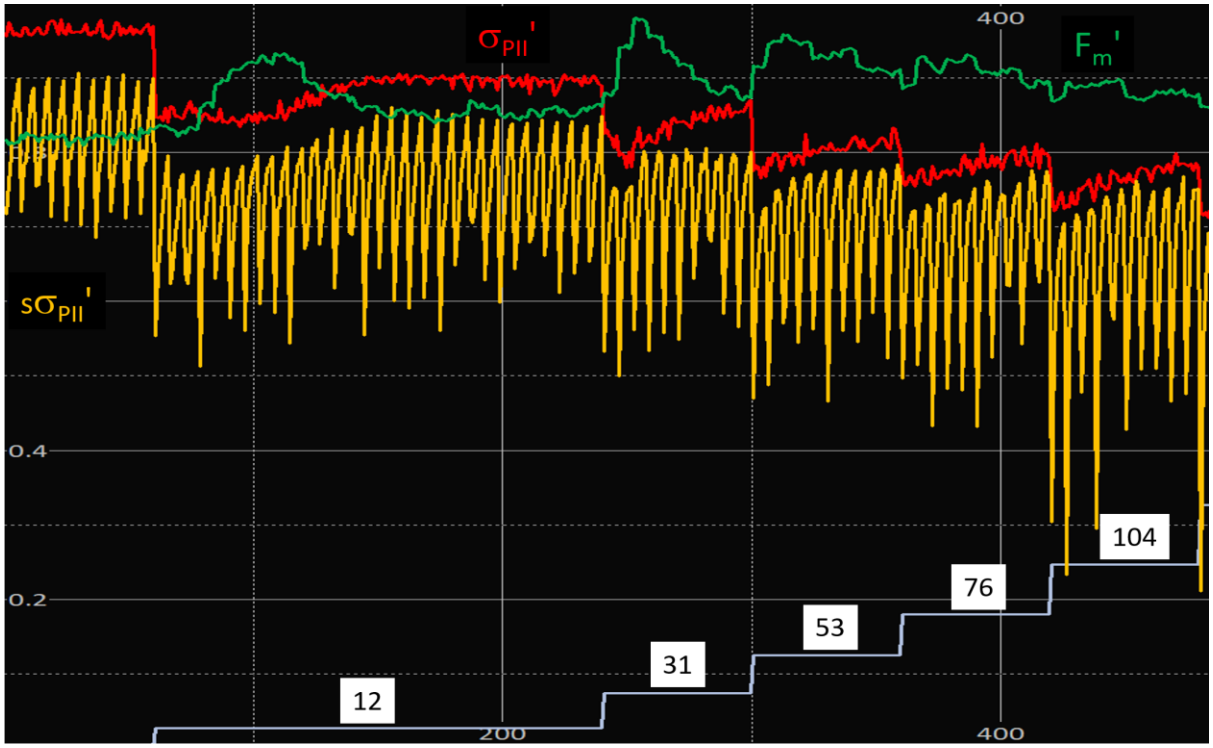

Figure 16.9: Crop from the RunSTAF data screen showing changes in $\sigma_{PII}{}'$, $s\sigma_{PII}{}'$ and $F_m{}'$ during the first steps of an FLC. The numbers in white squares are E (µmol photons m^{-2} s^{-1}). The oscillations in $s\sigma_{PII}{}'$ track with the gap steps during each DSP. The anti-parallel relationship between $\sigma_{PII}{}'$ (red line) and $F_m{}'$ (green line) is discussed, in the context of PSII heterogeneity, elsewhere within this document.

At a basic level, and under the assumption that charge separation at a closed PSII complex is best avoided, dimerization of PSII can be seen as being photoprotective. Protection is provided to a closed RCII within an open plus closed (oc) dimer, simply because an absorbed photon is much more likely to result in charge separation at the open RCII than the closed RCII.

The observed decrease between $\sigma_{PII}{}'$ and $s\sigma_{PII}{}'$ may reflect a secondary photoprotective process, activated by the formation of cc dimers. The working assumption is that the apparent 50% decrease observed between $\sigma_{PII}{}'$ and $s\sigma_{PII}{}'$ reflects a requirement for two charge separation events to close an open RCII in the first few hundred µs after formation of a cc dimer. In turn, it is assumed that this requirement is indicative of a deexcitation pathway within a closed RCII that is functional over that timescale. In other words:

- The absorption of a first photon within a cc dimer would have a low probability of inducing so-called acceptor side photoinactivation (Vass et al. 2009) because a transient deexcitation pathway provides a very effective escape route to prevent double reduction of Q_A and/or charge recombination between reduced phaeophytin and oxidised P_{680}.
- The putative escape route remains active for a few hundred µs to low ms after formation of the cc dimer, even if one or both of the RCII within the dimer re-opens during this time

Figure 16.10 provides a detailed view of the recovery of $s\sigma_{PII}{}'$ to $\sigma_{PII}{}'$ as the gap between the first and second ST pulses within a DSP sequence is increased.

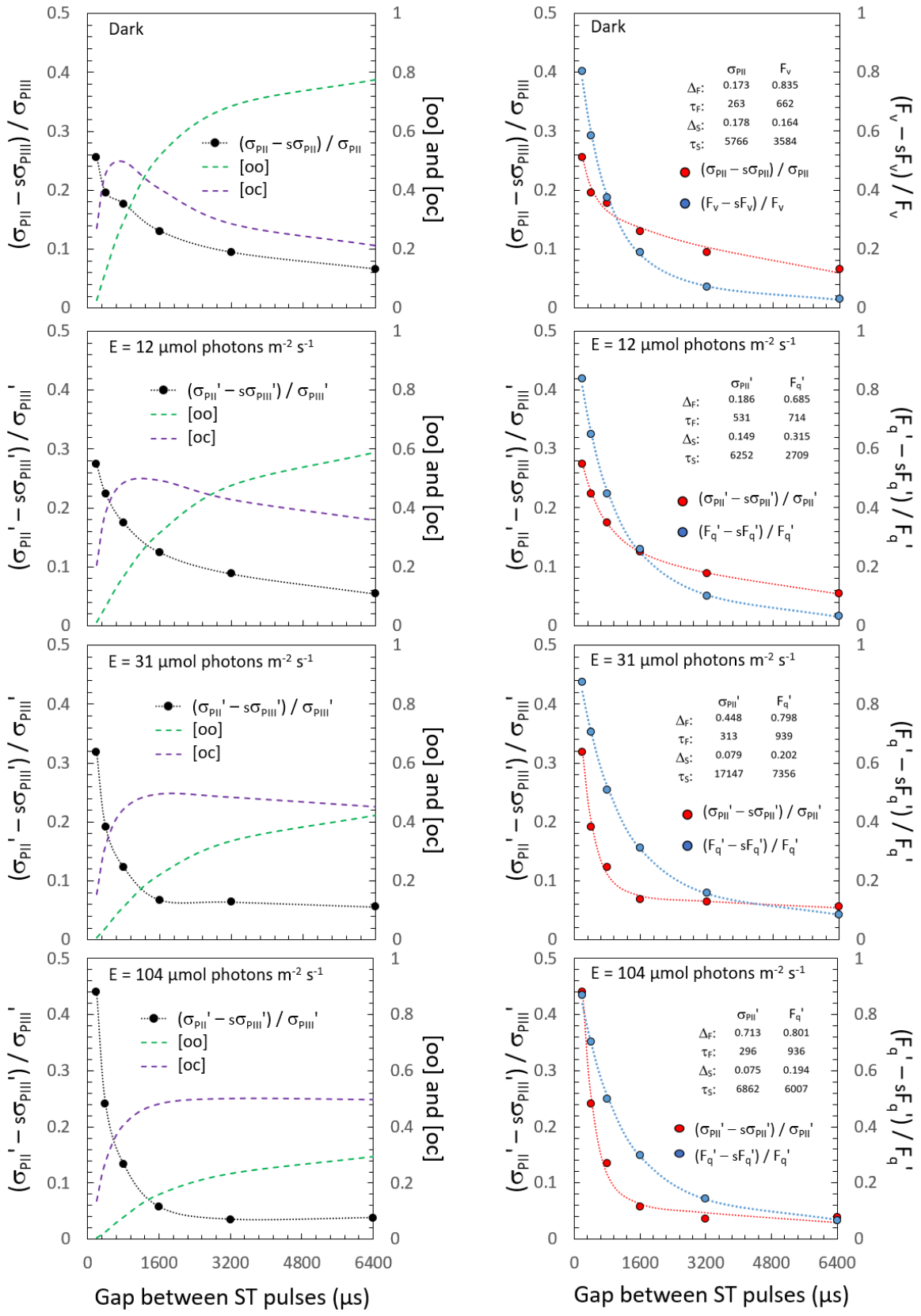

Figure 16.10: The left column shows the recovery of $\sigma_{PI}^{(')}$ with concurrent changes in [oo] and [oc]. The right column shows concurrent changes in the recovery of $\sigma_{PII}^{(')}$ and F_v or F_q'. The increase in [oc] relative to [oo] and the amplitude of the fast phase (Δ_F) of the $\sigma_{PII}^{(')}$ recovery, within increasing photon irradiance, are consistent with PSII dimerization being the main basis for connectivity among PSII complexes.

Moving through the graphs on the left hand side of Figure 16.10, increasing actinic photon irradiance (from dark to 104 µmol photons m^{-2} s^{-1}) results in a larger maximum decrease in $s\sigma_{PII}{}'$ and steeper recovery back to $\sigma_{PII}{}'$. These changes in amplitude and dynamics are matched by a shift in the relative fractions of oo and oc dimers at steady state. In the dark-adapted state, [oo] is at 100% and [oc] is zero. Within increasing actinic photon irradiance, the steady state fraction of oo dimers decreases and the fraction of oc dimers increases. At 104 µmol photons m^{-2} s^{-1} (the highest actinic photon irradiance used here), [oo] is 37% and [oc] is 48%.

Because the open centre within an oc dimer has much larger $\sigma_{PII}{}'$ than each of the two open centres within an oo dimer, the $\sigma_{PII}{}'$ of open centres at the first ST pulse in a DSP sequence will increase with the steady state value of [oc]. This feature of the dimer model provides a good explanation for the increase in the amplitude of the change in $\sigma_{PII}{}'$, between first and second ST pulses, that is clearly evident with increasing actinic photon irradiance.

As already noted, [oc] is zero at the start of the first ST pulse in the DSP sequence in the dark-adapted state and the measured σ_{PII} is defined by open PSII complexes within oo dimers. During the first 400 µs after the first ST pulse, there is a rapid accumulation of oc dimers, which pushes the $s\sigma_{PII}$ significantly higher than the σ_{PII} value for the first ST pulse. In the context of the model being proposed within this section, the increase between σ_{PII} and $s\sigma_{PII}$ due to the accumulation of oc dimers offsets the expected 50% decrease between σ_{PII} and $s\sigma_{PII}$ due to the proposed two photochemical event requirement for centre closure. The overall result is that the apparent decrease in σ_{PII} at t = 0 is approximately 25%.

At 104 µmol photons m^{-2} s^{-1}, the σ_{PII}' at the start of the first ST pulse in the DSP sequence is more indicative of a single open PSII complex within an oc dimer, simply because [oc] is at 48% while [oo] is at 37%. It follows that the 50% decrease between $\sigma_{PII}{}'$ and $s\sigma_{PII}{}'$ induced by the proposed requirement for two photochemical events to close an open PSII complex during the first few hundred microseconds after formation of a cc dimer will not be as strongly offset as oc dimers accumulate in the gap between ST pulses. The end result is that the 45% decrease in σ_{PII}' induced by the first ST pulse is much closer to the theoretical 50% decrease induced by the proposed two photochemical event requirement for centre closure.

The plots on the right hand side of Figure 16.10 compare the recovery of $\sigma_{PII}{}'$ with the recovery of variable fluorescence (F_v or F_q'). Clearly, the changes in the recovery of $\sigma_{PII}{}'$ with increasing actinic light are much greater than the relatively minor changes in the recovery of F_v or F_q'. This comparison highlights the value of a photochemical explanation for the decrease in $\sigma_{PII}{}'$ observed between the first and second ST pulses in a DSP sequence, rather than a mechanism linked to non-photochemical quenching. Put simply, the expectation for a 50% decrease in $\sigma_{PII}{}'$ through a non-photochemical process would be expected to decrease F_v or F_q' by an equivalent amount. This clearly does not happen. There is also no established non-photochemical quenching process that operates on the timescale involved.

Another notable feature of the data presented in Figure 16.9 is the approximately 10% decrease in $\sigma_{PII}{}'$ between dark and the first actinic light level (12 µmol photons m^{-2} s^{-1}). This feature cannot easily be linked in with the proposed mechanism covered within this section and is more likely to result from PSII heterogeneity.

17 Delivery pack

#	CTL reference	Item	Quantity
1	2408-024-AS	Peristaltic pump unit	1
2	200230	Peristaltic pump head with 6 mm bore tubing installed	1
3	2408-169-AS	Solenoid unit	1
4	2408-070-AS	Flow-through unit	1
5	2408-160-AS	Flow-through stirrer unit	1
6	2408-157-MD	Calibration plug	1
7	2408-158-MD	Sample chamber lid	1
8	2408-258-AS	LabSTAF and peristaltic pump power cables	2
9	2408-262-AS	Surface Go power cable	1
10	2408-259-AS	Peristaltic pump interface cable	1
11	2408-260-AS	Solenoid unit cable	1
12	2408-261-AS	LabSTAF to USB-C cable	1
13	925791278	Connectors: 7 – 11 mm + 11 – 16 mm	2
14	117250	8 mm ID silicon tubing	2 x 80 mm
15	118054	4 mm ID tubing	80 mm
16	114126	O-rings (spare)	4
17	113639	7 mL sachet of silicon grease	1
18	118842	Fischer 102 blanking plug (spare)	2
19	105243	Surface Go 3 and power supply	1
20	12052	Surface Go Keyboard	1

Table 17.1: Items stored within the LabSTAF accessory case.

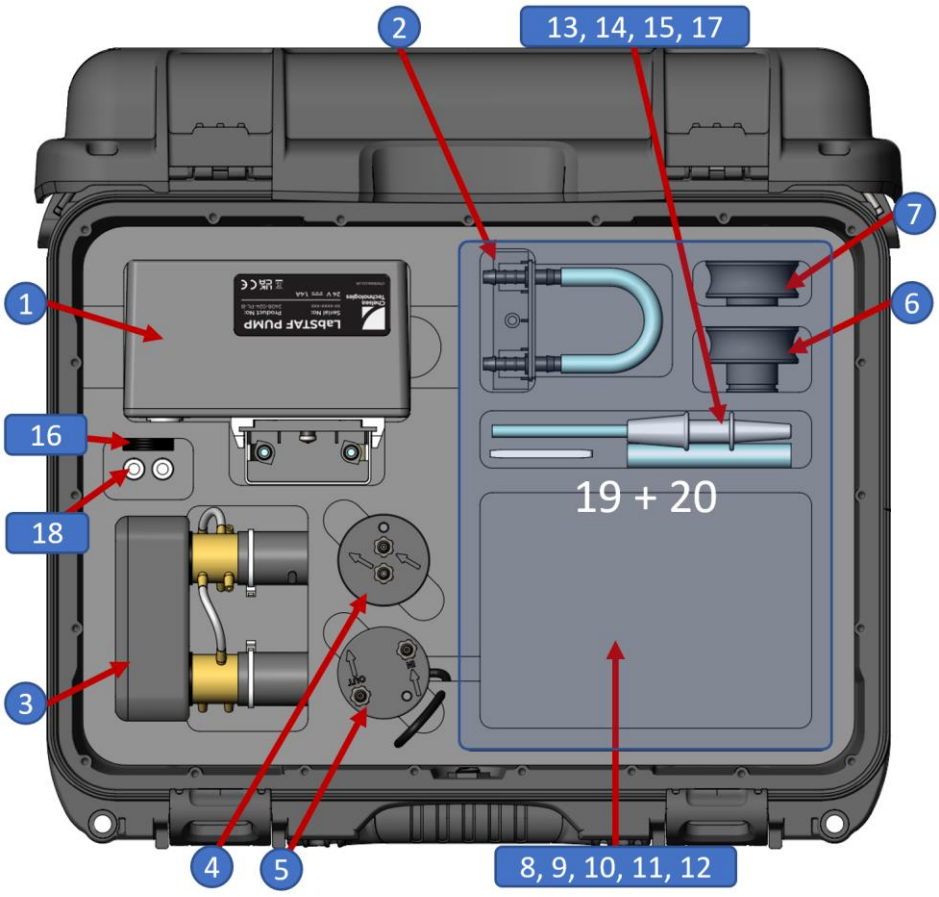

Figure 17.1: The LabSTAF Spares Case. The numbers correspond to the # column in Table 15.1. The Surface Go + keyboard (19 + 20) fit into a recess above other items.

18 LabSTAF hardware setup

18.1 Plumbing the flow-through unit, peristaltic pump and solenoid unit

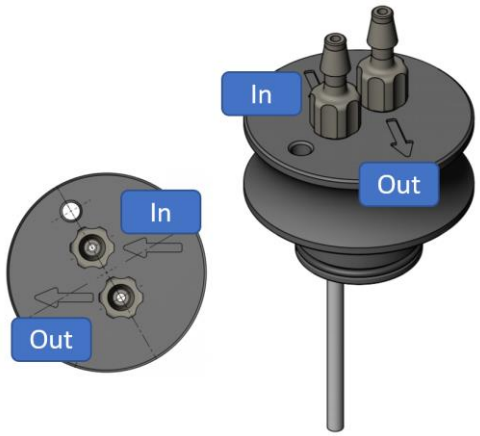

Figure 18.1: The LabSTAF flow-through unit with **In** and **Out** ports labelled. Make sure the connectors are screwed in tightly before using.

If the Auto FLC mode is being used without the solenoid unit, the **In** on the flow-through unit can be connected directly to the **Out** connector on the peristaltic pump unit. Otherwise, the **Out** on the flow-through unit should be connected to the **In** on the peristaltic pump unit.

When running the system in Auto FLC mode, the plumbing shown below must be adhered to.

Figure 18.2: This image shows a valve of the type used within the LabSTAF solenoid unit. The single port on the left is the Common port (**COM**). This is the output for each of the three valves (A, B and C) when the unit is plumbed in correctly. The upper port on the right is Normally Open (**NO**) and the lower port is Normally Closed (**NC**). Table 18.1 shows the status of each valve for each Auto FLC function.

The switch from NO to NC is driven by 24 V DC delivered from the LabSTAF unit through the **SOLENOID VALVE UNIT** connector located on the top panel.

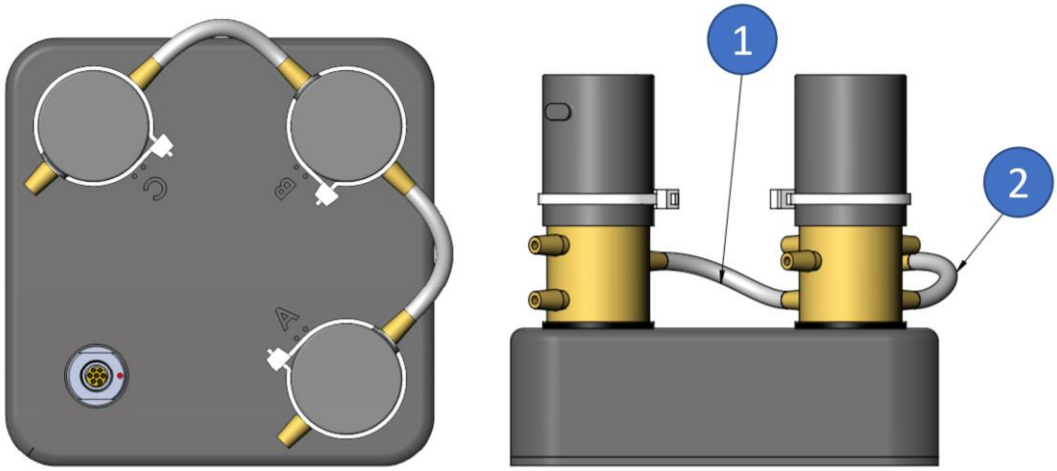

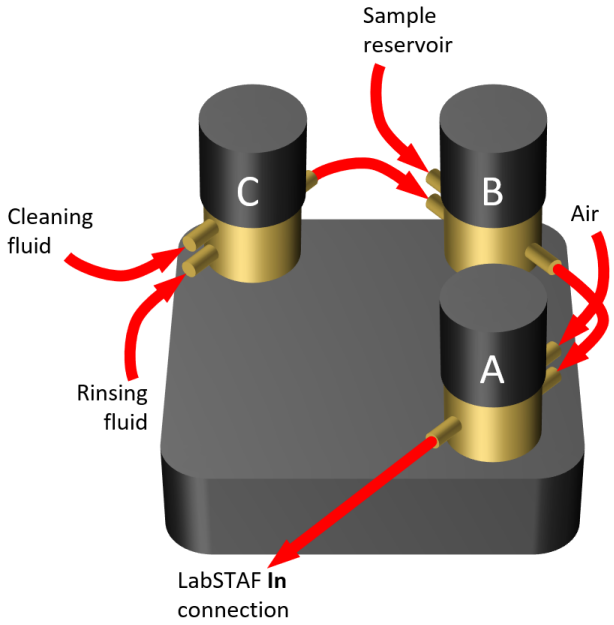

Figure 18.3: The images above show the solenoid unit as supplied from the factory. On the left, the unit is viewed from above to show the labelling of Solenoids **A**, **B** and **C**. On the right, the unit is oriented to show Solenoids A and C from the side. Tube **1** connects the common from Solenoid C to the Normally Closed (NC) on Solenoid B. Tube **2** connects the common from Solenoid B to the NC of Solenoid A. Both tubes are 60 mm lengths of 3 mm ID silicon.

The image left shows the inlets and outlets for the standard configuration, as detailed within the table below.

Solenoid connection	Connects to…
Solenoid A, COM	**In** connector on the LabSTAF flow through unit
Solenoid A, NO	No connection (air input)
Solenoid A, NC	Solenoid B, COM (sample exchange and/or cleaning)
Solenoid B, COM	Solenoid A, NC
Solenoid B, NO	Sample exchange reservoir
Solenoid B, NC	Solenoid C, COM (cleaning)
Solenoid C, COM	Solenoid B, NC
Solenoid C, NO	Cleaning fluid (first step of cleaning cycle)
Solenoid C, NC	Rinsing fluid (second step of cleaning cycle)

Table 18.1: Solenoid unit connections.

Figure 18.4: Image showing the LabSTAF peristaltic PUMP and Solenoid valve unit plumbed in with the Flow-through unit (2408-070-AS).

19 Using a SPAR sensor with LabSTAF and RunSTAF

At the time of writing, the calibration procedure for the Spectral PAR (SPAR) sensor is under development. This section has been added ahead of commercial release of the SPAR sensor because RunSTAF already incorporates a functional interface and the performance of the sensor has been verified.

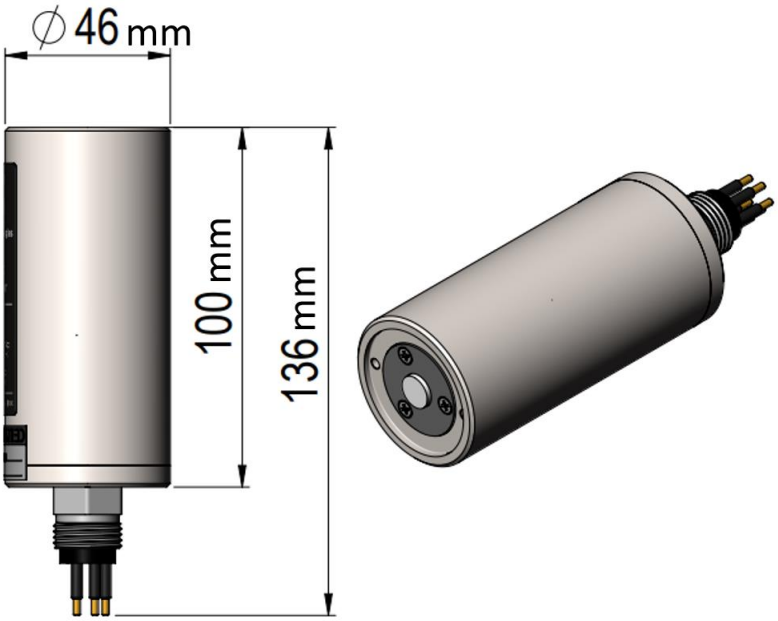

Figure 19.1: Dimensions of the Spectral PAR (SPAR) sensor. The six pin connector incorporates bi-directional RS232 and 5 V DC input.
CTL part number: 2408-250-PL

The SPAR sensor must be connected to a Surface Go or other PC running Windows 10 or 11 through a COM port. The COM port settings for data input from the SPAR sensor are as shown below. These values are automatically set by RunSTAF.

Baud rate:	115200
Byte size:	8
Parity:	NONE
Stop bits:	1
Flow control:	NONE

RunSTAF will only search for a connected SPAR sensor if the following selection is made from the menu:

Settings → Look for a SPAR sensor

Each SPAR sensor is supplied with a calibration file, which must be installed at the correct location:

C:\Users\...\Documents\CT-RunSTAF\SPAR\Calibration files

The filename is the serial number of the SPAR sensor, without dashes. The file extension is **spc**. For example, a SPAR sensor with serial number 22-1234-001 would require the following file:

221234001.spc

If the calibration file is missing, RunSTAF will show a LabSTAF message in the top left of the screen with this format:

Missing SPAR calibration file: 201234001.spc

The SPAR sensor will still work without the calibration file being installed. The default calibration values will provide indicative spectra. The primary data values from the SPAR sensor are always stored, to allow for reprocessing with the correct calibration values. When SPAR sensor values are used within the spectral correction of STAF data, the spectrally corrected STAF values are always

generated in real time. Consequently, updated STAF calibration values are automatically applied to dependent STAF values.

Although the SPAR sensor has primarily been developed to allow for real time spectral correction of STAF data, SPAR data can be acquired through RunSTAF without a LabSTAF being attached. With or without a LabSTAF attached, the SPAR sensor output and controls can be reached by selecting:

Settings → View SPAR sensor screen

from the menu bar. Figure 19.2 shows a crop from the SPAR sensor screen before a SPAR sensor has been attached and with all default values set for operation and calibration.

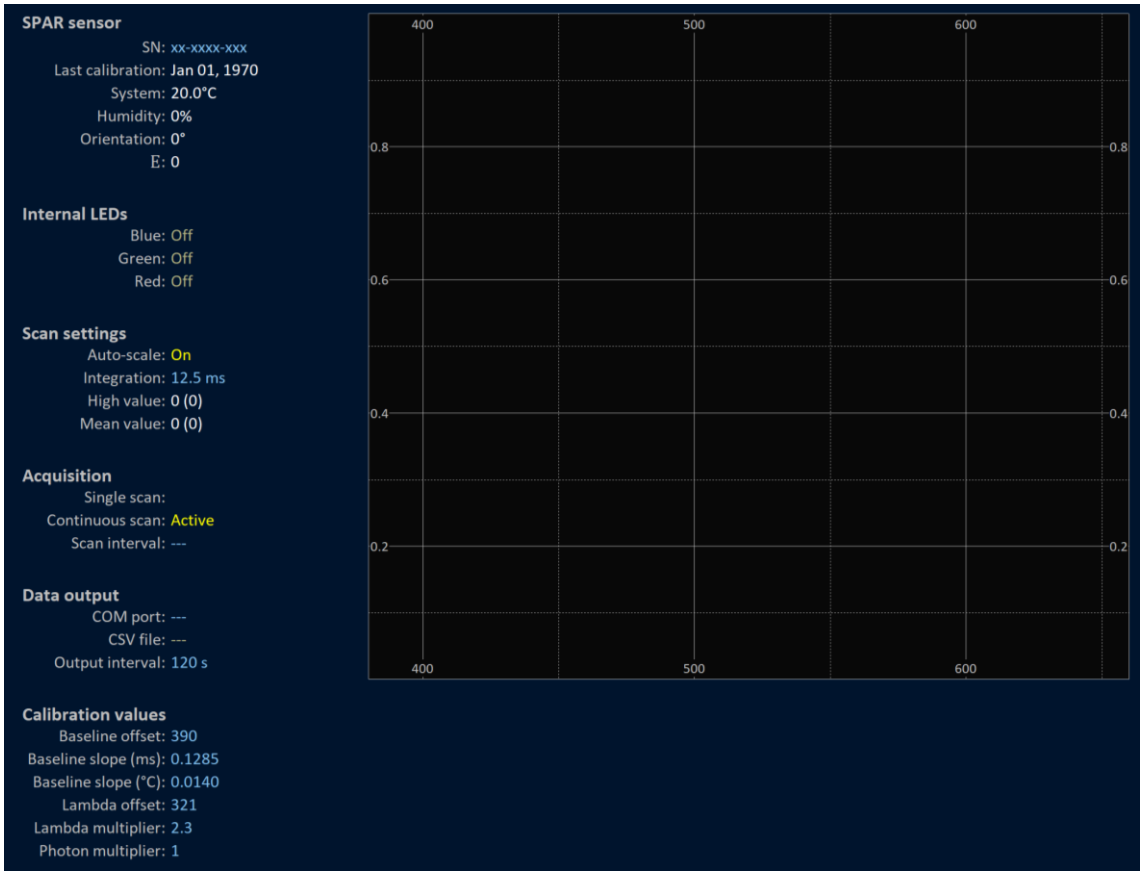

Figure 19.2: Screen crop from the SPAR sensor screen before a SPAR sensor has been connected. The COM port under data output is for data streaming from RunSTAF. The COM port the SPAR sensor is connected to is automatically located and set by RunSTAF.

Figure 19.3 shows the SPAR sensor screen while acquisition is running.

Under **SPAR sensor**:

- The system temperature is updated with every scan and is used to apply a temperature correction
- The Orientation is measured immediately before each scan
- The value of E has reported units of µmol photons m^{-2} s^{-1} and is derived from the scan range 380 to 660 nm, to match with the PEP and SCS data

The **Internal LEDs** provide an in-field calibration check

Under **Scan settings**:

- **Auto-scale** optimises the integration time, when active
- **Integration** shows the current integration time

- **High value** shows the highest value within the scan after baseline subtraction and before baseline subtraction in brackets
- **Mean value** shows the mean for the range of values plotted (380 to 660 nm) with and without baseline subtraction (without in brackets)

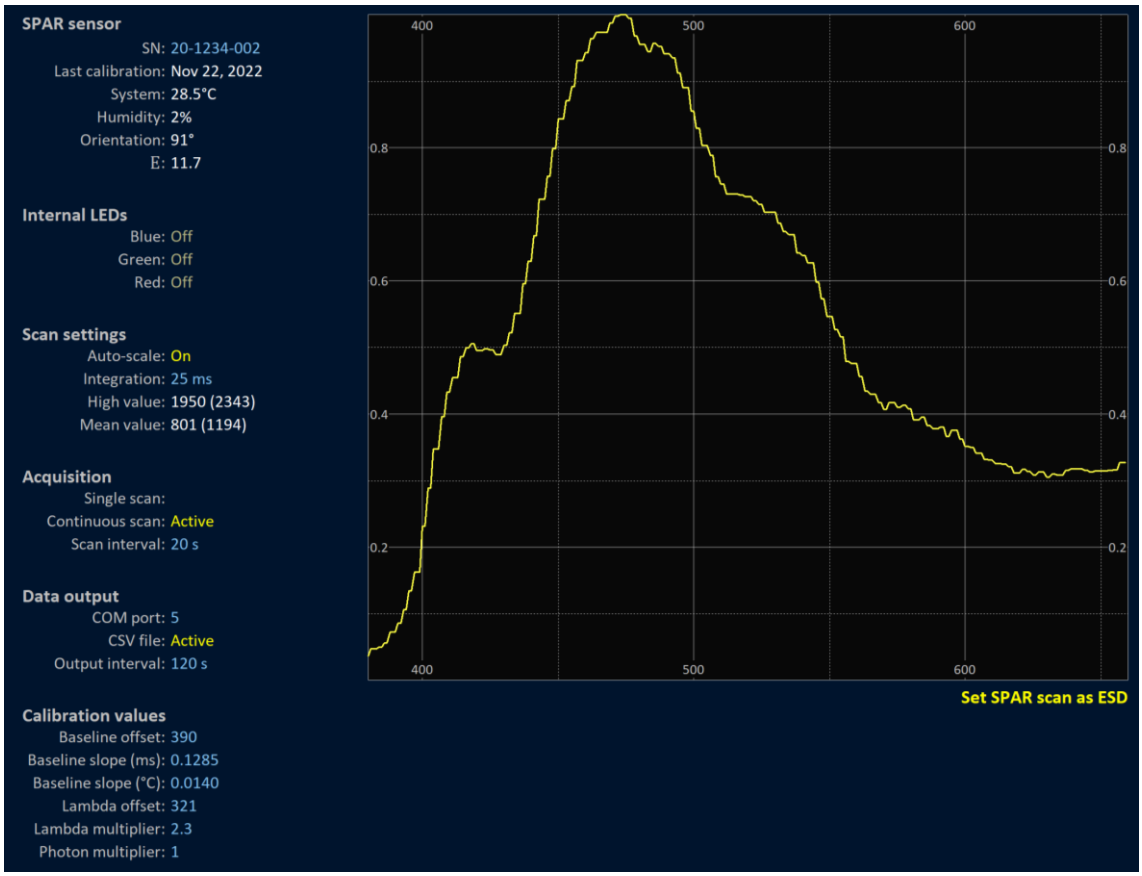

Figure 19.3: Screen crop from the SPAR sensor screen while acquisition is running. The **COM port** has been set to **5** and the **CSV file** output is **Active**, with a scan archived every **120 s**.

Under **Acquisition**:
If **Continuous scan** is deactivated, a single scan can be triggered at any point (Figure 19.4).

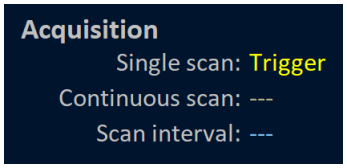

Figure 19.4: Screen crop of the **Acquisition** section of the SPAR sensor screen with **Continuous scan** deactivated.

If **Continuous scan** is active and **Scan interval** is not set, the scan will run at maximum frequency (around 0.5 to 1 Hz). The **Scan interval** can be used to slow the scan rate down by setting the required scan interval in seconds (Figure 19.5).

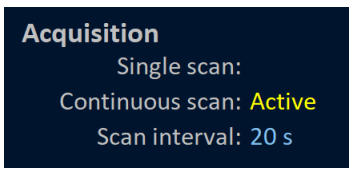

Figure 19.5: Screen crop of the **Acquisition** section of the SPAR sensor screen with **Continuous scan** deactivated.

Under **Data output** (Figure 19.3):

- COM port sets the COM port number for data streaming
- CSV file Activates the logging of data to a local file in CSV format

- The time set in Output interval applies to both the COM port and CSV file output
  See: **SPAR sensor COM and CSV file output**

Under **Calibration values**:

All values are included within this section are retrieved from the SPAR sensor calibration file if present. If the file is absent, the default values are used.

19.1 The integrated LEDs

The three LEDs integrated within the SPAR sensor allow for a check of the spectral calibration (Lambda offset and Lambda multiplier). Figure 19.3 shows output from each of the three LEDs recorded with the SPAR sensor face down over a sheet of white paper. The red line shows the selected lambda value (460 nm, 510 nm and 628 nm).

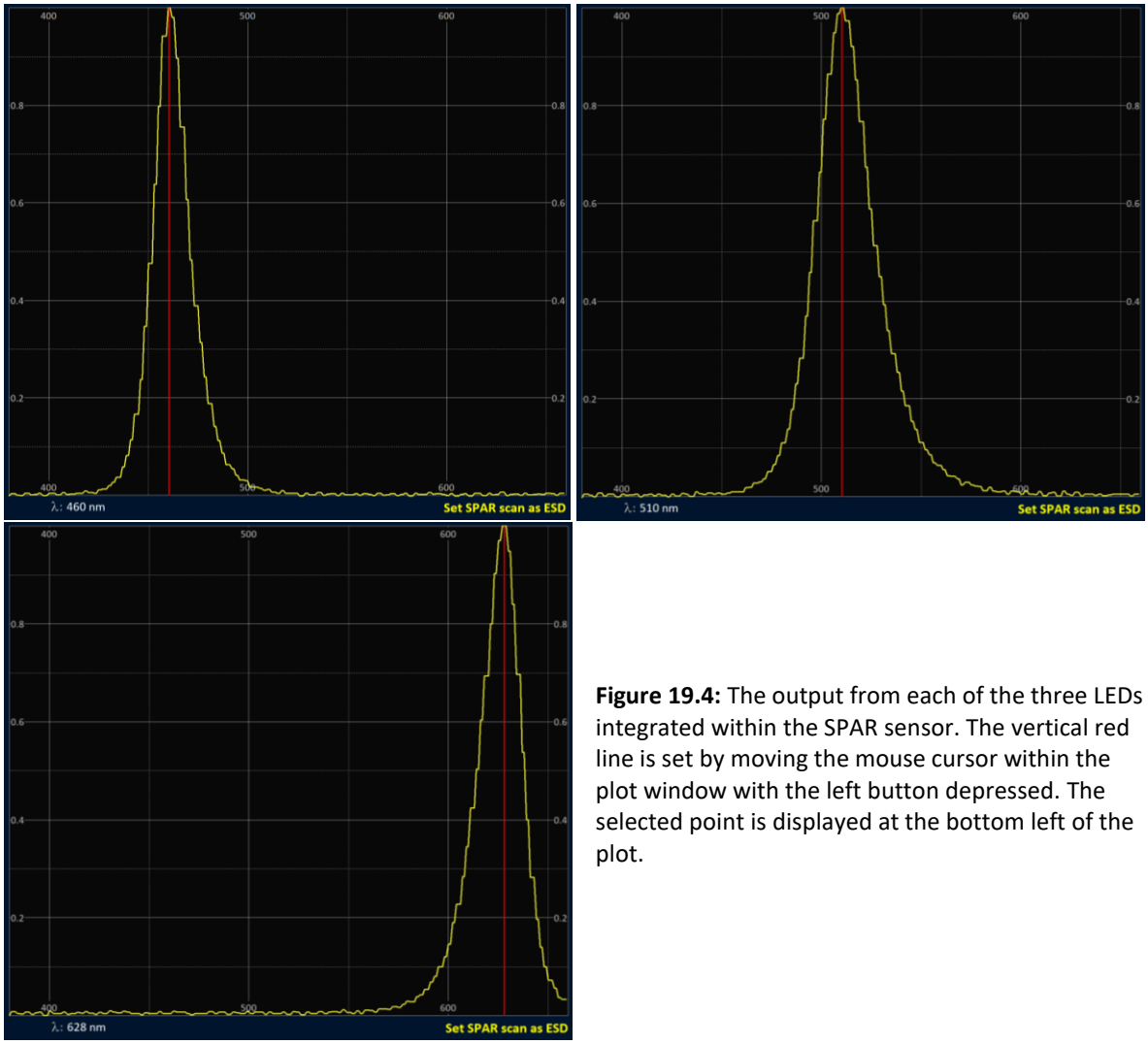

Figure 19.4: The output from each of the three LEDs integrated within the SPAR sensor. The vertical red line is set by moving the mouse cursor within the plot window with the left button depressed. The selected point is displayed at the bottom left of the plot.

19.2 Set SPAR scan as ESD

When the Auto FLC acquisition mode is set and a SPAR sensor is attached to RunSTAF, a SPAR sensor scan is automatically acquired at the start of the FLC and saved with the file. Pressing the **Set SPAR scan as ESD** button at the bottom right of the plot replaces this scan.
See: **Applying an ESD from a Spectral PAR (SPAR) sensor**

20 LabSTAF calibration

The calibration values used to process data are always saved within the RunSTAF file and are easily accessible. This approach maximises the options for reprocessing of primary data.

20.1 Calibration data stored within the LabSTAF unit

To view the calibration values, select…

Settings → Factory → View calibration data

From the menu bar. The screenshot crops within Figure 20.1 provide an example of the calibration values automatically loaded from an attached LabSTAF unit.

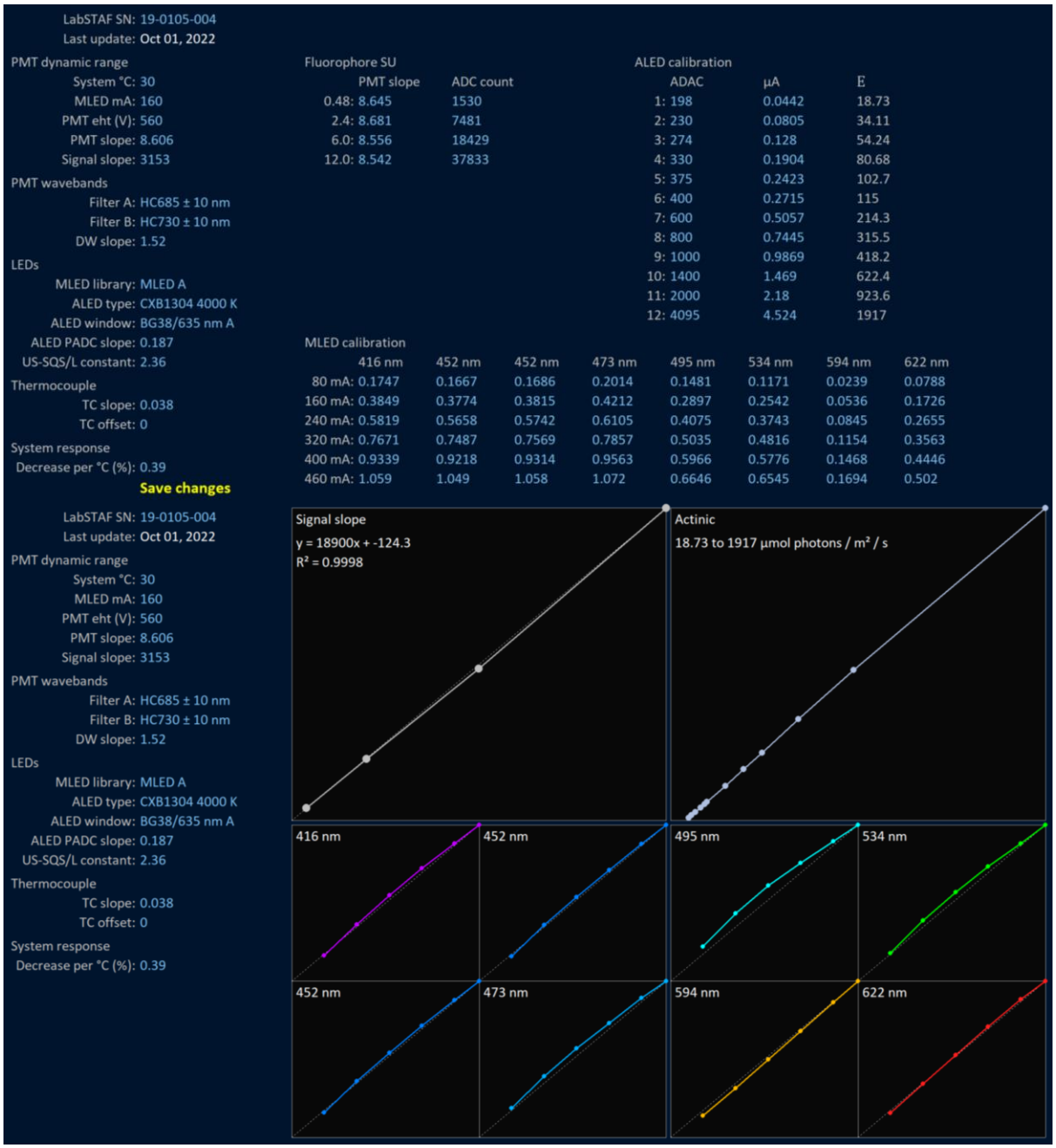

Figure 20.1: Screenshot crops from the RunSTAF calibration screen with a LabSTAF unit attached. The **Show plots** and **Hide plots** buttons (not shown here but located at bottom right of the full calibration screen) switch between the two screens. The **Save changes** button included within the upper screenshot is only shown after one or more values have been changed.

20.2 The spectral calibration spectra (scs) data file

In addition to the calibration data loaded from the attached LabSTAF, the spectral output of all seven MLED wavebands and the actinic LED within the LabSTAF unit are loaded from a spectral correction spectra (scs) file installed on the controlling computer. The scs filename is matched to a specific LabSTAF unit through the serial number without the dashes. For example, the LabSTAF unit attached in the above screenshots has the serial number 20-0325-001. The matching scs file is 200325001.scs. This file must be located within this folder:

Documents → CT-RunSTAF → Calibration files

The **Calibration files** folder is created by RunSTAF. The scs files for multiple LabSTAF units can be stored within this folder. RunSTAF will select the correct file based on the filename (matched to the serial number of the attached LabSTAF unit).

20.3 Creating a spectral calibration spectra (scs) data file

LabSTAF systems delivered from March 2022 onwards have the MLED spectral data supplied in text format. They are located at the following location:

Documents → CT-RunSTAF → Calibration files →Do not delete

Figure 20.2 shows the files included.

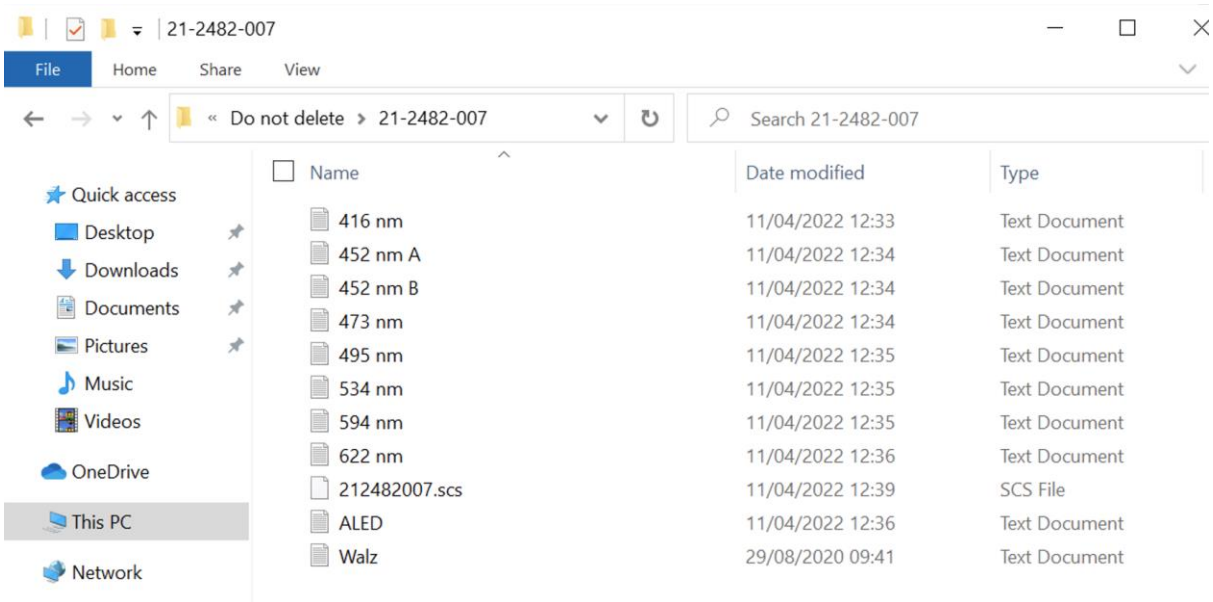

Figure 20.2: The text files providing MLED spectral data included on the Surface Go ex-factory (from March 2022). These files can be supplied for any existing LabSTAF system on request:

email: support@chelsea.co.uk

20.4 Create a local backup of the calibration data stored within LabSTAF

A local backup of the calibration data stored within an attached LabSTAF unit can be made by selecting…

Settings → Factory → Save calibration data

From the menu bar. This generates a file within this folder:

Documents → LabSTAF → Calibration files

The filename for the calibration backup is matched to a specific LabSTAF unit through the serial number without the dashes. The file extension is stc. For example, the LabSTAF unit attached in the above screenshots has the serial number 20-0325-001. The matching stc file is 200325001.stc. This

file can be used to overwrite any changes made to the calibration data. The file can be recovered by first selecting…

Settings → Factory → View calibration data

end then selecting…

Settings → Factory → Load calibration data

The **Save changes** button must be pressed to update the changes within the attached LabSTAF unit.

20.5 Post-processing with the Spectral Correction Spectra (SCS) data file

The SCS data are used to apply a spectral correction to RunSTAF data. This correction is required to generate values for a_{LHII}, J_{PII}, JV_{PII} and GO_{PII}. If the SCS file is absent during data acquisition, values for these parameters will not be generated in real time. However, it is possible to post-process the data to apply the spectral correction and generate values for J_{PII}, JV_{PII} and GO_{PII}.

To apply post-processing, the required SCS file must be copied to the **Calibration files** folder. Now, when RunSTAF data files are opened, the SCS file will be used to automatically apply spectral correction and generate values for a_{LHII}, J_{PII}, JV_{PII} and GO_{PII}. When the updated data file is saved, the SCS data are incorporated within it. This means it can be opened on another computer without the SCS data file being present.

20.6 On-site calibration of sample chamber temperature

The temperature within the sample chamber is monitored by an internal thermocouple. If there is a large difference between the ambient temperature and the temperature within the sample chamber, the reported value may be significantly higher than the actual sample chamber temperature. The steps below can be used to generate a more accurate value.

In most cases, a single point calibration can be run to generate a new TC slope. To activate the calibration mode, start RunSTAF and select…

Settings → Acquisition mode → Manual

…from the menu bar. Then select…

Settings → Factory → Manual calibration modes → Sample TC

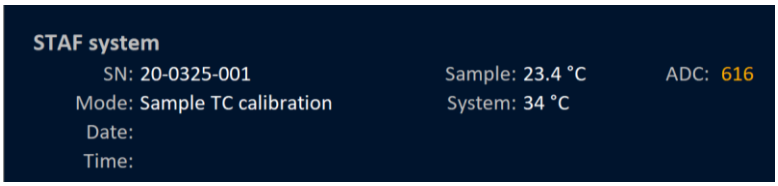

This will activate an ADC field next to the Sample temperature, as shown here.

The formula for using the ADC value to set the reported temperature is provided by Equation 20.1.

Sample °C = ADC x TC slope + TC offset Equation 20.1

In this example, the actual temperature within the sample chamber was 22.6 °C. The reported temperature (**Sample**) is **23.4 °C** and the reported **ADC** value is **616**.

To change the calibration values for the sample thermocouple, select…

Settings → Factory → View calibration data

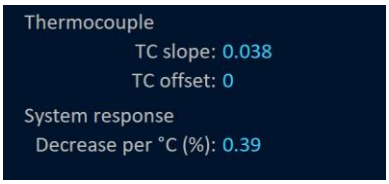

The current **TC slope TC offset** is **0.038**. Dividing the actual temperature by the reported ADC value of **616** gives a new TC slope of **0.0367**.

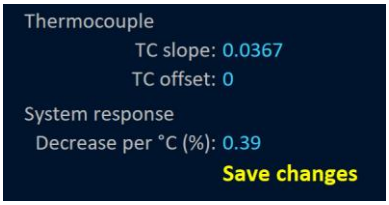

Changing the **TC slope** value activates the **Save changes** button. Pressing this button saves the changes to the attached LabSTAF unit.

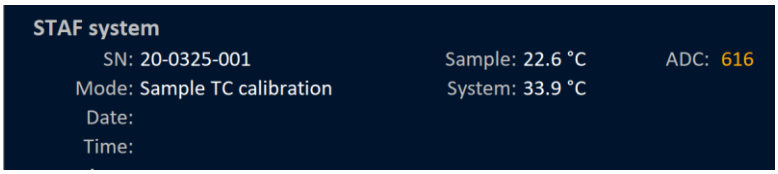

The reported value is now correct.

20.7 Updating calibration values across existing data files

This function has been incorporated within RunSTAF to allow for the updating of calibration data across data files when one or more incorrect values have been found. Although the most likely mismatch is the TC slope used to define the recorded sample temperature, all calibration values are assessed for changes and any required re-calculation of data is applied.

The function can be accessed through…

Settings → Factory → Update across files

21 Technical information and RunSTAF installation

21.1 Technical features

21.1.1 The Measurement LEDs (MLEDs) and PMT

The MLEDs are used to provide the ST pulses. There are eight channels with five LEDs in each, distributed between two four channel arrays (MLED1 and MLED2). Each array is connected to a four channel drive circuit which allows the drive current to be set independently for each channel.

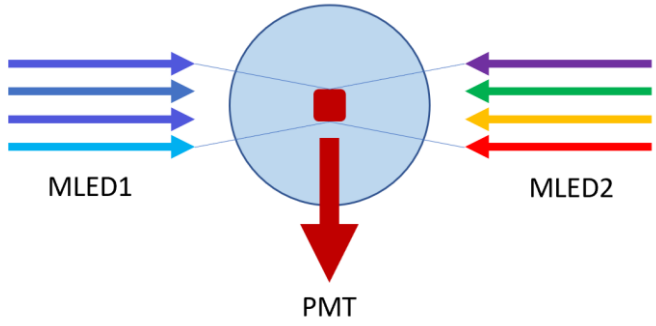

Figure 21.1: Two-stage MLED optics provide homogeneous illumination throughout an interrogated volume of approximately 0.5 mL.

The collimated MLED light from each array is passed through a shortpass filter before being directed through the interrogated volume. The fluorescence emission from the interrogated volume is Lambertian (uniformly spherically radiative). The first stage of the MLED and PMT optics collects a proportion of the emitted photons which are collimated through a bandpass filter (685 nm or 730 nm) and 630 nm longpass filter. The filtered emission is then focussed onto the active area of the PMT.

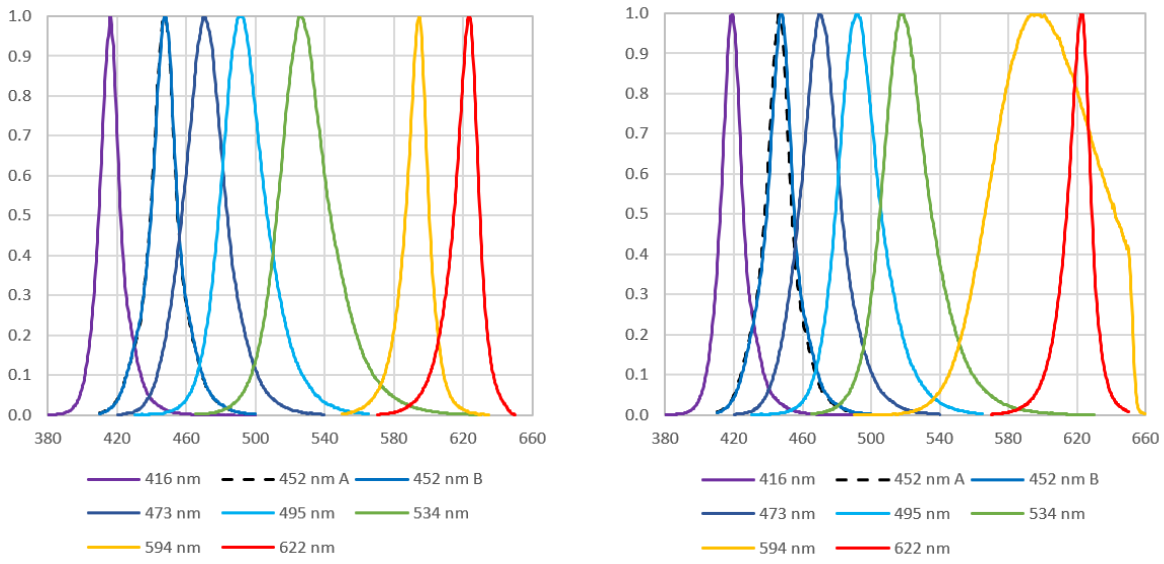

Figure 21.2: Emission spectra recorded from inside the LabSTAF sample chamber. The left plot is from a LabSTAF unit fitted with the MLED A configuration and the right plot is from a LabSTAF unit fitted with MLED B configuration. The only difference between the two is the 594 nm channel, which is very narrow in the MLED A configuration and much wider in the MLED B configuration. The sharp drop in output for the 594 nm channel within the MLED B configuration is due to the 650 nm shortpass filter located in front of the MLED2 array. The shortpass filter in front of the MLED1 array is a 635 nm shortpass.

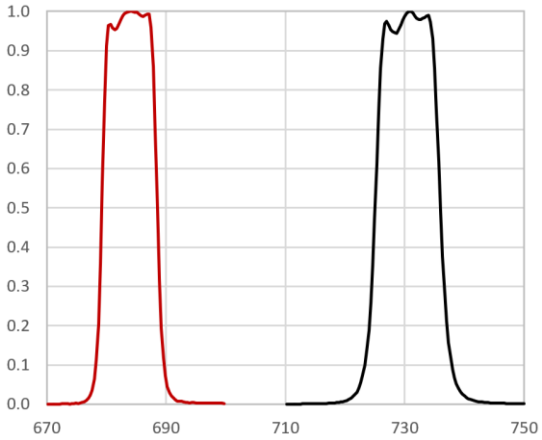

Figure 21.3: Transmission spectra for the 685 nm and 730 nm bandpass filters in front of the PMT. Both filters are ± 10 nm Full Width-Half Max FWHM.

21.1.2 The actinic light source (ALED)

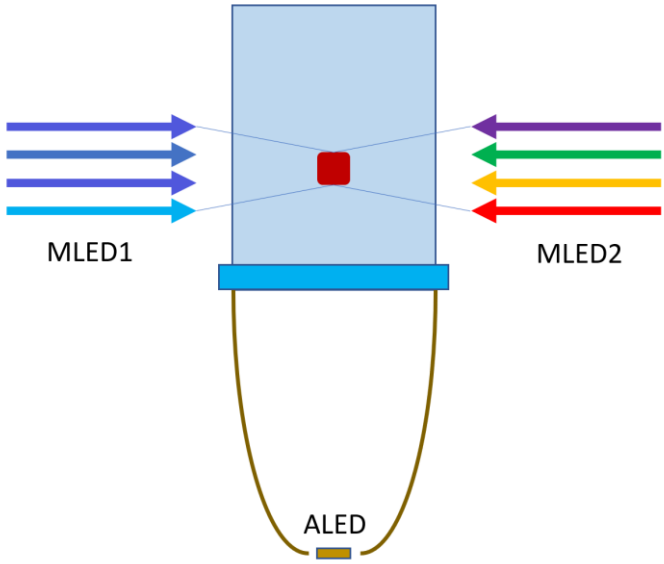

Figure 21.4: Actinic light is delivered to the entire sample from a single Actinic LED (ALED) via a collimating Compound Parabolic Collector (CPC). The base of the sample chamber is a 3 mm BG38 glass filter, sandwiched between two 0.5 mm layers of BK7 glass. A multi-layer coating on the BK7 surface facing the ALED provides a 635 nm shortpass filter.

The output range of 10 to >1600 µmol photons m^{-2} s^{-1} is provided by a single LED using a 12-bit constant current DC drive circuit. At very low current, where output is temperature sensitive, a photodiode integrated within the CPC monitors the actual output and adjusts the drive current to get as close as possible to the requested value.

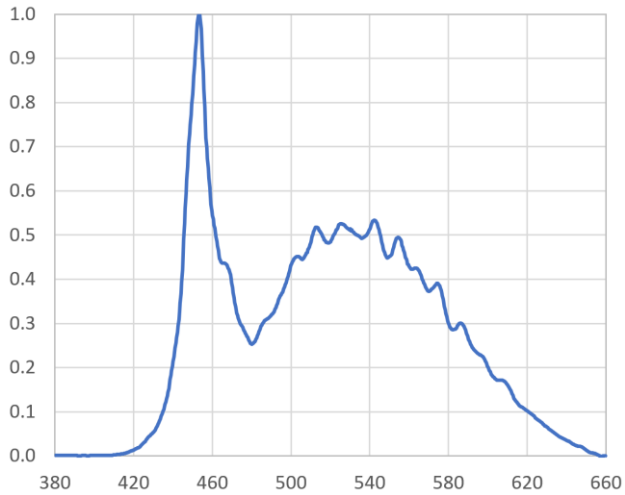

Figure 21.5: The emission spectrum from a LabSTAF ALED recorded from inside the LabSTAF chamber.

21.1.3 PMT temperature coefficient

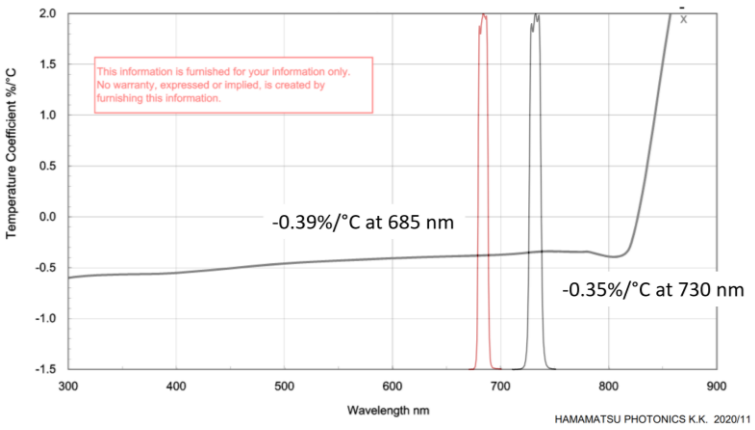

Figure 21.6: Continuous recording of the system temperature allows RunSTAF to apply an appropriate correction to the PMT output. The temperature coefficient applied is the 685 nm value from data provided by Hamamatsu.

21.1.4 Sample temperature control

The sample chamber thermal block is insulated from the main internal volume. However, this thermal block has a much better thermal connection to the internal optics than the internal electronics. Consequently, running the sample at very low temperature can result in the internal optics being cooled to the point where there is a significant temperature differential between the optics and the internal electronics. A humidity sensor has been incorporated within the main internal volume (the space occupied by the internal electronics) to check for the possibility of condensation forming on the optics. Table 21.1 provides a guide to the dew point on a mirror surface at different **System RH** values when the **System** temperature (inside the unit) is 32 °C.

Relative Humidity (RH) at 32 °C	Dew point
10%	-3.4 °C
12%	-1.0 °C
14%	1.1 °C
18%	4.7 °C
24%	8.9 °C
30%	12.2 °C
36%	15.0 °C
42%	17.5 °C

Table 21.1: Dew point values at different **System RH** values when the **System** temperature is 32 °C.

21.1.5 Summary of hardware specifications

Basic specifications of the LabSTAF unit	
Power requirements	Between 140 and 400 mA (3.4 and 9.7 W) at 24 V
Dimensions (w x d x h)	429 x 328 x 236 mm
Mass (approximate)	8.1 kg
Sample chamber	20 mL maximum sample volume
Excitation wavebands	Central wavelengths at: 416, 452 x 2, 473, 495, 534, 594, 622 nm
Actinic light source	Collimated output from 10 to >1600 µmol photons m^{-2} s^{-1}
Detection limit (approximate)	Can resolve F_v with an amplitude equivalent to the fluorescence signal generated under 452 nm excitation by 0.001 mg m^{-3} of chlorophyll
IP rating	IP64 (protected from water spray from any direction)

Table 21.2: Basic specification of LabSTAF unit (2408-040-AS).

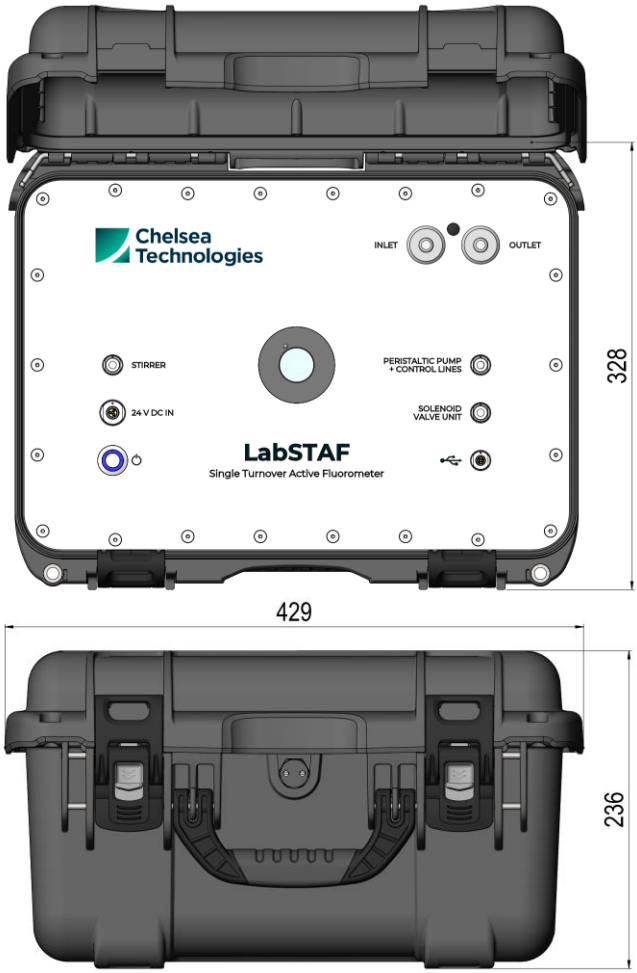

Figure 21.7: Dimensions of the LabSTAF unit with lid installed.

Basic specifications of the LabSTAF Power Pack	
Power requirements	Mains (110 to 220 V AC)
Dimensions (w x d x h)	259 x 201 x 114 mm
Mass (approximate)	?? kg
IP rating when closed	IP64 (protected from water spray from any direction)
IP rating when in use	IP40 (protected against entry by tools but not protected against moisture)

Table 21.2: Basic specification of the LabSTAF Power Pack (2408-040-AS).

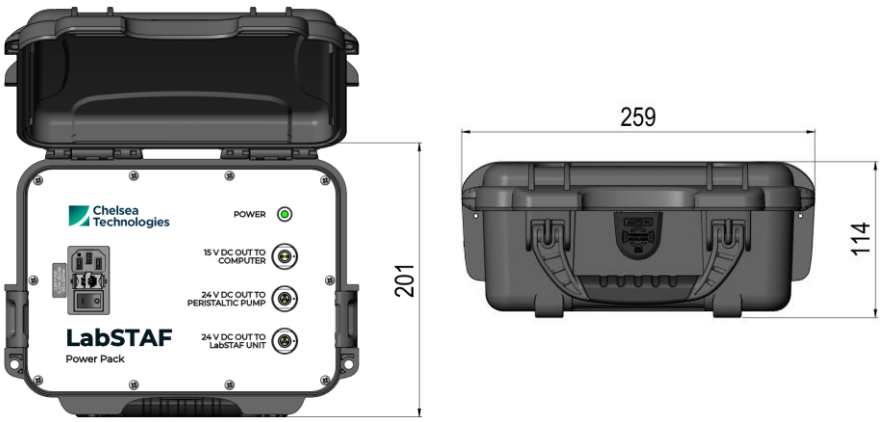

Figure 21.8: Dimensions of the LabSTAF Power Pack.

Basic specifications of the LabSTAF Spares Case	
Dimensions (w x d x h)	424 x 340 x 173 mm
Mass (approximate)	?? kg
IP rating when closed	IP64 (protected from water spray from any direction)

Table 21.2: Basic specification of the LabSTAF Spares Case (2408-179-AS).

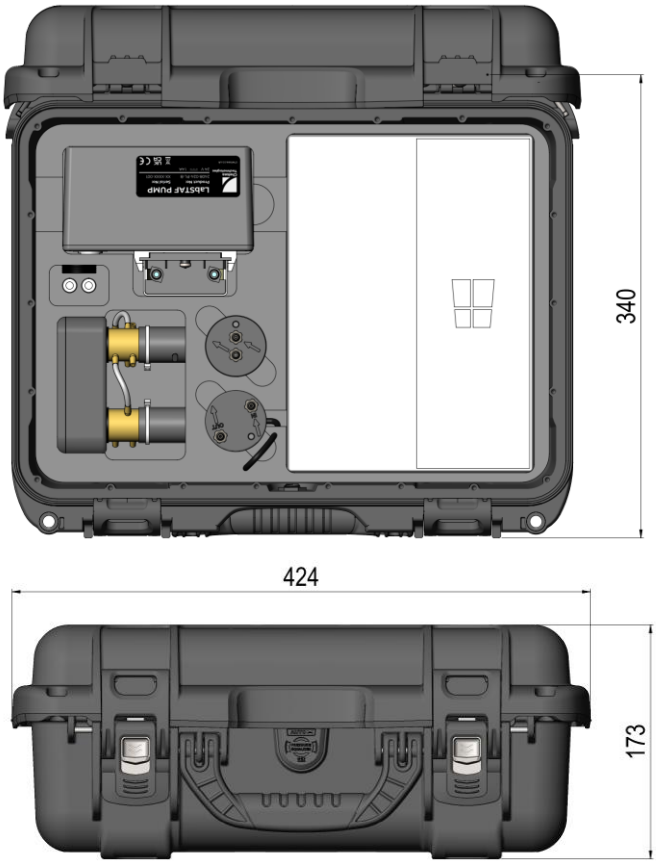

Figure 21.8: Dimensions of the LabSTAF Spares Case.

21.2 RunSTAF software

The Surface Go computer supplied as part of the LabSTAF system provides a reference platform for RunSTAF. Most Surface Go computers supplied will run Windows 11. At the time of writing, updates to RunSTAF are tested on the original Surface Go computers running Windows 10 and on version 2 and version 3 Surface Go computers running Windows 11. It is important to keep whichever version of Windows you are using up-to-date. RunSTAF is not demanding, in terms of computer hardware, and can be installed on most machines running Windows 10 or 11. The computer used to run the LabSTAF system should be set up specifically for this purpose. If you allow your IT department to impose limitations on the way the computer can be used, you are likely to run into problems – particularly with continuous acquisition over extended periods.

21.3 Updating an existing RunSTAF installation

This section provides instructions for updating RunSTAF under Windows 10. Updating under Windows 11 is very similar.

21.3.1 Access the most recent version of RunSTAF

To access the most recent version of RunSTAF, use this link…

https://1drv.ms/u/s!AkUtV8PHZSmVvJ9wFOm-fSR1FbwYGQ?e=w7SYaX

This provides access to the three folders shown here:

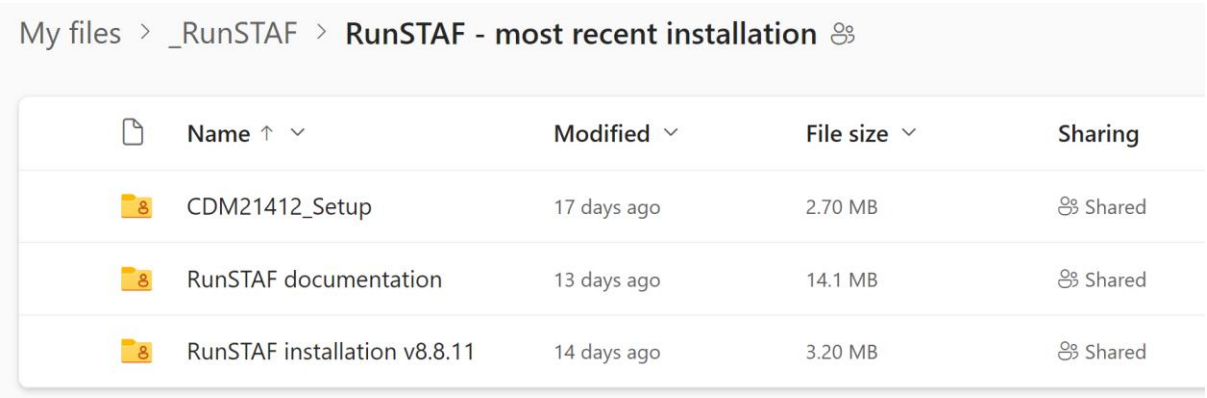

The **CDM21412_Setup** folder contains a single file which is also named **CDM21412_Setup**. This is an application file that will install essential drivers. This file is not required when updating RunSTAF as the required drivers will already be installed.

The **RunSTAF documentation** folder includes the most up-to-date version of this handbook plus other relevant documentation.

The **RunSTAF installation v8.8.11** folder includes two files named **RunSTAF setup** and **setup**. The first step is to compare the version number of this installation with the existing installation. To do this select **Help → About RunSTAF** from the RunSTAF menu bar.

In this example, the **About RunSTAF** dialog shows that the current installation is v6.9.0. Consequently, the update (v8.8.11) should be downloaded and installed following the instructions below.

21.3.2 Uninstall the existing RunSTAF

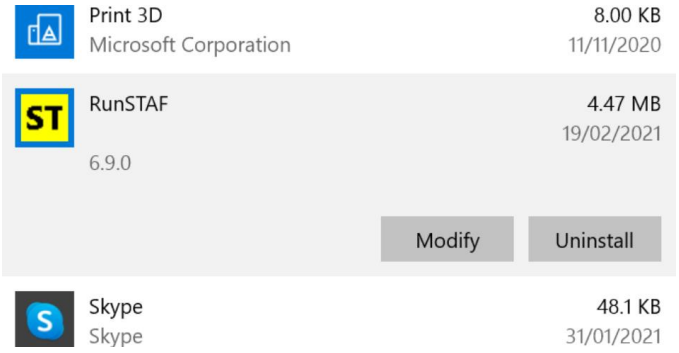

Go to **Add or remove programs** within Windows **System settings**. Under Apps & features, find the **RunSTAF** tab and select **Uninstall**.

Accept all the default options to complete the uninstall.

21.3.3 Install the new version of RunSTAF

Double click the **RunSTAF setup** Windows Installer Package.

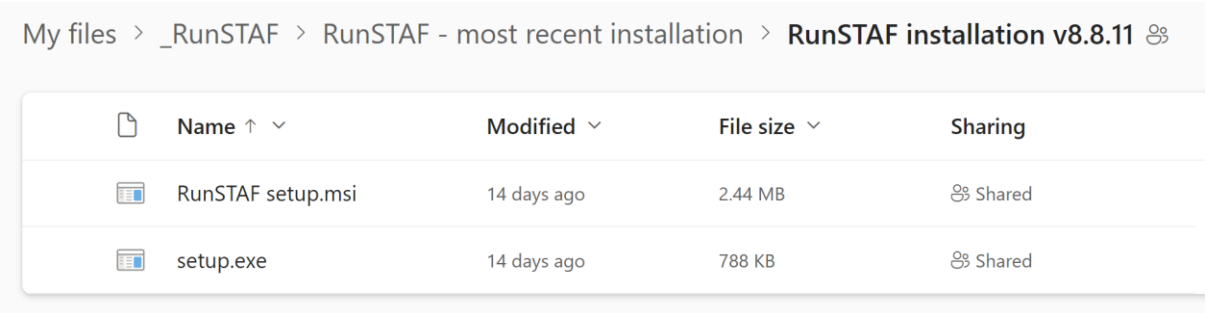

Accept all the default options to complete the installation.

21.4 Setting up a new computer for RunSTAF

The instructions below are slightly modified from the factory setup instructions for a new Surface Go computer running Windows 11.

21.4.1 First bootup

A Surface Go running Windows 11 is supplied with all LabSTAF systems. This provides the reference system for potential troubleshooting.

- The following setup steps are required during the first stage of the setup process for a new computer:

Language:	English (United Kingdom)
Country or region:	United Kingdom
Keyboard:	United Kingdom
Second keyboard:	Skip
Connect to a network:	As available

English (United Kingdom) and **United Kingdom** are used as the options to make them 100% compatible with the Surface Go keyboard supplied with the system and the RunSTAF software and handbook examples.

Run through all updates and make the following choices, where appropriate…

- Accept the **License agreement**
- **Skip** the **Device name** for now
- **Set up for personal use**

When you get to the Let's add your Microsoft account, select:

- **Sign in options**
- **Offline account**

At **What is a Microsoft account**, select:

- **Skip for now**

At **Who's going to use the device**, enter:

- **RunSTAF**

Leave the **Enter a password** field empty and press:

- **Next**

Let Microsoft and apps use your location:

- **No**

Find my device:

- **No**

Send diagnostic data to Microsoft:

- **Required only**

Improve inking and typing:

- **No**

Get tailored experiences with diagnostic data:

- **No**

Let apps use advertising ID:

- **No**

You have now reached the Checking for updates section. This can take more than a day to complete, in several stages. As you work through this process, accept all licensing agreements but reject all options that collect personal data.

21.4.2 Tidy the desktop

- Delete all icons from the desktop apart from the **Recycle Bin**

21.4.3 Change the background

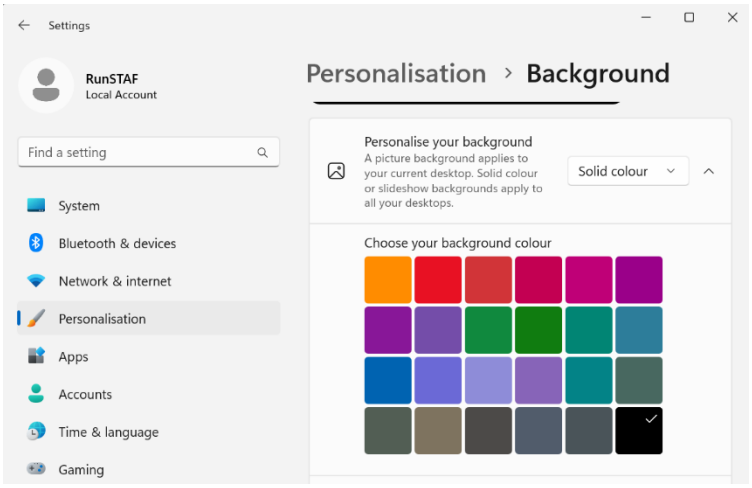

- Right click anywhere on the desktop and select **Personalize**
- Change the background setting from **Picture** to **Solid Colour**
- Keep the default of **Black**

21.4.4 Turn off sounds

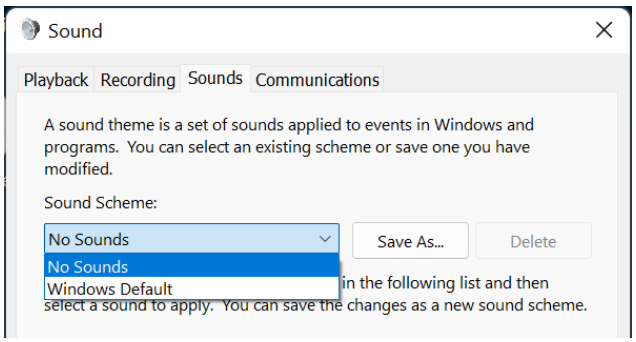

- Go to: **Control panel → Hardware and Sound → Sound → Change system sounds**
- switch to **No Sounds**…

21.4.5 Turn off notifications

- Go to: **System → Notifications**
- Turn off the overall **Notifications** option at the top of the window

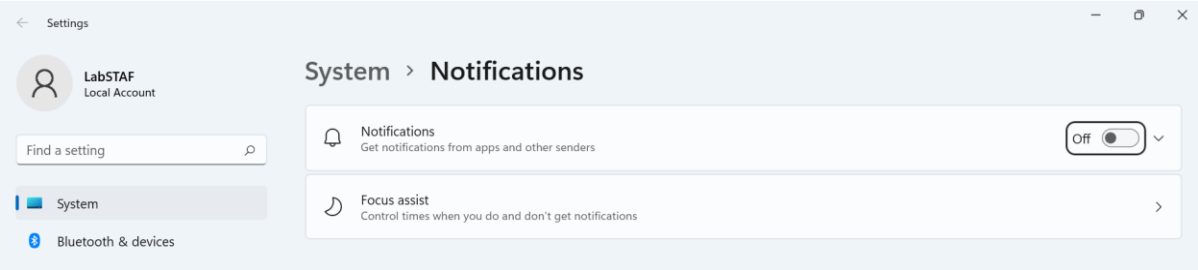

- Scroll down to the bottom of the window
- Deselect the three options there

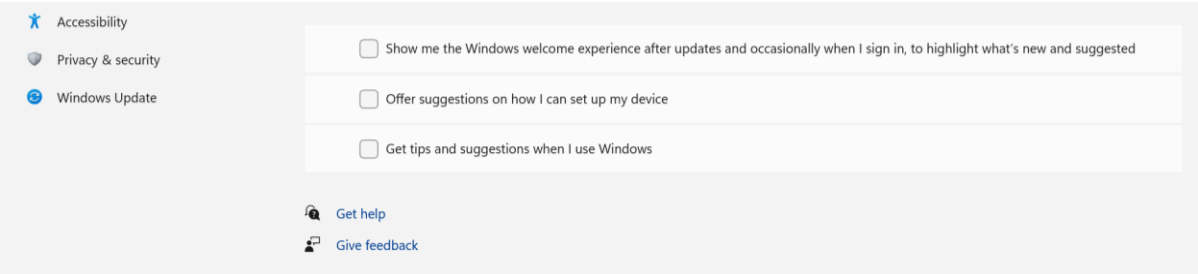

21.4.6 Turn off Teams and OneDrive as Startup Apps

- Go to: **Settings → Apps → Startup**
- Uncheck **Microsoft OneDrive**, **Microsoft Teams**, **Phone Link** and **Skype**

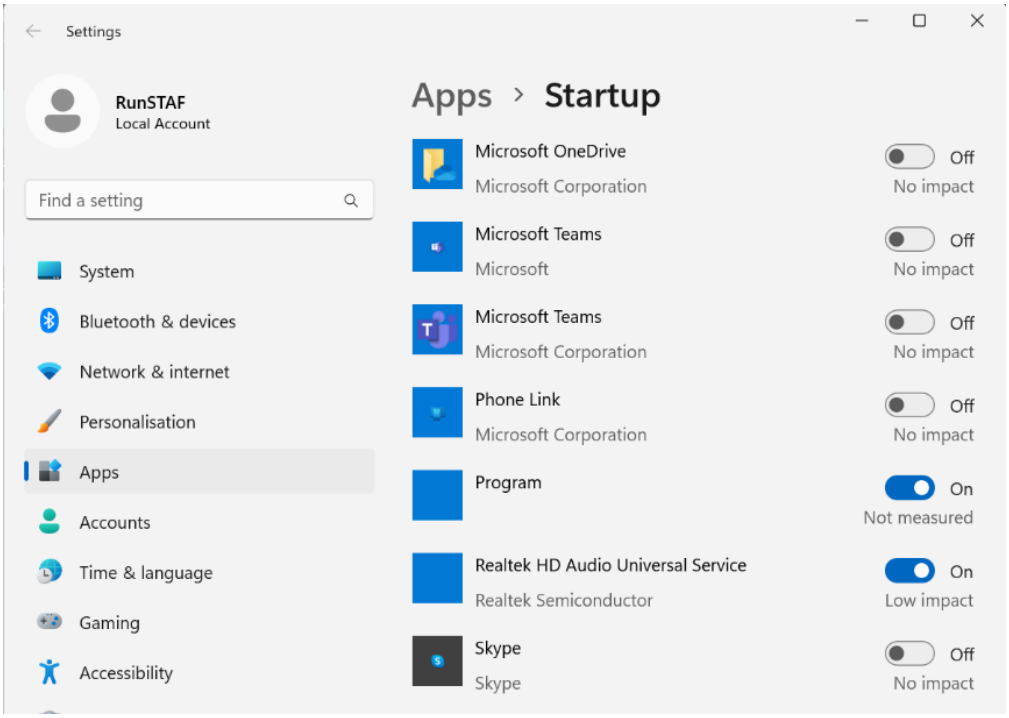

21.4.7 Power settings

- Go to: **System → Power & battery**
- Set the values shown below…

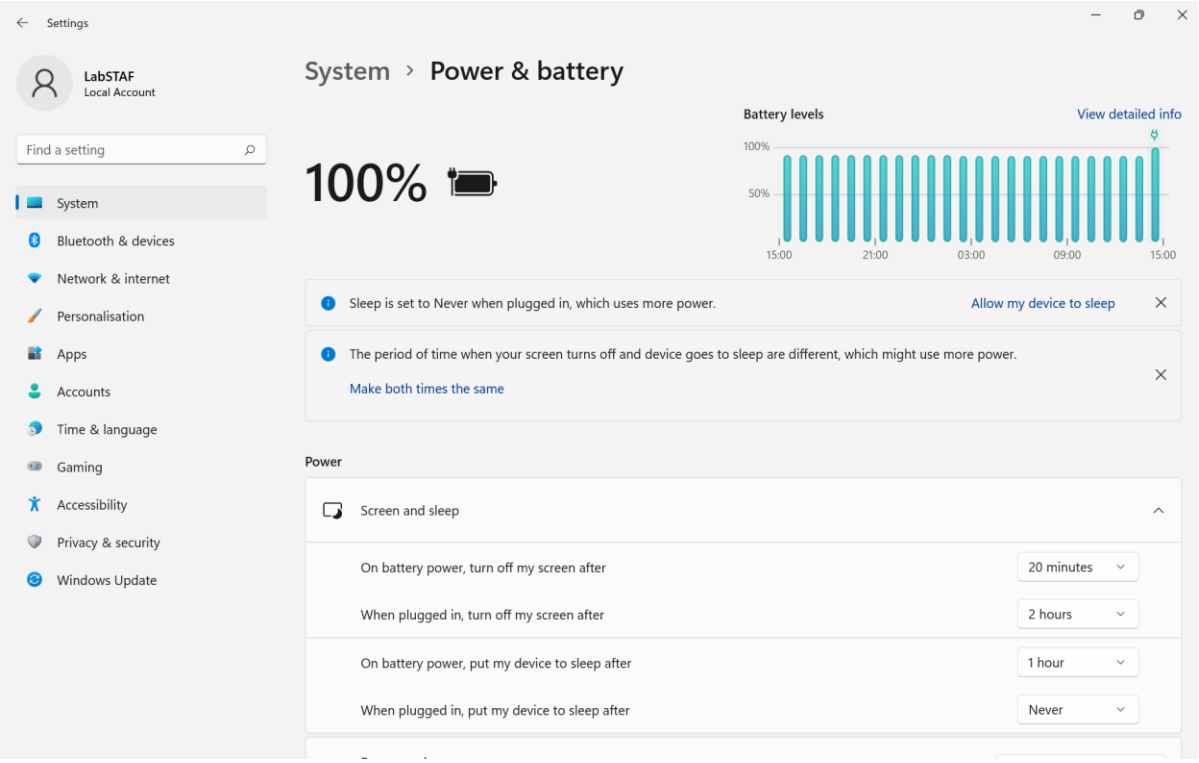

21.4.8 Install RunSTAF and optimise Windows

Use the link below to access the most recent release of RunSTAF and the handbook. At the time of writing, the handbook is the only document within the **RunSTAF documentation** folder.

https://1drv.ms/u/s!AkUtV8PHZSmVvJ9wFOm-fSR1FbwYGQ?e=w7SYaX

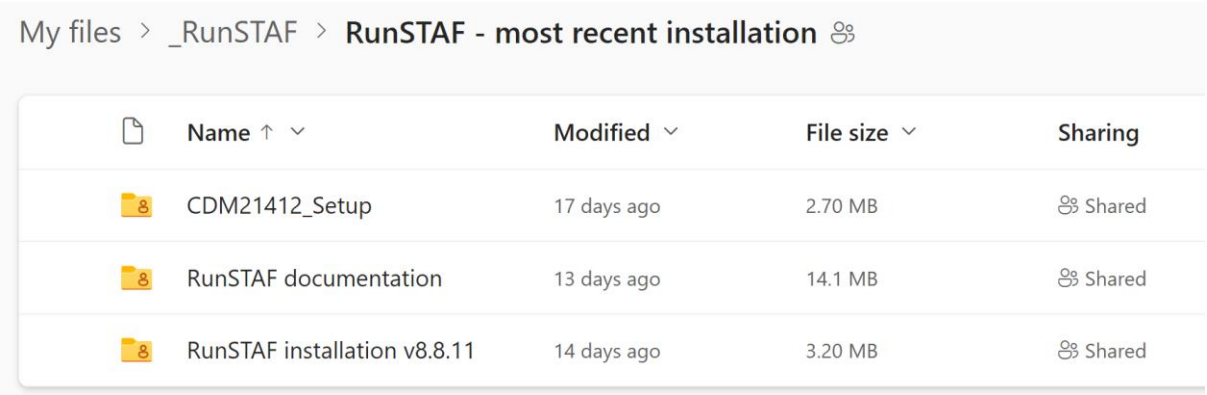

- Copy the **RunSTAF installation v8.8.11** folder (the version number will change regularly) and the handbook to a USB drive
- Open the folder on the USB drive and double click on either file to run the installation

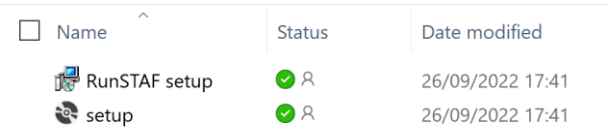

- Accept all the default options during the installation process
- Copy the handbook to the desktop
- Ensure that the handbook is named as **LabSTAF and RunSTAF handbook**

21.4.9 Set RunSTAF as a start-up program

- Go to start menu and type: **Run**
- Type **shell:common startup** and press **OK**
- Drag the **RunSTAF** icon from the desktop into the **Start-up** sub-folder

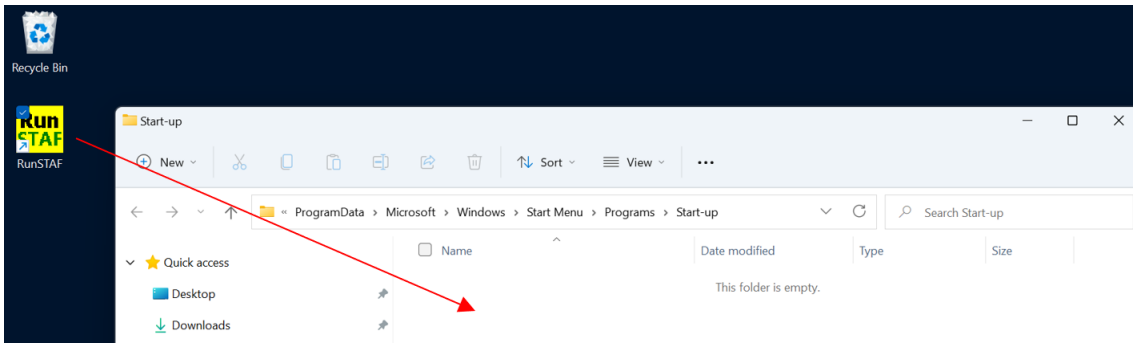

- Press **Continue** when prompted

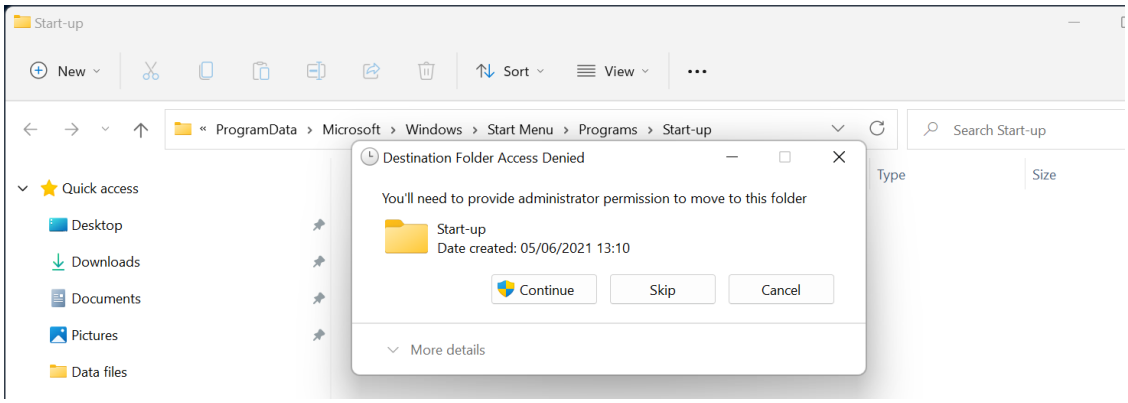

- Start RunSTAF
- Right click on the icon in the taskbar and select **Pin to taskbar**

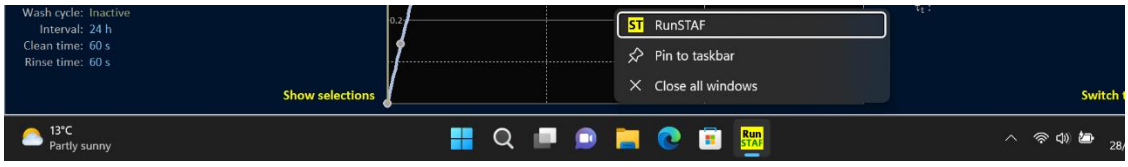

21.4.10 Block serial mouse detection on Startup

- Go to Windows Start Menu and type regedit
- Navigate to: **HKEY_LOCAL_MACHINE\SYSTEM\CurrentControlSet\Services\sermouse**
- Double click on the Start tag and change the **Value data** field from **3** to **4**
- Hit the **OK** button and close the **Registry Editor**

Exit Registry Editor and restart the computer

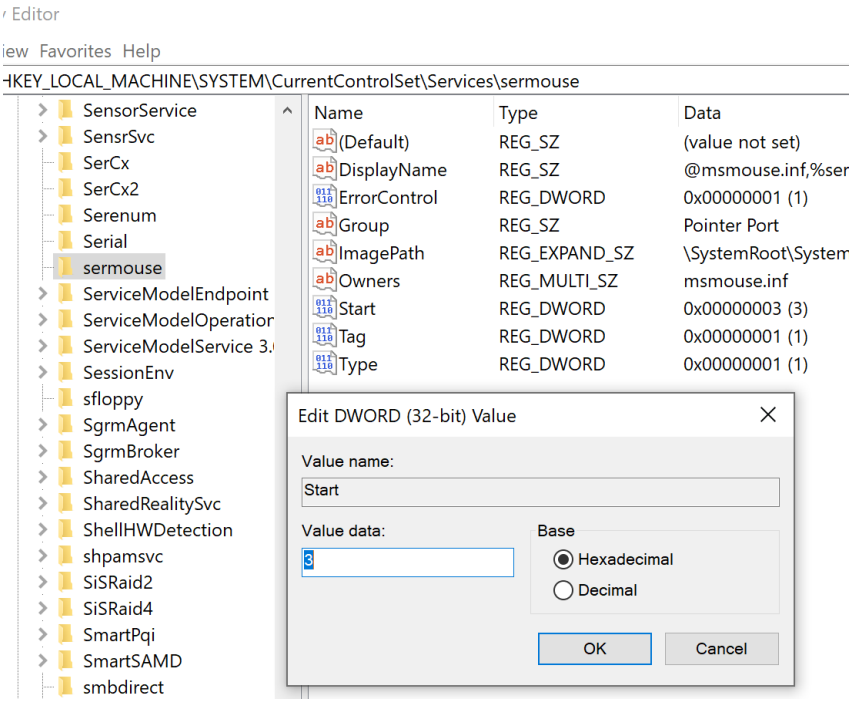

21.4.11 Block the Serial Enumerator

- Go to: **Device manager**

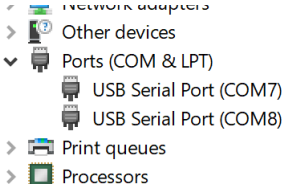

When LabSTAF is connected and powered up, you should see two USB Serial Ports. In this example, the LabSTAF ports are **USB Serial Port (COM7)** and **USB Serial Port (COM8)**.

- Right click on **USB Serial Port (COM7)** and open **Properties**
- Select the **Port Settings** tab and press the **Advanced…** button
- Within the **Advanced Settings for COM7** dialog, uncheck the **Serial Enumerator** box under **Miscellaneous Options**

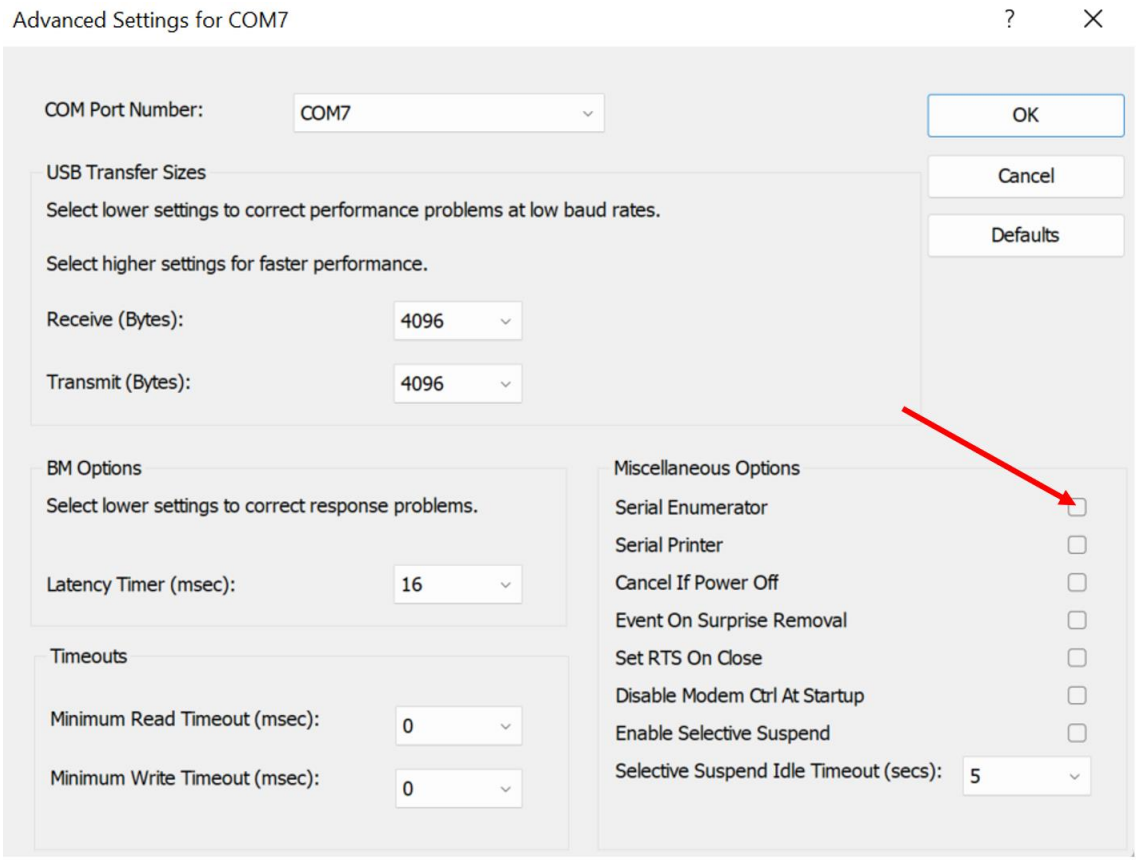

- Click the **OK** button to closed **Advanced Settings for COM7**
- Click **OK** again to close the **Properties** window
- Repeat for **USB Serial Port (COM8)**

21.4.12 Calibration documents

- Make a new folder called **Do not delete** in the file location: **Documents\CT-RunSTAF\Calibration files**

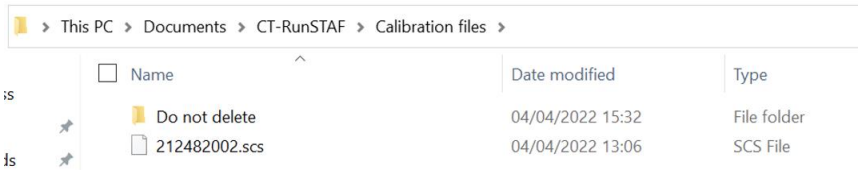

- Create a subfolder within **Do not delete** and name it the serial number of the LabSTAF
- Add the txt files of the spectra for the eight MLEDs, the ALED, and the Walz quantum sensor
- Copy the scs file to this location

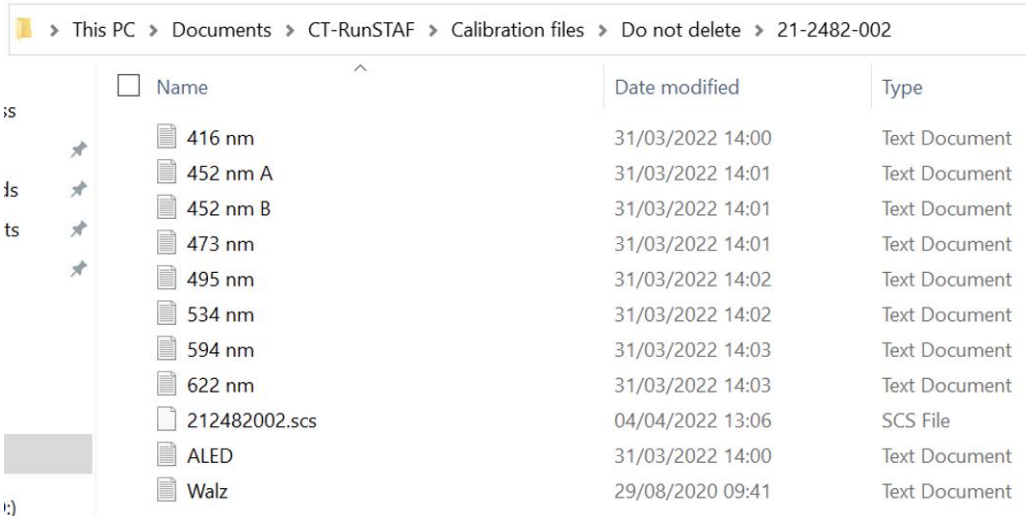

1. Check that the scs file is also saved in the file location:

   Documents\CT-RunSTAF\Calibration files

22 Glossary of terms

This section provides a summary of the terms used within this handbook. A more extensive list of terms used within the relevant literature has been compiled by Schuback et al. (2021).

22.1 Acronyms

22.1.1 CCAP

Culture Collection of Algae and Protozoa (https://www.sams.ac.uk/facilities/ccap/). Many of the examples provided within this handbook use cultures from CCAP.

22.2 Term modifiers

The base (unmodified) terms used within RunSTAF are valid for ST pulse measurements from a dark-adapted sample. There are four modifiers used to define terms that do not fit with this description.

22.2.1 The light-adapted state prime modifier (')

Within the relevant scientific literature, the prime symbol is widely used to signify that a parameter is from a light-adapted sample. Within LabSTAF, a prime is always used when the integrated actinic light source is turned on. It should be noted that no minimum exposure time is defined for inclusion of the prime symbol. Consequently, the prime symbol should not be taken as indicating that a sample is fully adapted to the currently light level.

Example: F_m in the dark becomes F_m' in the light

22.2.2 The baseline corrected modifier (c)

Baseline fluorescence (from any source other than photochemically active PSII complexes) contributes to the measured value of some fluorescence terms. Where a correction has been applied to subtract baseline fluorescence from the total signal, a lowercase c is added to the subscript of the fluorescence term. In situations where baseline fluorescence is zero, reported parameters with a subscripted c have the same value as reported parameters without the subscripted c.

Example: F_m becomes F_{mc} after baseline fluorescence has been subtracted

22.2.3 The second ST pulse modifier (s)

The dual pulse method incorporated within LabSTAF generates a number of additional parameters. A non-subscripted lower case s is used to define a second ST pulse parameter. This is added to the left of the main term.

Example: F_m for the first ST pulse becomes sF_m for the second ST pulse

22.2.4 The dimer modifier (d)

RunSTAF incorporates two fitting algorithms for ST curves: the widely used Rho ST fit and the RunSTAF-specific Dimer ST fit. A lower case d is used to indicate that a parameter was generated from the Dimer ST fit. This modifier is added to the left of the main term. When combined with a second ST pulse modifier, the dimer modifier is closest to the term.

Example: $s\sigma_{PII}$ for the Rho ST fit becomes $sd\sigma_{PII}$ for the Dimer ST fit

22.3 Basic STAF terms

Term	Meaning	SI units (reported units, if different)
ϕ_{xII}	Yield	dimensionless
k_{xII}	Rate-constant	s^{-1}
τ_{xII}	Time-constant	s
σ_{xII}	Absorption cross-section	m^2 $PSII^{-1}$ (nm^2 $PSII^{-1}$)
a_{xII}	Absorption coefficient	m^{-1}
J_{xII}	Photochemical flux per photosystem II	mol photons $PSII^{-1}$ s^{-1} (photons $PSII^{-1}$ s^{-1})
JV_{xII}	Photochemical flux per unit volume	mol photons m^{-3} s^{-1} (µmol photons m^{-3} s^{-1})

Table 22.1: STAF terms for PSII process 'x', where x is a placeholder for the terms in Table 22.2 (Boatman, Geider and Oxborough, 2019; Schuback et al. 2021).

Term	Meaning
LH	Light harvesting
P	Photochemistry
F	Fluorescence
D	Thermal Dissipation or non-radiative Decay

Table 22.2: Subscripts for use with STAF terms for each PSII process (Boatman, Geider and Oxborough, 2019; Schuback et al. 2021).

22.4 Dimer-specific STAF terms

Term	Definition
[oo]	The proportion of PSII dimers in the oo state (both centres open)
[oc]	The proportion of PSII dimers in the oc state (one centre open, the other closed)
[cc]	The proportion of PSII dimers in the cc state (both centres closed)

Table 22.3: Dimer-specific STAF terms

22.5 STAF relaxation phase terms

Term	Definition	SI units (reported units)
τ_F	Time-constant for the Fast component of the dual ST pulse relaxation phase	s (µs)
τ_S	Time-constant for the Slow component of the dual ST pulse relaxation phase	s (µs)
Δ_F	The fraction of the total amplitude of the dual ST pulse relaxation phase attributable to the Fast phase	dimensionless
Δ_S	The fraction of the total amplitude of the dual ST pulse relaxation phase attributable to the Slow phase	dimensionless

Table 22.4: STAF terms specific to the relaxation phase. Only dark terms are shown. The light-equivalent terms all carry a prime. For example, τ_F in the dark becomes τ_F' in the light.

22.6 Additional STAF terms

Term	Meaning	SI units (reported units, if different)
α_{PII}	The initial rate at which photons are used to drive PSII photochemistry during a ST pulse	mol photons $PSII^{-1}$ s^{-1} (photons $PSII^{-1}$ μs^{-1})
ρ	Apparent connectivity among PSII complexes	dimensionless
E_{ST}	Photon irradiance provided to the interrogated volume by the MLEDs during a ST pulse	mol photons m^{-2} s^{-1} (photons nm^{-2} [100 µs]$^{-1}$)
$[Q_A]$	Proportion of photochemically active PSII complexes in the open state	dimensionless

Table 22.5: Additional STAF terms. The parameter ρ can also be defined as the probability of a photon absorbed at a closed PSII being used to drive PSII photochemistry. Clearly, this requires that the photon is first transferred to an open PSII.

22.7 Basic fluorescence terms

Term	Definition
F_o	Measured as the extrapolation to t = 0 at the first ST pulse
F_m	At the asymptote of the first ST pulse (maximum fluorescence)
F_v	$F_m - F_o$ (variable fluorescence)
F	Any point between F_o and F_m
F_q	$F_m - F$ (fluorescence quenched by photochemistry)
F_b	Fluorescence signal not attributable to functional PSII centres
F_{oc}	The baseline subtracted value of F_o such that $F_{oc} = F_o - F_b$
F_{mc}	The baseline subtracted value of F_m such that $F_{mc} = F_m - F_b$
F_c	The baseline subtracted value of F such that $F_c = F - F_b$

Table 22.6: Basic fluorescence terms. Only dark terms are shown. The light-equivalent terms all carry a prime. For example, F_m in the dark becomes F_m' in the light. It is implicitly assumed that all photochemically active PSII complexes are in the open state when F_o is measured. Direct measurement of F_o' requires the inclusion of a pre-measurement dark phase to allow PSII complexes to open.

22.8 Additional fluorescence terms for the second ST pulse

Term	Definition
sF	Extrapolation to t = 0 at the second ST pulse
sF_m	At the asymptote of the second ST pulse
sF_q	$sF_m - sF$
sF_{mc}	The baseline subtracted value of sF_m such that $sF_{mc} = sF_m - F_b$
sF_c	The baseline subtracted value of sF such that $sF_c = sF - F_b$

Table 22.7: Additional fluorescence terms required for the second ST pulse in a dual pulse sequence. Only dark terms are shown. The light-equivalent terms all carry a prime. For example, sF_q in the dark becomes sF_q' in the light.

22.9 Derived fluorescence parameters

Parameter	Definition
F_v/F_m	Theoretically equivalent to ϕ_{PII} when all PSII centres are in the open state and $F_b = 0$
F_v/F_{mc}	As above with F_b subtracted
F_q/F_m	Theoretically equivalent to ϕ_{PII} when some centres are closed and $F_b = 0$
F_q/F_{mc}	As above with F_b subtracted
F_q/F_v	The so-called 'photochemical factor' (Baker and Oxborough, 2004)
F_o/F_v	Normalized Stern-Volmer equation when $F_b = 0$
F_{oc}/F_v	As above when non-zero F_b has been subtracted

Table 22.8: Derived fluorescence parameters. Only dark parameters are shown. The light-equivalent parameters all carry primes on each term. For example, F_q/F_m in the dark becomes F_q'/F_m' in the light.

22.10 Ek terms

Term	Definition	SI units (reported units)
E_k	Value derived from the Alpha phase of an rP-E curve fit	mol photons m^{-2} s^{-1} (µmol photons m^{-2} s^{-1})
E_{kS}	Derived as $1/ (\sigma_{PII}^{(')} \cdot \tau_s^{(')})$	mol photons m^{-2} s^{-1} (µmol photons m^{-2} s^{-1})
E_{kt}'	Downregulation-sensitive, transient value of E_k derived using F_q'/F_v'	mol photons m^{-2} s^{-1} (µmol photons m^{-2} s^{-1})
E_{kt}	Theoretical value of E_{kt}' in the absence of downregulation	mol photons m^{-2} s^{-1} (µmol photons m^{-2} s^{-1})
τ_t'	Time-constant for the recovery of PSII photochemistry derived from E_{kt}'	s (µs)

Table 22.9: STAF terms specific to the relaxation phase. Within the framework of RunSTAF, τ_t' is included under **Relaxation phase parameters**, to allow for direct comparison with the DSP-derived 'tau' parameters, τ_F and τ_S.

22.11 Acronyms and abbreviations

Term	Definition	SI units (reported units)
ALED	Actinic Light Emitting Diode See: **The actinic light source (ALED)**	NA
Acq	Acquisition See: **Data averaging terminology**	NA
cPEC	correction applied to fluorescence values on the SU scale (Package Effect Correction) See: **Applying the Package Effect Correction (PEC)**	dimensionless
DWM	Dual Waveband Measurement for Package Effect Correction (PEC)	NA
DSP	Dual Single Turnover Pulse See: **Dual ST Pulse (DSP)-based relaxation phase (tau) measurement**	NA
FLC	Fluorescence Light Curve	NA
Gaq	Group acquisition See: **Dual ST Pulse (DSP)-based relaxation phase (tau) measurement**	NA
MLED	Measurement Light Emitting Diode(s) See: **The Measurement LEDs (MLEDs) and PMT**	NA
PEC	Package Effect Correction See: **Applying the Package Effect Correction (PEC)**	dimensionless
PEP	Photochemical Excitation Profile See: **Photochemical Excitation Profiles (PEPs)**	NA
ST	Single Turnover See: **Single Turnover (ST)**	NA
SU	The STAF Units scale of fluorescence values See: **STAF Units of fluorescence (SU)**	unitless
Saq	Super acquisition See: **Data averaging terminology**	NA
Seq	Sequence of data points derived from a Single Turnover (ST) or Dual Single Turnover Pulse (DSP) measurement See: **Data averaging terminology**	NA

Table 22.10: Acronyms and abbreviations that are used within this handbook.

22.12 Alternative terminology

As already noted within this document, a structured approach has been taken to the terminology used within this document. As far as possible, terms are derived from core elements that have been in use for several decades. The aim has been to employ terminology that is both self-consistent and unambiguous. Inevitably, this has led to alternatives to some established terms being generated. This section compares the terminology used within this document with terminology used more widely.

See: **Key features and terminology**

22.12.1 Absorption cross sections

The most widely used equations for fitting ST curves to generate a value for the absorption cross section of PSII photochemistry were originally published by Kolber, Prášil and Falkowski (1998). Table 22.11 provides a comparison of the terminology used within this original publication and the terminology used here.

Units of nm^2 are used in preference to $Å^2$ because the Angstrom is not part of the SI system. Within the relevant scientific literature, the Greek letter Rho is now more widely used than an italicised p to define connectivity or energy transfer. Although 'functional absorption cross section' and 'effective absorption cross section' are widely used within the literature, they are inconsistent with the overall terminology used within this document. Within recent publications, the absorption cross section of PSII photochemistry is more likely to be reported as unit area per PSII (σ_{PII}) than unit area per photon ($\sigma_{PS\,II}$).

KPF term (reported units)	RunSTAF term (reported units)	KPF description	RunSTAF description
$\sigma_{PS\,II}$ ($Å^2$ $photon^{-1}$)	σ_{PII} (nm^2 $PSII^{-1}$)	Functional absorption cross section	Absorption cross section of PSII photochemistry
$a_{PS\,II}$ ($Å^2$ $photon^{-1}$)	σ_{LHII} (nm^2 $PSII^{-1}$)	Optical absorption cross section	Absorption cross section of PSII light harvesting
p (dimensionless)	ρ (dimensionless)	Extent of energy transfer	Apparent connectivity among PSII complexes

Table 22.11: KPF references Kolber, Prášil and Falkowski (1998).

23 Answers to FAQs and background material

This section covers a number of technical and theoretical issues that are not covered in earlier sections.

23.1 Deriving values of a_{LHII} and/or PSII concentration

As noted elsewhere within this document, the fluorescence values reported are on a defined STAF Unit (SU) scale. When incorporating fluorescence values within the derivation of a_{LHII} or PSII concentration, the reported fluorescence values should be divided by 10^6 to bring them onto the same scale as K_a (default value of 11,800 m^{-1}). Similarly, reported values for σ_{PII} and σ_{LHII} should be converted from nm^2 $PSII^{-1}$ to m^2 $PSII^{-1}$ to bring them onto the same scale as K_a.

The value of a_{LHII} reported by RunSTAF includes corrections for the package effect and spectral correction, using the cPEC and cPEP values shown under **Data processing** on the home screen. The value of cPEC is derived as the DWM-derived or user-set PEC value normalized to a default of 0.32. For example, a PEC of 0.16 generates a cPEC value of 0.16 / 0.32 = 0.5. The value of cPEP is derived from analysis of the MLED and ALED spectra incorporated within the scs calibration file.

Equation 23.1 should be used to derive a value for a_{LHII} that matches with the value generated by RunSTAF.

$$a_{LHII} = 10^{-6} \cdot K_a \cdot \frac{F_{mc} \cdot F_{oc}}{F_v} \cdot cPEC \cdot cPEP \qquad \text{Equation 23.1}$$

23.2 Deriving your own values of J_{PII}, JV_{PII} and GO_{PII}

RunSTAF applies a direct spectral correction to values of J_{PII}. This correction can only be applied if a PEP has been run and the scs calibration file for the LabSTAF sensor is available.

23.3 Dark Step F_v/F_m and F_v'/F_m' values

When running a FLC, it is common practice to include a dark step after the highest **Up** step and before the **Down** steps. Within the left panel of Figure 23.1, a 60 s Dark Step has been included after the **Up 12** (60 s at 456 µmol photons m^{-2} s^{-1}) and before the **Down 8** (120 s at 188 µmol photons m^{-2} s^{-1}), as indicated by the red arrows. The data values for the 456 µmol photons m^{-2} s^{-1} **Dark** step are highlighted by the yellow box within the right panel of Figure 23.1. These values are the dark equivalent of the light-adapted terms shown. For example, the **Dark** value in the F' line is F_o and the F_m' value is F_m.

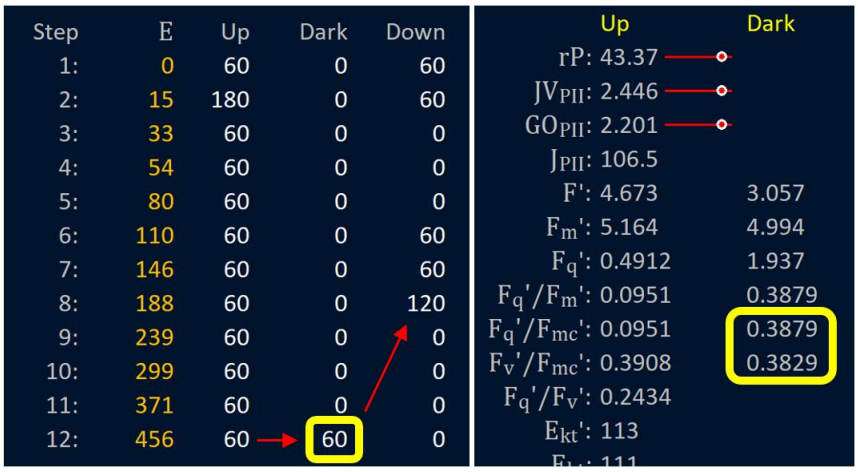

Figure 23.1: Dark FLC step comparison of F_v/F_m and F_v'/F_m' values.

In the case of F_q'/F_{mc}', the **Dark** value is F_v/F_{mc}. The values of F_o and F_m required to generate the Dark F_v/F_{mc} are from the ST data acquired during the **Dark** step.

In the case of F_v'/F_{mc}', the **Dark** value is also defined as F_v'/F_{mc}'. The value of F_{oc}' required for the **Dark** F_v'/F_{mc}' is generated using Equation 23.2 (Oxborough and Baker, 1997).

$$F_{oc}' = F_{oc}/\left(\frac{F_v}{F_{mc}} + \frac{F_{oc}}{F_{mc}'}\right) \qquad \text{Equation 23.2}$$

Within Equation 23.2, the only value measured from **Dark 12** is F_{mc}'. All the remaining values on the right-hand side are from **Up 1**.

By allowing for comparison between the F_v/F_{mc} measured directly in the dark and the calculated value, this process provides a check for the validity of F_v'/F_{mc}' and F_q'/F_v' parameters calculated from the same sample under illumination, which both require F_{oc}'.

23.4 The Stern-Volmer relationship, NPQ and NSV

NPQ has been in use for more than 20 years and NSV for around ten years. Although values for both parameters are generated by RunSTAF, they are not discussed within this handbook. This is mainly because neither parameter has any direct relevance to the assessment of primary productivity. This subsection has been included to provide a basic overview of their derivation.

The Stern-Volmer relationship provides a theoretical basis for the decrease in F_m to F_m' that is commonly observed under actinic illumination: so-called non-photochemical quenching. The basic concept of Stern-Volmer quenching within PSII is that quenching is induced by the accumulation of a class of molecules within the PSII light harvesting system with the capacity to accelerate the deactivation of excited light harvesting molecules. Under the Stern-Volmer relationship, this intermolecular quenching is in direct proportion to the concentration of quencher. Because this mechanism competes directly with photochemistry within the PSII complex, it is routinely described as downregulation (of PSII photochemistry).

It is important to note that Stern-Volmer quenching is not the only mechanism that can potentially change the value of F_m'. For example, so-called state-transitions can increase or decrease F_m' by modifying the physical cross section of the PSII light harvesting system. With some setups, a simple change in biomass within the interrogated volume could also be responsible for a measured increase or decrease in F_m'. It follows that while calculated values of NPQ and NSV are scaled to Stern-Volmer quenching, they may actually be tracking changes that are at least partly driven by other mechanisms. Because the assumption of Stern-Volmer quenching is intrinsic to both parameters, use of either parameter is not appropriate when other processes may be responsible for quenching of F_m'.

Non-photochemical quenching attributed to Stern-Volmer quenching is widely assumed to be at least partly regulated through the xanthophyll cycle in chlorophytes and brown algae and diadinoxanthin cycle in diatoms, dinoflagellates and haptophytes (See Goss and Latowski, 2020 for a recent review). Typically, the xanthophyll cycle is stimulated as incident light is increased beyond E_k. Within the chlorophytes and brown algae, violaxanthin is converted to zeaxanthin via the intermediate antheraxanthin. Within diatoms and dinoflagellates, diadinoxanthin is transformed into diatoxanthin (diatoms) or dinoxanthin (dinoflagellates). The conversion (de-epoxidation) of violaxanthin to zeaxanthin is typically reversed over tens of second to minutes in the dark. In contrast, de-epoxidation of diadinoxanthin may not reverse in the dark. If, for example, diatoms are rapidly taken from high light to darkness, downregulation may remain locked in. A routine method for reversing this is to apply low light treatment for several minutes. An incident photon irradiance of 10 – 20 µmol photons m^{-2} s^{-1} for 10 to 20 minutes at ambient temperature has been proposed as a reasonable starting point for establishing the optimum pre-FLC treatment conditions (Schuback et al. 2021).

Equation 23.3 provides a general equation for the Stern-Volmer relationship.

$$\frac{I_f^0}{I_f} = 1 + k_q \tau_0 \cdot [\mathrm{Q}] \qquad \text{Equation 23.3}$$

Where I_f^0 is the fluorescence intensity in the absence of the quencher, I_f is the fluorescence intensity in the presence of the quencher, k_q is the quencher rate-constant and τ_0 is the lifetime of the excited state of the fluorescent molecule in the absence of quencher. For PSII fluorescence, we can substitute the terms on the left-hand side of Equation 23.3 to form Equation 23.4.

$$\frac{\mathrm{F_m}}{\mathrm{F_{m'}}} = 1 + k_q \tau_0 \cdot [\mathrm{Q}] \qquad \text{Equation 23.4}$$

Although routine measurement of k_q and τ_0 is not practical, we can simplify Equation 23.4 to provide Equation 23.5.

$$[\mathrm{Q}] \propto \frac{\mathrm{F_m}}{\mathrm{F_{m'}}} - 1 \qquad \text{Equation 23.5}$$

To generate a value for NPQ, we simply replace the proportionality sign with an equal sign (Equation 23.6).

$$\mathrm{NPQ} = \frac{\mathrm{F_m}}{\mathrm{F_{m'}}} - 1 \qquad \text{Equation 23.6}$$

From Equations 23.3, 23.4 and 23.5 it should be clear that values for NPQ can only be compared if k_q and τ_0 are constant and $[\mathrm{Q}]$ is zero at $\mathrm{F_m}$. A significant problem with Equation 23.5 is that the calculated value of NPQ is sensitive to baseline fluorescence as well as $[\mathrm{Q}]$. It follows that that NPQ values cannot reliably be compared between samples with different values of $\mathrm{F_v/F_m}$.

NSV was used as an alternative to NPQ within McKew et al. (2013) to allow for comparison of downregulation between high light-grown and low light-grown cells of *Emiliania huxleyi* (clone CCMP 1516). Within this study, it was assumed that differences in $\mathrm{F_v/F_m}$ between high and low light-grown cells were due to differences in pigment composition, rather than differences in baseline fluorescence. This assumption was supported through HPLC analysis of pigments. Values for NSV can be generated using Equation 23.7.

$$\mathrm{NSV} = \frac{\mathrm{F_{o'}}}{\mathrm{F_{v'}}} \qquad \text{Equation 23.7}$$

While both NPQ and NSV can be used to track changes in downregulation with increasing incident photon irradiance within a single sample, NSV also allows for comparison between samples with different values of $\mathrm{F_v/F_m}$. In the study of McKew et al. (2013) there were no significant differences in NPQ values for the high light-grown and low light-grown cells between zero and 300 µmol photons m^{-2} s^{-1}. In contrast, the high light-grown cells had higher values of NSV at all points between zero and 1200 µmol photons m^{-2} s^{-1}.

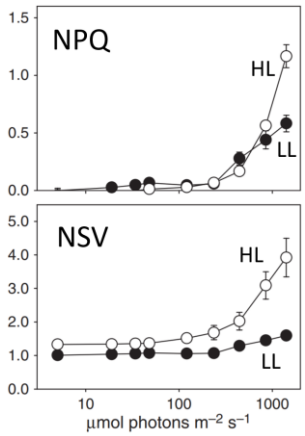

Figure 23.2: Comparison of NPQ and NSV data for High Light (HL) and Low Light (LL) grown cells of *Emiliania huxleyi* (clone CCMP 1516). The $\mathrm{F_v/F_m}$ values were 0.4 for the HL-grown cells and 0.5 for the LL-grown cells.

These data are from parts **d** and **e** of Figure 2 within McKew et al. (2013).

24 Troubleshooting guide

24.1 LabSTAF unit fails to attach or gets stuck at Starting…

The LabSTAF unit takes 30 s to boot up and attach to RunSTAF. If you power cycle the LabSTAF during the boot up process, it is very likely that you will crash the internal operating system. So please BE PATIENT!

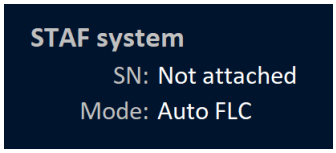

If the LabSTAF doesn't attach…

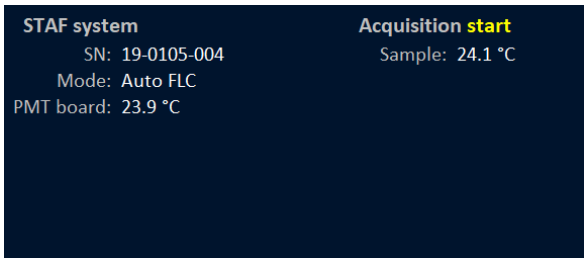

…and show the Acquisition **start** button

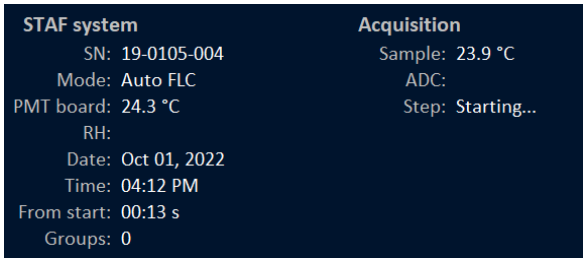

Or if acquisition gets stuck at **Starting…**

24.1.1 Option 1

- Close RunSTAF and power down the LabSTAF unit
- Wait at least 60 s
- Power up the LabSTAF unit and restart RunSTAF
- Remember that it takes 30 s for the LabSTAF unit to boot up and attach to RunSTAF

24.1.2 Option 2 (if Option 1 fails to fix the problem)

- Close RunSTAF and power down the LabSTAF unit
- Disconnect the USB cable used to connect the Surface Go to the LabSTAF unit
- Wait at least 60 s
- Reconnect the USB cable between the Surface Go and STAF unit
- Power up the LabSTAF unit and restart RunSTAF
- Remember that it takes 30 s for the LabSTAF unit to boot up and attach to RunSTAF

24.1.3 Option 3 (if Option 2 fails to fix the problem)

- Delete all files within the **…Documents/CT-RunSTAF/App** sub-folder
- Run through all **Option 2** steps

24.2 Clearing all Windows COM ports

If the LabSTAF is not running correctly, even after one or more power cycles of the system, it is worth clearing all COM ports through Device Manager.

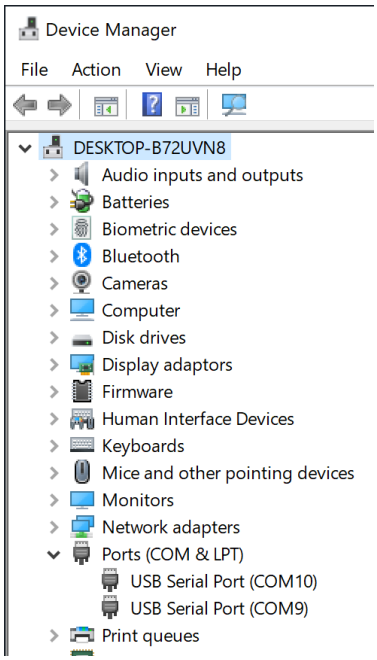

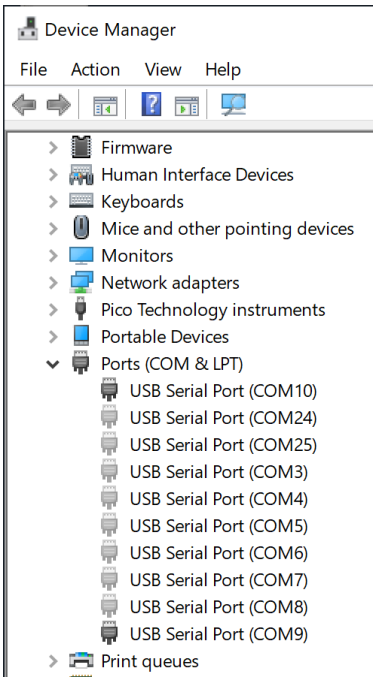

Figure 24.3: In both screen crops, the USB Serial Ports (COM9 and COM10) are provided by a LabSTAF unit that is plugged into the computer and powered up.

Selecting…
View → Show hidden devices from the menu adds the additional COM ports seen in the right screen crop to the list.

Right click over each **USB Serial Port (COM..)** and select **Uninstall device**. Include the two ports (**COM9** and **COM10**) in this process. Do not select the option to **Delete the driver software for this device** when uninstalling.

Once all **USB Serial Ports** have been deleted, reboot the computer. When the LabSTAF is connected and powered on, new **USB Serial Ports** should be created under **Ports (COM & LPT)** in **Device Manager**.

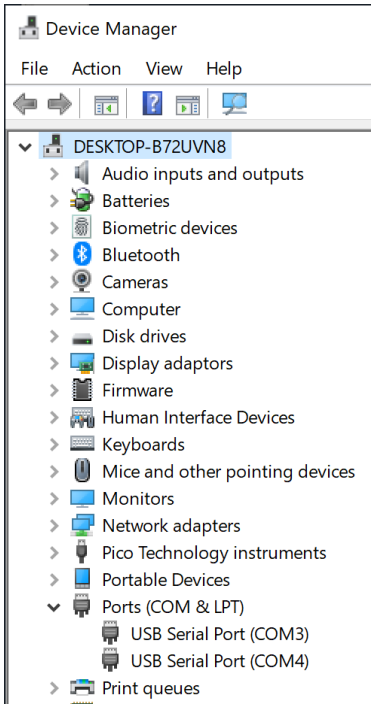

Figure 24.4: Within this screen crop, the two USB Serial Ports provided by the connected LabSTAF unit have been reassigned as COM3 and COM4.

24.3 RunSTAF messages

Most messages are presented within a dialog at the top left of the screen. Figure 24.4 provides an example.

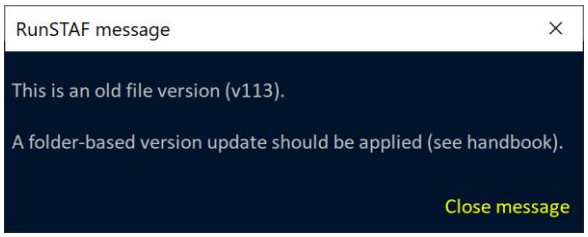

Figure 24.4: An example of a **RunSTAF message** dialog. This type of message is shown in the top left of the screen.

Within this subsection, the RunSTAF dialog message text is shown in bold.

24.3.1 RunSTAF messages on opening a file

The current data fit is out of date (v112).
A folder-based Saq refit should be applied (see handbook).

At least one of the curve fits applied at the time the file was created has been superseded within the version of RunSTAF being used to open the file.
See: **Refitting ST data**

This is an old file version (v116).
A folder-based version update should be applied (see handbook).

This file was created using an older version of RunSTAF. The message is based on the assumption that other files within the same folder will have been created with the same version. The version update can take anywhere from a few seconds, if no curve refits are required, to several minutes, if curve fits are required.
See: **Folder-based refitting and reprocessing**

Unsupported file version (v120).

The file may have been created using a more recent version of RunSTAF. Ensure that the version of RunSTAF being used is the most up-to-date available.
See: **Access the most recent version of RunSTAF**

24.4 Events log

A range of operational events are logged within a text file stored at the following location…

Documents → CT-RunSTAF → Events

A new file is created each day. As an example, an events file created on 14th October 2022 will be named…

221014 events.txt

The events recorded are **AB reset**, **ST reset**, **Auto MLED failed**, **DWM failed** and **PEP failed**.

The **AB reset** and **ST reset** events are triggered together after a successful system reset. A reset may be triggered by a high voltage spike through the mains supply.

The **Auto MLED failed**, **DWM failed**, and **PEP failed** events can be triggered by low signal to noise. Increasing the **Seq / Acq** value under **STAF setup** will often help with this.

25 References

Andrée, S. Weis, E. and Krieger, A. (1998) Heterogeneity and Photoinhibition of Photosystem II Studied with Thermoluminescence. *Plant Physiol.* 116: 1053–1061.

Dau, H. and Sauer, K (1991) Electric field effect on chlorophyll fluorescence and its relation to Photosystem II charge separation reactions studied by a salt-jump technique. *Biochim. Biophys. Acta* 1098: 49-60. https://doi.org/10.1016/0005-2728(91)90008-C

Baker, N.R. and Oxborough, K. (2004) Chlorophyll Fluorescence as a Probe of Photosynthetic Productivity. In: Chlorophyll *a* fluorescence. A signature of photosynthesis. pp. 65-82. George Papageorgiou and Govindjee Eds. Springer, Dordrecht, The Netherlands. ISBN 1-4020-3217-X

Behrenfeld, M. J., Prášil, O., Babin, M., and Bruyant, F. (2004). In search of a physiological basis for covariations in light-saturated photosynthesis. *J. Phycol.* 40: 4–25. https://doi.org/10.1046/j.1529-8817.2004.03083.x

Björn, L.O. (2015) Photobiology : The Science of Light and Life, 3rd Edition. *Elsevier*. ISBN13 9781493914678

Black, M.T., Brearley, T.H. and Horton P. (1986) Heterogeneity in chloroplast photosystem II. *Photosynth. Res.* 8: 193–207. https://doi.org/10.1007/BF00037128

Boatman, T.G., Geider R.J. and Oxborough, K. (2019) Improving the accuracy of single turnover active fluorometry (STAF) for the estimation of phytoplankton primary productivity (PhytoPP). *Front. Mar. Sci.* https://doi.org/10.3389/fmars.2019.00319

Geider, R. J., and MacIntyre, H. L. (2002). "Physiology and biochemistry of photosynthesis and algal carbon acquisition," in Phytoplankton Productivity: Carbon Assimilation in Marine and Freshwater Ecosystems, eds P. J. L. B. Williams, D. N. Thomas, and C. S. Reynolds (Oxford: Blackwell), 44–77. https://doi.org/10.1002/9780470995204.ch3

Geider, R. J. and Osborne, B.A. (1992) Algal Photosynthesis: Prentice Hall. ISBN 978-1-4757-2155-3

Gorbunov, M.Y., Shirsin, E., Nikonova, E., Fadeev, V.V., and Falkowski, P.G. (2020) A multi-spectral fluorescence induction and relaxation (FIRe) technique for physiological and taxonomic analysis of phytoplankton communities. *MEPS* 644: 1-13 https://doi.org/10.3354/meps13358

Goss, R. and Latowski, D. (2020) Lipid dependence of xanthophyll cycling in higher plants and algae. *Front. Plant. Sci.* https://doi.org/10.3389/fpls.2020.00455

Guenther, J.E., Melis, A. (1990) The physiological significance of photosystem II heterogeneity in chloroplasts. *Photosynth. Res.* 23: 105–109 https://doi.org/10.1007/BF00030070

Halsey, K. H., Milligan, A. J., and Behrenfeld, M. J. (2010). Physiological optimization underlies growth rate-independent chlorophyll-specific gross and net primary production. *Photosynth. Res.* 103: 125–137. https://doi.org/10.1007/s11120-009-9526-z

Johnson, M.P. and Ruban, A.V. (2014) Rethinking the existence of a steady-state ΔΨ component of the proton motive force across plant thylakoid membranes. *Photosynth. Res.* 119: 233 – 242. https://doi.org/10.1007/s11120-013-9817-2

Kolber, Z. S., Prášil, O., and Falkowski, P. G. (1998). Measurements of variable chlorophyll fluorescence using fast repetition rate techniques: defining methodology and experimental protocols. *Biochim. Biophys. Acta* 1367: 88–106. https://doi.org/10.1016/s0005-2728(98)00135-2

Lacour, T., Larivière, J., Ferland, J., Bruyant, F., Lavaud, J., and Babin, M. (2018). The role of sustained photoprotective non-photochemical quenching in low temperature and high light acclimation in the bloom-forming arctic diatom *Thalassiosira gravida*. *Front. Mar. Sci.* 5, 1–16.

https://doi.org/10.3389/fmars.2018.00354

Lavaud, J., and Goss, R. (2014). The Peculiar Features of Non-Photochemical Fluorescence Quenching in Diatoms and Brown Algae. In: *Advances in Photosynthesis and Respiration* (Springer, Dordrecht), 421–443. https://link.springer.com/chapter/10.1007/978-94-017-9032-1_20

Lawrenz, E., Silsbe, G., Capuzzo, E., Ylöstalo, P., Forster, R. M., and Simis, S. G. (2013) Predicting the electron requirement for carbon fixation in seas and oceans. *PLoS One* 8:e58137. https://doi.org/10.1371/journal.pone.0058137

Lee, Z., Marra, J. Perry, M.J. and kahru M. (2015) Estimating oceanic primary productivity from ocean color remote sensing: A strategic assessment. *J. Mar. Sys.* 149: 50-59. http://dx.doi.org/10.1016/j.jmarsys.2014.11.015

MacIntyre, H.L., Kana, T.M., Anning, T. and Geider, R.J. (2002). Photoacclimation of photosynthesis irradiance response curves and photosynthetic pigments in microalgae and cyanobacteria. *J. Phycol.* 38:17-38.

Marra, J. (2002). "Approaches to the measurement of plankton production," in Phytoplankton Productivity, eds P. J. L. B. Williams, D. N. Thomas, and C. S. Reynolds (Oxford: Blackwell Science Ltd), 78–108. https://doi.org/10.1002/9780470995204.ch4

Marchin, T. de, Ghysels, B., Nicolay, S. and Franck F (2014). Analysis of PSII antenna size heterogeneity of *Chlamydomonas reinhardtii* during state transitions. *Biochim. Biophys. Acta* 1837: 121-130. https://doi.org/10.1016/j.bbabio.2013.07.009

McKew, B.A., Davey, P., Finch, S.J., Hopkins, J., Lefebvre, S.C., Metodiev, M.V., Oxborough, K., Raines, C.A., Lawson, T. and Geider, R.J. (2013). The trade-off between the light-harvesting and photoprotective functions of fucoxanthin-chlorophyll proteins dominates light acclimation in *Emiliania huxleyi* (clone CCMP 1516). *New Phytol*. 200:74-85. https://doi.org/10.1111/nph.12373

Milligan, A. J., Halsey, K. H., and Behrenfeld, M. J. (2015). Advancing interpretations of 14C-uptake measurements in the context of phytoplankton physiology and ecology. *J. Plankt. Res.* 37, 692–698. https://doi.org/10.1093/plankt/fbv051

Montagnes, D. J. S., Berges, J. A., Harrison, P. J., and Taylor, F. J. R. (1994). Estimating carbon, nitrogen, protein, and chlorophyll *a* from volume in marine phytoplankton. *Limnol. Oceanogr.* 39: 1044–1060. https://doi.org/10.4319/lo.1994.39.5.1044

Nakayama, T., Nomura, M., Takano. Y., Tanifuji, G., Shiba, K., Inaba, K., Inagaki, Y., and Kawata, M. (2019) Single-cell genomics unveiled a cryptic cyanobacterial lineage with a worldwide distribution hidden by a dinoflagellate host. Proc. Natl. Acad. Sci. USA. 116(32):15973-15978 https://doi.10.1073/pnas.1902538116

Nield, J. and Barber, J. (2006) Refinement of the structural model for the photosystem II supercomplex of higher plants., *Biochim. Biophys. Acta* 1757: 353-361

Oxborough, K., Moore, C.M., Suggett, D.J., Lawson, T., Chan, H.G and Geider, R.J. (2012) Direct estimation of functional PSII reaction centre concentration and PSII electron flux on a volume basis: a new approach to the analysis of Fast Repetition Rate fluorometry (FRRf) data. *Limnol. Oceanogr.: Methods.* (10) 142-154 https://doi.org/10.4319/lom.2012.10.142

Oxborough, K. and Baker, N.R. (1997) Resolving chlorophyll *a* fluorescence images of photosynthetic efficiency into photochemical and non-photochemical components - calculation of q_P and F_v'/F_m' without measuring F_o'. *Photosynth. Res.* 54: 135-142 https://link.springer.com/article/10.1023/A:1005936823310

Platt, T., and Gallegos, C. L. (1980). "Modelling primary production," in Primary productivity in the Sea, ed. P. G. Falkowski (Boston, MA: Springer). pp 339–362 https://doi.org/10.1007/978-1-4684-3890-1_19

Quick, W.P. and Horton, P. (1984) Studies on the induction of chlorophyll fluorescence quenching by redox state and transthylakoid pH gradient. *Proc. R. Soc. Lond.* B 220: 371–382 https://royalsocietypublishing.org/doi/10.1098/rspb.1984.0006

Sakshaug, E., Bricaud, A., Dandonneau, Y., Falkowski, P. G., Kiefer, D. A., Legendre, L., Morel, A. Parslow, J. and Takahashi, M. (1997) Parameters of photosynthesis: definitions, theory and interpretation of results *J. Plank. Res.* 19: 1637-1670
https://doi.org/10.1093/plankt/19.11.1637

Schuback, N., Tortell P.D. and 22 others (2021) Single-turnover variable chlorophyll fluorescence as a tool for assessing phytoplankton photosynthesis and primary productivity: Opportunities, caveats and recommendations. *Front. Mar. Sci.*
https://doi.org/10.3389/fmars.2021.690607

Silsbe, G.M., Oxborough, K., Suggett, D.J., Forster R.M., Ihnken, S. Komárek, O. Lawrenz, E., Prášil, O., Röttgers, R., Sicner, M., Simis, S., Van Dijk, M.A. and Kromkamp, J.C. (2015). Toward autonomous measurements of photosynthetic electron transport rates: An evaluation of active fluorescence-based measurements of photochemistry. *Limnol. Oceanogr.: Methods.* 13: 138-155
https://doi.org/10.1002/lom3.10014

Suggett, D.J., MacIntyre, H.L. and Geider, R.J. (2004). Evaluation of biophysical and optical determinations of light absorption by photosystem II in phytoplankton. *Limnol. Oceanogr.: Methods.* (2) 316-332.

Suggett, D. J., Moore, C. M., and Geider, R. J. (2010). "Estimating aquatic productivity from active fluorescence measurements," in Chlorophyll a Fluorescence in Aquatic Sciences: Methods and Applications, eds D. Suggett, O. Prášil, and M. Borowitzka (Dordrecht: Springer), 103–127.
https://doi.org/10.1007/978-90-481-9268-7_6

Stirbet, A., Lazár, D., Papageorgiou, G.C. and Govindjee (2019) Chlorophyll *a* Fluorescence in Cyanobacteria: Relation to Photosynthesis. In: Cyanobacteria: From Basic Science to Applications (Academic Press). pp 79-130
https://doi.org/10.1016/B978-0-12-814667-5.00005-2

Umena, Y., Kawakami, K., Shen, JR. et al. Crystal structure of oxygen-evolving photosystem II at a resolution of 1.9 Å. *Nature* 473, 55–60 (2011).
https://doi.org/10.1038/nature09913

Vernotte, C. Etienne, A.L. and Briantais, J.M. (1979) Quenching of the system II chlorophyll fluorescence by the plastoquinone pool. *Biochim. Biophys. Acta* 545: 519-527

Watanabe, M., Iwai, M., Narikawa, R. and Ikeuchi, M. (2009) Is the Photosystem II complex a monomer or a dimer? *Plant Cell Physiol.* 50: 1674-1680
https://doi.org/10.1093/pcp/pcp112

Webb, W. L., Newton, M., and Starr, D. (1974). Carbon dioxide exchange of *Alnus rubra*. *Oecologia* 17, 281–291
https://doi.org/10.1007/BF00345747

Witt, H.T. (1971) Coupling of quanta, electrons, fields, ions and phosphorylation in the functional membrane of photosynthesis. *Quart. Rev. Biophys.* 4:365-477

Chelsea Technologies
A SONARDYNE COMPANY

55 Central Avenue
West Molesey
Surrey KT8 2QZ
United Kingdom

T +44 (0)20 8481 9000
E sales@chelsea.co.uk

chelsea.co.uk